# INFORMATION TO USERS

This manuscript has been reproduced from the microfilm master. UMI films the text directly from the original or copy submitted. Thus, some thesis and dissertation copies are in typewriter face, while others may be from any type of computer printer.

**The quality of this reproduction is dependent upon the quality of the copy submitted.** Broken or indistinct print, colored or poor quality illustrations and photographs, print bleedthrough, substandard margins, and improper alignment can adversely affect reproduction.

In the unlikely event that the author did not send UMI a complete manuscript and there are missing pages, these will be noted. Also, if unauthorized copyright material had to be removed, a note will indicate the deletion.

Oversize materials (e.g., maps, drawings, charts) are reproduced by sectioning the original, beginning at the upper left-hand corner and continuing from left to right in equal sections with small overlaps.

Photographs included in the original manuscript have been reproduced xerographically in this copy. Higher quality 6" x 9" black and white photographic prints are available for any photographs or illustrations appearing in this copy for an additional charge. Contact UMI directly to order.

Bell & Howell Information and Learning
300 North Zeeb Road, Ann Arbor, MI 48106-1346 USA

UMI®
800-521-0600

# EVALUATION OF THE SEISMIC LEVEL OF PROTECTION OF STEEL MOMENT RESISTING FRAME BUILDING STRUCTURES

By

AIMAN MAHMOUD SAMY BIDDAH

A Thesis

Submitted to the School of Graduate Studies

in Partial Fulfilment of the Requirements

for the Degree

Doctor of Philosophy

McMaster University

# EVALUATION OF THE SEISMIC LEVEL OF PROTECTION OF STEEL MOMENT RESISTING FRAME BUILDING STRUCTURES

DOCTOR OF PHILOSOPHY (1998)
(Civil Engineering)

McMater University
Hamilton, Ontario

TITLE: Evaluation of the seismic level of protection of steel moment resisting frame building structures.

AUTHOR: Aiman Mahmoud Samy Biddah, B.Sc. (Ain Shams University)
M.Eng. (McMaster University)

SUPERVISOR: Professor A.C. Heidebrecht

NUMBER OF PAGES: xxiii, 295

## ABSTRACT

A large number of low and medium-rise buildings have steel moment resisting frames as the primary lateral load resisting system. During the past few decades, much confidence has been placed on this type of structural system for resisting seismic loads. However, after recent earthquakes (e.g. Northridge, California, in 1994, and Kobe, Japan, in 1995) the confidence in this system was reduced as a result of various types of damage that moment resisting steel frames have suffered. This resulted in a recognition of the need to evaluate the performance criteria on which current provisions are based. While there have not been any major casualties due to earthquakes in Canada during the past few decades, in fact there is an actual seismic hazard which affects significant regions of the country, for example, the cities of Victoria, Vancouver, Quebec City, Montreal, and Ottawa. The design peak ground motions in such regions are moderate in comparison with those in California or Japan, however the uncertainties associated with estimating the expected ground motions are such that twice or three times the seismic design level motions are likely to occur.

The main objectives of this research study are: (i) to evaluate the seismic level of protection afforded to steel moment resisting frame building structures designed in accordance with the current Canadian provisions (i.e. NBCC (1995) and CAN/CSA-S16.1-94), and (ii) to investigate the effect of the different design philosophies and seismic hazard design levels on the inelastic dynamic response of multi-storey steel frame structures.

Six storey office buildings located in regions of high, intermediate, and low seismic hazard, and a ten storey office building located in a region of intermediate seismic hazard are designed in accordance with the current Canadian provisions using three design philosophies, namely strong-column weak-beam (SCWB), weak-column strong-beam (WCSB), and strong-column weak-panel zone (SCWP). The scope of the research program includes: (a) modelling of the structural elements; (b) nonlinear push over static analyses / inelastic dynamic analyses, and (c) evaluation of the damage potential associated with each design.

In the study analytical models are modified and incorporated into the PC-ANSR computer program in order to perform the inelastic dynamic analyses of the frames. The inelastic models take into account the spreading of inelastic deformations in beam-column elements, connection flexibility and panel zone deformations. A cyclic model for the panel zone element is developed and introduced into PC-ANSR. The performance of the frames is evaluated both statically using monotonically increasing lateral load (nonlinear push over static analyses), and dynamically by subjecting the inelastic model to an ensemble of actual strong ground motion records (time-history analyses).

The main ensemble of time-histories used in the study consists of twelve earthquake ground motion records selected on the basis of Newmark-Hall design spectra amplification factors. An additional ensemble of time-histories (twelve records) is selected based on the uniform hazard spectrum for Vancouver which describes the new seismic hazard information given by the Geological Survey of Canada. The additional ensemble is used to investigate the implication of the new seismic hazard information on the performance of the six storey frames in the intermediate seismic hazard region.

The results of the inelastic dynamic analyses are presented in terms of statistical measures of the maximum response parameters determined during the time-history analyses. Also, the results of the nonlinear push over analyses are presented and compared with those of the dynamic analyses. The performance expectations of the frames are evaluated in order to assess both the overall level of protection provided to the frames and the preferred design philosophy.

It is concluded from the analyses that in high and intermediate seismic hazard regions, a well-designed and detailed ductile moment resisting frame (i.e. SCWB or SCWP) can withstand ground motions of twice the design level with a very little likelihood of collapse, while an ill-conditioned designed frame (i.e. WCSB) may develop a collapse mechanism even at the design level excitation. In regions of low seismic hazard activity, the three frame design types perform satisfactorily, and can withstand twice the design level excitations with only a moderate amount of damage.

## ACKNOWLEDGEMENTS

I wish to express my sincere appreciation to my research supervisor, Prof. A.C. Heidebrecht for his guidance and encouragement throughout the course of this study. I am grateful to his dedication and the number of hours that he spent with me on this research.

I am indebted to my Supervisory Committee members, Prof. R.M. Korol and Prof. M. Dokainish for their valuable comments and suggestions on my research and also their time in reviewing this thesis.

Financial support from McMaster University and the Natural Sciences and Engineering Research Council of Canada are gratefully acknowledged.

Finally, much appreciation is extended to my parents and my brothers for their encouragement and support during the course of this study.

To my dear parents and brothers

## TABLE OF CONTENTS


| | | Page |
|---|---|---|
| **ABSTRACT** | | iii |
| **ACKNOWLEDGEMENTS** | | vi |
| **TABLE OF CONTENTS** | | viii |
| **LIST OF TABLES** | | xiii |
| **LIST OF FIGURES** | | xvi |
| **CHAPTER 1** | **INTRODUCTION** | 1 |
| 1.1 | BACKGROUND AND MOTIVATION | 1 |
| 1.2 | REVIEW OF PREVIOUS STUDIES | 4 |
| 1.3 | OBJECTIVES AND SCOPE | 9 |
| 1.4 | ORGANIZATION OF THE THESIS | 11 |
| **CHAPTER 2** | **SEISMIC BEHAVIOUR OF MOMENT RESISTING STEEL FRAMES** | 14 |
| 2.1 | GENERAL | 14 |
| 2.2 | JOINT BEHAVIOUR | 16 |
| | 2.2.1 Behaviour of beam-column panel zones | 16 |
| | 2.2.2 Behaviour of beam-column connections | 18 |
| 2.3 | SEISMIC DAMAGE ASSESSMENT | 21 |
| 2.4 | EFFECT OF FLEXIBILITY OF CONNECTIONS AND DEFORMATION OF PANEL ZONES | 24 |
| 2.5 | DEFINITION OF DESIGN PHILOSOPHIES | 26 |

**Table of contents (cont'd)**


| | | | |
|---|---|---|---|
| | 2.5.1 | Strong-column weak-beam (SCWB) design | 27 |
| | 2.5.2 | Weak-column strong-beam (WCSB) design | 29 |
| | 2.5.3 | Strong-column weak-panel zone (SCWP) design | 30 |
| 2.6 | | LEVEL OF PROTECTION FRAMEWORK | 31 |
| **CHAPTER 3** | | **COMPUTER MODELLING AND RESPONSE PARAMETER DEFINITION** | 47 |
| 3.1 | | COMPUTATIONAL TOOL: PC-ANSR | 47 |
| | 3.1.1 | Static analysis | 49 |
| | 3.1.2 | Dynamic analysis | 50 |
| | 3.1.3 | P-Delta effect (Geometric stiffness) | 52 |
| | 3.1.4 | Element modelling | 53 |
| 3.2 | | MODELLING OF ELEMENTS | 54 |
| | 3.2.1 | Beam-column element | 55 |
| | 3.2.2 | Panel-zone finite element | 60 |
| | 3.2.3 | Spring connection element | 70 |
| | 3.2.4 | Validation of the element modelling | 72 |
| 3.3 | | RESPONSE PARAMETER DEFINITION | 75 |
| | 3.3.1 | Overall response parameters | 76 |
| | 3.3.2 | Local member response parameters | 77 |
| **CHAPTER 4** | | **DESIGN OF STEEL OFFICE BUILDINGS** | 104 |
| 4.1 | | GENERAL LAYOUT AND NOTATIONS | 104 |
| 4.2 | | MATERIAL PROPERTIES AND DESIGN LOADING | 105 |
| | 4.2.1 | Material properties | 105 |
| | 4.2.2 | Gravity loading | 105 |
| | 4.2.3 | Seismic loading | 107 |
| | 4.2.4 | Load combinations | 109 |
| 4.3 | | DESIGN PROCESS | 110 |
| | 4.3.1 | Steel design computer program | 110 |
| | 4.3.2 | Design philosophies | 111 |
| | 4.3.3 | Code regulations and limitations | 111 |

**Table of contents (cont'd)**


| | | |
|---|---|---|
| 4.4 | FINAL STRUCTURAL CONFIGURATION OF THE FRAMES | 113 |
| 4.5 | NATURAL PERIODS AND MODE SHAPES | 114 |
| 4.6 | WEIGHTS OF STEEL REQUIRED TO CONSTRUCT THE FRAME SKELETONS | 115 |
| **CHAPTER 5** | **INPUT GROUND MOTIONS** | 131 |
| 5.1 | GENERAL | 131 |
| 5.2 | EARTHQUAKE DATA SET | 132 |
| | 5.2.1 The first ensemble of time-histories (Ensemble "A") | 133 |
| | 5.2.2 The second ensemble of time-histories (Ensemble "B") | 136 |
| 5.3 | TRUNCATION OF TIME-HISTORIES | 137 |
| **CHAPTER 6** | **NONLINEAR PUSH OVER STATIC ANALYSES** | 146 |
| 6.1 | GENERAL | 146 |
| 6.2 | BASE SHEAR-ROOF DEFLECTION RELATIONSHIPS | 149 |
| | 6.2.1 Six storey frames | 149 |
| | 6.2.2 Limited drift designed six storey frames | 153 |
| | 6.2.3 Ten storey frames | 154 |
| 6.3 | BASE SHEAR-MAXIMUM STOREY DRIFT RELATIONSHIPS AND LOCATIONS OF PLASTIC DEFORMATIONS | 155 |
| 6.4 | IMPLICATIONS OF THE DESIGN PHILOSOPHIES | 156 |
| 6.5 | IMPLICATIONS OF THE SEISMIC HAZARD DESIGN LEVEL | 157 |
| 6.6 | FLOOR DISPLACEMENTS AND STOREY DRIFT RATIOS DISTRIBUTION | 159 |
| 6.7 | BEAM PERFORMANCE | 160 |

**Table of contents (cont'd)**


| | | |
|---|---|---|
| 6.8 | COLUMN PERFORMANCE | 163 |
| 6.9 | JOINT PERFORMANCE | 165 |
| 6.10 | MAXIMUM PLASTIC DEFORMATIONS | 167 |
| 6.11 | MAXIMUM STATIC STOREY DRIFT-MAXIMUM ELEMENT PERFORMANCE PARAMETERS RELATIONSHIPS | 169 |
| 6.12 | SUMMARY OF OVERALL PERFORMANCE | 170 |
| **CHAPTER 7** | **INELASTIC DYNAMIC ANALYSES** | 197 |
| 7.1 | GENERAL | 197 |
| 7.2 | SCALING OF THE TIME-HISTORIES | 198 |
| | 7.2.1 Ensemble "A" | 198 |
| | 7.2.2 Ensemble "B" | 199 |
| 7.3 | MAXIMUM STOREY DRIFT RATIOS | 200 |
| | 7.3.1 Statistical analyses of maximum storey drifts | 200 |
| | 7.3.2 Base shear-maximum storey drift relationships | 203 |
| 7.4 | BASE SHEAR-MAXIMUM ROOF DEFLECTION RELATIONSHIPS | 206 |
| 7.5 | HEIGHT-WISE DISTRIBUTION OF OVERALL RESPONSE PARAMETERS | 210 |
| | 7.5.1 Floor displacements | 210 |
| | 7.5.2 Storey drifts | 211 |
| | 7.5.3 Storey shears | 213 |
| 7.6 | BEAM PERFORMANCE | 214 |
| | 7.6.1 Performance parameters | 214 |
| | 7.6.2 Concluding comments | 216 |
| 7.7 | COLUMN PERFORMANCE | 217 |
| | 7.7.1 Exterior column performance parameters | 217 |
| | 7.7.2 Interior column performance parameters | 218 |

**Table of contents (cont'd)**


| | | |
|---|---|---|
| | 7.7.3 Concluding comments | 220 |
| 7.8 | JOINT PANEL PERFORMANCE | 220 |
| | 7.8.1 Exterior panel performance parameters | 221 |
| | 7.8.2 Interior panel performance parameters | 222 |
| | 7.8.3 Concluding comments | 223 |
| 7.9 | EFFECT OF PEAK GROUND VELOCITY LEVEL | 224 |
| 7.10 | MAXIMUM STOREY DRIFT-MAXIMUM ELEMENT PERFORMANCE PARAMETERS RELATIONSHIPS | 227 |
| 7.11 | SUMMARY OF OVERALL PERFORMANCE | 230 |
| | 7.11.1 Summary of maximum plastic deformations | 230 |
| | 7.11.2 Overall performance in relation to potential collapse | 231 |
| **CHAPTER 8** | **CONCLUSIONS** | 272 |
| 8.1 | SUMMARY | 272 |
| 8.2 | CONCLUSIONS | 275 |
| | 8.2.1 Push over static analyses | 275 |
| | 8.2.2 Inelastic dynamic analyses | 277 |
| | 8.2.3 Overall performance | 279 |
| 8.3 | RECOMMENDATIONS FOR FUTURE RESEARCH | 280 |
| **REFERENCES** | | 282 |
| **APPENDIX (I)** | **STRAIN-DISPLACEMENT MATRIX OF THE WEB PANEL FINITE ELEMENT MODEL** | 291 |
| **APPENDIX (II)** | **PERFORMANCE OF EXTERIOR COLUMNS DURING PUSH OVER ANALYSES** | 292 |
| **APPENDIX (III)** | **PERFORMANCE OF EXTERIOR PANEL ZONES DURING PUSH OVER ANALYSES** | 294 |

## LIST OF TABLES


| Table | Title | Page |
|---|---|---|
| 2.1 | Damage states and performance level thresholds | 34 |
| 2.2 | Global damage indicator | 35 |
| 2.3 | Cross-section properties of members | 35 |
| 2.4 | Dimensions of panel zones (cm) | 36 |
| 2.5 | Natural periods of the frames (in sec.) | 36 |
| 2.6 | Mode shapes of the frames | 37 |
| 3.1 | Comparison between the experimental and predicted load-deflection relationship characteristics | 81 |
| 3.2 | Comparison between the experimental and predicted applied moment-joint shear strain relationship characteristics | 81 |
| 4.1 | Design cases included in the study and notation of each designed frame | 117 |
| 4.2 | Material properties | 118 |
| 4.3 | The design base shear ($V_{frame}$) for each of the moment resisting frames | 118 |
| 4.4 | Member sizes and panel zone designs for the H6 set of frames | 119 |
| 4.5 | Member sizes and panel zone designs for the I6 set of frames | 120 |
| 4.6 | Member sizes and panel zone designs for the L6 set of frames | 121 |
| 4.7 | Member sizes and panel zone designs for the SP.I6 set of frames | 122 |
| 4.8 | Member sizes and panel zone designs for the I10 set of frames | 123 |

**List of Tables (cont'd)**


| Table | Title | Page |
|---|---|---|
| 4.9 | Vibrational periods of the first two modes for each of the moment resisting frames | 124 |
| 4.10 | Deformed mode shapes for the I6 set of frames | 125 |
| 4.11 | Deformed mode shapes for the I10 set of frames | 126 |
| 4.12 | Comparison between the weights of steel (skeleton only) to be used in constructing each of the moment resisting frames | 127 |
| 5.1 | Newmark-Hall spectrum velocity amplification factors for horizontal elastic response | 139 |
| 5.2 | Target values of $S_a(T)/v_{max}$ from Newmark-Hall design spectrum against actual values of $S_a(T)/v_{max}$ determined from ensemble "A" | 139 |
| 5.3 | Description of time-histories included in ensemble "A" | 140 |
| 5.4 | Probabilistic seismic hazard estimates or Vancouver Uniform Hazard Spectra (Geological Survey of Canada) | 141 |
| 5.5 | Target mean spectral shape for selection of time-histories of ensemble "B" against actual mean spectral shape determined from ensemble "B" | 141 |
| 5.6 | Description of time-histories included in ensemble "B" | 142 |
| 6.1 | Normalized base shears and maximum storey drift ratios at 1% and 2% roof deflections | 174 |
| 6.2 | Normalized base shears and roof deflections at 2% and 2.5% maximum storey drift ratios | 175 |
| 6.3 | Maximum plastic deformations at 2.5% maximum storey drift | 176 |
| 6.4 | Overall performance at 2.5% maximum storey drift | 177 |
| 7.1 | Maximum storey drift ratios for excitation at twice the design level | 236 |

**List of Tables (cont'd)**


| Table | Title | Page |
|---|---|---|
| 7.2 | Drift and roof deflection ductility factor | 237 |
| 7.3 | Summary of maximum plastic deformations (Excitation at twice the design level) | 238 |
| 7.4 | Summary of overall performance (Excitation at twice the design level) | 239 |

## LIST OF FIGURES


| Figure | Description | Page |
|---|---|---|
| 1.1 | Plan of the research program | 13 |
| 2.1 | Different failure mechanisms in steel frames | 38 |
| 2.2 | Typical beam-column joint in steel frame (after Osman, 1991) | 38 |
| 2.3 | Forces acting on a typical beam-column panel-zone | 39 |
| 2.4 | Typical shear force-distortion behaviour of a joint panel zone | 40 |
| 2.5 | Relation between average displacement and shear deformation of the joint panel zone and end deformations of the adjacent beam and column | 40 |
| 2.6 | Rotational stiffness of steel connections (after Nader and Astaneh, 1992) | 41 |
| 2.7 | Beam-to-column connections used in steel frames (after Nader and Astaneh, 1992) | 41 |
| 2.8 | Classification of connections based on their moment-rotation relationship (after Nader and Astaneh, 1992) | 42 |
| 2.9 | Connection moment-rotation curves for different types of connections (after Chen and Lui, 1991) | 42 |
| 2.10 | Linear moment-rotation models for connections (after Chen and Lui, 1991) | 43 |
| 2.11 | Typical top-and-bottom plate connections (after Nader and Astaneh, 1992) | 43 |
| 2.12 | Typical extended-end plate connections (after Nader and Astaneh, 1992) | 44 |
| 2.13 | Typical top-and-bottom seated angles with web connections (after Nader and Astaneh, 1992) | 44 |
| 2.14 | Three storey moment resisting steel frame | 45 |

**List of Figures (cont'd)**


| Figure | Description | Page |
|---|---|---|
| 2.15 | Effect of connection flexibility on the behaviour of steel frames subjected to lateral loads | 45 |
| 2.16 | Effect of panel zone deformation on the behaviour of steel frames subjected to lateral loads | 46 |
| 2.17 | Typical locations of plastic deformations in moment resisting steel frames designed using different design philosophies | 46 |
| 3.1 | Newton-Raphson iteration procedure | 82 |
| 3.2 | P-Delta effect due to axial force and relative lateral displacement | 82 |
| 3.3 | Modelling of different structural elements in a steel MRF | 83 |
| 3.4 | Beam-column element | 83 |
| 3.5 | Panel zone element | 84 |
| 3.6 | Deformation modes of a joint panel zone | 84 |
| 3.7 | Analytical models for discrete member idealization | 85 |
| 3.8 | Degrees of freedom for the beam-column element | 86 |
| 3.9 | Idealized moment-curvature relationship | 86 |
| 3.10 | Bilinear hysteretic model for moment-curvature relationship | 87 |
| 3.11 | Effect of axial force on the moment-curvature relationship (after Chen and Lui, 1991) | 87 |
| 3.12 | Interaction curve for beam-column model (class 1 sections) | 88 |
| 3.13 | Finite element models for the web and flanges of a joint panel zone (after Lui and Chen, 1986) | 88 |

**List of Figures (cont'd)**


| Figure | Description | Page |
|---|---|---|
| 3.14 | Idealized stress-strain curve for steel | 89 |
| 3.15 | Gauss points of the panel web element | 89 |
| 3.16 | Degrees of freedom of a joint panel | 90 |
| 3.17 | Face numbering of a joint panel | 90 |
| 3.18 | Rigid link connecting a column and a panel zone, and transition element connecting a beam and a panel zone | 91 |
| 3.19 | Parallel component model | 91 |
| 3.20 | Scaling back to yield surface | 92 |
| 3.21 | Moment-rotation behaviour of the connection element | 92 |
| 3.22 | Idealization of semi-rigid connection element | 93 |
| 3.23 | The connection element components | 93 |
| 3.24 | Details of specimen CB-1 and its loading history (after Osman, 1991) | 94 |
| 3.25 | Theoretical and experimental tip load-deflection relationship for specimen CB-1 | 95 |
| 3.26 | Theoretical and experimental applied moment-versus panel average shear strain for specimen CB-1 | 96 |
| 3.27 | Details of specimen CC-1 and its loading history (after Osman, 1991) | 97 |
| 3.28 | Theoretical and experimental tip load-deflection relationship for specimen CC-1 | 98 |

**List of Figures (cont'd)**


| Figure | Description | Page |
|---|---|---|
| 3.29 | Theoretical and experimental applied moment-versus panel average shear strain for specimen CC-1 | 99 |
| 3.30 | Details of specimen CC-2 and its loading history (after Osman, 1991) | 100 |
| 3.31 | Theoretical and experimental tip load-deflection relationship for specimen CC-2 | 101 |
| 3.32 | Theoretical and experimental applied moment-versus panel average shear strain for specimen CC-2 | 102 |
| 3.33 | Determination of maximum rotation capacity for steel beams | 103 |
| 3.34 | Neutral axis location for a steel section subjected to axial load and bending moment about the major axis | 103 |
| 4.1 | Floor plan of the steel office buildings | 128 |
| 4.2 | Elevation of the six storey moment resisting steel frame (column line A) | 129 |
| 4.3 | Elevation of the ten storey moment resisting steel frame (column line A) | 130 |
| 5.1 | Trifunac and Brady definition of strong-motion duration | 143 |
| 5.2 | Mean and mean+one standard deviation response spectra for time-histories of ensemble "A" | 144 |
| 5.3 | Response spectra for time-histories of ensemble "A" | 144 |
| 5.4 | Median uniform hazard spectrum for Vancouver, B.C. | 145 |
| 5.5 | Mean spectral shape for time-histories of ensemble "B" compared with Vancouver median uniform hazard spectral shape | 145 |
| 6.1 | Base shear-roof deflection relationships for the six storey frames | 178 |

**List of Figures (cont'd)**


| Figure | Description | Page |
|---|---|---|
| 6.2 | Base shear-roof deflection relationships for the six storey frames designed for special storey drift limit of 1% | 179 |
| 6.3 | Base shear-roof deflection relationships for the ten storey frames | 179 |
| 6.4 | Base shear-maximum storey drift relationships for the six storey frames | 180 |
| 6.5 | Base shear-maximum storey drift relationships for the six storey frames designed for special storey drift limit of 1% | 181 |
| 6.6 | Base shear-maximum storey drift relationships for the ten storey frames | 181 |
| 6.7 | Locations of plastic deformations in the six storey frames at 1.5% maximum drift | 182 |
| 6.8 | Locations of plastic deformations in the ten storey frames at 1.5% maximum drift | 183 |
| 6.9 | Locations of plastic deformations in the six storey frames at 2.5% maximum drift | 184 |
| 6.10 | Locations of plastic deformations in the ten storey frames at 2.5% maximum drift | 185 |
| 6.11 | Effect of the seismic hazard design level on the overstrength factors and roof deflections of the frames | 186 |
| 6.12 | Height-wise distribution of floor displacements and storey drifts for the six storey frames at 2.5% maximum storey drift | 187 |
| 6.13 | Height-wise distribution of floor displacements and storey drifts for the special drift limit designed six storey frames at 2.5% maximum storey drift | 188 |
| 6.14 | Height-wise distribution of floor displacements and storey drifts for the ten storey frames at 2.5% maximum storey drift | 188 |

**List of Figures (cont'd)**


| Figure | Description | Page |
|---|---|---|
| 6.15 | Height-wise distribution of floor displacements for all frames at a common roof deflection of 2% of the building height | 189 |
| 6.16 | Beam performance parameters for the six storey frames at 2.5% maximum storey drift | 190 |
| 6.17 | Beam performance parameters for the special drift limit designed six storey frames at 2.5% maximum storey drift | 191 |
| 6.18 | Beam performance parameters for the ten storey frames at 2.5% maximum storey drift | 191 |
| 6.19 | Interior column performance parameters for the six storey frames at 2.5% maximum storey drift | 192 |
| 6.20 | Interior column performance parameters for the special drift limit designed six storey frames at 2.5% maximum storey drift | 193 |
| 6.21 | Interior column performance parameters for the ten storey frames at 2.5% maximum storey drift | 193 |
| 6.22 | Interior panel zone performance parameters for the six storey frames at 2.5% maximum storey drift | 194 |
| 6.23 | Interior panel zone performance parameters for the special drift limit designed six storey frames at 2.5% maximum storey drift | 195 |
| 6.24 | Interior panel zone performance parameters for the ten storey frames at 2.5% maximum storey drift | 195 |
| 6.25 | Maximum critical element performance parameters-maximum storey drift relationships | 196 |
| 7.1 | Scaling level for the time-histories in ensemble "B" | 240 |
| 7.2 | Base shear-maximum storey drift relationships for the SCWB frames, evaluation of the different time-history responses | 241 |

**List of Figures (cont'd)**


| Figure | Description | Page |
|---|---|---|
| 7.3 | Base shear-maximum storey drift relationships for the WCSB frames, evaluation of the different time-history responses | 243 |
| 7.4 | Base shear-maximum storey drift relationships for the SCWP frames, evaluation of the different time-history responses | 245 |
| 7.5 | Base shear-maximum roof deflection relationships for the SCWB frames, evaluation of the different time-history responses | 247 |
| 7.6 | Base shear-maximum roof deflection relationships for the WCSB frames, evaluation of the different time-history responses | 249 |
| 7.7 | Base shear-maximum roof deflection relationships for the SCWP frames, evaluation of the different time-history responses | 251 |
| 7.8 | Height-wise distribution of maximum floor displacements, M+SD values | 253 |
| 7.9 | Height-wise distribution of maximum storey drifts, M+SD values | 254 |
| 7.10 | Height-wise distribution of maximum storey shears, M+SD values | 255 |
| 7.11 | Beam performance parameters, M+SD values | 256 |
| 7.12 | Exterior column performance parameters, M+SD values | 258 |
| 7.13 | Interior column performance parameters, M+SD values | 260 |
| 7.14 | Exterior panel zone performance parameters, M+SD values | 262 |
| 7.15 | Interior panel zone performance parameters, M+SD values | 264 |
| 7.16 | Comparison between M+SD maximum storey drifts at the design level and twice the design level excitations | 266 |
| 7.17 | Comparison between M+SD interior column performance parameters at the design level and twice the design level excitations | 267 |

**List of Figures (cont'd)**


| Figure | Description | Page |
|---|---|---|
| 7.18 | Effect of the peak ground velocity level on the maximum storey drifts and maximum roof deflections of the I6 frames | 268 |
| 7.19 | Effect of the peak ground velocity level on the critical element maximum performance parameters in the I6 frames | 269 |
| 7.20 | Maximum critical element performance parameters-maximum storey drift relationships | 270 |
| 7.21 | Maximum column performance parameters-maximum storey drift relationships for the SCWB and SCWP frames | 271 |
| II.1 | Exterior column performance parameters for the six storey frames at 2.5% maximum storey drift | 292 |
| II.2 | Exterior column performance parameters for the special drift limit designed six storey frames at 2.5% maximum storey drift | 293 |
| II.3 | Exterior column performance parameters for the ten storey frames at 2.5% maximum storey drift | 293 |
| III.1 | Exterior panel zone performance parameters for the six storey frames at 2.5% maximum storey drift | 294 |
| III.2 | Exterior panel zone performance parameters for the special drift limit designed six storey frames at 2.5% maximum storey drift | 295 |
| III.3 | Exterior panel zone performance parameters for the ten storey frames at 2.5% maximum storey drift | 295 |

# CHAPTER 1

# INTRODUCTION

## 1.1 BACKGROUND AND MOTIVATION

A major objective of seismic design is the generation of structures that can survive earthquakes. Traditional building structures are usually designed in accordance with provisions in building codes and standards such as the National Building Code of Canada (NBCC, 1995) and the Uniform Building Code (UBC, 1994). The code provisions are intended to achieve satisfactory performance of buildings under various loads imposed by users or nature (such as earthquakes) during the life-time of buildings in service. Commentary "J" (effects of earthquakes) associated with the 1995 edition of the NBCC states that satisfactory performance under earthquake loads means that buildings, designed according to the code provisions, will:

1- resist minor earthquakes without any damage.

2- resist moderate earthquakes without significant structural damage.

3- resist severe earthquakes without collapse.

The above statement on seismic performance is described in a qualitative manner and the codes do not provide quantitative measure of the actual performance of the code-designed buildings.

Building codes usually employ simplified formulas in the provisions in order to facilitate the design process. For example, estimating seismic hazard in terms of zones having different peak ground acceleration and peak ground velocity, also the equivalent static design forces are stipulated in building codes to represent the seismic forces which are dynamic and random in nature. The effects of frequency content, duration of ground motions, structural dynamic characteristics, and structural redundancy are not explicitly accounted for in seismic design.

There is no doubt that building codes should utilize simplified rules and formulas to facilitate operational convenience of design process. However, the validity of these rules and formulas and their impact on building safety are questionable. Since the code provisions are intended to achieve satisfactory performance of structural systems due to seismic loads during the life-time of structures, it is essential to evaluate the actual performance of code designed structural systems under earthquakes.

During the past few decades, the population of the world has increased significantly. Currently, a large percentage of the world population lives and works in urban areas; some of those areas are associated with extreme seismic activity. During devastating earthquakes that have occurred in different places all over the world, a number of building structures designed and built in accordance with current building codes have been subjected to strong ground motion shaking which equals or exceeds the levels for which they have been designed. While damage assessment during these events enabled engineers to learn and improve the design codes and construction techniques of buildings located in seismically active zones, there remains considerable concern about the level of protection afforded to buildings

designed in accordance with those codes. For example, steel moment resisting frames (MRFs), which have long been considered the most efficient earthquake lateral force resisting systems for low-rise and medium-rise buildings, suffered a surprising amount of damage during the 1994 Northridge earthquake in California (Bertero et al., 1994; Tremblay et al., 1995) and the 1995 Hyogo-ken Nanbu (Kobe) earthquake in Japan (Tremblay et al., 1996).

In the US, this concern resulted in a re-evaluation of the performance criteria on which current provisions are based. The Structural Engineers Association of California (SEAOC) recognized the need for such a re-evaluation even before the Northridge earthquake occurred. In 1992, the Vision 2000 committee was formed, which later in 1995 presented its initial report (SEAOC, 1995) that includes recommendations concerning performance based seismic resistive design and construction of buildings.

In Canada, seismic loading provisions have been included in the National Building Code of Canada (NBCC) since 1953. The code has been updated in new editions from 1965 through 1995, during which the changes in the code have been substantial (Heidebrecht, 1997). However, there has not been a comprehensive systematic evaluation of the resulting level of protection against strong seismic ground motions. In 1992, the Canadian National Committee on Earthquake Engineering (CANCEE), which has the responsibility for preparing and recommending the seismic loading provisions of the NBCC, recognized the need to evaluate the seismic level of protection before further major changes in these provisions (Heidebrecht et al., 1995).

This study comprises a comprehensive research program on the evaluation of seismic level of protection afforded by the current Canadian provisions (NBCC, 1995 and CAN/CSA-

S16.1-94) to medium-rise (six and ten storeys) steel moment resisting frame buildings. The study involves three different design philosophies: a) Strong-Column Weak-Beam (SCWB), b) Weak-Column Strong-Beam (WCSB) and c) Strong-Column Weak-Panel zone (SCWP), and three levels of seismic hazard activity which range from low to high.

In this study, the seismic level of protection is concerned with the performance of the structures during strong seismic shaking. Thus, seismic level of protection is defined as the damage potential for both life-safety and operational considerations. Damage is associated directly with structural response parameters, e.g. lateral deflections, interstorey drifts, and damage indices expressed in terms of accumulated element plastic deformations.

## 1.2 REVIEW OF PREVIOUS STUDIES

A very large number of research studies, either experimentally and/or analytically using a limited number of earthquake ground motions, have been conducted on the seismic performance of steel MRFs. Each study has focused on examining a specific structural aspect in such frames. Most of the previous research studies have mainly investigated the effect of connection semi-rigid action and/or the role of panel zone deformation on the frame performance.

The objective of this section is to briefly summarize some of the previous studies which are believed to be relevant for the current study, i.e. those involve analytical assessment of the performance of such frames when subjected to seismic excitations. Additional references concerning the behaviour of steel beam-to-column subassemblages are mentioned where applicable throughout the thesis.

Krawinkler and Mohasseb (1987) investigated the role of joint panel zone strength and deformation on frame performance. A study was performed on two frame configurations comprising seven storey and ten storey frames. Beam-column joints were modelled as a pair of scissor-type elements connected by a hinge and a rotational spring that allows relative rotation between the elements. Results of nonlinear static analysis and inelastic dynamic analysis using one earthquake record (Taft, Kern County earthquake 1952) were presented. Results showed that the joint panel zone shear deformations may have a significant effect on the structure strength and stiffness and on the distribution of inelastic deformations in a frame structure subjected to earthquake excitations.

Sivakumaran (1988) examined the effect of connection semi-rigid action on frame behaviour. The study was based on the analyses of ten and twenty storey frames taking the connection flexibility into consideration, modelled as a bilinear moment rotation behaviour. The static analyses showed that the connection flexibility increases the building deflections at specified loads, but the strength is marginally affected. The dynamic analyses, for which the El Centro 1940 earthquake was used as an input, showed an increase in deflections.

Tsai and Popov (1988) focused on the effects of yielding in the beam-column panel zones and the beam-column connections on the behaviour of the frames. They conducted an analytical investigation on the performance of six storey and twenty storey steel MRFs using four earthquake records. Based on the analytical results, it was demonstrated that the panel zone shear deformations in a MRF may be significant and should be considered explicitly in the response analyses under static or dynamic forces.

Popov et al. (1989) presented a study that is devoted to a discussion of joints and connections for MRFs. The demand placed on such joints during four different earthquake ground motions was examined using time-history analyses for low-rise and high-rise buildings with perimeter framing. The results were compared with the experimentally determined capacities of such joints.

Nader and Astaneh-Asl (1992) investigated the dynamic response of three steel buildings (four, seven, and ten storeys) with different beam-to-column semi-rigid connections. The connection type used was either top-and-bottom seated angles with tee connections to transfer the shear, top-and-bottom plate moment connections with double angles to transfer the shear, or extended end-plate connections. Two time-history earthquake ground motions were used. It was concluded that semi-rigid connections, designed according to the capacity design method, were capable of supplying the rotational ductilities and plastic rotations that are required in the event of a severe earthquake.

Osman et al. (1993) conducted an analytical study to investigate the effect of joint flexibility, in particular extended end-plate joints, on the response of MRFs. Different design cases of an eight storey frame were considered in the study. Using spring element models, both the connection flexibility and panel zone deformation were included. Three earthquake records were used as input for the dynamic analyses. It was concluded that both the connection flexibility and panel zone deformation contribute to the frame response. The energy dissipation mechanisms and plastic hinging patterns can be substantially altered as a result of joint flexibility.

There have been a few investigations concerning the implications of different design philosophies for the seismic response of steel MRFs, for example:

Redwood et al. (1990) presented a review of the earthquake resistant design of steel MRFs in the Canadian code provisions, and an example of eight storey frame was used to illustrate the impact of the provisions. The provisions are based on a philosophy of capacity design, in which the weakest structural elements meeting at a joint are identified, and are then detailed to provide ductile behaviour. About 70% of the frame joints were studied, and it was notable that the joint panel zone was critical in all cases if minimum size doubler plates are selected.

Roeder et al. (1993) conducted an analytical investigation into the performance of steel MRFs designed for SCWB and WCSB philosophies. Neither the connection flexibility nor the panel zone yielding and deformation were considered. The study included the dynamic analyses of a three, eight, and twenty storey frames. The inelastic responses of these frames were determined for a range of three different earthquake accelerations conditions. The analyses showed that the SCWB frames result in much smaller storey drifts and better distribution of inelastic deformation among structural elements than comparable WCSB frames. The differences were most significant with earthquake accelerations that cause significant yielding. The study suggested that the SCWB frames should be capable of sustaining the required deformations, but it did not provide a clear answer for WCSB frames.

Osman et al. (1995) investigated the implications of design philosophies on the seismic performance of steel MRFs. Typical six storey frames were designed using SCWB, WCSB, and SCWP philosophies. Nonlinear static and inelastic dynamic analyses were performed on

the frames. Panel zone deformation was included but flexibility of connections was not. Three earthquake records were used as inputs for the dynamic analyses. Analyses showed that the strength of the panel zone is a key issue in frame performance.

Schneider and Amidi (1998) investigated the behaviour of steel frames with deformable panel zones, which were modelled using two bilinear rotational springs. The analyses included eight storey frames designed for SCWB and WCSB philosophies. In addition, panel zones were designed and doubler plates were added where applicable. Static push over analysis and dynamic inelastic analyses were performed on the frames. Four earthquake records were used as inputs for the dynamic analyses. Results showed that simple models that do not include panel zone deformations result in unconservative estimates of drift and lateral strength of the frame. Neglecting panel zone distortions underestimated drift by 10% and overestimated the base shear strength by 30%. It was also concluded that the current code provisions governing the minimum strength design of panel zones might result in joints with high shear distortions.

Previous studies have concentrated mainly on examining, either experimentally or analytically using some sophisticated models, the influence of the connection flexibility and panel zone deformation on the MRFs seismic behaviour. Previous studies that involved time-history analyses of MRFs have usually been done using very limited number of earthquake ground motions; the records were not scaled in order to simulate a specific seismic hazard activity level. In addition, the seismic response of a MRF to each ground motion record was evaluated separately rather than evaluating the seismic performance of the frame based on the statistical results of all the time-history responses.

## 1.3 OBJECTIVES AND SCOPE

The objectives of this research study are:

a) To evaluate the seismic level of protection provided by the current Canadian provisions (i.e. NBCC, 1995, and CAN/CSA-S16.1-94) for medium-rise moment resisting steel frames, in particular, to evaluate their seismic performance when subjected to strong earthquake ground motions, taking into account the connection flexibility and panel zone deformations. The evaluation of the seismic level of protection is based on investigating the damage potential associated with such structural system due to seismic excitations.

b) To investigate the effect of the different design philosophies on the inelastic seismic response of multi-storey steel frame structures.

c) To investigate the effect of the design seismic hazard activity level on the inelastic seismic response of multi-storey steel frame structures.

To accomplish the objectives outlined above, the scope of this research program, which is schematically outlined in Figure 1.1, consists of the following phases:

1) Presenting the assumptions on which each frame design philosophy is based. The design philosophies include, strong-column weak-beam, weak-column strong-beam, and strong-column weak- panel zone.

2) Defining the seismic level of protection framework as well as the drift based performance criteria that is to be used in the evaluation process. In addition, the overall and local member performance parameters are defined.

3) Developing a cyclic model for the panel zone which is capable of predicting its inelastic dynamic behaviour, and incorporating the model into the PC-ANSR computer program. The validity of the model is examined by comparing the predicted response (i.e. from the model) with experimental results.

4) Incorporating other appropriate structural element analytical models into the PC-ANSR computer program. The models are a beam-column element and a spring connection element. The models represent the behaviour of those structural components in a moment resisting steel frame subjected to seismic excitation.

5) Designing typical six and ten storey moment resisting steel frames of office buildings in accordance with the current Canadian provisions (NBCC,1995, and CAN/CSA-S16.1-94). The design includes cases of the different design philosophies in combination with three levels of seismic hazard activities, i.e. high, intermediate, and low.

6) Selecting the appropriate input excitations (earthquake time-history records) to be used in the dynamic analyses. Two ensembles of time-histories are selected, each consisting of twelve records; one ensemble is based on the traditional Newmark-Hall design response spectrum, while the other is based on the new seismic hazard information in the from of the uniform hazard spectrum. The different time-histories give an opportunity to evaluate structural response and damage potential statistically.

7) Performing nonlinear push over static analyses of the frames when subjected to monotonically increased lateral loading, determining the critical elements, the actual strength, and the lateral capacity of each frame.

8) Performing inelastic dynamic analyses of the frames subjected to the selected earthquake excitations. The dynamic responses of the frames are analyzed statistically. Thus, the results of statistical analyses of the maximum values of lateral displacements, storey drifts, element performance parameters are used to evaluate the vulnerability and damage potential associated with each design, including the implications of different frame heights, different design philosophies, and different levels of seismic hazard activities.

The performance expectations of the various frames are evaluated and compared, leading to conclusions regarding the overall level of protection provided by the current Canadian provisions to such frames, and the frame design type that exhibits the best performance in each seismic hazard activity region.

## 1.4 ORGANIZATION OF THE THESIS

The thesis consists of eight chapters. A brief introduction and review of previous studies, followed by the objectives and scope are given in Chapter 1.

In Chapter 2, the behaviour of the beam-column joint is discussed, including the panel zone and the connection. This chapter also includes the definitions of the design philosophies, and the seismic level of protection frame-work.

In Chapter 3, the description of the computer program PC-ANSR is presented. The chapter also presents the proposed structural element models that are incorporated into the program for the static and dynamic analyses of the frames. At the end of the chapter, the response parameters to be used in the evaluation of performance are mentioned, including overall and local parameters.

In Chapter 4, the detailed description and design of the moment resisting steel frames considered in the study are given.

In Chapter 5, the earthquake data sets, i.e. the two ensembles of ground motion records, are described, including the different characteristics of each record as well as the whole ensemble.

In Chapter 6, the nonlinear behaviour of the steel frames subjected to monotonically increased lateral loading (i.e. push over static analyses of the frames) is studied. The results included in this chapter are considered significant since they provide background information for the evaluation of the inelastic dynamic responses of the frames to earthquake excitations described in Chapter 7.

In Chapter 7, the inelastic dynamic responses of the designed frames to the earthquake ground motions are analyzed statistically. The statistical results of the responses and the performance parameters are used to evaluate the vulnerability and damage potential of the frames at high ground motion levels. The performance expectations and damage acceptability of the various frames are evaluated and compared. Finally, the overall seismic level of protection provided to such frames are presented.

Finally, Chapter 8 presents a summary and the significant conclusions of this study, as well as recommendations for future research.

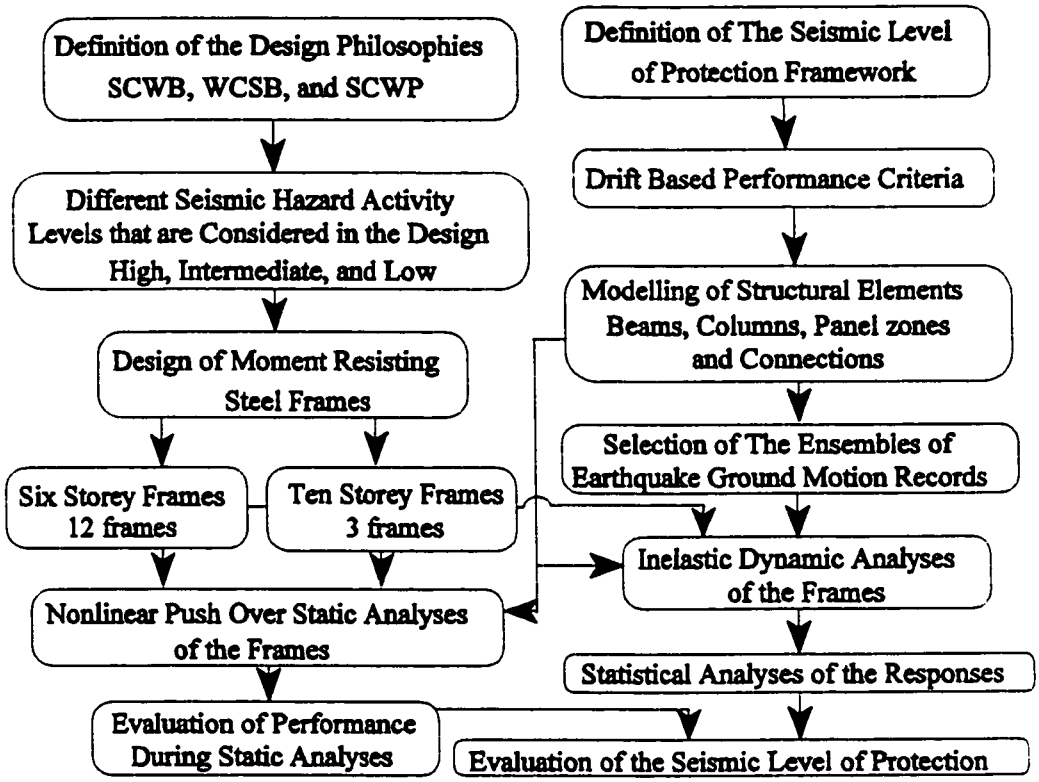


Figure 1.1 Plan of the research program.

# CHAPTER 2

## SEISMIC BEHAVIOUR OF MOMENT RESISTING STEEL FRAMES

### 2.1 GENERAL

Moment resisting steel frames (MRFs) are one of the leading structural systems used in seismic zones. When subjected to a major earthquake ground motion, these frames are expected to undergo relatively large inelastic deformations. Therefore, the need for ductile behaviour in the members and joints subjected to severe load reversals is essential. The basic philosophy behind the design of steel MRFs is to prevent non-ductile failure modes and to concentrate deformations in regions having a capacity for ductile behaviour. This is normally achieved by special detailing requirements in those regions where plastic hinges are expected to form. Plastic hinges in steel MRFs subjected to lateral loads can form at the beam-column joint and/or in the vicinity of the mid-span of the beam depending on the extent of gravity loads (Figure 2.1).

In the conventional analysis and design of steel frameworks, frames are analyzed and designed under the simplification that the beam-to-column joints behave either as ideally pinned or fully rigid. Although the use of these idealized joints simplifies drastically the analysis and design procedures, the predicted response of the frame may not be realistic as most joints behave in a semi-rigid manner. The joints' semi-rigid behaviour is due to a

combination of two main sources, the connection flexibility and the panel zone shear deformation. The connection is the medium that connects the beam to the column and is located at the beam-column interface, while the panel zone comprises the column web and column flanges adjacent to the connection (Figure 2.2).

In the seismic design philosophy, it is assumed that during a small or moderate earthquake a building frame must provide the necessary stiffness and strength to prevent damage and to remain serviceable after the event. On the other hand, during a major earthquake, a building frame must provide the necessary strength and ductility such that the structure will not collapse, i.e. the frame must be able to dissipate the seismic energy with a minimal loss of strength.

Ductile behaviour and inelastic energy absorption may occur in three elements at the joints of a moment frame: (1) the beams, (2) the columns and (3) the panel zones. Flexural hinges may occur in the beams and/or the columns. Shear yielding may take place in the panel zones. It is recommended that inelastic behaviour in the beam-column connections be prevented to reduce the probability of brittle failures in the welding.

To successfully design a steel MRF to achieve desirable behaviour, each of the following elements:

(1) beam and column sections;

(2) beam-column panel zones, and

(3) beam-column connections

should have the required strength, stiffness, ductility and deformation capacity (CAN/CSA-S16.1-94).

## 2.2 JOINT BEHAVIOUR

Several studies have been conducted to investigate the behaviour of the different elements in MRFs, especially the behaviour of the joints under earthquake loading. These studies included the behaviour of connections, as well as the behaviour of panel zones (Krawinkler et al., 1971; Popov et al., 1985; Popov, 1987; Popov and Tsai, 1989; Osman, 1991).

In case of semi-rigid structures in seismic zones, the basis of the design philosophy is to spread the inelastic deformation in the beam-column joint. All the ductile elements in the beam-column joint contribute to the required ductility, but any non-ductile failure is prevented. Thus, semi-rigid connections in semi-rigid structures will be designed for strength, ductility, and stiffness. In semi-rigid connections it is much easier to supply the demand of rotational ductility than in the rigid connection case, since semi-rigid connections are allowed to have some flexibility in the elastic stage. This type of rotational flexibility that is introduced in the elastic stage will also enhance the dynamic behaviour of the structure.

### 2.2.1 Behaviour of beam-column panel zones

When a steel frame is subjected to horizontal earthquake forces, high shears are developed in the beam-column panel zone. Assuming that the maximum moments occur at column ends, and that the points of contraflexure (inflection) are near the column mid-heights, the forces acting around an interior structural joint of a MRF are shown in Figure 2.3. The shear force in the panel, $V_{pn}$, can be estimated as:

$$V_{pn} = (M_{b1} / d_{b1}) + (M_{b2} / d_{b2}) - H_c \qquad (2.1)$$

where, $$H_c = (M_{c1}+M_{c2})/L_c \quad (2.2)$$

and the panel moment, $M_{pn}$,

$$M_{pn} = (M_{b1}+M_{b2}) = (M_{c1}+M_{c2}) \quad (2.3)$$

where, $M_{b1}$ and $M_{b2}$ are the beam bending moments acting on either side of the joint, $M_{c1}$ and $M_{c2}$ are the column bending moments acting on either side of the joint, $d_{b1}$ and $d_{b2}$ are the beam depths at both sides of the panel, and $L_c$ is the column height as shown in Figure 2.3. The panel shear, $V_{pn}$, can also be expressed as:

$$V_{pn} = ( M_{pn} / d_b) \ (1 - \kappa) \quad (2.4)$$

where, $\kappa = d_b / L_c$ and $d_b = (d_{b1} + d_{b2})/2$.

When the joint is subjected to lateral loads, shear stresses develop with their highest value at the panel centre. These shear stresses propagate from the centre of the panel towards its corners until the whole panel has completely yielded. In the elastic range, the panel possesses very high stiffness. Once the panel is yielded, the surrounding elements are the main components that are resisting the panel zone deformation. Thus, the panel stiffness decreases until it reaches a constant stiffness equal to the strain hardening stiffness. Once the mechanism is formed in the elements surrounding the panel (i.e. column flanges and stiffeners), the only resistance provided by the panel is due to its material strain hardening.

Therefore, there are two distinct stiffnesses in the panel zone shear force deformation response (Chen and Lui, 1991): an elastic stiffness, followed by a small range of gradually decreasing stiffness (may be ignored), and then stabilizing to a small constant post-yield stiffness (3-8% of the elastic stiffness) for a long range of deformation as shown in Figure 2.4. The post-yield stiffness is due to: (i) the resistance of the boundary plate elements such as the

column flanges and the stiffeners of the panel zone; (ii) the strain hardening of the panel zone web, and (iii) the restraint from the beam flanges connecting the joint panel. For cyclic loading, tests of steel panel zones show stable hysteresis loops and remain ductile under reversed loading for a range of large plastic deformations (Krawinkler et al., 1971; Tsai and Popov, 1988, and Osman, 1991).

The panel has three rigid body displacements, $u^p$ , $v^p$ , and $\theta^p$ , as well as a shear deformation (distortion) variable $\gamma$ (Figure 2.5). Panel, beam, and column deformations are inter-related as follows:

$$\theta^b = \theta^p \quad \text{and} \quad \theta^c = \theta^b + \gamma \tag{2.5}$$

where, $\theta^b$ is the beam end rotation and $\theta^c$ is the column end rotation.

In the past two decades the cyclic behaviour and seismic design of beam-column panel zones in steel MRFs have been studied quite extensively, particularly at the University of California at Berkeley, for example, Krawinkler et al. (1975); Krawinkler and Popov (1982); Popov et al. (1989) and Tsai and Popov (1988). Studies on beam-column panel zones by Tsai and Popov (1988) and Popov et al. (1989) showed that a well-detailed beam-column panel zone, designed to undergo some shear yielding before the beam reaches its flexural plastic capacity, enhances the dynamic behaviour of steel MRFs. Thus, joints are required to possess adequate ductility and to provide sufficient stiffness and strength (Popov, 1983).

### 2.2.2 Behaviour of beam-column connections

When subjected to strong motions, steel MRFs designed in accordance with current code provisions are expected to yield in the vicinity of beam-column joints. However, the

design codes prevent the beam-column connections from contributing to this inelastic capacity. This restriction is due to the belief that rigid connections have inadequate rotational ductility capacity.

Connections in structural steel work are classified as pinned or simple, semi-rigid, or rigid. The critical characteristic of a connection that determines its classification is the moment-rotation relationship, where the rotation is defined as the relative angular change of the center lines of the beam and the column meeting at the joint.

Nader and Astaneh (1989) defined a rigid connection as one that is capable of developing a moment at the beam end more than or equal to 90% of the fixed end moments, while the end rotation is less than or equal to 10% of the rotation in a pin supported beam. Thus, for rigid connection, its rotational stiffness should be at least $(18\ EI_x/L)_{beam}$, where E is the elastic modulus of steel, $I_x$ is the beam moment of inertia, and L is the beam span.

A pinned connection is defined as one that can develop a moment at the beam end less than 20% of the fixed end moment, while the end rotation is more than or equal to 80% of the end rotation in a pin supported beam. Thus, a pinned connection should have a rotational stiffness less than or equal to $(EI_x/2L)_{beam}$.

A semi-rigid connection is one which is stiffer than a pin connection, but more flexible than a rigid one. In addition, semi-rigid connections can be divided into two types: stiff semi-rigid connection and flexible semi-rigid connection (Figure 2.6).

The elastic rotational stiffness of the connection, $(K_e)$, relative to the elastic bending stiffness of the connected beam, $(EI_x/L)_{beam}$, best defines its rigidity as shown in Figures 2.6, 2.7, and 2.8 (Nader and Astaneh, 1992). Thus, the factor (m) is defined as:

$$m = K_e / (EI_x/L)_{beam} \qquad (2.6)$$

If $m < 0.5$ then the connection is a simple or pinned connection (type A)

If $0.5 \leq m < 8$ then the connection is flexible semi-rigid (type B)

If $8 < m < 18$ then the connection is stiff semi-rigid (type C)

If $m \geq 18$ then the connection is rigid (type D)

The moment-rotation relationship for most steel connections is nonlinear as shown in Figure 2.9. In studying the overall behaviour of steel MRFs it is sufficient to model this relationship by a bilinear model as shown in Figure 2.10. To define the bilinear model, it is convenient to use the elastic stiffness $K_e$, the yield moment $M_y$, and the post-yield stiffness $K_p$.

The ductility is defined as the ratio of the maximum rotation ($\theta_{max}$) to the yield rotation ($\theta_y$). During an earthquake, if a connection is designed to contribute in dissipating the input seismic energy, it must be capable of deforming inelastically for a number of cycles without failure.

Connections that are commonly used in seismic zones are (Nader and Astaneh, 1992):

1) Top and bottom plate moment connections (Figure 2.11).

2) Extended end plate connections ( Figure 2.12).

3) Top and bottom seated angles with web connections (Figure 2.13).

These types are of particular interest in the research area of MRFs located in seismic zones. This is because these types of connections, if well designed and detailed, are expected to exhibit bilinear moment-rotation relationship with relatively large elastic stiffness, and sufficient ductility.

The behaviour and capacity design of these connections have been studied both experimentally and theoretically by several researchers. For example:

i) Harriot and Astaneh (1990); Popov and Bertero (1973); Pinkey and Popov (1967), and Chen and Patel (1981) studied the cyclic and the monotonic behaviour of top and bottom plate moment connections.

ii) Tsai and Popov (1988, 1989, and 1990); Popov et al. (1989); Ghobarah et al. (1990); Osman et al. (1990); Osman (1991), and Packer and Morris (1977) studied the cyclic and the monotonic behaviour of extended-end plate connections.

iii) Frye and Morris (1975); Harper et al. (1990), and Nader and Astaneh (1989) studied the cyclic and the monotonic behaviour of top and bottom seated angle connections with web connections.

In order to represent the commonly used types of connections (i.e. in seismic zones), an average value of m=15 is selected as a basis for modelling connections for steel frames in this study, i.e. the assumed connections are to behave in a stiff semi-rigid manner.

## 2.3 SEISMIC DAMAGE ASSESSMENT

This section gives a brief overview of seismic damage conditions and how this damage can be assessed. For economic reasons, structures located in seismically active zones are usually designed to undergo inelastic deformation. When a structure undergoes large inelastic excursions, it suffers a considerable amount of damage in preselected zones such as beam or column junctions. Damage in a structural member or in the structure as a whole has usually been defined in terms of ductility demand parameters that may depend on displacement,

rotation, stiffness limits, or even dissipated strain energy (Cheng et al., 1979; Oliveira, 1975; Banon et al., 1981; Powell and Allahabadi, 1988). However, these damage indicators alone are insufficient. The reason is that under severe earthquake loading, structural elements undergo large inelastic displacements accompanied by a substantial number of smaller inelastic excursions. These large number of smaller inelastic excursions can cause significant damage in the elements of a MRF in the form of low cycle fatigue magnified by local buckling. Under such conditions, the energy dissipation capacity of elements designed or selected on the basis of maximum displacement only will be much smaller than required. Thus any local structural element damage model should reflect the repeated inelastic effects which appear in the form of low-cycle fatigue characteristics. For these reasons, a number of mathematical models for damage assessment have been proposed in the literature in the past two decades. Some involve a combination of normalized maximum displacements and normalized dissipated energy (Banon and Veneziano, 1982; Park and Ang, 1985), while others are based on cumulative damage theory in the form of low cycle fatigue relationships (Krawinkler and Zohrei, 1983; Daali and Korol, 1994). Daali and Korol (1996) presented a damage model for steel beams under earthquake-type loading. The model uses the maximum response and the repeated inelastic deformations in the form of low-cycle fatigue. Cosenza et al. (1993) summarized the use of damage functions in earthquake engineering, and presented a comparison between different methods found in the literature.

For designers, the maximum storey drift ratio (defined as the relative lateral deflection between two consequent floors divided by the storey height) is considered the preferred damage indicator. As damage is a consequence of deformations, therefore for any structure

that is responding in the inelastic (plastic) region, the degree or level of damage depends upon the amount of plastic deformation that the structure undergoes. The primary disadvantage of the maximum storey drift is that it cannot account for effects of cumulative damage due to repeated inelastic deformation.

As the storey drift is related to the performance of a structure when subjected to seismic motions, the Vision 2000 committee from Structural Engineers Association of California (SEAOC) developed a framework for defining the relation between the maximum transient storey drift and the overall seismic performance level (SEAOC, 1995). Table 2.1 summarizes the relation between the performance level and the maximum transient storey drift.

The recommended performance objective for the seismic design of basic facilities (buildings) is that they should have a minimum of "life-safe" performance at the rare earthquake design level (475 years recurrence interval, i.e. 10% probability of exceedance in 50 years). A similar relationship between the maximum storey drift and a global damage indicator (G.D.I.) is also given by Sozen (1981), in which the G.D.I. is calculated using the following equation:

$$\text{G.D.I.} = [(2*\text{maximum storey drift \%}) - 1] / 4 \qquad (2.7)$$

Table 2.2 presents the values of G.D.I calculated using equation 2.7 and their relation with performance levels (i.e. damage state). Consequently, the storey drift is used as a primary global performance parameter in this study, while damage indices in the form of accumulated plastic deformations (Chapter 3, section 3.3) are used as local structural element performance parameters.

## 2.4 EFFECT OF FLEXIBILITY OF CONNECTIONS AND DEFORMATION OF PANEL ZONES

The inclusion of the connection and panel zone flexibilities in the analysis lengthens the natural periods of frames. However, this increase is not normally more than 10%. There is also a slight change in mode shapes. On the other hand, incorporation of panel zone deformations and connection flexibilities in the analysis may significantly change the distribution of internal forces throughout the structure. Incorporating the connection in the analysis, especially those types recommended for seismic zones, changes slightly the static and dynamic characteristics of frames (Nader and Astaneh, 1992; Osman, 1991). Under dynamic loads, allowing yielding to take place in panels results in a more uniform distribution of dissipated energy and imposes less rotational demands on the beams in the MRFs.

A three storey moment resisting frame is selected to further investigate the effect of connection flexibility and panel zone deformation on the behaviour of moment resisting frames subjected to lateral loading. The frame is the same as designed by Liew and Chen (1995) and the modelling used in the analysis (which includes connection flexibilities as well as panel zone deformations) is as described in Chapter 3. The elevation of the frame is shown in Figure 2.14 and the properties of the beam and column sections are given in Table 2.3, while panel zone dimensions are given in Table 2.4. Five frames with different characteristics are studied:

**Frame A:** basic frame assuming rigid panels and connections;

**Frame B:** same as frame "A" but with stiff semi-rigid beam-column connections (i.e. m=15);

**Frame C:** same as frame "A" but with flexible semi-rigid beam-column connections (i.e. m=5);

**Frame D:** same as frame "A" but with panels of thickness equal to three times the column web thickness (strong panels);

**Frame E:** same as frame "A" but with panels of thickness equal to twice the column web thickness (intermediate panels) and

**Frame F:** same as frame "A" but with panels of thickness equal to the column web thickness (weak panels).

In order to assess the effects of the connection flexibility and the panel zone deformation on the global behaviour of each frame, the frames were subjected to an increasing monotonic lateral load of uniform distribution (push over analysis). The effect of the connection flexibilities and panel thicknesses on the natural periods and mode shapes were investigated. Table 2.5 presents the first three natural periods, while Table 2.6 presents the mode shapes for the first period. From the tables, it can be concluded that both the connection flexibilities and the panel zone deformations tend to increase the natural period of a frame; the largest increases are in the order of 15% and 8% respectively. Similarly, there is a minor change in mode shapes, where the roof deflections tend to increase by 10% and 5% respectively in relation to the first floor deflection.

Figure 2.15 shows the base shear-roof deflection (top displacement) relationships for frames A, B, and C. The connection flexibility has an effect on the global stiffness of the frame and consequently its lateral deflection. The global stiffness of the frame was reduced and the lateral deflection was increased by reducing the stiffness of the connections (i.e.

increasing the connection flexibilities). The flexibility of connections does not affect the overall lateral strength capacity of the frames (i.e. the overstrength). Figure 2.16 shows the base shear-top displacement relationships for frames D, E, and F. The thickness of the panel zone, which is the main factor controlling the panel zone shear deformation, has a significant effect on the frame behaviour. Although the panel thickness has a minor (almost negligible) effect on the initial elastic stiffness of the frame, the global overall lateral strength of the frame is significantly reduced as the panel thickness decreases.

## 2.5 DEFINITION OF DESIGN PHILOSOPHIES

This section deals with the different types of design philosophies for moment resisting frames (MRFs) located in seismic regions, as the type of design philosophy is one of the main factors that affect the performance of these frames when subjected to seismic ground motions. The widely accepted design philosophy for MRFs is that of strong-column weak-beam (SCWB). According to this philosophy, the columns are detailed to be stronger than the adjoining beams. Consequently, inelastic action is forced to take place in the beams which are the main energy dissipators.

In the past two decades, several studies were conducted to investigate the cyclic response of other components of the MRFs such as columns and joint panel zones. It was determined that these elements can participate efficiently in dissipating the earthquake input energy with limited signs of deterioration, provided certain design requirements are satisfied. Popov et. al. (1975) investigated the cyclic response of beam-to-column subassemblages with weak columns. They demonstrated that columns can perform satisfactorily under cyclic loading conditions, provided the maximum axial force is less than 50% of the column yield

force. Bertero et al. (1972), Tsai and Popov (1988) and Ghobarah et al. (1992) examined the cyclic behaviour of joint panel zones. They concluded that panel zones possess stable restoring force characteristics and excellent ability to dissipate earthquake input energy.

New seismic design philosophies for MRFs have evolved and have been implemented by some of the current seismic steel design specifications, such as the Canadian steel standard (CAN/CSA-S16.1-94) and the Uniform Building Code (UBC, 1994). According to these standards, earthquake input energy is allowed to be dissipated in MRFs through inelastic deformation in one or more of the three elements meeting at the beam-to-column joint, i.e. in beams, columns or joint panel zones. Consequently, in addition to the conventional design concept of SCWB, other design philosophies such as weak-column strong-beam (WCSB) and strong-column weak-panel zone (SCWP) may also be considered acceptable if certain conditions are satisfied. Osman et al. (1995) presented a study regarding the implications of design philosophies for seismic response of steel moment frames.

In the current research study, moment resisting steel frames are designed using the three different design philosophies, i.e. SCWB, WCSB, and SCWP.

### 2.5.1 Strong-column weak-beam (SCWB) design

In this design philosophy, the beams are detailed to be weaker than the adjoining columns and are designed to be the critical elements that undergo inelastic deformations. This criterion is satisfied by ensuring that the strength of the columns at each joint is higher than the overstrength of the adjoining beams using the following relationship (Osman et al., 1995):

$$\sum M_{pc} (1-C_s/C_y) / 0.85 > 1.2 \sum M_{pb} \qquad (2.7)$$

where 1.2 is the overstrength factor, $M_{pc}$ and $M_{pb}$ are the plastic moment capacities of the

columns and the beams, respectively, and $C_s$ and $C_y$ are the specified gravity load and column yield axial load values respectively. The factor 0.85 is the parameter used in the ultimate strength interaction relationship. Since the beams are the main energy dissipators in the SCWB design, they must conform to Class 1 section requirements, while columns may conform to either Class 1 or 2 section requirements, according to clause 11 of the CAN/CSA-S16.1-94. Figure 2.17a illustrates the anticipated pattern of inelastic action when a SCWB frame is subjected to large lateral loads.

Panel zones are detailed to yield under the same moment as the adjacent beams. The panel yield shear resistance is equal to the shear force delivered by the beams framing into the panel when they develop their plastic moment capacity $M_{b1}$ and $M_{b2}$, satisfying the following relation:

$$0.55\ \sigma_y\ d_c\ t_{cw}\ \geq\ [\ M_{b1}/0.95\ d_{b1}] + [\ M_{b2}/0.95\ d_{b2}] - H_c \qquad (2.9)$$

where $\sigma_y$ is the column yield stress, $d_c$ is the column depth, $t_{cw}$ is the thickness of the column web panel including the thickness of doubler plates, if any, $d_{b1}$ and $d_{b2}$ are the beam depths at both sides of the panel, and $H_c$ is the column shear (see Equation 2.2). The factor 0.95 is the effective depth factor of a section, while the factor 0.55 is the product of the effective depth factor and $1/\sqrt{3}$ (which is the factor used to define the Von Mises average shear yield stress value, $\sigma_y/\sqrt{3}$). This design criterion results in relatively strong panels with thick doubler plates and only limited inelastic panel action. For this design (SCWB), while the panels are expected to yield after the neighbouring beams, there is a possibility that they may experience a limited amount of plastic deformations.

For the connections, the design criterion proposed by Korol et al. (1990) is used. In this criterion, the connection is assumed to have adequate resistance to transmit a moment of

1.25 times the plastic moment of the adjacent beam; consequently, the connection rotation can be limited and inelastic action in the connection can be avoided. Stiff semi-rigid connection type is used as mentioned in section 2.2.2, i.e. the elastic stiffness of the connection is selected as $(15\ EI_x/L)_{beam}$, where $EI_x/L$ is the elastic stiffness of the adjacent beam.

### 2.5.2 Weak-column strong-beam (WCSB) design

In this design philosophy, the columns are the critical elements that dissipate the earthquake input energy. This situation normally arises in low-rise buildings, where the beam design is dominated by gravity loads and drift requirements, while that of the column is governed by earthquake forces. The WCSB approach is allowed provided that in seismic zones 4 or higher (zonal velocity 0.2 m/sec or higher), the axial factored load on any column, under any load combination, does not exceed $(0.3\ A\sigma_y)$, where A is the column cross sectional area and $\sigma_y$ is the column yield stress. Moreover, the columns conform to Class 1 section, while the beam flanges conform to Class 1 section and the beam webs may conform to either Class 1 or Class 2 section requirements, according to clause 11 of the CAN/CSA-S16.1-94. In this design (WCSB), the minimum strength of the beams relative to the columns is 1.2. The panel zone and connection designs are based on the same assumptions as stated for the SCWB philosophy. Figure 2.17b illustrates the anticipated pattern of inelastic action when a WCSB frame is subjected to large lateral loads; note the soft-storey type collapse mechanism in the lowest storey.

### 2.5.3 Strong-column weak-panel zone (SCWP) design

The beams, columns, and connections are the same as those for SCWB design philosophy. However, joint panel zones are designed to be the weakest elements in the frame (i.e. the critical elements). Most of the inelastic action is expected to take place in the joint panel zones, which have stable and ductile restoring force characteristics. According to CAN/CSA-S16.1-94, the factored shear force resulting from gravity loads combined with seismic forces should not exceed the factored panel shear resistance $V_r$:

$$V_r = 0.55\ \phi\ d_c\ t_{cw}\ \sigma_y\ \left[\ 1 + \left(3\ b_c\ t^2_{cf} /\ d_c\ d_b\ t_{cw}\right)\ \right] \qquad (2.10)$$

where $d_c$ and $d_b$ are the depths of the column and beam respectively, $b_c$ and $t_{cf}$ are the column flange's width and thickness, and $t_{cw}$ is the column web thickness. The performance factor $\phi$ is equal to 0.9. Equation 2.10 represents a lower bound for the joint panel strength. An upper bound to the joint panel strength is that it should not exceed that required to develop $0.8\sum M_{bi}$ (plastic moments) of the beams framing into the column flanges. This will ensure that the joint panels will yield prior to the yielding of the beams framing into them, thus:

$$M_{pa} = 0.55\ \sigma_y\ d_c\ d_b\ t_{cw} < 0.8\sum M_{bi} \qquad (2.11)$$

The proposed upper limit for the strength of the panels in the SCWP design is similar to that given by UBC(1994), even though the contribution of the column flanges is omitted in equation (2.11). The anticipated pattern of inelastic action in a SCWP frame subjected to large lateral loads is shown in Figure 2.17c .

For all the design philosophies, the current Canadian design code (CAN/CSA-S16.1-94) provides some additional requirements as follows:

a) The element or elements at a joint that may undergo large plastic deformations are termed critical elements, and they shall be identified. An element undergoing large

plastic deformations shall be assumed to apply relevant loads to the other elements at the joint equal to 1.2 times its unfactored yield resistance.

b) In order to preclude premature local buckling, and thus ensure adequate hinge rotation, compression elements in regions of plastic moment must have width-thickness ratios no greater than those specified for class 1 (plastic design) sections in clause 11.2 .

c) Slenderness ratios limits that define class 1 and class 2 sections (based on flanges and web slenderness) are given in clause 11.

d) For seismic zone 2 and higher (i.e. zonal velocity $v \geq 0.1$ m/sec), the ratio of the sum of panel zone depth and width to panel zone thickness shall not exceed 90. Doubler plate thickness may be included with web thickness in calculating this ratio. Doubler plates, if present shall be placed against the column web.

## 2.6 LEVEL OF PROTECTION FRAMEWORK

In Canada, seismic loading provisions have been included in the National Building Code of Canada (NBCC) since 1953. The code has been updated in new editions from 1965 through 1995, during which changes have been substantial (Heidebrecht, 1997). In 1992, the Canadian National Committee on Earthquake Engineering (CANCEE) recognized the need to evaluate the seismic level of protection before further major changes in these provisions (Heidebrecht et al., 1995).

The current edition of the National Building Code of Canada (NBCC, 1995) defines the seismic hazard of different locations in the country through seismic zoning maps developed by Basham et al. (1985) which have contours of seismic zones having different

peak ground acceleration and peak ground velocity for probability of exceedance of 10% in 50 years. In the current NBCC (1995) peak ground velocity is used explicitly, while peak ground acceleration is used implicitly.

During the last decade, improvements have been made in the methodology for seismic hazard computations (i.e. the incorporation of various uncertainties involved in the seismic hazard). New seismicity data helps to improve the knowledge about the seismic potential of different regions of the country. The preparation of new seismic maps using the state-of-the-art seismic hazard methodology which includes both random and modelling uncertainities are preliminary given by Adams et al. (1995) and the detailed results are given by Adams et al. (1996). The new seismic hazard results are expressed in the form of uniform hazard spectral values at both the median (50%) and median plus one standard deviation (84%) levels of confidence.

While new seismic hazard knowledge is available, it is essential that the the seismic level of protection provided by the NBCC (1995) be evaluated before any further major seismic loading provisions are introduced in the NBCC. The level of protection frame work as defined by Heidebrecht (1997) involves seismic hazard, seismic design, seismic response/damage, vulnerability, and seismic risk.

Seismic level of protection of steel moment resisting frames in this study is concerned with damage related-performance expectations during strong seismic shaking. Structural performance is based on different response parameters: overall lateral deflection, storey drift, and a damage index (Chapter 3, section 3.3).

As the damage assessment (response/damage evaluation) is the main subject of this research study, the steps for assessing seismic damage are as follows:

1- determine the appropriate seismic hazard parameter(s) for the given location.

2- determine the seismic code loading for the structure.

3- design and detail the structure for seismic loading, in combination with gravity loads.

4- develop an appropriate inelastic model for each structural component.

5- determine appropriate damage models (parameters) which are to be calculated during the analysis (e.g. overall lateral displacement, interstorey drift, damage index).

6- select appropriate seismic input excitations for use in dynamic analysis (10-15 time-histories); the input excitation should simulate the actual seismic hazard.

7- conduct inelastic dynamic analyses of the structure using the 10 to 15 time-histories determined in step 6.

8- calculate the damage parameters for each analysis and evaluate these on a statistical basis.

While buildings are designed according to specific seismic codes, however due to the uncertainties of seismic hazard, the actual ground motion that may excite a building structure may be two or three times higher than the values used in design (Heidebrecht, 1995). Consequently, analyses at excitation several times code design levels are needed to determine if the building can resist these higher ground motion with a moderate to high level of damage, but without structural collapse. This damage evaluation is required for life-safety objectives, i.e. determining whether or not the damage, during very strong seismic ground motions, is likely to cause collapse of the structure.

Table 2.1 Damage states and performance level thresholds.

| Damage state and performance level | Description of damage | Maximum transient storey drift (%) |
|---|---|---|
| **Fully operational** (negligible damage) | No damage, continuous service. | drift < 0.2% |
| **Operational** (light damage) | Most operations and functions can resume immediately. Repair is required to restore some non-essential services. Damage is light. | 0.2% ≤ drift < 0.5% |
| **Life-safe** (moderate damage) | Damage is moderate. Selected building systems, features or contents may be protected from damage. Life-safety is generally protected. | 0.5% ≤ drift < 1.5% |
| **Near collapse** (severe damage) | Structural collapse prevented. Non-structural elements may fall. Structural damage is severe but collapse is prevented. | 1.5% ≤ drift < 2.5% |
| **Collapse** (complete damage) | Portions of primary structural systems collapse or complete structural collapse. | 2.5% ≤ drift |

Table 2.2 Global damage indicator.

| Maximum transient storey drift (%) | Global damage indicator | Damage state |
|---|---|---|
| 0.5% | 0.0 | Negligible |
| 1.0% | 0.25 | Light |
| 1.5% | 0.50 | Moderate |
| 2% | 0.75 | Severe |
| 2.5% | 1.00 | Collapse |

Table 2.3 Cross-section properties of members

| Members | A ($cm^2$) | $I_X$ ($cm^4$) | $I_Y$ ($cm^4$) |
|---|---|---|---|
| IPE330 | 62.6 | 11,770 | 788 |
| IPE360 | 72.7 | 16,270 | 1,043 |
| IPE400 | 84.5 | 23,130 | 1,318 |
| HEB220 | 91.0 | 8,091 | 2,843 |
| HEB240 | 106.0 | 11,260 | 3,923 |
| HEB260 | 118.0 | 14,920 | 5,135 |

Table 2.4 Dimensions of panel zones (cm)

| Storey | Panel location | Beam depth $d_b$ | Column depth $d_c$ | Web thickness $t_w$ | Flange thickness $t_{cf}$ |
|---|---|---|---|---|---|
| 1 | Exterior | 40 | 22 | 0.95 | 1.6 |
| | Interior | 40 | 26 | 0.10 | 1.6 |
| 2 | Exterior | 36 | 22 | 0.95 | 1.6 |
| | Interior | 36 | 26 | 0.10 | 1.6 |
| 3 | Exterior | 33 | 22 | 0.95 | 1.6 |
| | Interior | 33 | 24 | 0.95 | 1.7 |

Table 2.5 Natural periods of the frames (in sec.)

| Frame type | A | B | C | D | E | F |
|---|---|---|---|---|---|---|
| 1st period | 1.254 | 1.347 | 1.483 | 1.254 | 1.287 | 1.353 |
| 2nd period | 0.434 | 0.452 | 0.477 | 0.434 | 0.441 | 0.453 |
| 3rd period | 0.256 | 0.259 | 0.262 | 0.256 | 0.257 | 0.259 |

Table 2.6 Mode shapes of the frames

| Frame type | A | B | C | D | E | F |
|---|---|---|---|---|---|---|
| 1st storey | 0.314 | 0.314 | 0.314 | 0.314 | 0.314 | 0.314 |
| 2nd storey | 0.696 | 0.723 | 0.756 | 0.696 | 0.706 | 0.723 |
| 3rd storey | 1.0 | 1.05 | 1.11 | 1.0 | 1.02 | 1.05 |

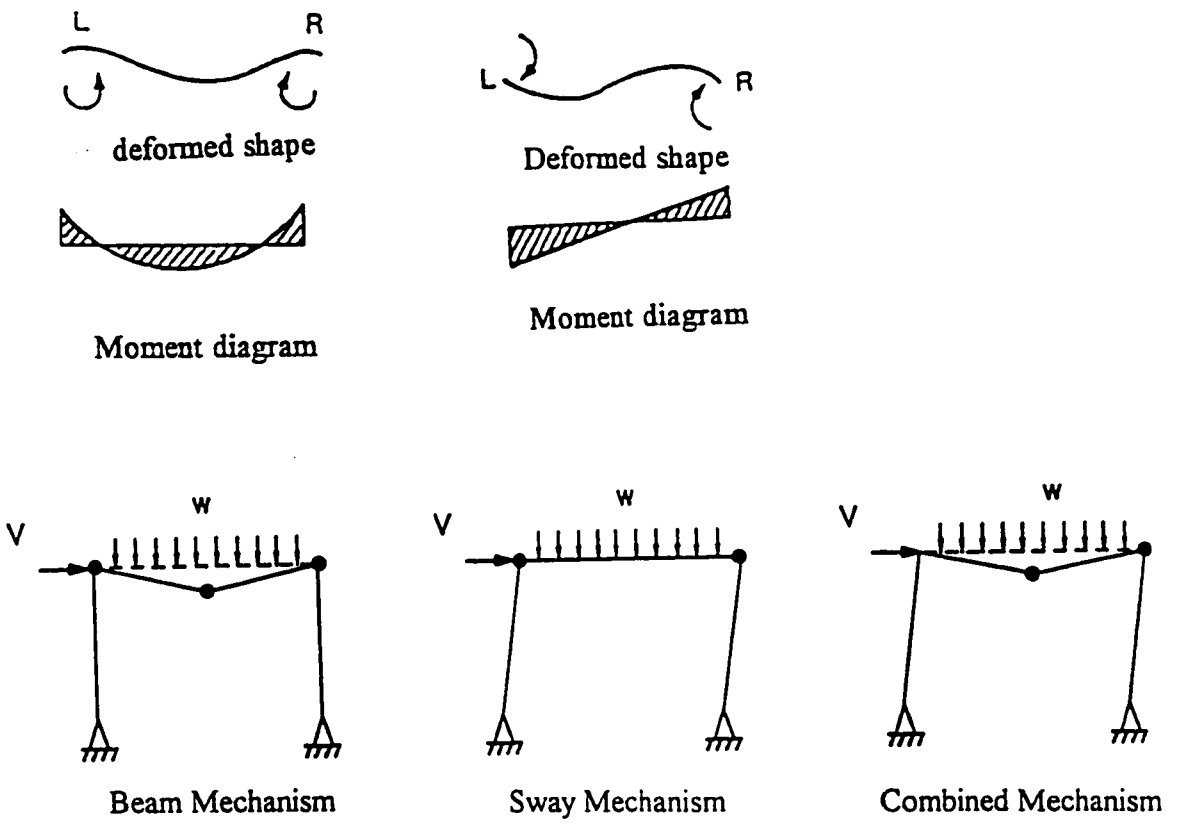


Figure 2.1 Different failure mechanisms in steel frames.

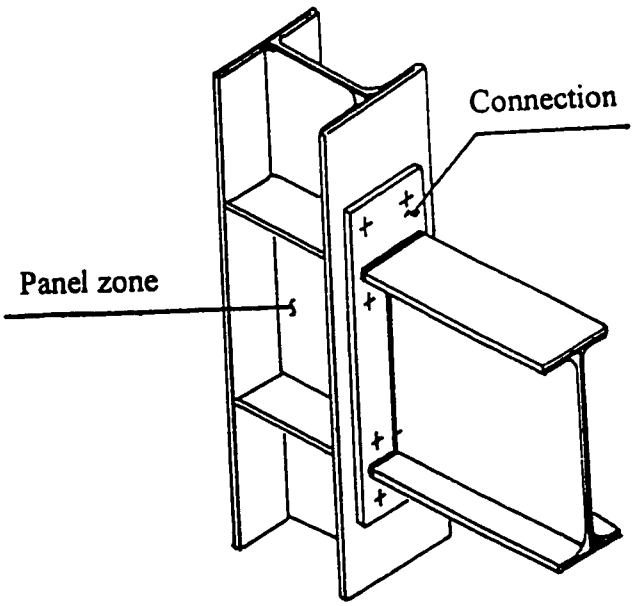


Figure 2.2 Typical beam-column joint in steel frame (after Osman, 1991).

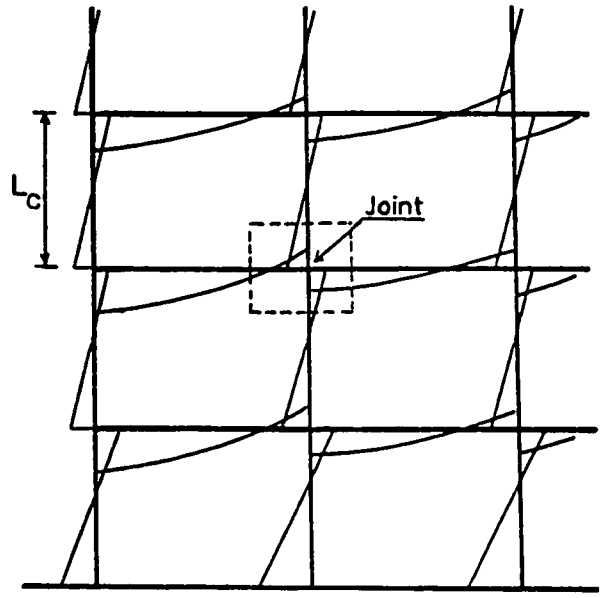


a) Bending moment distribution in portion of a MRF subjected to lateral loading.

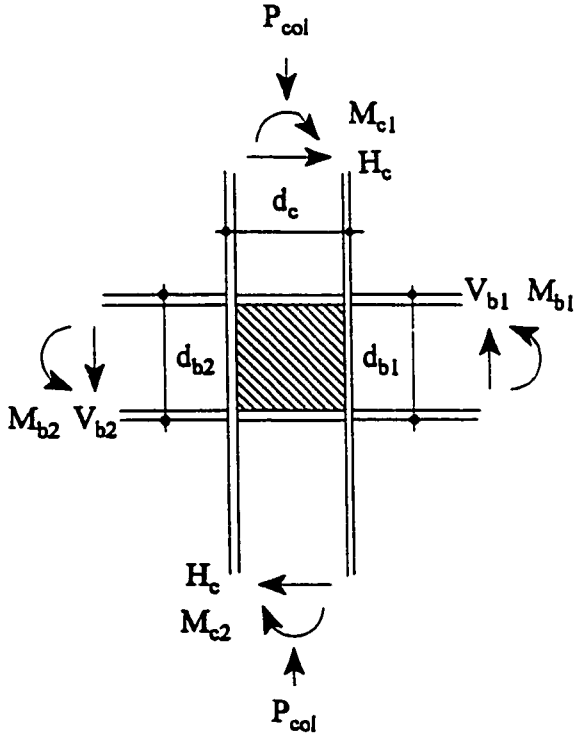


b) Typical beam-column panel zone subjected to lateral loading.

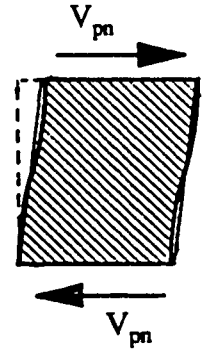


c) Deformed shape of beam-column panel zone.

Figure 2.3 Forces acting on a typical beam-column panel-zone.

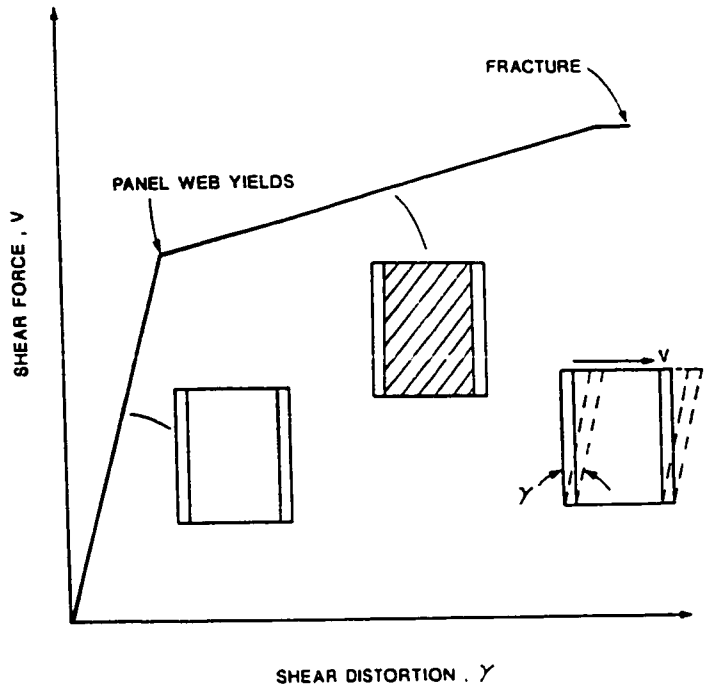


Figure 2.4 Typical shear force-distortion behaviour of a joint panel zone.

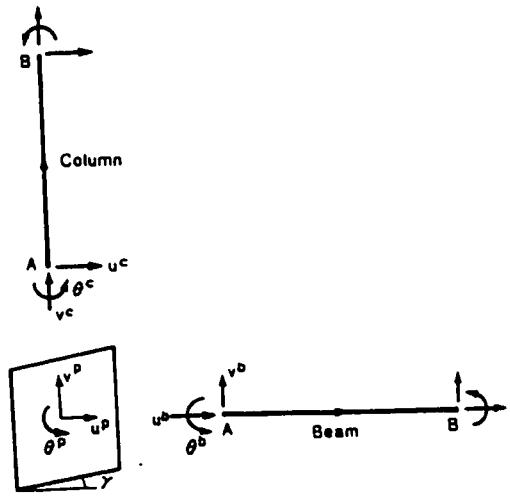


Figure 2.5 Relation between average displacement and shear deformation of the joint panel zone and end deformations of the adjacent beam and column.

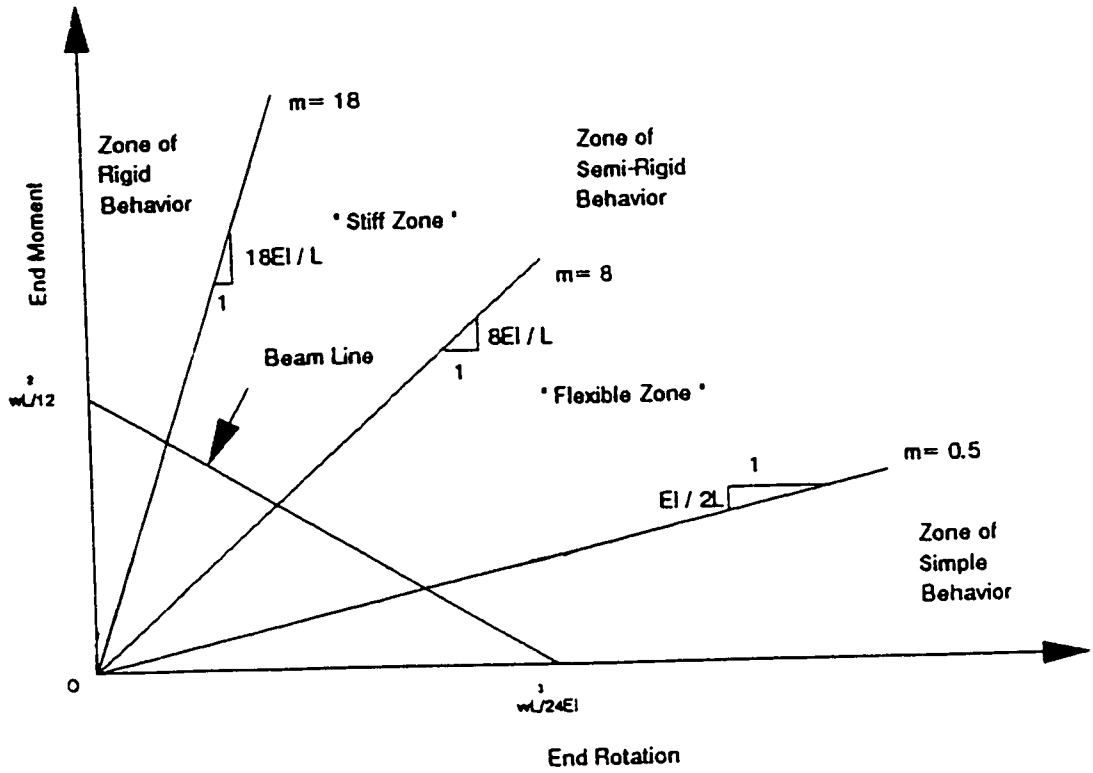


Figure 2.6 Rotational stiffness of steel connections (after Nader and Astaneh, 1992).

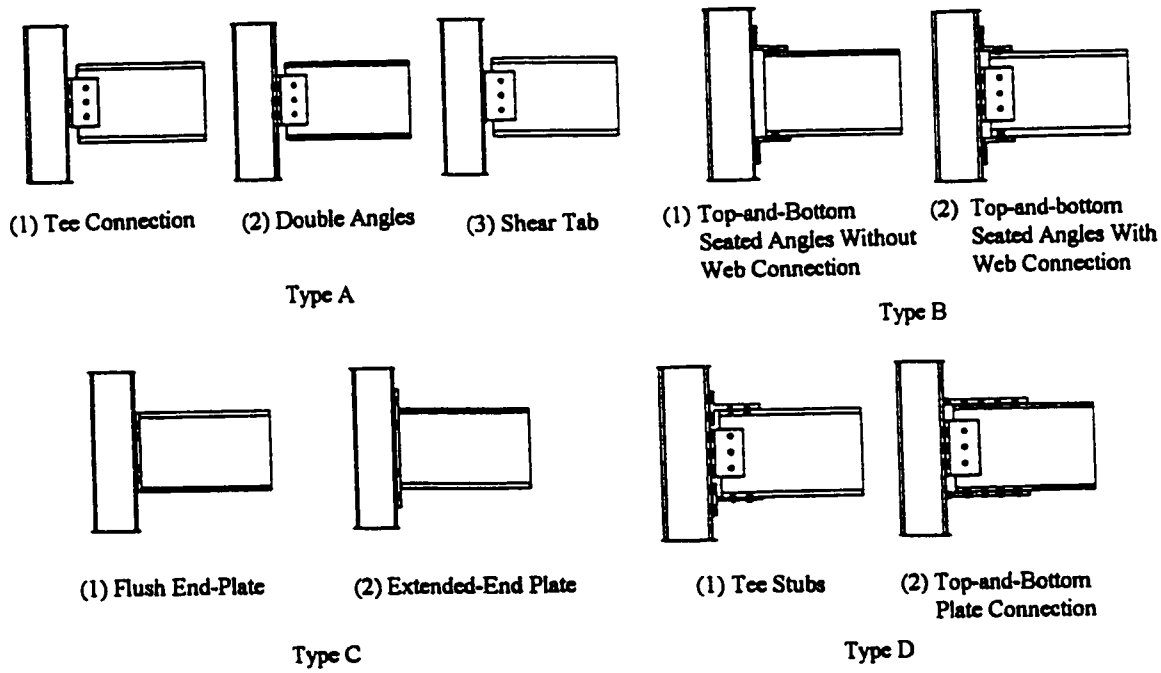


Figure 2.7 Beam-to-column connections used in steel frames (after Nader and Astaneh, 1992).

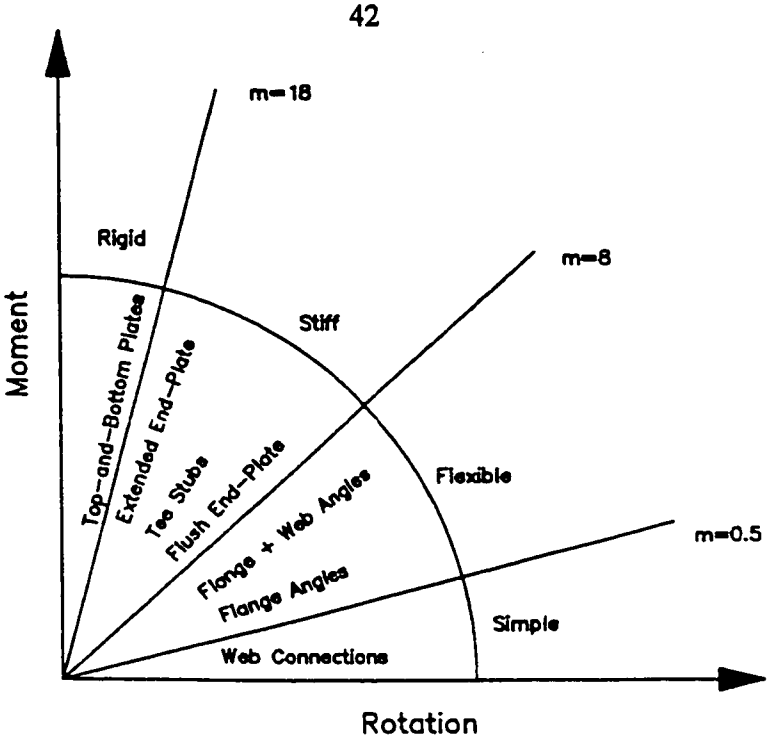


Figure 2.8 Classification of connections based on their moment-rotation relationship (after Nader and Astaneh, 1992).

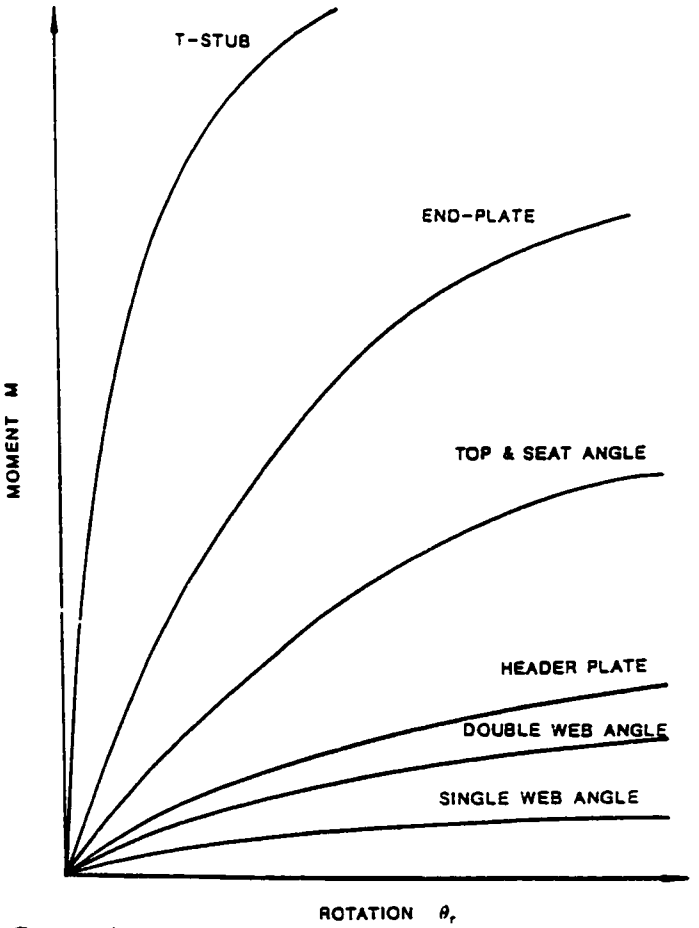


Figure 2.9 Connection moment-rotation curves for different types of connections (after Chen and Lui, 1991).

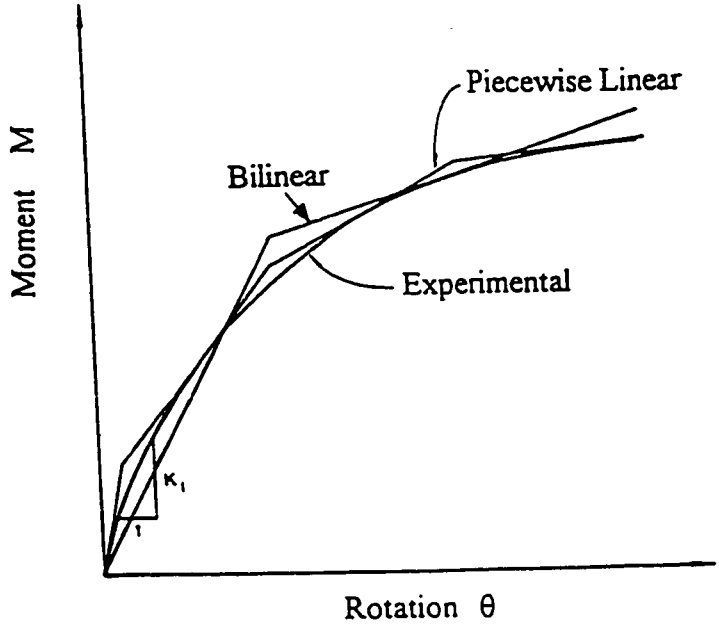


Figure 2.10 Linear moment-rotation models for connections (after Chen and Lui, 1991).

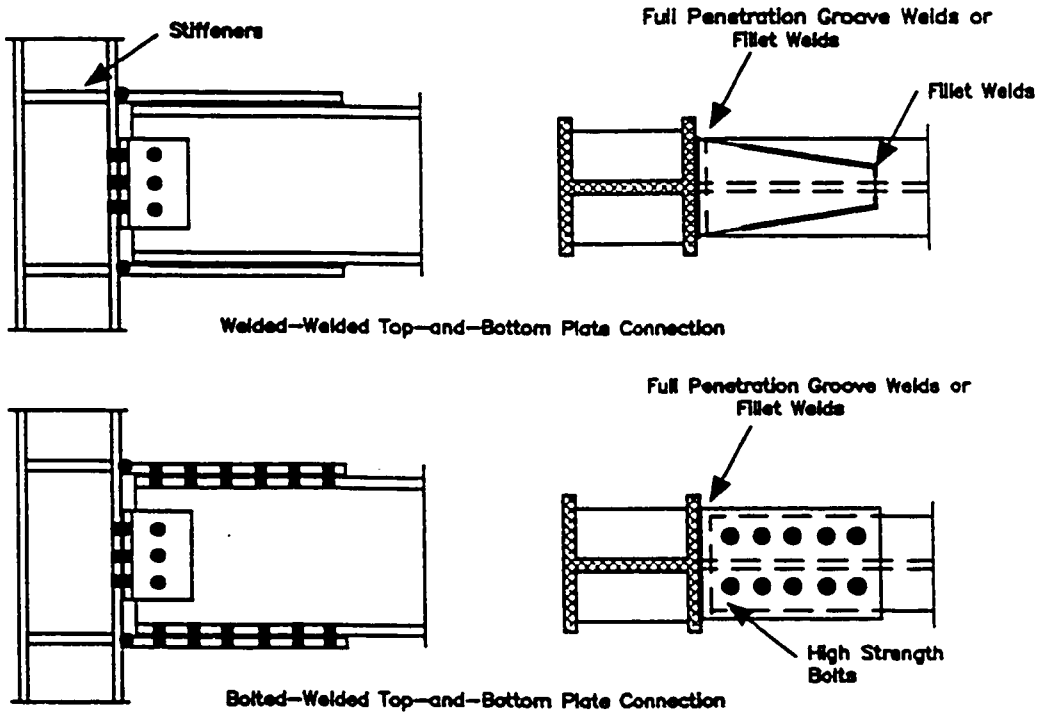


Figure 2.11 Typical top-and-bottom plate connections (after Nader and Astaneh, 1992).

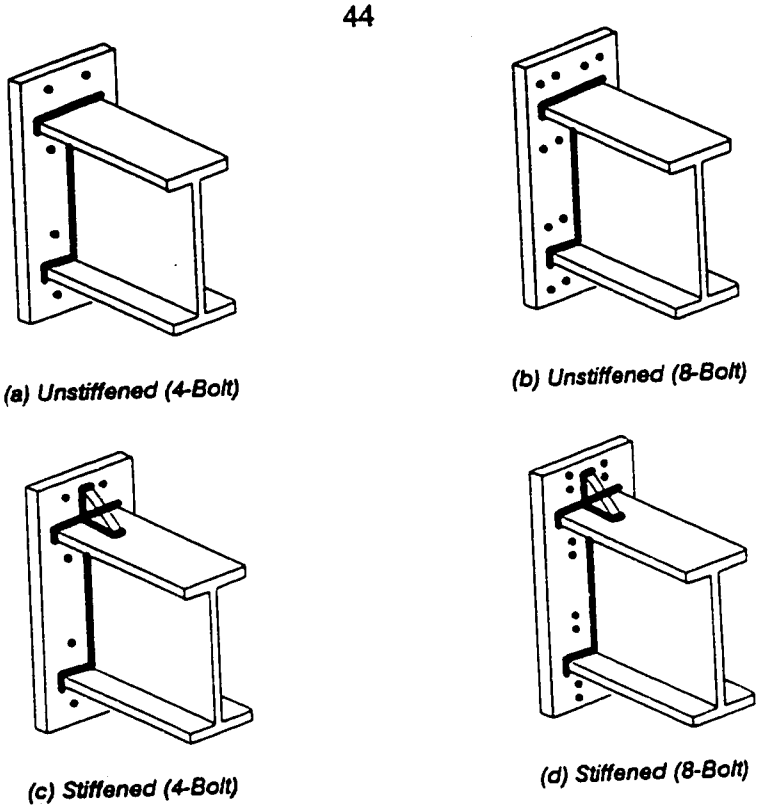


Figure 2.12 Typical extended-end plate connections (after Nader and Astaneh, 1992).

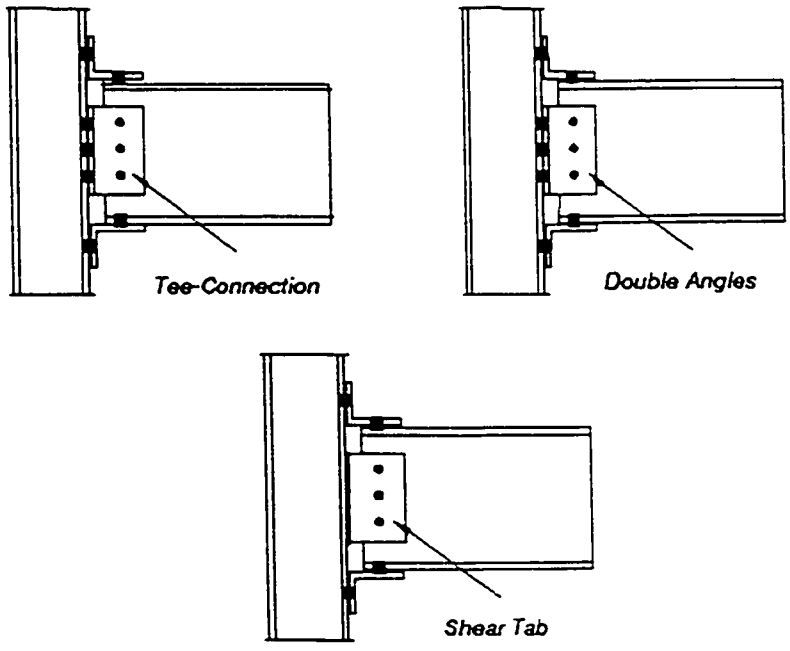


Figure 2.13 Typical top-and-bottom seated angles with web connections (after Nader and Astaneh, 1992).

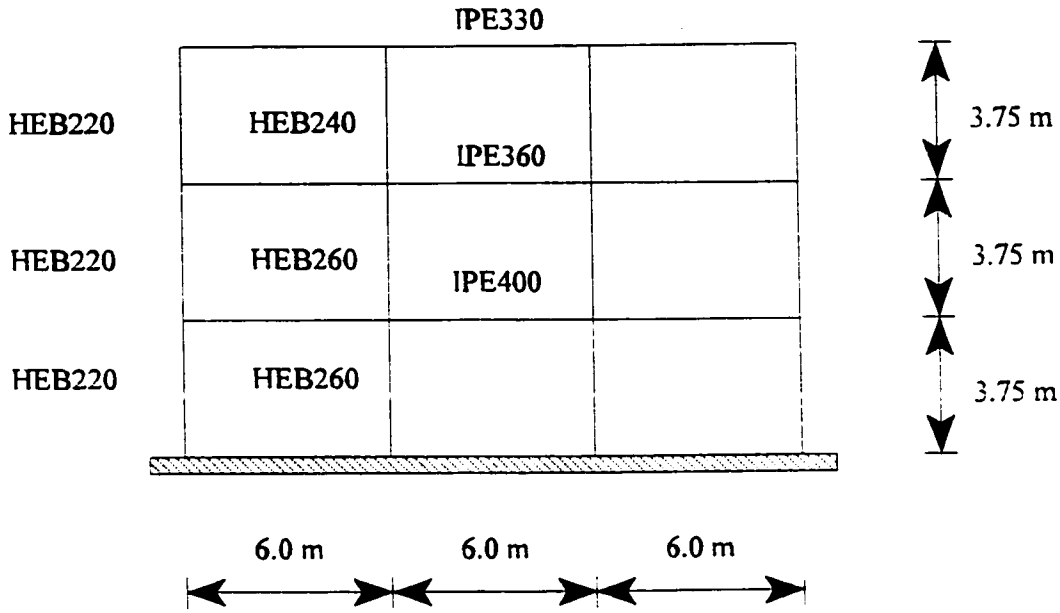


Figure 2.14 Three storey moment resisting steel frame

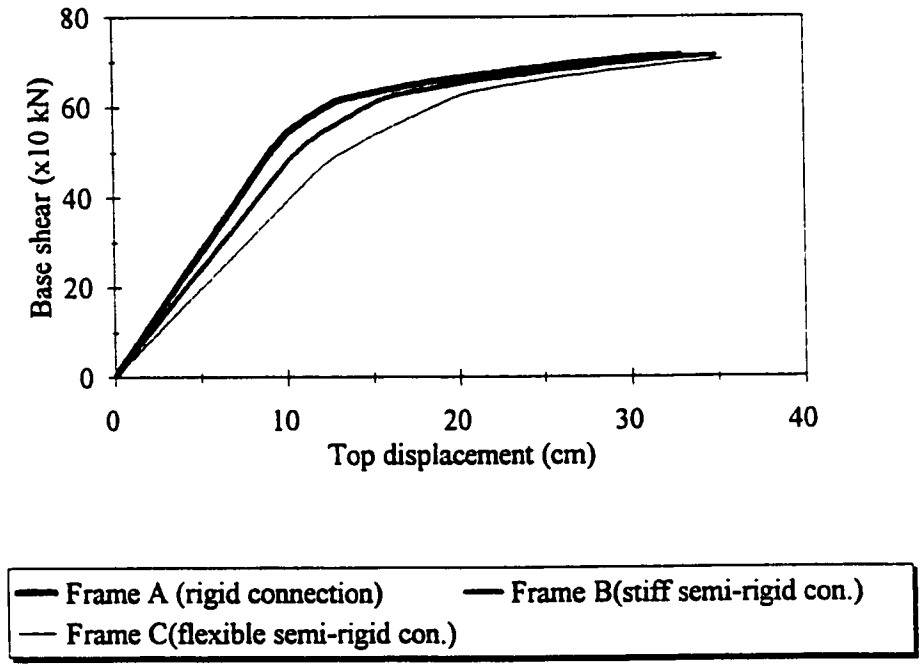


Figure 2.15 Effect of connection flexibility on the behaviour of steel frames subjected to lateral loads

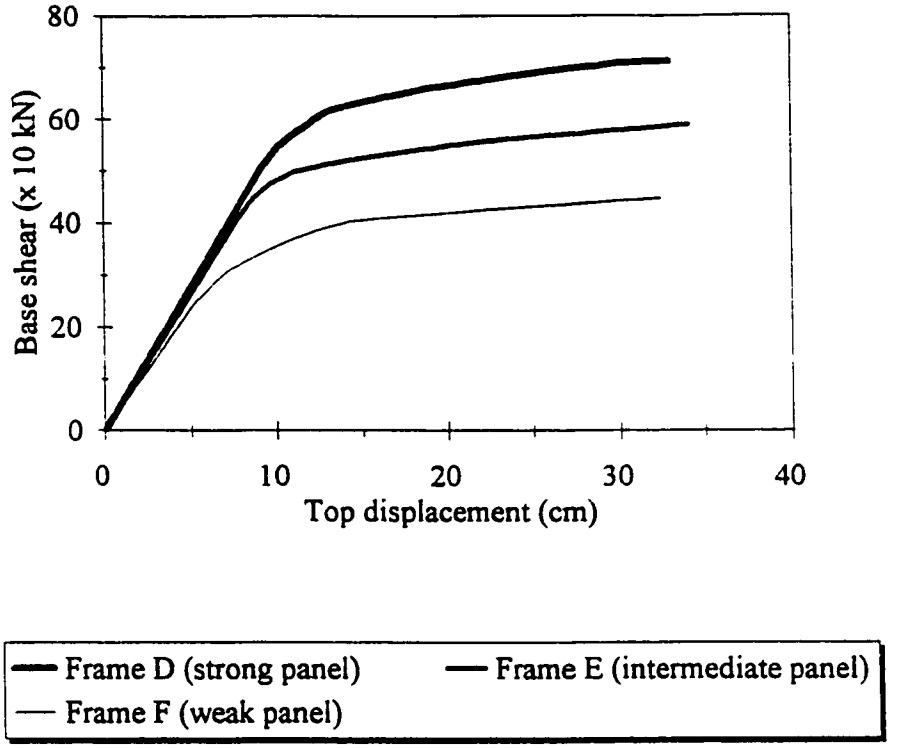


Figure 2.16 Effect of panel zone deformation on the behaviour of steel frames subjected to lateral loads

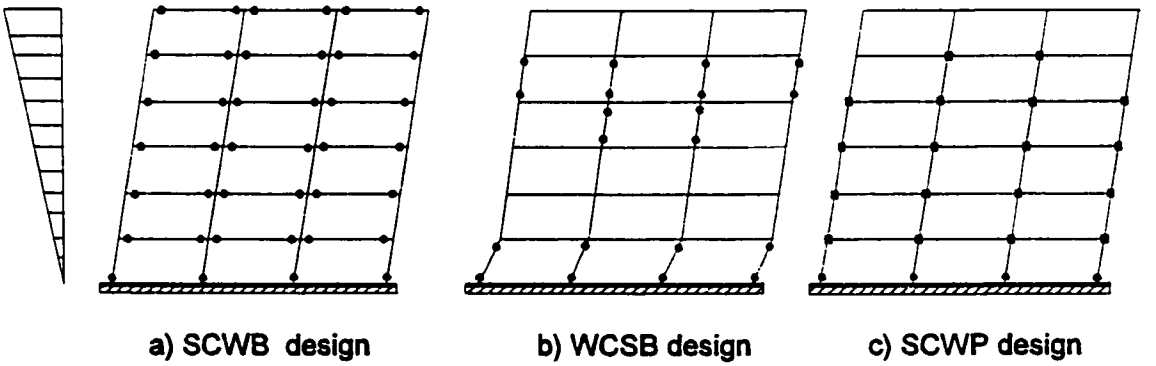


Figure 2.17 Typical locations of plastic deformations in moment resisting steel frames designed using different design philosophies.

# CHAPTER 3

# COMPUTER MODELLING AND RESPONSE PARAMETER DEFINITIONS

## 3.1 COMPUTATIONAL TOOL: PC-ANSR

The inelastic static and dynamic analyses in the study were performed using a modified version of the program PC-ANSR (Maison, 1992). The program was modified by adding three elements to be used in modelling the behaviour of moment resisting steel frames when subjected to either static loading or dynamic loading. A detailed description of the original program PC-ANSR was presented by Maison (1992).

PC-ANSR is based on the ANSR-1 program (Mondkar and Powell, 1974 and 1975) originally developed for use on main frame type computers. PC-ANSR is a PC version essentially the same as ANSR-1. Hence, the descriptions of ANSR-1 formulation and solution techniques apply to PC-ANSR as well.

PC-ANSR is organized in such a way that new finite elements can be added by developing new subroutines, without changing the existing main program. This has been achieved by structuring the program as a base program to which a number of auxiliary programs can be added.

The structural idealization in the program can be summarized as follows:

1- the structure is idealized as an assemblage of discrete elements (macro-elements

and/or finite elements) connected at nodes. A macro-element is based on the direct formulation of the structural element stiffness matrix, while the structural element stiffness matrix of a finite element is based on the integral of the product of the strain-displacement matrix and the stress-strain matrix.

2- the theory and solution procedure are based on the finite element formulation of the displacement method, with nodal displacements as the field variables (Mondkar and Powell, 1975).

3- each node may possess up to six displacement degrees of freedom (three translational and three rotational), as in a typical three dimensional frame analysis.

4- the structure's mass is assumed to be lumped at the nodes, so that the mass matrix is diagonal.

5- Viscous damping effects may be included. Damping effects proportional to mass, initial elastic stiffness, and/or tangent stiffness can be specified.

6- material nonlinearity is considered by using bilinear force-deformation relationships for members and joints, while geometric nonlinearity (arising from column P-$\Delta$ effects) is approximated by including geometric stiffness terms in the element stiffness formulation.

The loading assumptions in the program are as follows:

1- loads are assumed to be applied only at the nodes. Static and/or dynamic loads may be specified; however, static loads, if any, must be applied prior to the dynamic loads.

2- for static analysis, the static force patterns must be specified. Static loads are then applied in a series of load increments.

3- the dynamic loading may consist of earthquake ground accelerations, time dependent nodal loads, and prescribed initial values of nodal velocities and accelerations.

4- earthquake excitations are defined by time-histories of ground acceleration.

5- the dynamic response is computed by step-wise time integration of the incremental equations of motion using Newmark's $\beta$-$\gamma$-$\delta$ operator (Newmark, 1959 and 1962)

6- for both analyses (i.e. static and dynamic analysis), Newton-Raphson iteration procedure is used for nonlinear analysis.

### 3.1.1 Static analysis

The gravity loads are applied as nodal forces prior to lateral loading. The lateral loads are distributed at storey levels based on the distribution formula of the NBCC (1995). The load distribution shape remains unchanged during the loading process. The magnitude of the lateral loading is increased monotonically in small increments. The Newton-Raphson iteration method (Figure 3.1) is used, and the structural stiffness matrix is reformed at every load step. Because of nonlinearities developed within the load step an iterative procedure is required in order to satisfy equilibrium. If the solution does not converge within the maximum number of iterations for any load step the execution will terminate. This accounts for any plastification that has occurred in any of the structural elements. The analysis is continued until the maximum global displacement exceeds some specified value (for example top displacement of 2% of the total height of a frame structure), or the number of iterations exceed the maximum number specified in the analysis.

### 3.1.2 Dynamic analysis

The dynamic response of a structural system is obtained by solving the equations of motion for that system. In case of nonlinear dynamic analyses, incremental and iterative procedures are used to obtain the response. The masses are lumped at each floor level and viscous damping is assumed (Clough and Penzien, 1993) resulting in the following discrete equations of motion at any time t:

$$[M]\{\ddot{u}\} + [C]\{\dot{u}\} + [K_t]\{u\} = \{P_t\} \tag{3.1}$$

and at time $t+\Delta t$ the equations of motion become as follows:

$$[M](\{\ddot{u}\}+\{\Delta\ddot{u}\}) + [C](\{\dot{u}\}+\{\Delta\dot{u}\}) + [K_t](\{u\}+\{\Delta u\}) = \{P_{t+\Delta t}\} \tag{3.2}$$

Thus, the incremental form of equations of motion is:

$$[M]\{\Delta\ddot{u}\} + [C]\{\Delta\dot{u}\} + [K_t]\{\Delta u\} = \{P_{t+\Delta t}\} - ([M]\{\ddot{u}\} + [C]\{\dot{u}\} + [K_t]\{u\}) \tag{3.3}$$

where [M] is the mass matrix of the system, [C] is the damping matrix of the system and $[K_t]$ is the tangent stiffness matrix of the system at time t.

$\{u\}$, $\{\dot{u}\}$, $\{\ddot{u}\}$ are the nodal displacement, velocity and acceleration at time t.

$\{\Delta u\}$, $\{\Delta\dot{u}\}$, $\{\Delta\ddot{u}\}$ are the increments of nodal displacement, velocity and acceleration, $\{P_t\}$ and $\{P_{t+\Delta t}\}$ are the external applied loads at time t and $t+\Delta t$. In the case of seismic excitation, the external applied loads are the inertia forces caused by the ground acceleration at time t as follows:

$$\{P_t\} = [M]\{r\}\ \{\ddot{u}_g(t)\} \tag{3.4}$$

where $\{\ddot{u}_g(t)\}$ is the ground acceleration of support at time t and $\{r\}$ is the vector relating

static nodal displacements to the support motions (Clough and Penzien, 1993). It should be mentioned that in this dynamic analysis, only one horizontal excitation is considered for each analysis; also, soil-structure interaction and differential support excitation are not considered.

The integration of the equations of motion is carried out by dividing the time domain into a number of time steps. The Newmark's $\beta$-$\gamma$-$\delta$ operator is used to carry out the integration. The "constant average acceleration" operator (with value of $\beta = 0.25$, a value of $\gamma = 0.5$, and a value of $\delta$ = zero) is the most commonly used scheme in nonlinear analysis. It is assumed that increments of velocity and acceleration are functions of the increment in displacement and the state of motion at time t. Due to nonlinearity, an integration algorithm can be designed in which iterations are performed within a time step to satisfy equilibrium subjected to a specified tolerance. Thus, a path-dependant state determination is used, and stiffness is reformed at every time step. If the solution does not converge within the maximum number of iterations for any time step, the execution will terminate.

A time increment of 0.01 seconds is used in the study for all the frames. A sensitivity study using a reduced increment of 0.005 seconds time was performed. The results are comparable (differences less than 5%) to those using a time increment of 0.01 seconds.

Viscous type damping is used in the study. The damping matrix for the viscous damping is assumed to be Rayleigh type, and it is expressed as a linear combination of the mass matrix and the stiffness matrix. The damping matrix is derived by assuming accepted values of modal damping ratios for the modes which are considered to be important (first and second modes). In PC-ANSR the orthogonal damping matrix for multi-degree of freedom system is defined to be proportional to the mass matrix and stiffness matrix as follows:

$$[C] = c_1 [M] + c_2 [K] + c_3 [K_t] \tag{3.5}$$

where [C] is the damping matrix, [M] is the mass matrix, [K] is the elastic stiffness matrix, $[K_t]$ is the tangential stiffness matrix and $c_1$, $c_2$, $c_3$ are the proportional constants. In the dynamic analysis in this study, a damping matrix proportional to both mass and elastic stiffness is used. Thus, the proportional constants ($c_1$ and $c_2$) can be determined from the modal damping ratios of the first two modes. In this study, a damping ratio of 3% is assigned for both the first and the second modes. Therefore, $c_1$ and $c_2$ are determined based on the following expression:

$$\begin{bmatrix} c_1 \\ c_2 \end{bmatrix} = \frac{2\omega_1\omega_2}{\omega_2^2 - \omega_1^2} \begin{bmatrix} \omega_2 & -\omega_1 \\ \frac{-1}{\omega_2} & \frac{1}{\omega_1} \end{bmatrix} \begin{bmatrix} \beta_1 \\ \beta_2 \end{bmatrix} \tag{3.6}$$

where $\omega_1$, $\omega_2$ are the undamped frequencies of the first and second mode respectively and $\beta_1$, $\beta_2$ are the damping ratios of the first and second mode respectively, and both are assigned a value of 3% as mentioned above. The global stiffness matrix is then obtained by assembling individual element stiffness matrices. The structural stiffness matrix for the current time step is evaluated at the end of the previous time step and assumed to remain constant during the time increment. The structural stiffness matrix is updated at the end of the current time step for the next time step.

### 3.1.3 P-Delta effect (Geometric stiffness)

Axial force in a column produces secondary moments due to the relative lateral displacement between its nodes (P-$\Delta$ effect). These second-order moments tend to increase

inelastic deformations. In this study, a linearized solution (Wilson and Habibullah, 1987) has been assumed. The axial force on a column in its deformed shape can be decomposed into two components. One is parallel to the line joining the two ends of the deformed column, and the other is perpendicular. If the column deflection $\Delta$ is small as compared to its length L, the perpendicular component is equal to $P\Delta/L$. Thus, the total shear acting at each end of the column is the sum of the original shear V and the shear ($P\Delta/L$) resulting from the moment induced by P acting through the deflection $\Delta$ (Figure 3.2). Therefore, the shear terms in an element (column) stiffness matrix are modified by subtracting the following geometric stiffness matrix:

$$[K_g] = \frac{P}{L}\begin{bmatrix} 1 & -1 \\ -1 & 1 \end{bmatrix} \tag{3.7}$$

The axial force P is based on the unfactored gravity loading. During the application of monotonically increased lateral loading or the dynamic response, the axial force is allowed to change, i.e. the structural stiffness matrix has to be modified at each load step or time step.

### 3.1.4 Element modelling

Structural elements of a steel moment resisting frame are beams, columns, panel zones, and connections. In the current study, a model for each of the previous structural elements (Figure 3.3) is incorporated into PC-ANSR to represent the behaviour of moment resisting frames subjected to either static or dynamic loading. Three elements are incorporated into the computer program:

a) *beam-column element:* which is subdivided into three zones, an elastic zone in the centre and two inelastic finite zones at the ends (Figure 3.4). These two finite inelastic zones represent the gradual spreading of inelastic deformations into the element, which take place when the end moments exceed the yielding moment. The length of each plastic zone varies during the response history as a function of the moment distribution along the element length. The element is modified in order to take into account the effect of column axial load on the moment-curvature relationship.

b) *connection element:* which is a nonlinear rotational spring of zero length located at the beam-column interface.

c) *panel zone element:* which is based on the finite element formulation; the element consists of a column web and two column flanges adjacent to the connection (Figure 3.5). The element is capable of simulating the real modes of deformation (extension, shear, and bending) of the panel zone (Figure 3.6). A proposed cyclic model for the panel zone element is introduced in order to perform the dynamic analyses.

Complete descriptions of these elements are given in the following section.

## 3.2 MODELLING OF ELEMENTS

In order to predict the response of a moment resisting frame to seismic excitations, structural elements should be properly modelled. In steel frames, all joints behave in a semi-rigid manner. The joints' semi-rigid behaviour arises from two main sources: connection flexibility, and panel zone deformation. In this study, the joints' semi-rigid behaviour is

accounted for (section 3.2.2 and 3.2.3).

### 3.2.1 Beam-column element

In the literature, three analytical models are used to simulate the inelastic behaviour of a structural member in the discrete member idealization as follows:

a) Single component model (Giberson, 1969 and Otani and Sozen, 1972): a structural member is represented by an elastic line element with inelastic springs attached at its two ends (Figure 3.7a). Thus, inelastic deformation is assumed to be concentrated at the two member ends, and the inelastic rotation at one end is independent of that at the other end.

b) Dual component model (Otani,1974): a structural member is represented by an elastic component and elastic-plastic component in parallel (Figure 3.7b). Inelastic deformation is associated with the elastic-plastic component and assumed to be concentrated at the two ends of the member. The elastic component represents the strain-hardening effect. In the dual component model the inelastic rotation at one end affects the inelastic rotation at the other end. This approach results in a non-symmetric flexibility matrix, unless the inelastic deformations are concentrated at the member ends or the contraflexure point is assumed fixed at the midspan of the member.

c) Inelastic zone model (Soleimani et al., 1979, and Meyer et al., 1983): gradual spreading of the inelastic zones at the two ends of a structural member takes place (Figure 3.7c). The reduced flexural rigidity is assumed to be uniform within the inelastic zone at each end and depends on the moment-curvature relationship of the end section. In order to determine the length of the two end inelastic zones, the distribution of the bending moment along the

member is usually assumed to vary linearly along the member which is true for members in frames dominated by lateral load.

Anagnostopoulos (1981) studied the applicability of point-hinge models in studying the seismic response of steel members. He pointed out that point-hinge models are incapable of reproducing the gradual change of stiffness of a member in the post-yield range. The stiffness matrix of a member which is now a function of the spring stiffness remains constant throughout yielding. Moreover, given a moment acting at one end, the rotation of the corresponding spring is determined as if it were independent of the spring at the other end. From the above discussion, it can be concluded that although the concept of concentrated plastic hinges simplifies the computational effort, it leads to some inconsistency.

To overcome the inconsistencies developed by using the concentrated plastic hinge concept, the inelastic zone model is used in this study as shown in Figure 3.8. The model represents a beam-column element with a finite length of plastic zone at each end, and each plastic length varies during the response as a function of the moment distribution along the element length. To compute the tangent stiffness of a typical frame member, the element is subdivided into three regions: (1) an inelastic region of length $X_i$ at node i, having the average stiffness $(EI)_i$ ; (2) an inelastic region of length $X_j$ at node j, having the average stiffness $(EI)_j$ and (3) a central region of length $(L - X_i - X_j)$ having the initial elastic stiffness EI. The assumptions considered for using this model in the present study are as follows:

1- plane sections remain plane after deformation.

2- the primary moment-curvature relationship of a cross-section can be approximated by a bilinear function (Figure 3.9).

3- the hysteretic loops for the moment-curvature relationship follow a bilinear kinematic hardening model (Figure 3.10).

4- the original inelastic zone model proposed by Soleimani et al.(1979) and Meyer et al. (1983) did not take into account the effect of axial load. Since the the presence of an axial force in a member modifies the primary moment-curvature relationship; high axial force reduces the yield moment and curvature of the cross-section (Figure 3.11), the model is modified in order to consider the effect of axial load. A yield moment-axial force interaction diagram describes the effect of column axial force on its flexural yield strength. The interaction surface for this study is expressed by the following equations according with the Canadian design provisions for steel structure (CAN/CSA-S16.1-94):

for class 1 members (Figure 3.12),

$$(C_f/C_y) + 0.85\,(M_{fx}/M_p) \le 1.0 \qquad (3.8)$$

and,

$$M_{fx}/M_p \le 1.0 \qquad (3.9)$$

for class 2 members,

$$(C_f/C_y) + (M_{fx}/M_p) \le 1.0 \qquad (3.10)$$

and,

$$M_{fx}/M_p \le 1.0 \qquad (3.11)$$

where $C_f$ and $M_{fx}$ are the factored axial load and bending moment about the major axis due to gravity and lateral loads while $C_y$ and $M_p$ are the axial compressive resistance ($A\sigma_y$) and the moment resistance respectively. This is applicable only for WWF and W steel sections bent about their major axis. Member stability considerations are excluded while yielding is assumed to take place in the finite plastic

zones at the element ends.

5- axial deformation is not considered for the beams due to the assumption of rigid diaphragms in the planes of the floors.

6- P-Delta effect for columns is considered by adding the geometric stiffness matrix (given in section 3.1.3) to the element stiffness to give the final beam-column element stiffness matrix.

**Yield interaction surface:**

1) for beams, the yield surfaces are considered to be affected only by bending moment, i.e. the beam yield strength is equal to $Z\sigma_y$, where Z is the plastic modulus of the cross-section and $\sigma_y$ is the yield stress.

2) for columns, the yield interaction surfaces take into account effect of axial force on determining the yielding moment. For any combination of axial force and bending moment within a yield surface, the element end is assumed to be elastic. If the axial force-moment combination lies on or outside the surface, plastic zone starts to be introduced at that end. The interaction is taken into account until yield and is ignored after yield. In case the combination lies outside the yield surface, corrective moments are applied in the next load (time) step or iteration.

For six planar degrees of freedom identified in Figure 3.8, the symmetric tangent frame element stiffness can be written as :

$$[K] = \begin{bmatrix} K_{11} & 0 & 0 & K_{14} & 0 & 0 \\ 0 & K_{22} & K_{23} & 0 & K_{25} & K_{26} \\ 0 & K_{32} & K_{33} & 0 & K_{35} & K_{36} \\ K_{41} & 0 & 0 & K_{44} & 0 & 0 \\ 0 & K_{52} & K_{53} & 0 & K_{55} & K_{56} \\ 0 & K_{62} & K_{63} & 0 & K_{65} & K_{66} \end{bmatrix} \qquad (3.12)$$

where,

$K_{11} = K_{44} = - K_{14} = EA/L$

$Q_i = EI / (EI)_i$

$Q_j = EI / (EI)_j$

$f_{ii} = [1/3EIL^2] * [(Q_j - 1) X^3_j - (Q_i - 1)(L-X_j)^3 + Q_i L^3 ]$

$f_{jj} = [1/3EIL^2] * [(Q_i - 1) X^3_i - (Q_j - 1)(L-X_j)^3 + Q_j L^3 ]$

$f_{ij} = [1/3EIL^2] * [(Q_j - 1) X^2_j (1.5 L - X_j) + (Q_i - 1) X^2_i (1.5 L - X_i) + L^3/2 ]$

$K_{33} = f_{jj} / (f_{ii} f_{jj} - f^2_{ij})$

$K_{66} = f_{ii} / (f_{ii} f_{jj} - f^2_{ij})$

$K_{36} = -f_{ij} / (f_{ii} f_{jj} - f^2_{ij})$

$K_{23} = - K_{35} = (K_{33} + K_{36}) / L$

$K_{26} = - K_{56} = (K_{36} + K_{66}) / L$

$K_{22} = K_{55} = - K_{25} = (K_{33} + 2 K_{36} + K_{66}) / L^2$

The length $X_i$ and the stiffness ratio $Q_i$ of the plastic region at node i depends on the current branch of the M-$\phi$ diagram. For elastic loading or unloading $X_i = 0$, and $Q_i = 1.0$; for inelastic loading:

$$X_i = [M_i - M_y] * L / [M_i + M_j] \quad (3.13)$$

$$Q_i = EI / (EI)_i \quad (3.14)$$

in which $(EI)_i = p\,EI$, where p is the hardening coefficient. $X_i$ remains the maximum plastic region reached (during loading) in any previous load step. For inelastic unloading, stiffness degradation is assumed to be negligible and the member reloads with its elastic stiffness (EI). Similarly, $X_j$ and $Q_j$ can be obtained.

### 3.2.2 Panel-zone finite element

Experimental studies as well as recent earthquakes have shown that panel zone deformation has a pronounced influence on frame behaviour. The system of forces that acts on the joint panel was discussed in Chapter 2. Under the action of these forces, the joint panel deforms in various deformation modes as shown in Figure 3.6. These forces may cause premature yielding of the panel zone resulting in a reduction in strength and stiffness of the frame. Many experimental tests on steel beam-column subassemblages have been performed (e.g. Becker, 1975; Bertero et al., 1972; Kato, 1982, and Krawinkler, 1978) to investigate the load-deformation behaviour of the joint panel. Particular attention was given to the shear capacity of the panel zone and the effect of panel zone shear deformation on the strength and stiffness of the subassemblages. From the test results, it was concluded that there are two distinct stiffnesses in the joint shear force-shear distortion response of the panel (as mentioned in Chapter 2), an elastic stiffness followed by a smaller, almost constant, stiffness for a long range of deformation as showed in Figure 2.4. Moreover, the joint panel experiences a large ductility before failure, and finally the failure of the panel is usually caused by fracture of the

welds or beam flange on the face of the column flange. Several models have been proposed in the literature for the panel zone (e.g. Nakao, 1975; Krawinkler, 1978; Tsai and Popov, 1988, and Osman, 1991). Most of these models are simple, semi-empirical in nature and based on an idealized joint model calibrated against experimental results. Other models as Kato et al. (1988) are based on the matrix stiffness formulation.

To simulate the panel zone behaviour, a model initially developed by Lui and Chen (1986) for static nonlinear frame analysis is selected, modified in order to consider cyclic behaviour, and incorporated into PC-ANSR. The model, which is based on the finite element formulation and models the real geometry of the panel, accounts not only for the shear mode of deformation but also for the extension and bending deformation modes. The model also accounts for the effect of axial force on panel zone deformation. Figure 3.13 shows the finite element models for the web and flanges of a joint panel.

The model takes into consideration yielding and strain hardening of the web panel and the post-yield resistance of the joint from surrounding elements. The model is based on the following assumptions:

1- an idealized elastic-plastic bilinear stress-strain behaviour for the web panel is assumed, with a strain hardening ratio of 3% as shown in Figure 3.14.

2- no local buckling or lateral torsional buckling of the panel is allowed.

3- yielding of the web of the joint panel occurs when the state of stress reaches the yield surface described by Von Mises ($J_2$) theory.

4- the plasticity model with parallel branches concept is used to describe the subsequent yield or loading surfaces. A nonlinear kinematic hardening model can be obtained by

observing that a uniaxial stress-strain curve can be decomposed into an elastic-perfectly plastic branch in addition to an elastic branch to represent the hardening branch. The parallel branches concept was used for inelastic finite element analysis by Chi and Powell (1973) at the Universtiy of California (Berkeley) and was also given by Mondkar and Powell (1975).

5- fracture of the material is not considered.

The development of the stiffness matrix of the joint panel follows a standard finite element formulation. The finite element model of the panel zone, shown in Figure 3.13, consists of three separate elements: one web element, and two flange elements.

1- Web element:

The web element has four nodes and each node has three degrees of freedom u, v, and θ. The displacement field for this element can be written as:

$$\begin{bmatrix} u \\ v \\ \theta \end{bmatrix} = \begin{bmatrix} u(\xi,\eta) \\ v(\xi,\eta) \\ \dfrac{-\partial u(\xi,\eta)}{\partial y} \end{bmatrix} \tag{3.15}$$

in which u is linear in $\xi$, cubic in $\eta$; while v is linear in both $\xi$ and $\eta$. The formulation of the strain-displacement (B) matrix (Lui and Chen, 1986), where the strains are related to the nodal displacements, is as follows:

$$\epsilon_w = \begin{bmatrix} \epsilon_{xx} \\ \epsilon_{yy} \\ \gamma_{xy} \end{bmatrix} = [B_w]_{3x12} \; [u_1 \;\; v_1 \;\; \theta_1 \;\; u_2 \;\; v_2 \;\; \theta_2 \;\; u_3 \;\; v_3 \;\; \theta_3 \;\; u_4 \;\; v_4 \;\; \theta_4]^T \tag{3.16}$$

where $[B_w]$ is given in Appendix (I). Using the common notations used in the finite element

method and from the principal of virtual work, the stiffness matrix of the web element is obtained from the integral:

$$K_w = \int_v B_w^T D B_w dV = t_w \int_{-1}^{1}\int_{-1}^{1} B_w^T D B_w |J| d\xi d\eta \quad (3.17)$$

where $t_w$ is the thickness of the column web in the panel zone and $|J|$ is the Jacobian matrix given by:

$$|J| = \begin{bmatrix} \frac{w}{2} & 0 \\ 0 & \frac{h}{2} \end{bmatrix} = \frac{hw}{4} \quad (3.18)$$

where h is the height of the column web in the panel zone and w is the width of the panel web.

The integration is carried out by applying the numerical integration method over 2 x 4 Gauss-Legendre quadrature (Figure 3.15). Thus, the incremental stiffness matrix of the web panel zone ($K_w$) is given by:

$$K_w = \frac{h\ w\ t_w}{4} \Sigma_{i=1}^{2}\Sigma_{j=1}^{4} W_i W_j [B_w^T D B_w]_{\xi=\xi_i,\eta=\eta_j} \quad (3.19)$$

where $t_w$ is the thickness of the panel, D is the stress-strain relationship, $W_i$ and $W_j$ are weight coefficients.

2- Flange element

The stiffness matrices used for these flange elements are those of the ordinary six degree of freedom flexure frame elements. For the left flange (for example), the incremental stiffness matrix is as follows:

$$K_{lf} = \frac{EI_f}{h^3}\begin{bmatrix} 12 & 0 & -6h & -12 & 0 & -6h \\ 0 & \frac{h^2 A_f}{I_f} & 0 & 0 & \frac{-h^2 A_f}{I_f} & 0 \\ -6h & 0 & 4h^2 & 6h & 0 & 2h^2 \\ -12 & 0 & 6h & 12 & 0 & 6h \\ 0 & \frac{-h^2 A_f}{I_f} & 0 & 0 & \frac{h^2 A_f}{I_f} & 0 \\ -6h & 0 & 2h^2 & 6h & 0 & 4h^2 \end{bmatrix} \tag{3.20}$$

where h is the height of panel zone, $I_f = b_f t_f^3 / 12$, $A_f = b_f t_f$, $b_f$ is the width of column flange and $t_f$ is the thickness of column flange. The right flange has similar incremental stiffness matrix but with change in the signs of few coefficients.

Once the incremental stiffness matrices for the web and flanges of the panel are developed, the incremental stiffness matrix for the joint panel zone shown in Figure 3.16 is obtained by assembly. However, since the degrees of freedom of the joint panel do not coincide with the degrees of freedom of the web and flange elements, it is necessary to offset the latter degrees of freedom using offset transformation matrices before assembly. The stiffness matrix of the panel zone with respect to local coordinate system can be written as follows:

$$K_p = T_{olf}^T K_{lf} T_{olf} + T_{ow} K_w T_{ow} + T_{orf}^T K_{rf} T_{orf} \tag{3.21}$$

where $T_{olf}$ is the offset transformation matrix of left flange element, $T_{ow}$ is offset transformation matrix of the web element and $T_{orf}$ is the offset transformation matrix of the right flange element given as follows:

$$T_{olf} = \begin{bmatrix} H_{lf} & . \\ . & H_{lf} \end{bmatrix}, \quad H_{lf} = \begin{bmatrix} 1 & 0 & 0 \\ 0 & 1 & \frac{t_f}{2} \\ 0 & 0 & 1 \end{bmatrix} \tag{3.22}$$

$$T_{orw} = \begin{bmatrix} H_{lw} & . & . & . \\ . & H_{lw} & . & . \\ . & . & H_{rw} & . \\ . & . & . & H_{rw} \end{bmatrix}, \quad H_{lw} = \begin{bmatrix} 1 & 0 & 0 \\ 0 & 1 & t_f \\ 0 & 0 & 1 \end{bmatrix}, \quad H_{rw} = \begin{bmatrix} 1 & 0 & 0 \\ 0 & 1 & -t_f \\ 0 & 0 & 1 \end{bmatrix} \tag{3.23}$$

$$T_{orf} = \begin{bmatrix} H_{rf} & . \\ . & H_{rf} \end{bmatrix}, \quad H_{rf} = \begin{bmatrix} 1 & 0 & 0 \\ 0 & 1 & \frac{-t_f}{2} \\ 0 & 0 & 1 \end{bmatrix} \tag{3.24}$$

If a panel element is present at the end of a frame element, the 3 degrees of freedom at the end of the frame element must be related to the 6 degrees of freedom on the face of the panel element (Figure 3.17). Faces 1 and 3 are treated differently than faces 2 and 4 because a frame element attaches to face 1 or 3 of the panel element through a connection, whereas for face 2 or 4, the junction of the frame and panel elements is physically continuous.

A rigid link is proposed and used for faces 2 and 4 to relate the 3 degrees of freedom at the end of a column to the 6 degrees of freedom on the face of the panel element. The rigid link is assumed to form a linear relationship between the deformations along the face, i.e. the deformations of frame element (column) are the average of the deformations of the two nodes of the panel along this face.

A transition element (Figure 3.18) is proposed and used for faces 1 and 3 to relate the 3 degrees of freedom at the end of a beam to the 6 degrees of freedom on the face of the panel element. The transition element is composed of three nodes (each has three degrees of freedom); two nodes are connected to the face of the panel zone (where the transition element is compatible with the panel face), while the third node is connected to the beam element. The formulation of the strain-displacement (B) matrix for the transition element are:

(a) for the left element connected with face 1:

$$[B]_{3x9}^{\text{transition}} = \begin{bmatrix} -\frac{1}{w} & 0 & \frac{1}{2}\frac{h}{w}\eta & \text{same as for nodes 3; 4} \\ 0 & 0 & 0 & \text{of the original web element} \\ 0 & -\frac{1}{w} & -\frac{1}{2}(1-\xi) & \text{see Appendix (I)} \end{bmatrix} \qquad (3.25)$$

(b) for the right element connected with face 3:

$$[B]_{3x9}^{\text{transition}} = \begin{bmatrix} \text{same as for nodes 1; 2} & \frac{1}{w} & 0 & -\frac{1}{2}\frac{h}{w}\eta \\ \text{of the original web element} & 0 & 0 & 0 \\ \text{see Appendix (I)} & 0 & \frac{1}{w} & -\frac{1}{2}(1+\xi) \end{bmatrix} \qquad (3.26)$$

The validity of the transition elements were evaluated by conducting the following three analyses:

1- simple shear force acting at the face with one node. The stresses and the end deflection were examined. Shear stresses are constant (shear force/shear area), and the deflection is equal to the theoretical value (PL/GA).

2- simple tension force acting at the face with one node. The stresses and the end horizontal

displacement were examined. Normal stresses are constant (normal force/cross-sectional area) across the face, and the horizontal displacement is equal to the theoretical value (PL/EA).

3- simple bending moment acting at the face with one node. The stresses at the gaussian points were examined. The normal stresses follow the triangular distribution and the values of the stresses are equal to the theoretical values.

**Panel zone plasticity:**

Usually, the isotropic hardening plasticity model is simple to use but it cannot account for the Bauschinger effect exhibited by most structural materials subjected to stress reversals. In this study, the stress-strain relationship is assumed to follow a kinematic hardening model. A nonlinear kinematic hardening model is obtained by observing that a uniaxial stress-strain curve can be decomposed into an elastic-perfectly plastic component and an elastic component acting in parallel (Figure 3.19). Thus, the constitutive tensor for the resultant stress-strain relationship is obtained by simple addition of the two matrices ($D_1$ for elastic and $D_2$ for elastic-perfectly plastic) representing the two components (Mondkar and Powell, 1975).

For the first component (the elastic), the slope of the uniaxial stress-strain relationship is $E_1 = \alpha E$, where $\alpha$ is the strain hardening ratio and E is the elastic modulus of steel. Thus, $D_1$ for the case of plane stress element is given by:

$$D_1 = \frac{E_1}{1 - \nu^2} \begin{bmatrix} 1 & \nu & 0 \\ \nu & 1 & 0 \\ 0 & 0 & \frac{1-\nu}{2} \end{bmatrix} \qquad (3.27)$$

where ν is poisson's ratio. $D_1$ can also be written in tensor notation as:

$$(D_{ijkl})_1 = \lambda_1 \delta_{ij} \delta_{kl} + \mu_1 (\delta_{ik} \delta_{jl} + \delta_{il} \delta_{jk}) \qquad (3.28)$$

where $\delta_{ij}$ is the kronecker delta, and $\lambda_1$ and $\mu_1$ are Lame's constants where,

$\lambda_1 = E_1 \nu / (1+\nu)(1-2\nu)$, and $\mu_1 = E_1 / 2(1+\nu)$.

For the second component (the elastic-perfectly plastic), the slope of the uniaxial stress-strain relationship before yielding is $E_2 = (1-\alpha)E$ , and the yielding stress is $\sigma_{y2} = (1-\alpha)\sigma_y$ , where $\sigma_y$ is the yield stress of the material under a uniaxial tension test. When the state of stress calculated from the second component reaches a limit defined by Von Mises ($J_2$) theory, i.e. $f = J_2 - [\sigma_{y2}]^2 / 3 = 0$, the column web of the panel is assumed to be yielded. For the plane stress case, $J_2 = 1/3 [\sigma_{xx}^2 - \sigma_{xx} \sigma_{yy} + \sigma_{yy}^2 + 3 \tau_{xy}^2]$, in this case the stresses are calculated from the elastic-perfectly plastic component. In terms of tensor notation, the yield function in case of elastic perfectly-plastic component is given by :

$$f(\sigma_{ij}) = F(\sigma_{ij}) - K = 0 \qquad (3.29)$$

where K is a constant, or it can be written as $f(\sigma_{ij}) = J_2 - k^2 = 0$ in case of flow rule associated with Von Mises yield function, where $k^2 = [\sigma_{y2}]^2 / 3$, $J_2 = 1/2 S_{ij} S_{ij} = \sigma_{eff}^2 / 3$, the deviatoric stress component $S_{ij} = \sigma_{ij} - 1/3 \sigma_{mm} \delta_{ij}$ , and the effective stress $\sigma_{eff} = (3/2 S_{ij} S_{ij})^{1/2} = (3 J_2)^{1/2}$.

$f(\sigma_{ij}, K) = 0$ and $df = [\partial f / \partial \sigma_{ij}] d\sigma_{ij} = 0$ is the criterion for loading, while

$f(\sigma_{ij}, K) = 0$ and $df = [\partial f / \partial \sigma_{ij}] d\sigma_{ij} < 0$ is the criterion for unloading.

It should be mentioned that in some cases, a finite load increment may bring the state of stress from the second component (the elastic-perfectly plastic) outside the yield surface

(point Q, Figure 3.20) . If this is the case, the load increment (from point P to point Q) is scaled down by a factor (r) to the yield surface (point R), (r) is defined as:

$$r = ( -b + \sqrt{b^2 - 4ac} ) / 2a \qquad (3.30)$$

where,

$a = \Delta\sigma^2_{xx} + \Delta\sigma^2_{yy} - \Delta\sigma_{xx}\Delta\sigma_{yy} + 3\Delta\tau^2_{xy}$

$b = 2\sigma_{xx}\Delta\sigma_{xx} + 2\sigma_{yy}\Delta\sigma_{yy} - \sigma_{xx}\Delta\sigma_{yy} - \sigma_{yy}\Delta\sigma_{xx} + 6\,\tau_{xy}\,\Delta\tau_{xy}$

$c = \sigma^2_{xx} + \sigma^2_{yy} - \sigma_{xx}\sigma_{yy} + 3\tau^2_{xy} - [\,\sigma_{y2}\,]^2$

and,

$\Delta\sigma_{ij}$ = increment of stress induced in the second component by the load increment assuming elastic behaviour.

$\sigma_{ij}$ = state of stress from the second component before the load increment.

During elastic loading or during unloading (where plastic deformations vanish), the $D_2$ matrix is given as follows:

$$(D_{ijkl})_2 = (D_{ijkl})^e_2 = \lambda_2\delta_{ij}\delta_{kl} + \mu_2(\delta_{ik}\delta_{jl} + \delta_{il}\delta_{jk}) \qquad (3.31)$$

where $\delta_{ij}$ is the kronecker delta, and $\lambda_2$ and $\mu_2$ are Lame's constants where,

$\lambda_2 = E_2\,\nu / (1+\nu)(1-2\nu)$ and $\mu_2 = E_2 / 2(1+\nu)$.

During plastic loading, the $D_2$ matrix is given as follows:

$$(D_{ijkl})_2 = (D_{ijkl})^{ep}_2 = (D_{ijkl})^e_2 - \frac{3\mu_2}{\sigma^2_{eff}} S_{ij}\, S_{kl} \qquad (3.32)$$

The constitutive tensor for the resultant stress-strain relationship that is used in evaluating the panel incremental stiffness matrix is obtained by simple addition of the two components:

$$D_{ijkl} = (D_{ijkl})_1 + (D_{ijkl})_2 \tag{3.33}$$

The state of strain $\epsilon_{ij}$ (i.e. $\epsilon_{xx}$, $\epsilon_{yy}$, $\gamma_{xy}$) at any point in the web panel is the same as that of the first or the second component in the model, while the state of stress $\sigma_{ij}$ (i.e. $\sigma_{xx}$, $\sigma_{yy}$, $\tau_{xy}$) is the summation of the state of stress of both the first and the second component.

### 3.2.3 Spring connection element

In the past, several researchers have tried to simulate connection behaviour under general loading conditions. Different models have been presented, the models range from purely empirical curve fitting of test data; or by, analogy and semi-empirical techniques, to comprehensive models, (e.g. Frye and Morris, 1975, Ang and Morris, 1984, and Mzzalani, 1987).

The degree of model sophistication required and its capability of predicting with sufficient accuracy the connection response depends mainly on the purpose for which the model is to be used. In cases like studying the overall response of MRFs, simple models that are capable of handling the key aspects of the connection response are considered to be adequate, as properly designed connections remain in the elastic range.

To simulate the connection behaviour a simplified model (Tsai and Popov, 1988, and Osman, 1991) is considered in this study. The model selected for the connection is

incorporated into PC-ANSR for inelastic static and dynamic analysis. The connection is represented as a rotational spring element, in which the moment-rotation relationship is approximated by a bilinear piece-line curve (Figure 3.21). The curve is completely defined by three parameters: (1) the connection elastic stiffness $K_e$, (2) the connection post-elastic stiffness $K_{pc}$ and (3) the connection plastic moment $M_{pc}$.

The model can be used to simulate the behaviour of the connection under both monotonic and cyclic loading conditions (Figure 3.21). The model ignores the effect of connection stiffness degradation. Only flexural deformation of the connection is considered. A one degree of freedom connection element is introduced at the beam-column interface. To model the M-θ relationship, the connection element joins two nodes and is only influenced by the relative rotation between the nodes. The deformation of the element is defined as the change of angle between the connected beam and column due to connection rotation. It is assumed that the two connected nodes at both ends of the element have identical translational displacements (Figure 3.22).

The M-θ relationship for a connection is modeled as the summation of an elastic and elastic-plastic component in parallel as shown in Figure 3.23. A plastic hinge is introduced into the elastic-plastic component once the connection yield moment is reached. Kinematic hardening of the connection is modeled by specifying the appropriate percentage of strain hardening ratio of the M-θ relationship.

The relative rotation between the connected nodes is related to the node rotations as follows:

$$d\theta^{relative} = [1 \quad -1] \begin{bmatrix} d\theta_i \\ d\theta_j \end{bmatrix} \tag{3.34}$$

where $d\theta^{relative}$ is the increment of relative rotation (connection element deformation) and $d\theta_i$ and $d\theta_j$ are the increments of rotation of the connected nodes. The inelastic deformation is the amount of relative rotation beyond yield of the elastic-plastic component of the element. The element tangent stiffness relationship is given by:

$$dM = K_T \, d\theta^{relative} \tag{3.35}$$

In this study, the post-yield stiffness $K_p$ is considered as 15% of the elastic stiffness $K_e$ based on the experimental research done by Osman (1991). However, since the connection capacities are designed to avoid inelastic action, only the connection elastic stiffness is required. The validity of the bilinear moment-rotation relationship of the spring element was tested using a simple cantilever beam. The beam had the element at its fixed end (to represent a semi-rigid connection) and was subjected to cyclic concentrated point load at its free end.

### 3.2.4 Validation of the element modelling

Validation of the models incorporated into the nonlinear dynamic computer program is carried out by comparing the analytical results with experimental laboratory results done by other researchers. The experimental results of specimens (Figures 3.24, 3.27, and 3.30) tested by Osman (1991) are used to verify the validity of the models for MRFs. Each specimen consists of a single column 2800 mm long with cantilever beam on one side of the column at its mid-height. The length of the cantilever beam was 2300 mm from the point of loading to the centre line of the column. The material used for all the specimens was CSA-

G40.21-M300W steel. Three specimens were modelled using the proposed elements: CB-1, CC-1 and CC-2.

The details of specimen CB-1 are shown in Figure 3.24. The connection used is an extended end-plate connection with a 28 mm thick end-plate welded by fillet weld to the beam and bolted with eight 25 mm diameter, grade ASTM A490M, bolts to the column flange. In this specimen, the panel zone was designed to be the weakest element in the subassemblage. Thus, the behaviour was expected to be dominated by that of the panel zone. Twelve displacement cycles were applied to the beam tip. A constant axial force of 600 kN was applied to the column (25% of the column yield axial load). The loading history is shown in Figure 3.24. Figure 3.25 shows a comparison between the experimental and theoretical load-deflection relationship, while Figure 3.26 shows a comparison between the experimental and theoretical moment-average panel shear strain relationship.

The details of specimen CC-1 are shown in Figure 3.27. The connection used is an extended end-plate connection with a 28 mm thick end-plate welded by fillet weld to the beam and bolted with eight 25 mm diameter, grade ASTM A490M, bolts to the column flange. In this specimen, the panel zone was expected to yield at approximately the same load as the beam. Thus, the inelastic action of both the beam and the panel zone during loading could be expected. Fourteen displacement cycles were applied to the beam tip. A constant axial force of 600 kN was applied to the column (12% of the column yield axial load). The loading history is shown in Figure 3.27. Figure 3.28 shows a comparison between the experimental and theoretical load-deflection relationship, while Figure 3.29 shows a comparison between the experimental and theoretical moment-average panel shear strain relationship.

The details of specimen CC-2 shown in Figure 3.30 are similar to specimen CC-1, except that a 9 mm thick doubler plate was welded to the column web at the panel zone area to increase the panel shear capacity leading to a relatively strong panel. The behaviour of this specimen was expected to be dominated by the behaviour of the beam. Twelve displacement cycles were applied, and a 600 kN constant axial force acting on the column. The specimen represents a case of strong panel, where most of the inelastic action is forced to take place in the beam, imposing high ductility demand on the beam. The loading history is shown in Figure 3.30. Figure 3.31 shows a comparison between the experimental and theoretical load-deflection relationship, while Figure 3. 32 shows a comparison between the experimental and theoretical moment-average panel shear strain relationship.

Although the experimental relationships are more rounded during the change from one stiffness to another than the theoretical relationships (because of the theoretical bilinear representation), the comparison of the theoretical and experimental results indicates a very good agreement among the main factors that define a relationship (i.e. relationship characteristics) in both cases. During studying the overall response of MRFs, the important factors in a force-deformation relationship are:

1) The elastic stiffness and the post-elastic stiffness.

2) The force at which yielding deformation occurs (i.e. change from one stiffness to another).

3) The maximum level of deformation.

4) The shape of the hysteretic loops and the energy dissipating during each cycle.

Comparisons between theoretical and experimental results, which are listed in Tables 3.1 and 3.2, show that the model is capable of predicting the above main relationship

characteristics. The only drawback in the model is that in some cases the area calculated under one hysteretic loop may be higher by 10%-15% than the experimental case, which is basically because of the bilinear representation. The proposed model can accurately predict the overall behaviour of steel moment resisting frames subjected to either static or dynamic loading. The observed differences between the experimental and theoretical shapes (which are mainly during the change from the elastic stiffness to the plastic stiffness) can be eliminated by using a curved or multi-linear force-deformation model, in addition to taking into account the influence of local buckling on reducing the stiffness as well as the effect of local instability in the plastic range. Other more sophisticated inelastic models, such as plate or shell elements, can also be used to account for the smooth curved change from one stiffness to another. However, the use of such sophisticated models when performing inelastic dynamic analyses for multistorey frame structutres may result in complexity and computational inefficiency.

Based on the parametric study done by Engelhardt et al. (1995) on the inelastic modelling of steel frames, it is found that the predicted locations of yielding can be sensitive to the modelling. Therefore, the detailed sequence of plastic hinge formation that are included in this thesis may be modelling dependent. However, the objective is to identify broad pattern of plastic deformations rather than the detailed sequence of hinge formation.

## 3.3 RESPONSE PARAMETER DEFINITIONS

In order to describe the amount of damage that a building structure sustains during its seismic response, damage parameters need to be defined. Damage parameters can be

divided into two groups, the first is related to overall response, and the second is associated with localized member (element) response.

Damage parameters may also be divided into two categories based on the type of loading. The first category is related to damage caused by sudden large inelastic deformation excursions, and the second is associated with low-cycle fatigue-type damage during sustained reversals of inelastic deformation.

### 3.3.1 Overall response parameters

The response of a structure to a certain kind of loading is related directly to how much deformation the structure undergoes due to this load. For a structural frame model subjected to lateral loading, either due to static lateral forces or horizontal seismic excitation, the roof deflection (i.e. top displacement) is a key parameter in determining to what extent the frame has deformed laterally. Thus, the normalized top displacement $\Delta_{top}$ represents an important parameter in evaluating the overall response of the structure. The normalized top displacement $\Delta_{top}$ is defined as:

$$\Delta_{top} = \delta_{max} / H \quad \text{(in percentage form)} \tag{3.36}$$

where $\delta_{max}$ is the maximum top displacement and H is the overall height of the frame structure.

When a frame is subjected to monotonically increased lateral loading (push over static analysis), the relation between the normalized base shear (base shear/design base shear) and the normalized top displacement gives a good assessment of the global behaviour of the frame. This relation shows the overstrength that the frame possesses and the overall ductility

demand it can sustain.

The overall response parameters also include storey level response parameters such as maximum storey displacement, and maximum storey drift. The maximum storey drift is defined as the maximum storey displacement divided by the storey height as follows:

$$\text{storey drift for } i^{th} \text{ storey} = (\Delta_{i+1} - \Delta_i) / h_i \qquad (3.37)$$

where $\Delta_{i+1}$ is the displacement of $(i^{th}+1)$ floor, $\Delta_i$ is the displacement of $i^{th}$ floor and $h_i$ is the height of $i^{th}$ storey.

The storey drift is more important than the overall normalized roof deflection. This is because during seismic shaking, the damage that each storey suffers is a function of the relative displacement between its two neighbouring floors, i.e. the storey drift. Moreover, the value of the roof deflection alone can sometimes be a misleading parameter because of the concentration of lateral deflection in only one floor, while the other floors experience relatively small deflections, e.g. the case of soft first storey. For damage evaluation, one should examine the roof deflection in addition to storey drifts and their distribution along the structure's height.

### 3.3.2 Local member response parameters

Performance of beams and columns is expressed in terms of element rotational ductility and element damage index. Ductility reflects damage caused by large inelastic deformation excursions. The rotational ductility, $\mu_\theta$, is defined as the ratio of the maximum rotation, $\theta_{max}$, to the rotation at yield, $\theta_y$. In order to estimate the yield rotation, an assumption needs to be made regarding the deformed shape of the member at first yielding.

It is usually assumed that the member (in a frame subjected to lateral loading) yields in antisymmetric bending. Therefore, the yield rotation for beams is given by:

$$\theta_y = M_p L / 6 EI_x \tag{3.38}$$

where L is the member length, $M_p$ is the plastic moment of the element, E is the modulus of elasticity and $I_x$ is the moment of inertia. In case of columns, the presence of axial force will reduce the yield rotation from that calculated for beams. It should be noted that for a column which is subjected to the combination of axial force and moment, such combination varies with time during an earthquake, or during push over analysis due to change of lateral load at every load step. This makes it more complex to predict the inelastic behaviour of a column. However, the axial force caused by gravity load is usually the dominant axial force of a column. Therefore, the column is assumed to be a member subjected to alternating bending with constant axial force due to gravity loads. The proposed yield rotation is (Chen and Atsuta, 1976):

$$\theta_y = (M_p L / 6 EI) * (1 - (P/P_y)) \tag{3.39}$$

where P is the unfactored axial force on the column due to gravity load, and $P_y$ is the column yielding load.

For static analysis, the damage index for beams and columns is:

$$\text{Damage Index (D.I.)} = \theta^p / (\theta_{um} - \theta_y) \tag{3.40}$$

where $\theta^p$ is the maximum plastic rotation of the element under static loading and $\theta_{um}$ is the ultimate rotational capacity of the element under monotonic loading.

For dynamic analysis, the damage index for beams and columns is defined as the accumulation of the ratio of the $i^{th}$ reversal of maximum plastic rotation $\theta^p_i$ (either positive

or negative) to the ultimate monotonic plastic rotational capacity, $\theta^p_{um} = (\theta_{um} - \theta_y)$. Based on Miner's (1945) rule of linear damage accumulation, and the research study done by Daali and Korol (1996) on the energy deterioration per reversal, then for N variable amplitude reversals of different ductilities, the damage index (DI) can be expressed as:

$$DI = \sum_{i=1}^{N} \{\theta^p_i / (\theta_{um} - \theta_y)\}^{1.15} \qquad (3.41)$$

Estimates of $\theta^p_{um}$ for beams are calculated based on their slenderness ratios. Daali and Korol (1995) presented an equation for the prediction of rotational capacity, $R_m$ , as follows:

$$R_m = (\theta_{um} / \theta_y) - 1 = l\,[(2s-1) + (e\,l)/(1 - l)] \qquad (3.42)$$

where $e = E/E_T$, where $E_T$ is the tangent modulus of elasticity (i.e. e = 36), s is the ratio of strain at the beginning of strain hardening to the yield strain (i.e. s = 9), and $l$ is the yield length of the flange which corresponds to the optimal wave length initiating the local buckling to the overall length. The value of $l$ can be calculated as follows:

$$l = 0.3997 - [\alpha_f^{\,2} / (E/480)] - [\alpha_w^{\,2} / (E/5.695)] \qquad (3.43)$$

where $\alpha_f = (b / t_f) * \sqrt{\sigma_y/300}$, and $\alpha_w = (h / t_w) * \sqrt{\sigma_y/300}$

in which b is half the flange width, $t_f$ is the flange thickness, h is the web depth, and $t_w$ is web thickness. Using this equation, one can predict the rotational capacity of a W-shape steel beam, or simply the rotation corresponding to the maximum moment (Figure 3.33).

In case of columns, the ultimate rotational capacities are calculated based on the values of ultimate curvatures determined from the yield stress and the ultimate stress of steel. Given the yield stress as 300 MPa and the ultimate stress as 450 MPa, and assuming a stress-strain curve with hardening 3%, the yield strain and the ultimate strain can be obtained (Figure

3.14). Determining the position of the neutral axis of the cross-section based on the axial force due to gravity load on the column (Figure 3.34), the ultimate curvature can be estimated, then the ultimate rotation is the product of the ultimate curvature and the plastic hinge length which is assumed to be equal to the depth of the column section (Chen, 1994).

The parameters used to express the performance of a joint panel zone are similar to those used for the beam-column element, except that rotations are replaced by shear strains, i.e. performance is expressed in terms of panel zone shear ductility, $\mu_\gamma$, and panel damage index. The panel zone shear ductility is defined as the ratio of the maximum panel shear strain ($\gamma_{max}$) to the panel shear strain at yield ($\gamma_y$). The shear strain at yield $\gamma_y = \tau_y / G$, where the yield shear stress $\tau_y = \sigma_y / \sqrt{3}$, the shear modulus $G = E/2(1+\nu)$, E is the elastic modulus, and Poisson's ratio for steel $\nu = 0.3$. The column axial load has a negligible effect on determining $\gamma_y$ (Tsai and Popov, 1988). A reduction factor of $(1-(P/P_y)^2)^{1/2}$ given by Popov (1968) can be applied to ($\gamma_y$) to account for the axial load effect, however, for low levels of axial loads ($P/P_y \leq 0.3$), the reduction can be practically ignored (i.e. reduction of ≈ 5%). For well designed joints, the ultimate joint distortion is in the order of $20\gamma_y$ (Kato et al., 1988).

The damage index for joint panel zones is similar to that defined for the beams and columns but it is function of the shear strain rather than the end rotation. It should be mentioned that a damage index = zero means an elastic response with no damage to that element, and a damage index ≥ 1.0 means complete failure of the element.

Table 3.1 Comparison between the experimental and predicted load-deflection relationship characteristics

| Specimen | Elastic stiffness (kN/mm) | | Plastic stiffness (kN/mm) | | Yielding load (kN) | | Yielding tip deflection (mm) | | Maximum tip deflection (mm) | |
|---|---|---|---|---|---|---|---|---|---|---|
| | Exp. | Model | Exp. | Model | Exp. | Model | Exp. | Model | Exp. | Model |
| CB-1 | 5 | 5.3 | 0.50 | 0.45 | 100 | 110 | 20 | 21 | 140 | 140 |
| CC-1 | 6.1 | 6.3 | 0.50 | 0.54 | 160 | 175 | 26 | 28 | 130 | 135 |
| CC-2 | 6.4 | 6.6 | 0.53 | 0.61 | 175 | 185 | 27 | 28 | 115 | 120 |

Table 3.2 Comparison between the experimental and predicted applied moment-joint shear strain relationship characteristics

| Specimen | Elastic stiffness (kNm/mm/mm) x $10^5$ | | Plastic stiffness (kNm/mm/mm) x $10^5$ | | Yielding moment (kNm) | | Yielding shear strain (mm/mm) x $10^{-3}$ | | Maximum shear strain (mm/mm) x $10^{-3}$ | |
|---|---|---|---|---|---|---|---|---|---|---|
| | Exp. | Model | Exp. | Model | Exp. | Model | Exp. | Model | Exp. | Model |
| CB-1 | 0.95 | 1 | 0.04 | 0.04 | 220 | 230 | 2.3 | 2.3 | 30 - 38 | 33 |
| CC-1 | 1.57 | 1.61 | 1.4 | 1.3 | 360 | 370 | 2.3 | 2.3 | 15 | 16 |
| CC-2 | 2.2 | 2.3 | 0.1 | 0.08 | 500 | 520 | 2.3 | 2.3 | 4 | 3.5 |

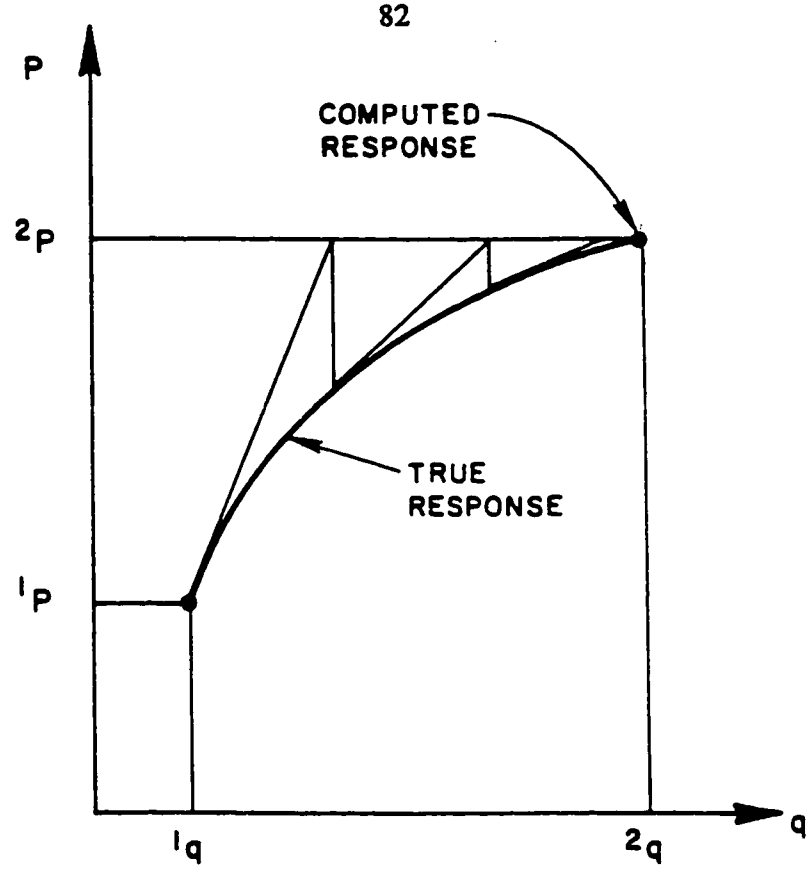


Figure 3.1 Newton-Raphson iteration procedure.

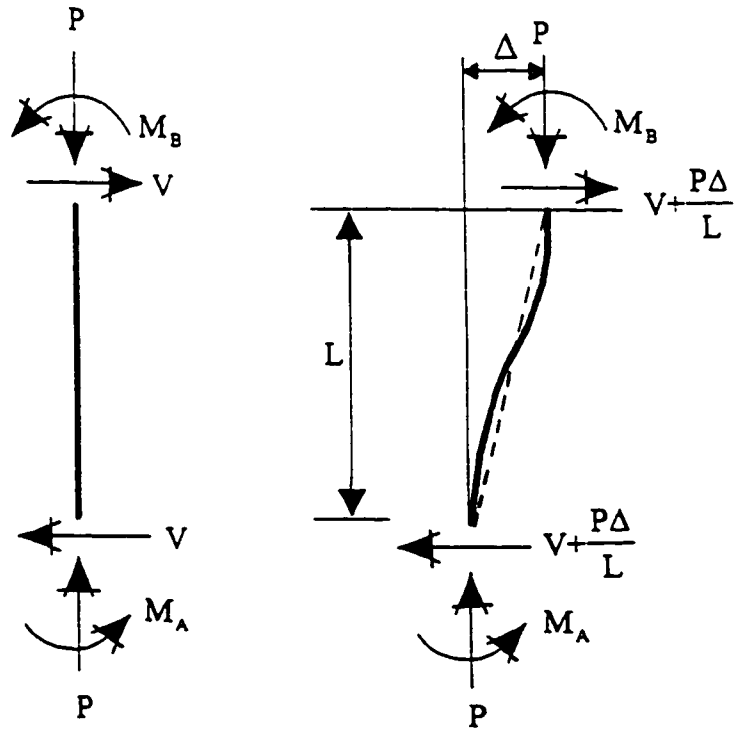


Figure 3.2 P-Delta effect due to axial force and relative lateral displacement.

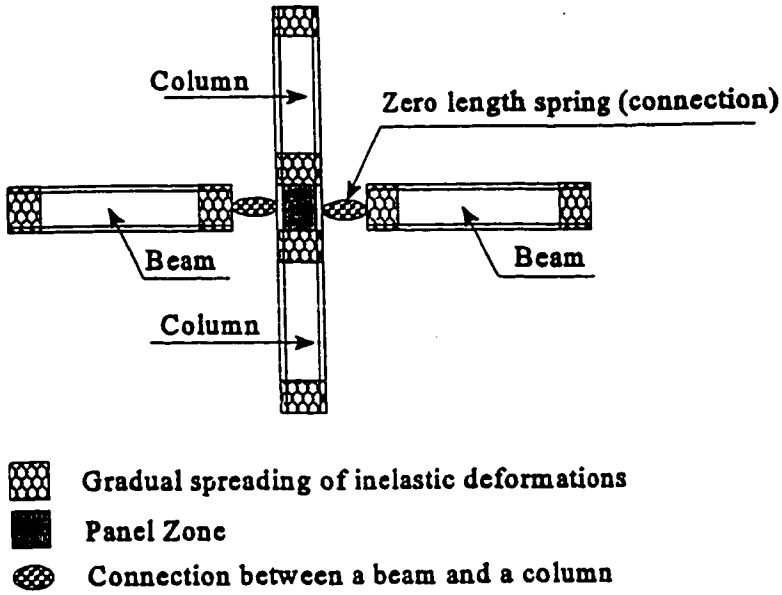


Figure 3.3 Modelling of different structural elements in a steel MRF.

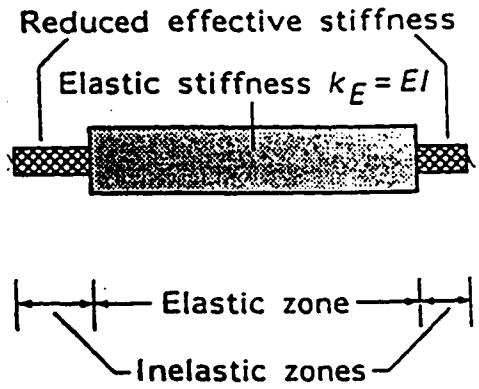


Figure 3.4 Beam-column element.

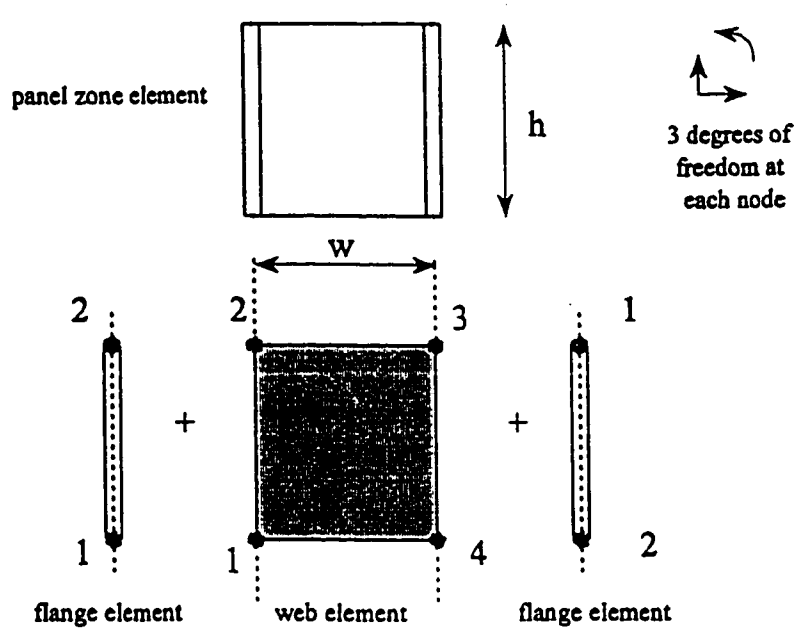


Figure 3.5 Panel zone element.

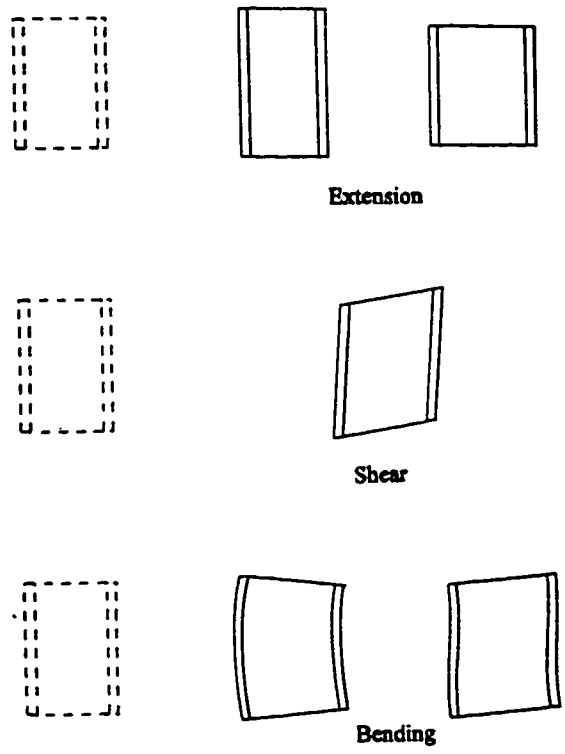


Figure 3.6 Deformation modes of a joint panel zone.

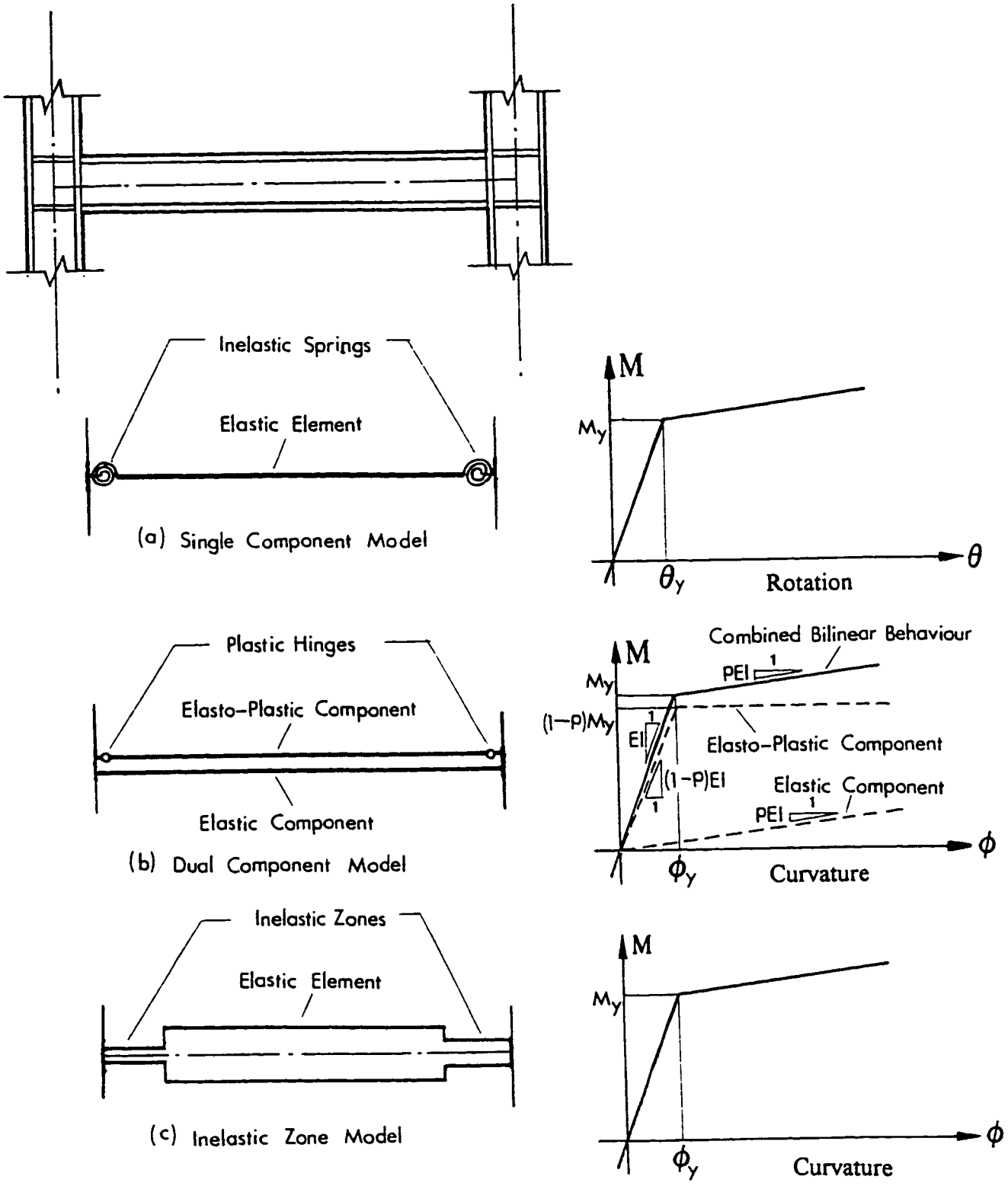


Figure 3.7 Analytical models for discrete member idealization

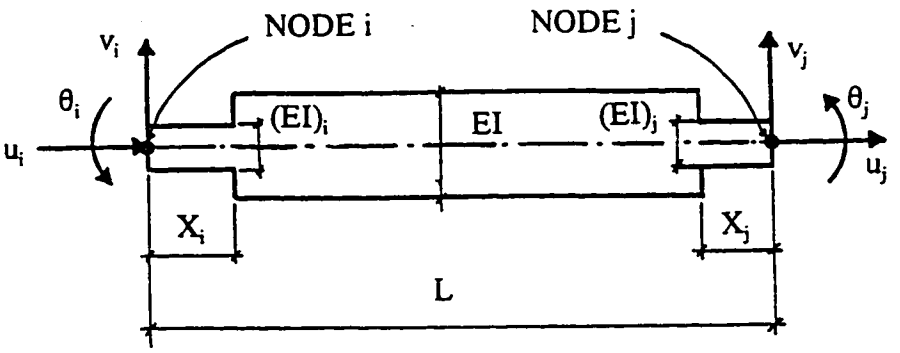


Figure 3.8 Degrees of freedom for the beam-column element.

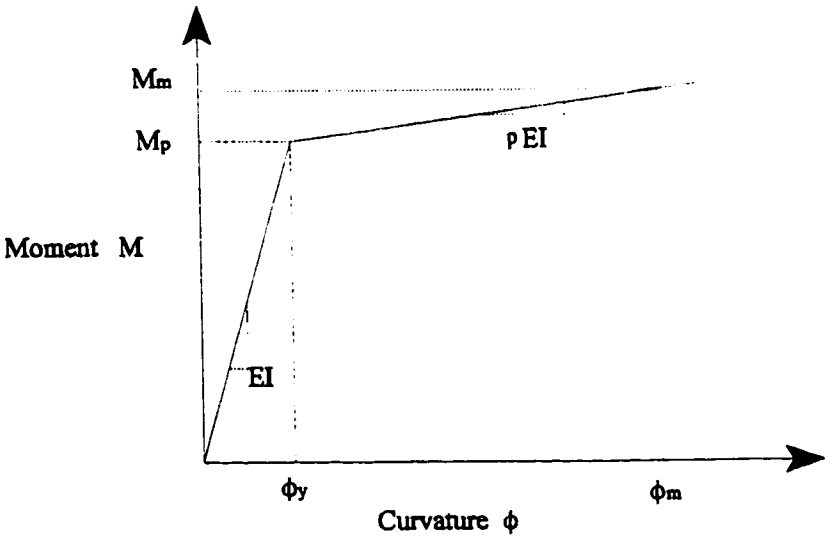


Figure 3.9 Idealized moment-curvature relationship.

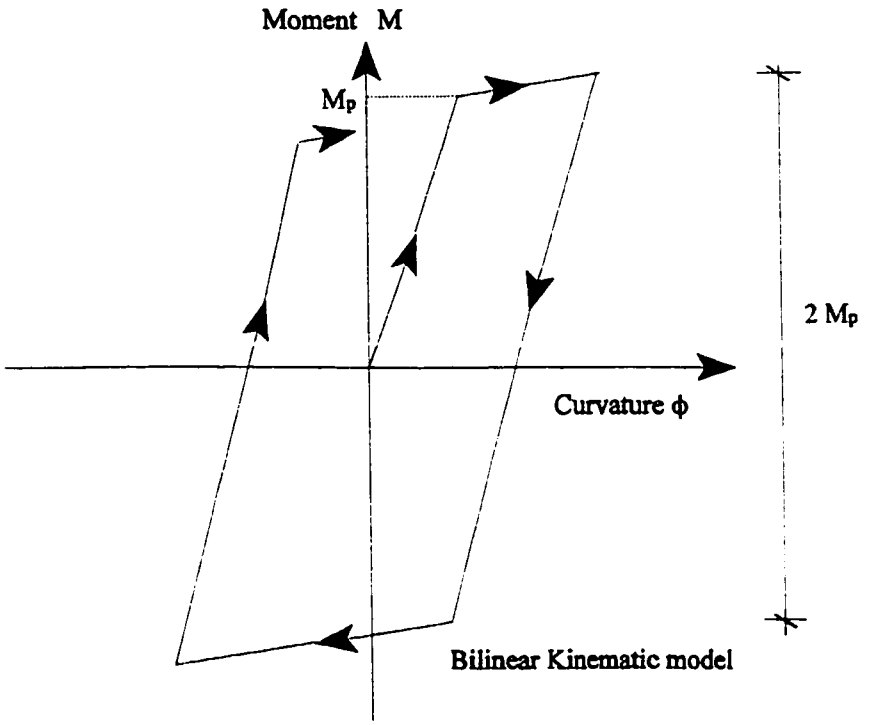


Figure 3.10 Bilinear hysteretic model for moment-curvature relationship.

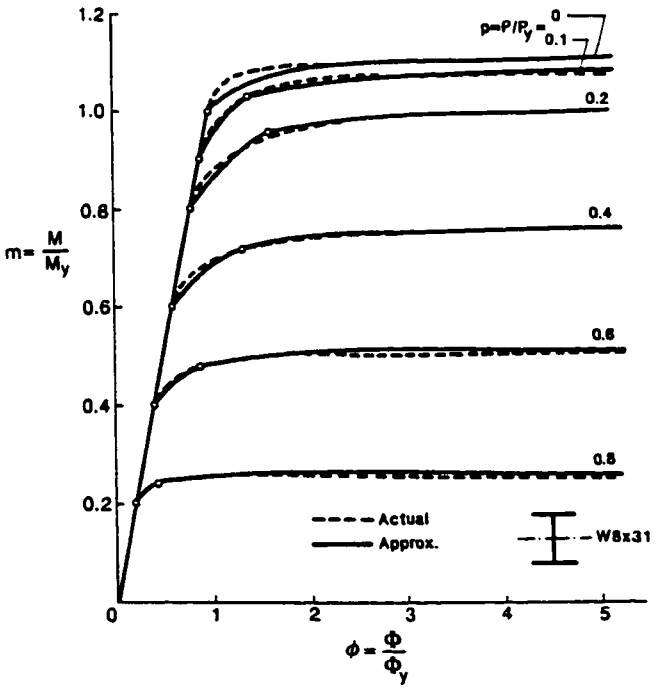


Figure 3.11 Effect of axial force on the moment-curvature relationship (after Chen and Lui, 1991).

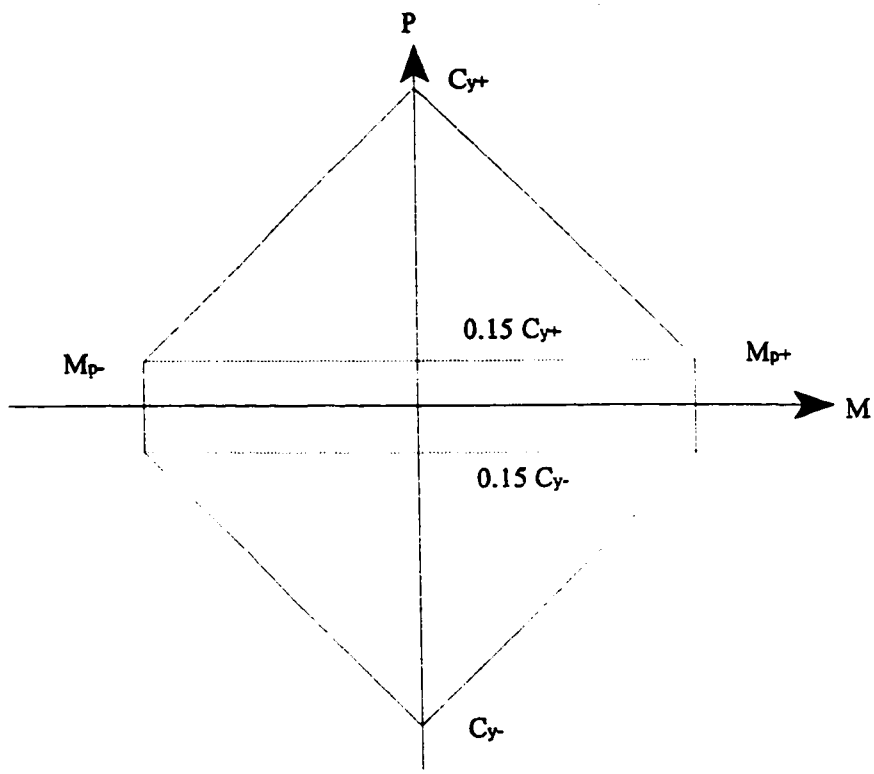


Figure 3.12 Interaction curve for beam-column model (class 1 sections).

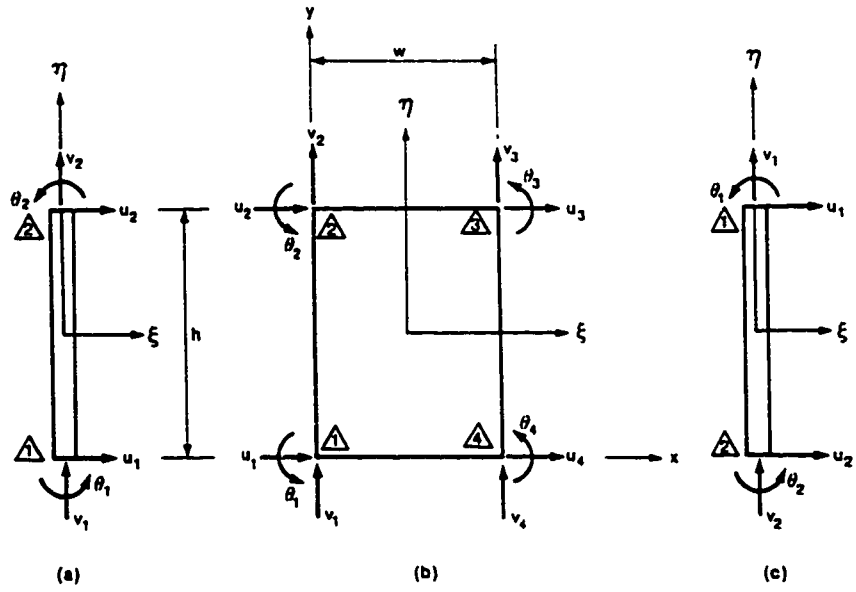


Figure 3.13 Finite element models for the web and flanges of a joint panel zone (after Lui and Chen, 1986).

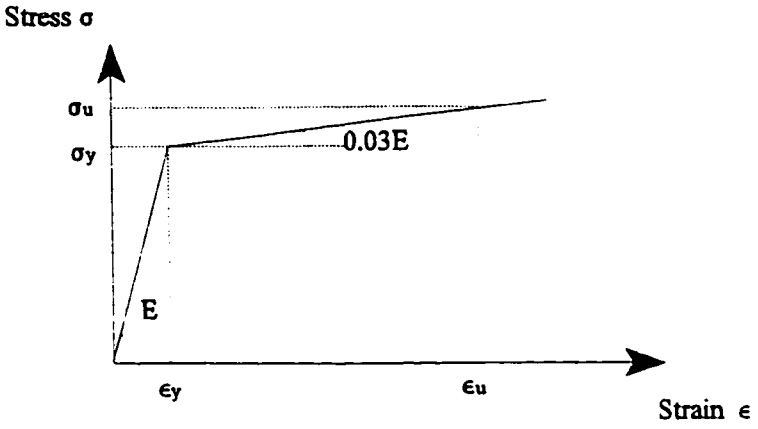


Figure 3.14 Idealized stress-strain curve for steel.

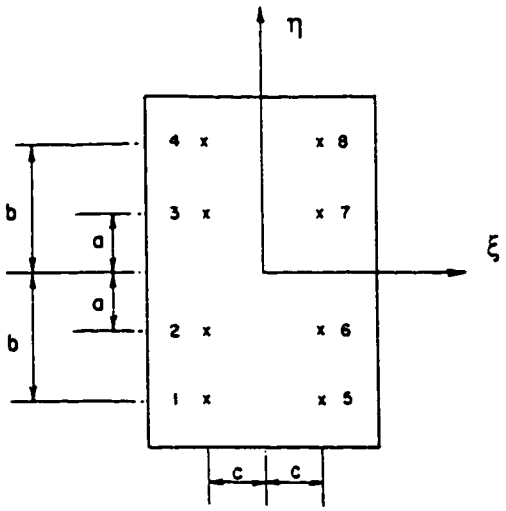


| Gauss point | Weight coefficients $W_i$ | $W_j$ |
|---|---|---|
| 1 | 1.00000 | 0.34785 |
| 2 | 1.00000 | 0.65215 |
| 3 | 1.00000 | 0.65215 |
| 4 | 1.00000 | 0.34785 |
| 5 | 1.00000 | 0.34785 |
| 6 | 1.00000 | 0.65215 |
| 7 | 1.00000 | 0.65215 |
| 8 | 1.00000 | 0.34785 |

a = 0.33998 h

b = 0.86114 h

c = 0.57735 w

Figure 3.15 Gauss points of the panel web element.

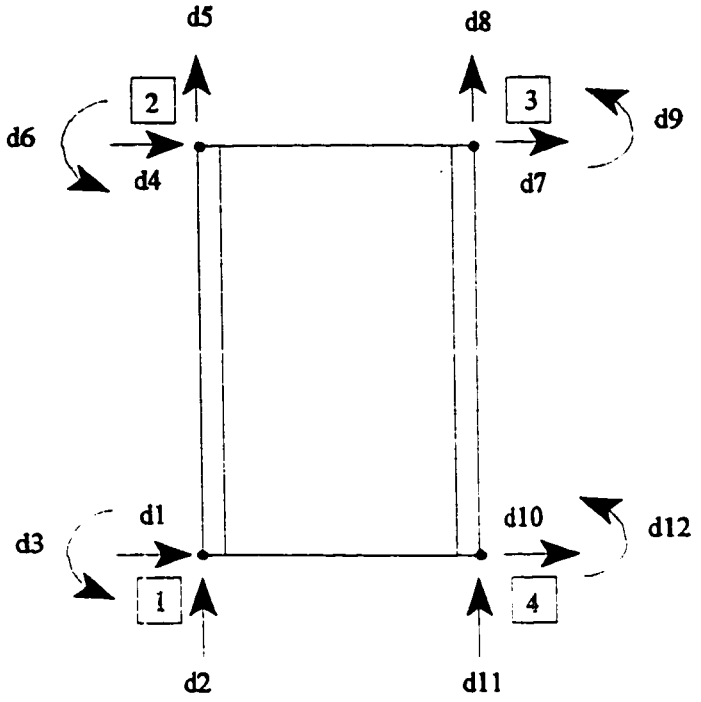


Figure 3.16 Degrees of freedom of a joint panel.

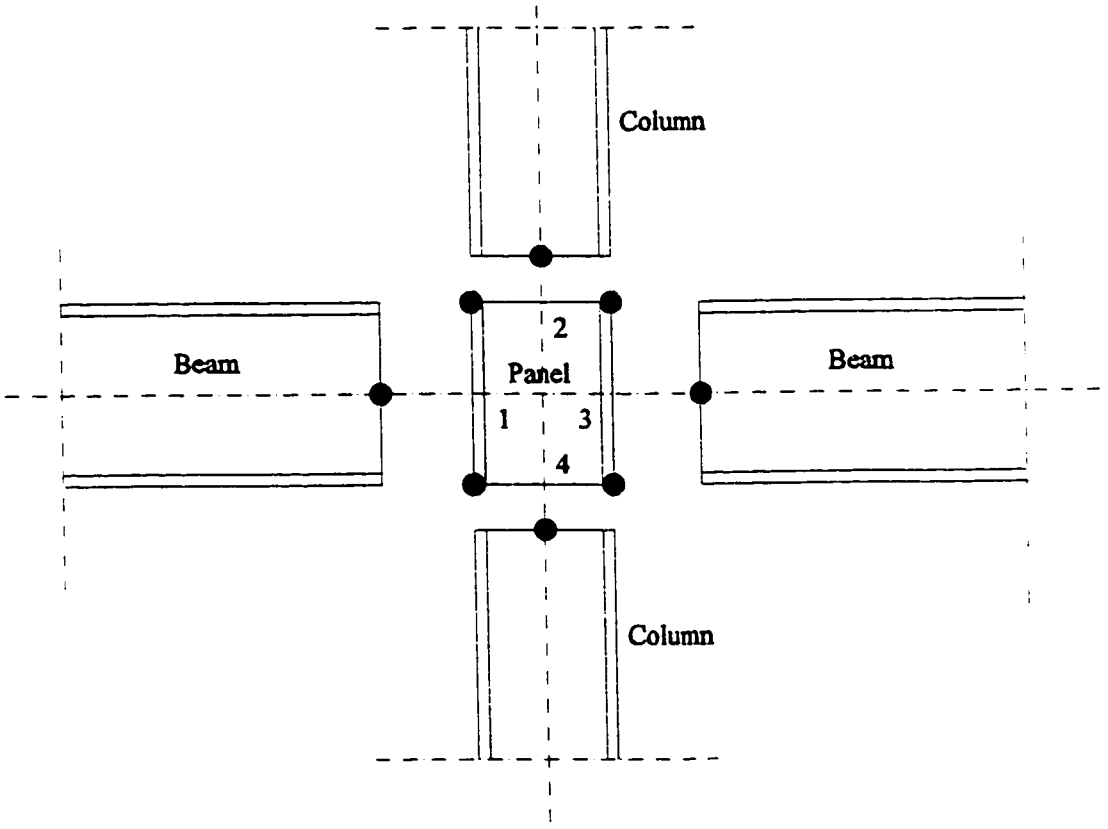


Figure 3.17 Face numbering of a joint panel.

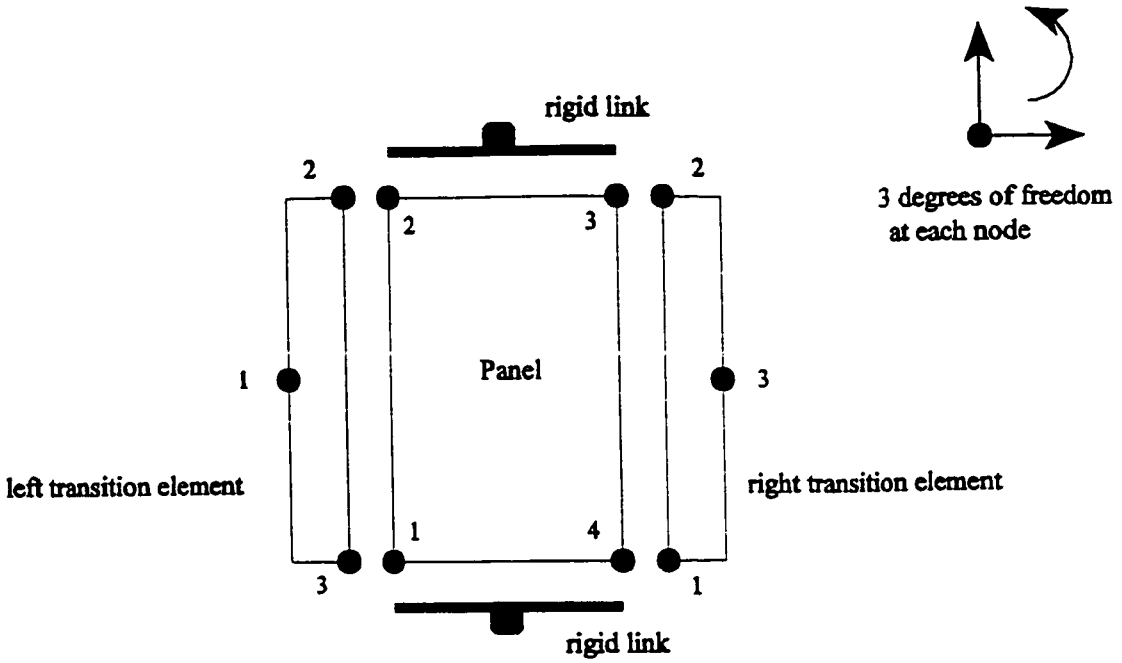


Figure 3.18 Rigid link connecting a column and a panel zone, and transition element connecting a beam and a panel zone.

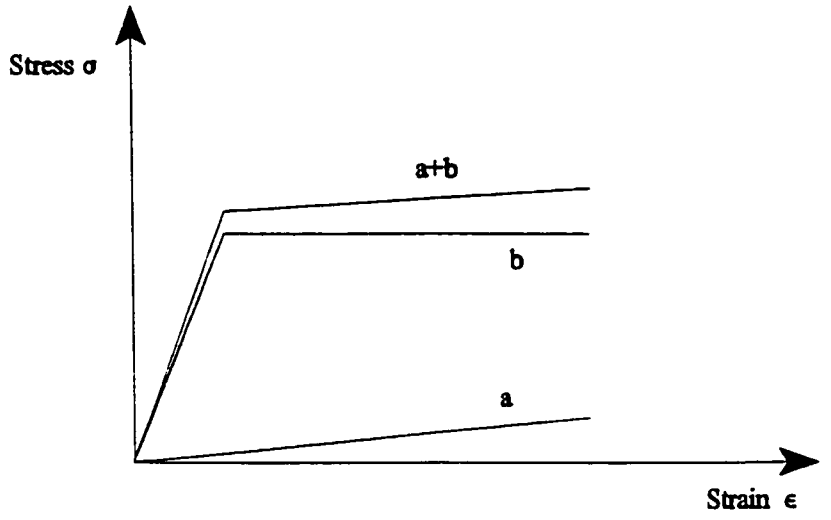


Figure 3.19 Parallel component model.

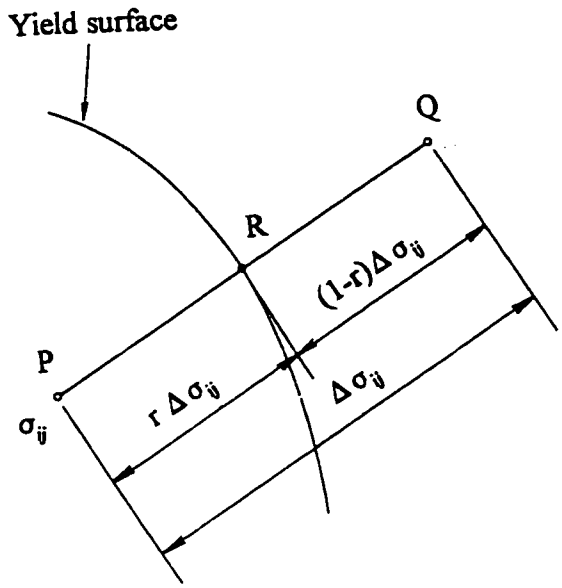


Figure 3.20 Scaling back to yield surface.

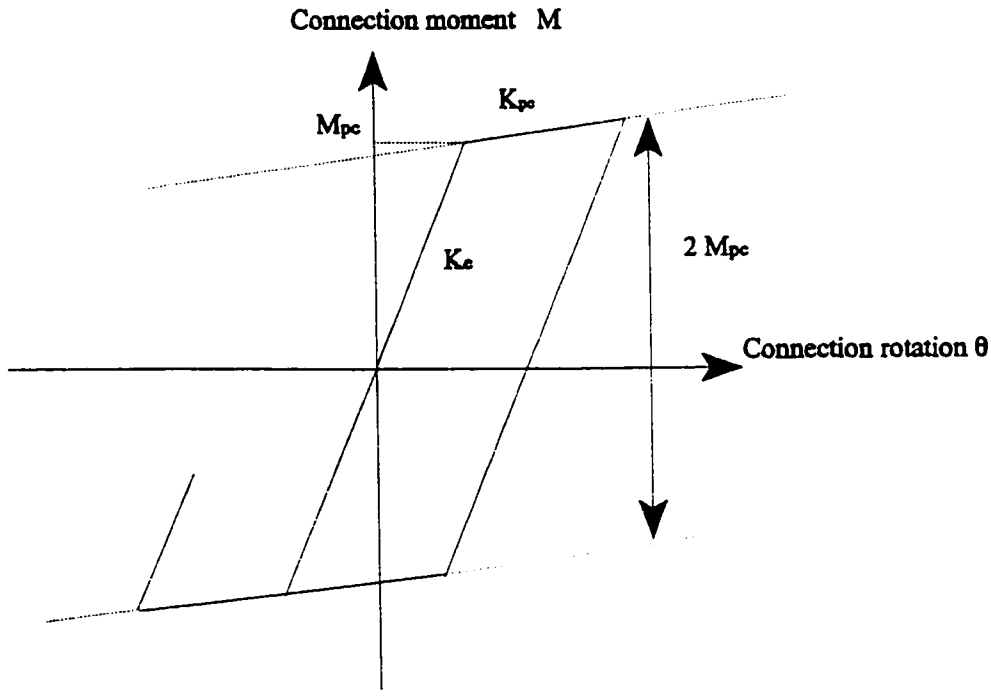


Figure 3.21 Moment-rotation behaviour of the connection element.

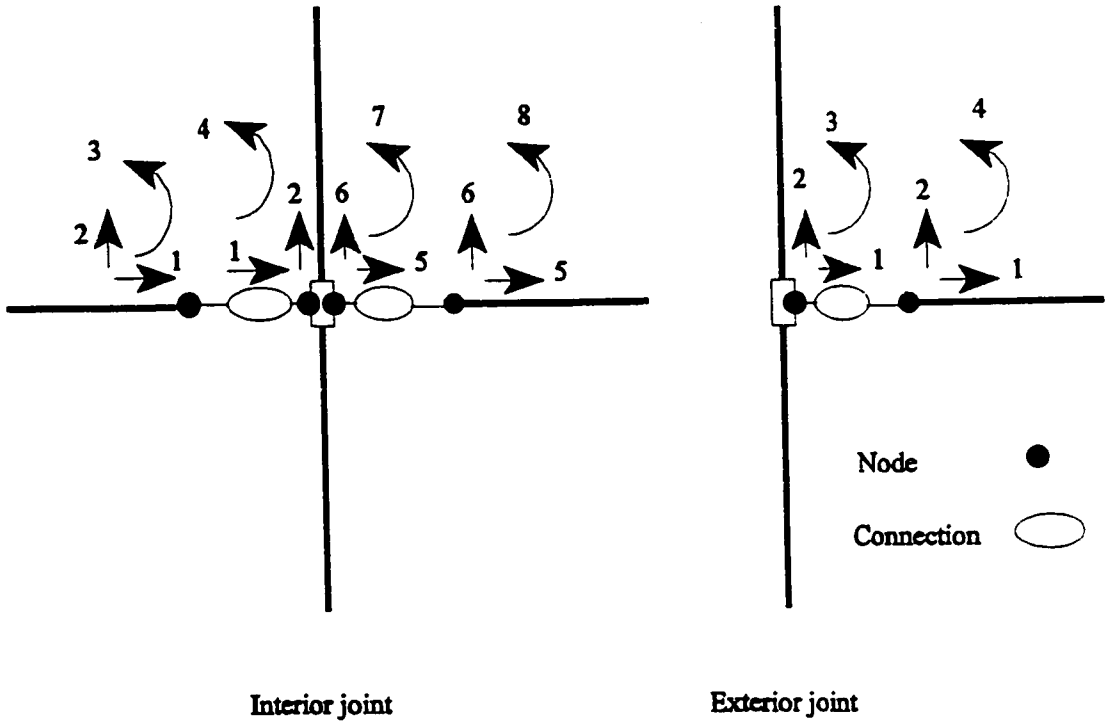


Figure 3.22 Idealization of semi-rigid connection element.

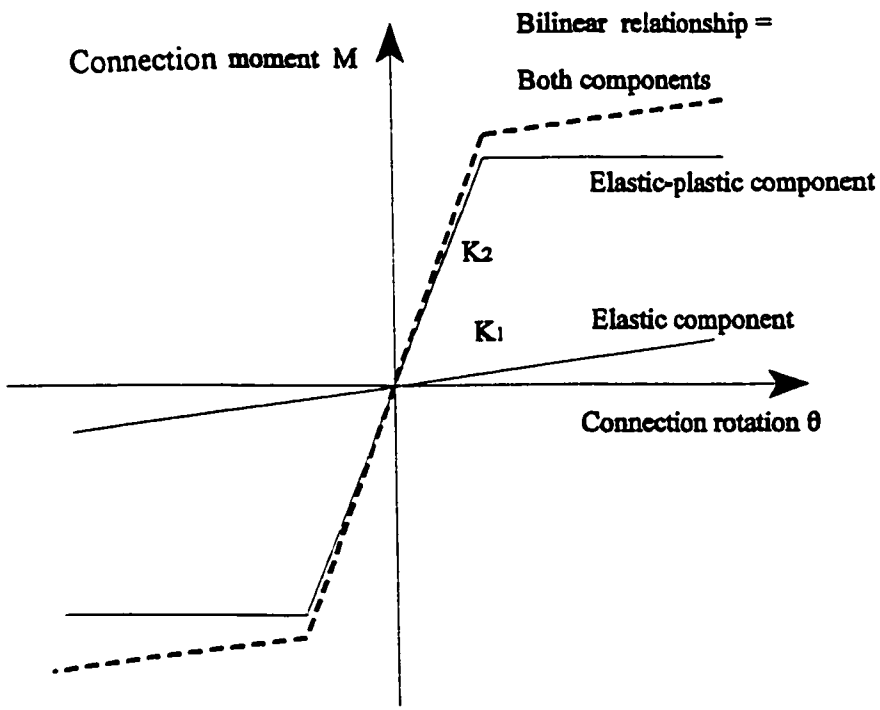


Figure 3.23 The connection element components.

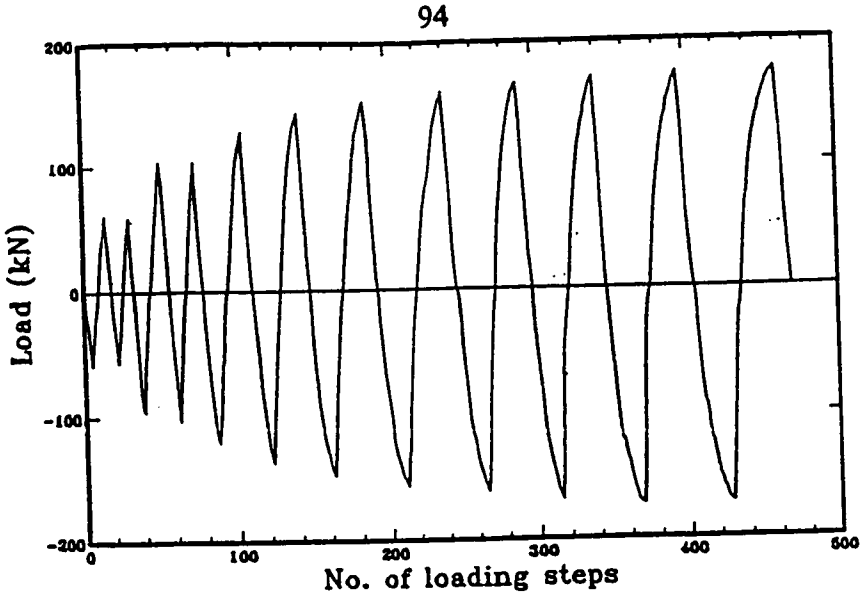


Loading history for specimen CB–1.

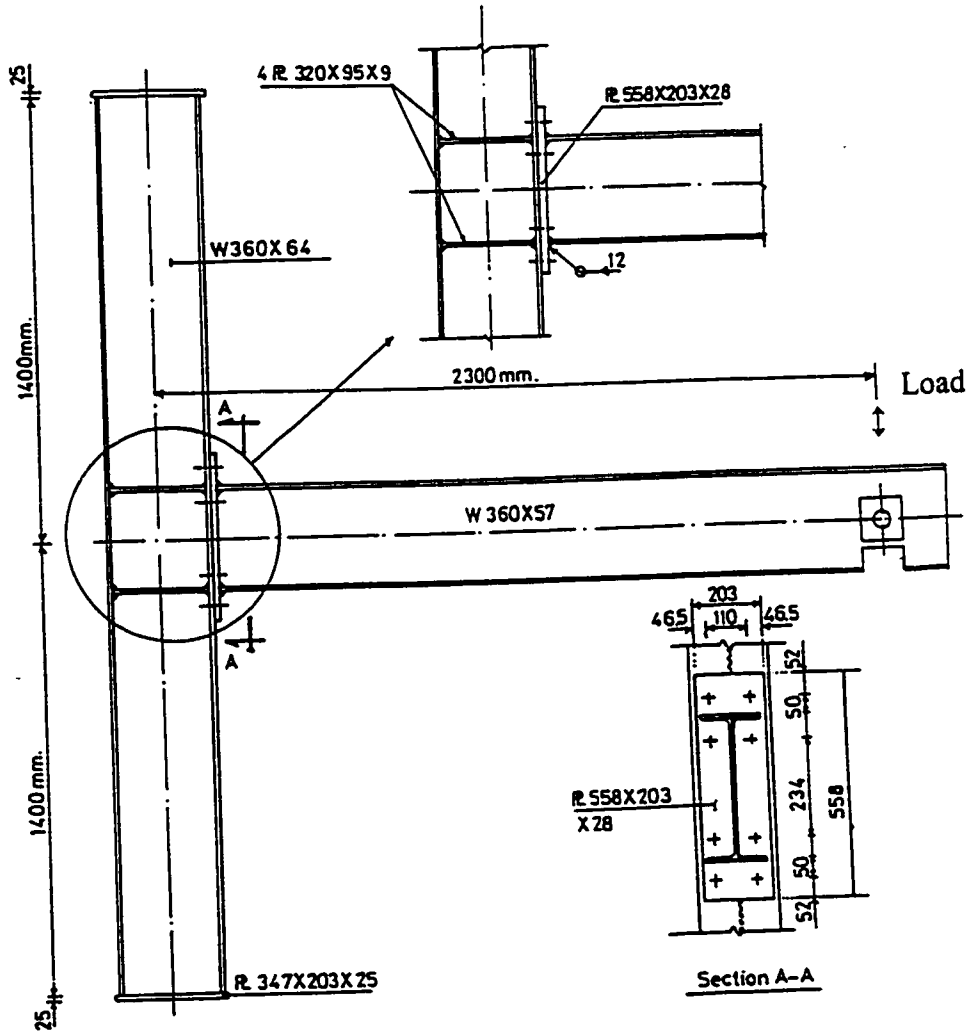


Figure 3.24 Details of specimen CB-1 and its loading history (after Osman, 1991).

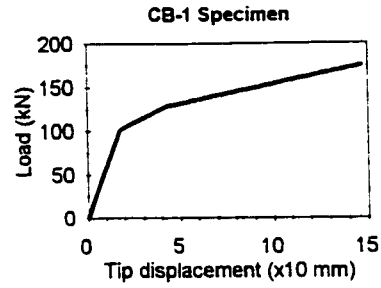


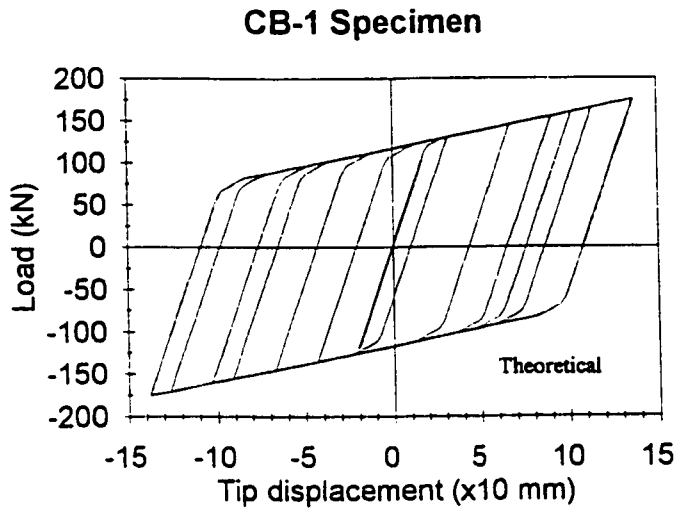


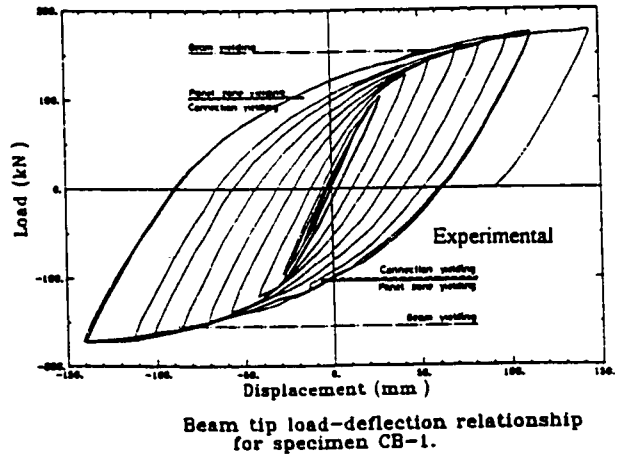


Beam tip load–deflection relationship for specimen CB–1.

Figure 3.25 Theoretical and experimental tip load-deflection relationship for specimen CB-1.

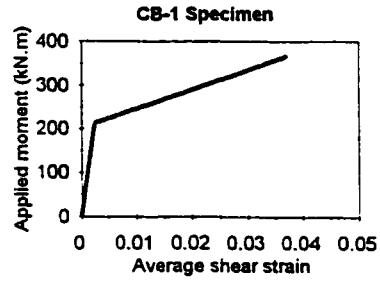


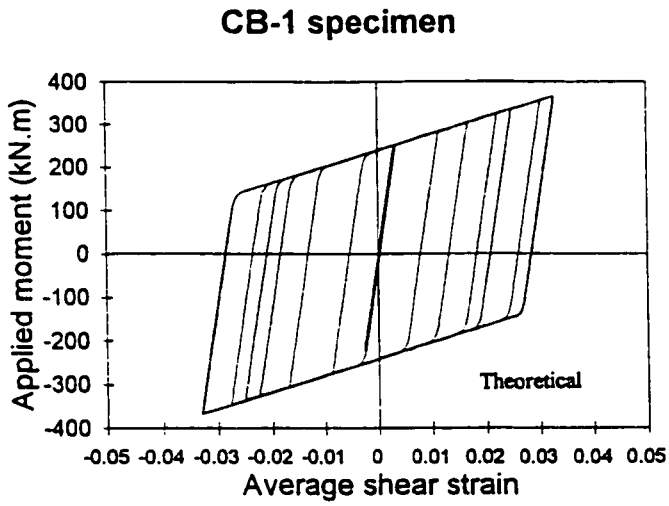


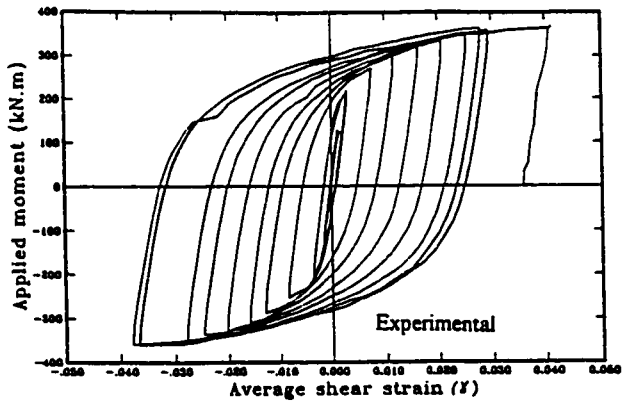


Figure 3.26 Theoretical and experimental applied moment-versus panel average shear strain for specimen CB-1.

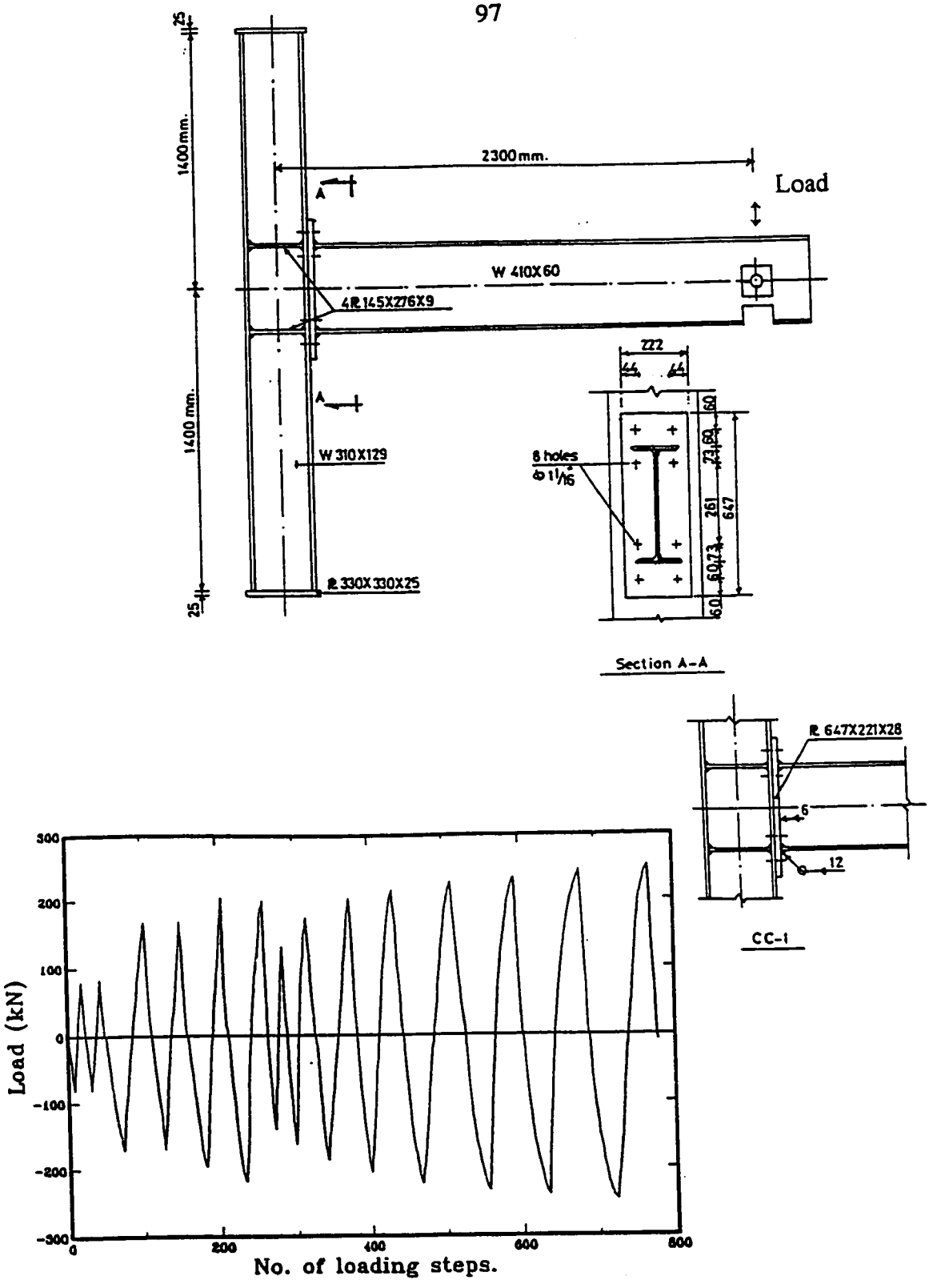


Figure 3.27 Details of specimen CC-1 and its loading history (after Osman, 1991).

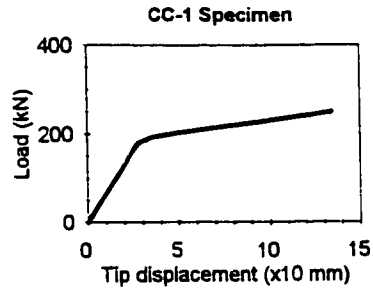


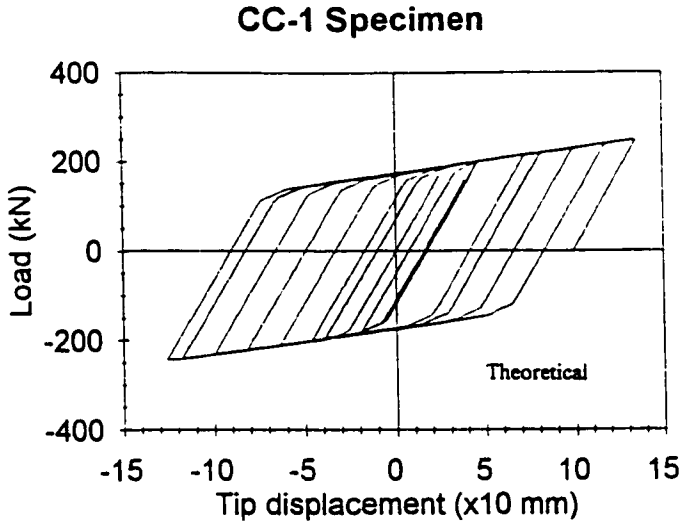


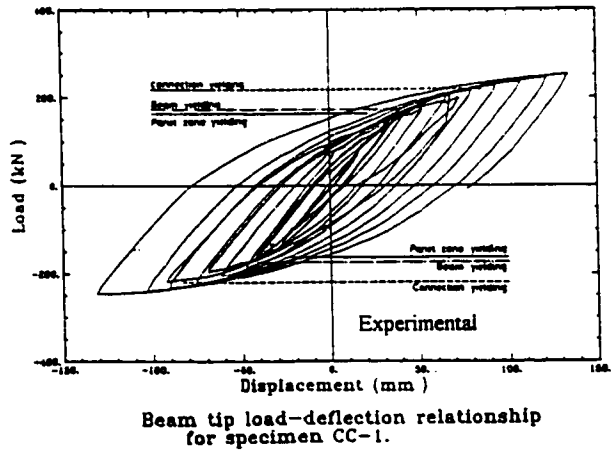


Beam tip load-deflection relationship for specimen CC-1.

Figure 3.28 Theoretical and experimental tip load-deflection relationship for specimen CC-1.

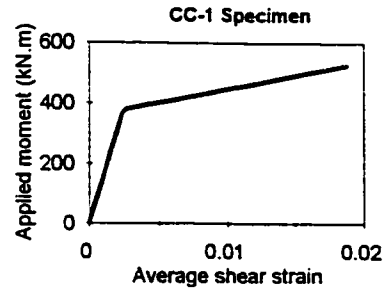


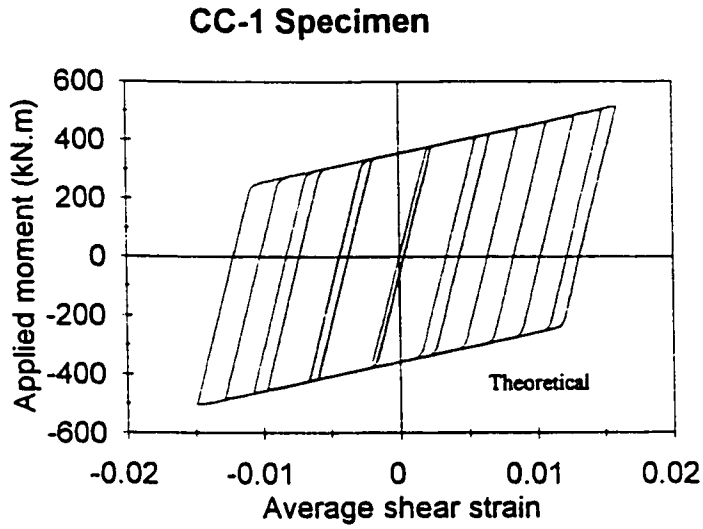


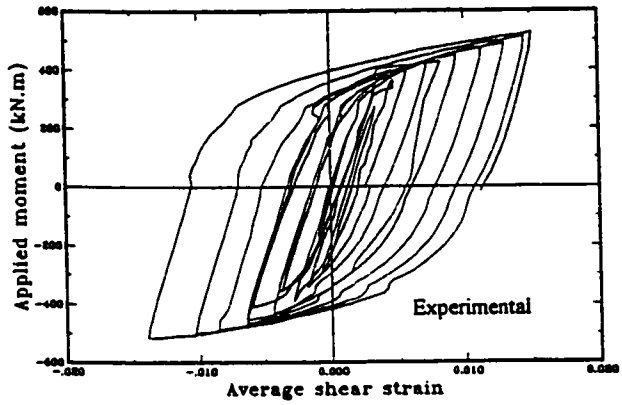


Figure 3.29 Theoretical and experimental applied moment-versus panel average shear strain for specimen CC-1.

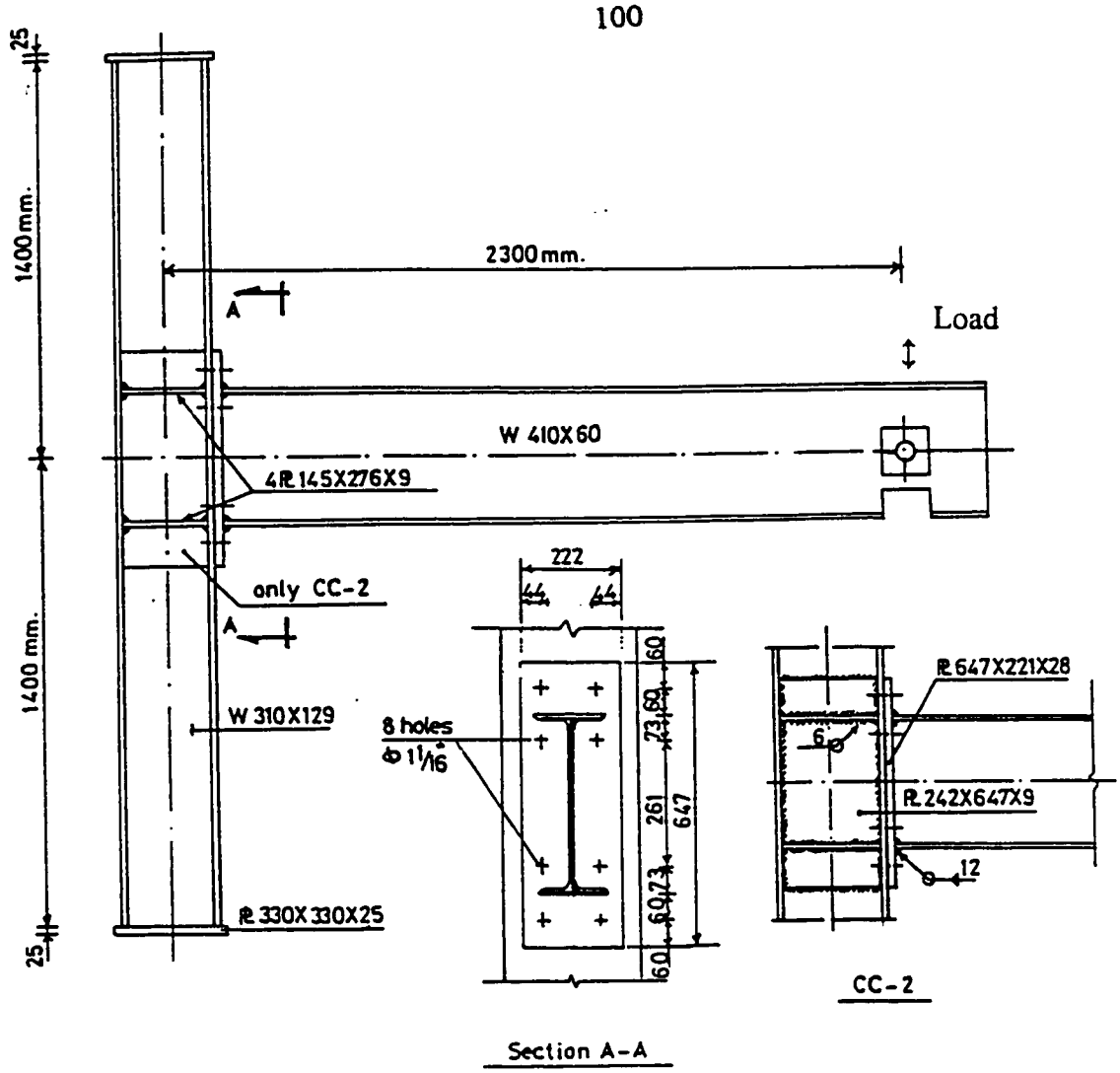


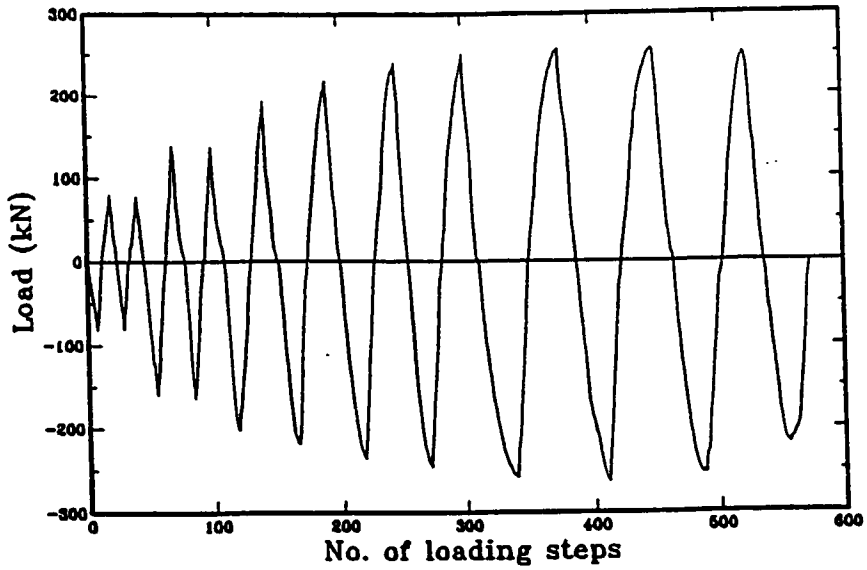


Figure 3.30 Details of specimen CC-2 and its loading history (after Osman, 1991).

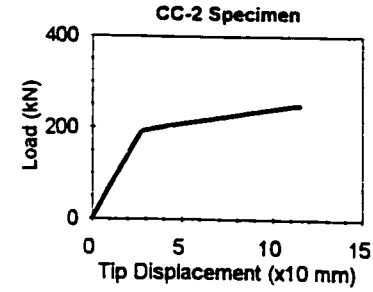


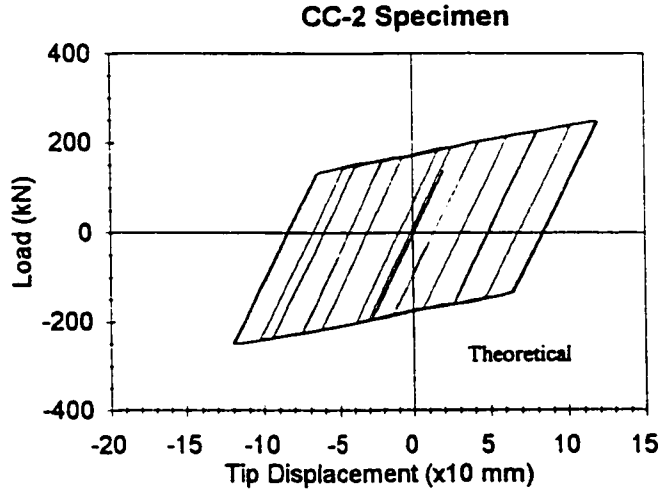


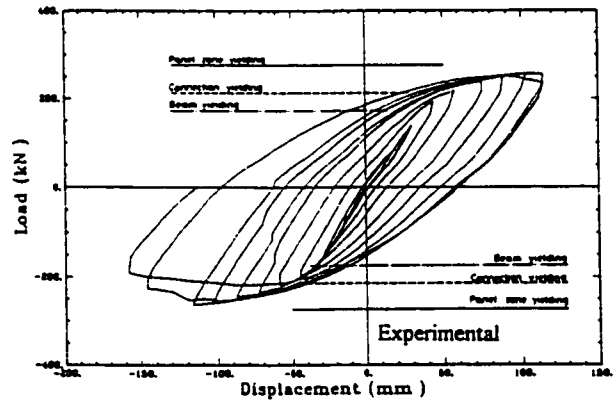


Beam tip load-deflection relationship for specimen CC-2.

Figure 3.31 Theoretical and experimental tip load-deflection relationship for specimen CC-2.

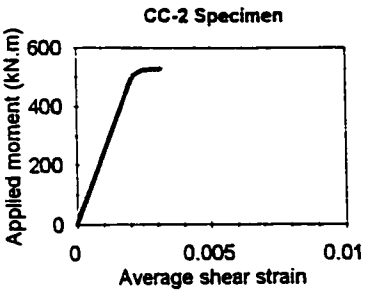


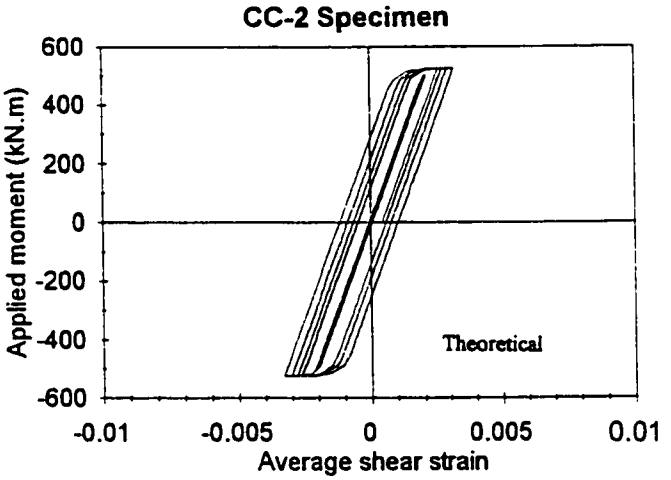


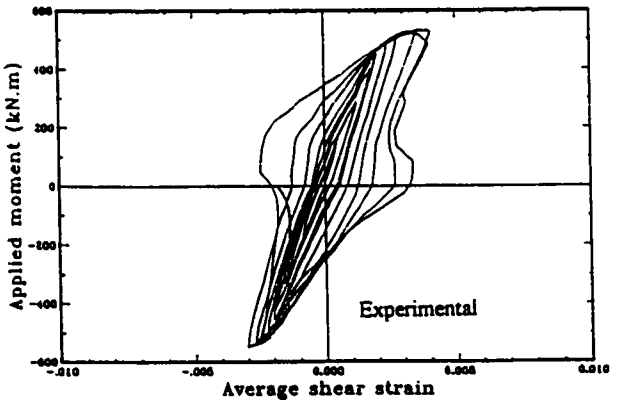


Figure 3.32 Theoretical and experimental applied moment-versus panel average shear strain for specimen CC-2.

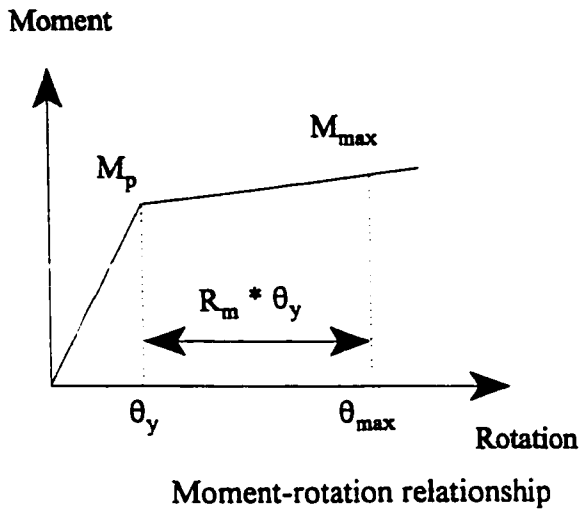


Figure 3.33 Determination of maximum rotation capacity for steel beams.

$c = p / 2 t_w \sigma_y$ if neutral axis is in the web

$c = (p - A_g \sigma_y + d b_f \sigma_y) / 2 b_f \sigma_y$ if neutral axis in the flange

$A_g$ = gross cross-section area
$\sigma_y$ = yield stress

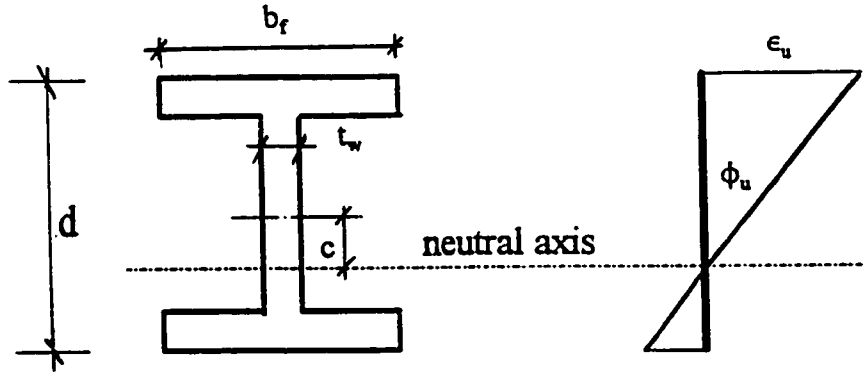


Figure 3.34 Neutral axis location for a steel section subjected to axial load and bending moment about the major axis.

# CHAPTER 4

# DESIGN OF STEEL OFFICE BUILDINGS

## 4.1 GENERAL LAYOUT AND NOTATIONS

Ductile moment resisting steel frames are widely used as structural framing systems for low to medium height office buildings located in seismic regions. To cover a wide range of different cases in this study, two basic office buildings with heights of six and ten storeys are considered. The two buildings have the same floor plan, as shown in Figure 4.1, which represents a three-bay by four-bay rectangular steel office building that has a floor area of 768 $m^2$. The total height of the six and ten storey buildings are 22.5 m and 36.9 m as shown in Figures 4.2 and 4.3 respectively. The bay width in both directions (E-W, and N-S) is 8 m. The storey height for the buildings is 4.5 m for the ground floor, and 3.6 m for all other floors. The lateral load resisting system of the buildings consists of perimeter braced steel frames in the N-S direction (column lines 1 and 4) and perimeter moment resisting steel frames in the E-W direction (column lines A and E). The gravity load is supported by interior core columns in addition to the perimeter system. Therefore, the interior columns carry gravity loads only.

In this study, the perimeter moment resisting steel frames are considered for analysis and design. Thus, a typical perimeter MRF in the E-W direction is expected to resist 50%

of the lateral load in that direction but carry only 12.5% of the total gravity loads. This system is similar to systems widely used in North America (Tahara and Kamei, 1988). Therefore, the results and conclusions of this thesis are applicable for the case in which the ratio of gravity load to lateral load tributary area is in the neighbourhood of 1:4

The frame design cases that are included in the study and the notation given for each frame are shown in Table 4.1. The classification of seismic hazard levels in Table 4.1 is in accordance with Canadian seismic zoning (NBCC, 1995), in which seismic hazard is represented explicitly by the zonal peak horizontal ground velocity (v) at an exceedance probability of 10% in 50 years. Examples of each level are: **i) High** seismic hazard (e.g. **Victoria**, B.C., v = 0.3 m/s), **ii) Intermediate** seismic hazard (e.g. **Vancouver**, B.C., v = 0.2 m/s) and **iii) Low** seismic hazard (e.g. **Montreal**, Que., v = 0.1 m/s).

## 4.2 MATERIAL PROPERTIES AND DESIGN LOADING

### 4.2.1 Material properties

For the purpose of design, nominal values are taken for the material properties in this study. Structural steel used is grade 300 W in accordance with standard CAN/CSA-G40.21-92 (CSA, 1992), where the yield strength is 300 MPa and the steel is weldable steel. Slabs are made of normal density concrete. The material properties used in this study are summarized in Table 4.2.

### 4.2.2 Gravity loading

The design gravity loading for the buildings consists of dead and live loads. The design

dead load includes the following:

1) weight of the flooring system (metal deck; concrete slab and cement-lime topping): this was assumed as 3.4 kPa for the typical floors, and 4.0 kPa for the mechanical floor.

2) the exterior window wall system: this was assumed as 1.65 kPa over the exterior surface of the building for the office floors.

3) the interior core walls for the mechanical floor: this was assumed as 2.0 kPa over the wall surface area.

4) the load of permanent equipment on the mechanical floor: this was assumed as 2.0 kPa.

5) the self-weight of columns and beams: this was assumed as an average 2.5 and 2.0 kN/m height for exterior and interior columns respectively, and 1.5 kN/m span for the beams.

6) superimposed load on floor slabs: this is to account for tiled ceiling and suspended system; ducts; pipes; wiring allowance; carpeting; and partitions. The assumed load for this purpose is 0.5 kPa for the mechanical floor and the roof, and 1.6 kPa for typical floors.

7) Snow; ice; and rain loads: these vary with location according to NBCC(1995); for the purpose of the study a typical value of 1.5 kPa on the roof was assumed.

The design live loads were taken as those suggested by NBCC (1995) for ordinary office buildings. The selected values are 2.4 kPa for typical floors; 3.6 kPa for the mechanical floor, and a minimum value of 1.0 kPa for the roof.

Typical structural distribution of the above loads, where the concrete slabs are one-way type and simply supported by beams through steel deck, was done using the tributary area method provided in NBCC(1995) to determine gravity loads (dead and live) acting on each perimeter moment resisting steel frame.

### 4.2.3 Seismic loading

In order to be consistent in comparing the seismic behaviour of frames located in regions of different seismic hazard levels, it was assumed that lateral loads in all cases would be dominated by earthquake loads rather than wind loads. For determining the base shear as specified in the NBCC(1995), the weights of the six and ten storey buildings were calculated as dead load (including the permanent equipment load on the mechanical floor) plus 25% of snow load on the roof. The weight of the six storey building was 31300 kN, while the weight of the ten storey building was 52500 kN. The minimum base shear V was determined as specified in NBCC 1995 (Clause 4.1.9.1):

$$V = \left( \frac{V_e}{R} \right) U \qquad (4.1)$$

where, $V_e$ = the equivalent lateral seismic force representing elastic response.

R = the force modification factor.

U = a force calibration factor equal 0.6.

"R" was selected as 4, which is applicable for ductile moment resisting steel frame buildings. The elastic design base shear, $V_e$, is given by:

$$V_e = v\ S\ I\ F\ W \qquad (4.2)$$

where, v = the zonal velocity ratio.

S = the seismic response factor.

I = the seismic importance factor.

F = the foundation factor.

W = the weight of the structure, consisting of dead load plus 25% of the

design snow load.

The seismic response factor is calculated as:

$$S = \frac{1.5}{\sqrt{T}} \quad \text{for } T \geq 0.5 \text{ sec} \tag{4.3}$$

where, T = fundamental period of vibration of the structure in sec.

= 0.1 N

where, N = total number of storeys of the building.

while another formula is also given by the NBCC(1995) for calculating the fundamental period of a moment resisting frame structure, i.e.:

$$T = 0.085(H)^{3/4} \tag{4.4}$$

where H is the total height of the moment resisting frame in metres, the formula T=0.1N was used in this study, thus resembling actual design practice. Also, the formula T=0.1N generates the largest design base shear forces, i.e. the most conservative approach.

The buildings are of normal importance and are assumed to be located on rock or stiff soil, so that both I and F are equal to 1.0.

The frames base shears for all the design cases are listed in Table 4.3. The lateral seismic base shear on a frame, $V_{frame}$, was distributed to each floor using the equation given in the NBCC(1995):

$$F_x = \frac{(V_{frame} - F_t)\, W_x\, h_x}{\sum_{i=1}^{N} W_i\, h_i} \tag{4.5}$$

where,

$W_i$ , $W_x$ = portion of W assigned to level i or x respectively.

$h_i$ , $h_x$ = heights of level i or x above ground.

N = total number of storeys in the building.

$F_x$ = lateral load at level x.

$F_t$ = portion of $V_{frame}$ to be concentrated at the top of the structure in addition to $F_N$.

level "i" is any level in the building, and level "x" is that level under consideration.

$F_t$ is intended to account for higher mode effects and it is given as:

$$F_t = 0.07TV_{frame} < 0.25V_{frame}, \text{ if } T>0.7 \text{ s} \quad (4.6)$$

$$F_t = 0.0 \quad , \text{ if } T<0.7 \text{ s} \quad (4.7)$$

Thus, $V_{frame}$ was distributed to each floor as shown in Figures 4.2 and 4.3 for the six storey and ten storey frames respectively.

### 4.2.4 Load combinations

The frames are designed for the critical combinations of gravity and seismic loading based on the limit states design of steel structures (CAN/CSA-S16.1-94). Thus, the load combinations considered in the study are as follows:

$$1.25\,D + 1.5\,L \quad (4.8)$$

$$1.0\,D + 1.0\,E \quad (4.9)$$

$$1.0\,D + (0.5\,L + 1.0\,E) \quad (4.10)$$

in which D is the dead load, L is the live load, and E is the specified equivalent seismic load.

## 4.3 DESIGN PROCESS

### 4.3.1 Steel design computer program

The design was performed using the software computer program (SODA, Structure Optimization Design and Analysis), Version 3.3.1, developed by a research group in the Solid Mechanics Division, Civil Engineering Department, University of Waterloo (Waterloo Engineering Software, 1996).

The program automatically designs a steel framework under static loads (vertical and/or lateral loads), provided the structural geometry, member properties and loading conditions (load factors for load combinations) are given. SODA supports the use of several codes, including Canadian and American design codes. In this study, SODA was used to comply with CAN/CSA-S16.1-94.

The column sizes were allowed to change at every two floors, but exterior and interior columns were treated as different groups. Beams on the same floor level were specified to have the same section. The computer program was directed to select member sections first from a W shape (rolled wide flange sections) data base; if this was not possible, WWF shape (welded wide flange sections) was to be chosen. The member sizes follow the Canadian metric designation, where the member shape (W or WWF), is followed by nominal depth of the member in millimetres times the mass of the member per unit length in kilogrammes per meter.

In case of lateral loads, SODA takes into account the second order effect (P-$\Delta$) during the analysis and design of the frames. The analysis and design of the frames were carried out in an iterative process assuming rigid joints and based on centre-line to centre-line

dimensions, an approach likely to be followed in actual design practice. The gravity loads acting on the leaning interior gravity columns are not considered in the (P-Δ) analysis performed for the design.

### 4.3.2 Design philosophies

Based on the definition of each design philosophy, SCWB; WCSB and SCWP, trials were done during which the computer program was directed by assigning sections for different elements which satisfy both the conditions that defined the design philosophy (mentioned in Chapter 2) and the requirements of the Canadian steel design code. The analysis was refined until the final member sizes were selected. The final design for each frame was verified according to the design conditions of strength and displacement.

### 4.3.3 Code regulations and limitations

Storey drift is one of the major aspects in assessing the performance of a structure under earthquake loads. Seismic codes specify drift limits to be satisfied during the design in order to minimize nonstructural damage during earthquakes. NBCC(1995) specifies in Clause 4.1.9.2 that the storey drift obtained from an elastic analysis using the loads given in equation 4.5 will be multiplied by "R" and limited to 2% of the storey height. In the design process, the standard frames were assigned this drift limit in accordance with NBCC(1995).

As there is a direct link between the performance level and the maximum permissible storey drift, designers often tend to use a more conservative drift value than that specified by code provisions in order to reduce levels of damage, even for buildings of normal importance.

The special drift designed six storey frames (i.e. SP.I6SCWB; SP.I6WCSB and SP.I6SCWP) were assigned a drift limit of 1% rather than 2%.

The set of six storey frames (SP.I6 set) designed for such special drift limitation (i.e. 1%) gives an opportunity to investigate the effect of using such conservative drift limitation on the seismic performance and damage of steel MRFs.

During the design, all members were subjected to the following constraints conformed to clauses in (CAN/CSA-S16.1-94):

1) Maximum slenderness ratio limits (clauses 10.2.1 and 10.2.2)

2) Maximum width-thickness ratios for class 1 and class 2 sections (clause 11)

3) Axial compression strength (clause 13.3)

4) Section shear strength (clause 13.4.1.4)

5) Section bending strength (clauses 13.5 and 13.6)

6) Cross-sectional strength (clause 13.8.1a or 13.8.2 a)

7) Overall member strength ( clause 13.8.1b or 13.8.2 b)

8) Lateral torsional buckling strength ( clause 13.8.1 c or 13.8.2 c)

It was assumed that the secondary beams can provide bracing against lateral-torsional buckling at places where they are framed into the beams of the moment resisting frames. Therefore, the unbraced length for the beams of the frames was taken as 2.67m. For columns, out-of-plane bracing was assumed at both ends, so the effective length factors about both major and minor axis were taken as 1.0.

## 4.4 FINAL STRUCTURAL CONFIGURATION OF THE FRAMES

The design software gives only the column and beam sections. Hand calculations were made to ensure the relation between the strength of beams and the strength of columns at a beam-column joint, section classes, slenderness ratios, percentage of axial load on columns with respect to yield axial loads, panel zones strength and slenderness ratios and other rules mentioned in Chapter 2 were satisfied in accordance with the specification of each design philosophy. A number of trials were done, during which modifications were made in the sections selected for beams and columns, before a final design was achieved for each moment resisting frame. The final designs were verified to make sure that they conformed to clauses in CAN/CSA-S16.1-94. For the design of panel zones, depending on the requirements of the corresponding design philosophy, doubler plates were sometimes added to the thickness of the column webs to provide the panel zones web thicknesses that satisfy the required shear strength.

For cases of high and intermediate seismic hazard, drift limitations governed the design, while in the case of low seismic hazard the strength requirements governed the design. The final designs for the cases are presented in Tables 4.4 to 4.8. For each set of frames, i.e. H6, I6, L6, SP.I6 or I10, the beam and column sections in the SCWB and SCWP designs are the same; the SCWB panels are reinforced using doubler plates. The beams and columns in the WCSB design are different than in the other two designs; doubler plates are also required in WCSB design.

## 4.5 NATURAL PERIODS AND MODE SHAPES

Natural periods of a structure are important in determining its dynamic properties. An eigenvalue analysis for natural periods was performed using the PC-ANSR; masses are assumed to be lumped at nodes. Table 4.9 shows the vibrational periods of the first two modes for the different frame cases considered in this study. From this table, it can be seen that periods of the six storey frames are function of the level of seismic hazard, i.e. by increasing the level of seismic hazard the frames become stiffer and consequently the periods decrease. On the other hand, for frames designed for the same level of seismic hazard, but using different design philosophies, periods increase in the order: WCSB design, SCWB design and SCWP design. This indicates that the WCSB design philosophy results in the highest frame stiffness among the design philosophies due to the high beam stiffnesses used, then followed by the traditional SCWB design philosophy which results in lower beam stiffnesses, while the SCWP is the most flexible design philosophy due to the reduced panel thicknesses (i.e. reduced stiffnesses). However, the effect of the different design philosophies on the vibrational periods does not exceed 10%.

It can be observed that the fundamental periods of all the frames are much longer than the value $T = 0.1$ N suggested by NBCC(1995) for static design. This is because the analysis involved bare steel frames where:

1) the effects of floor connected with beams (diaphragm action) were not taken into account.

2) the stiffness contribution of the non structural elements, as infill walls, partitions was neglected.

In addition, the code would tend to under-estimate $T_1$ (i.e. to be conservative) rather than overestimate it. Goel and Chopra (1996) evaluated the code formulas for fundamental period of buildings. They found from the database of building periods (the database includes 42 steel MRF buildings) that the code formula leads to periods that are generally shorter than measured periods. Many measured period values exceed 1.5 times the calculated code values. Moreover, based on measured data obtained from actual steel frame buildings, Housner et al. (1963) found that the periods of steel frame buildings (fixed at the base) can be described by the equation:

$$T = 1.08 \sqrt{N} - 0.86 \qquad (4.11)$$

For N = 6 and N = 10 storeys considered in this study, the predicted periods would be 1.8 sec. for the six storey frames and 2.6 sec. for the ten storey frames. Those predicted values are comparable to the values calculated by PC-ANSR using eigenvalue analysis.

The mode shapes for the frames were also calculated. The design philosophy has very little effect on the first and second mode shapes in the elastic stage. For example, Tables 4.10 and 4.11 show the first and second mode shapes for the I6 and I10 sets of frames respectively. The most noticeable difference between the first mode shapes of the different designs is that the bottom floors in the WCSB design tend to have higher deflections relative to the top than those in the other designs.

## 4.6 WEIGHTS OF STEEL REQUIRED TO CONSTRUCT THE FRAME SKELETONS

In order to compare the amount of steel material used in the construction of each

frame, the weight of steel in each frame was calculated. In this study, the term "weight" refers to the frame skeleton only, i.e. weights of connection parts are not included. Assuming that moment resisting frames having the same height and designed under same load conditions have the same labour content and framing cost, then the frame that has the least weight of steel material is likely to be the most economical.

The weight of each of the steel frames is given in Table 4.12. In case of the H6, SP.I6 and I10 set of frames, the WCSB design requires more steel than the SCWB design, and this increase is in the order of about 15 to 20%. For both the I6 and L6 set of frames, the differences between steel requirements of the different design philosophies are small (i.e. practically negligible). The table also shows that the SCWP design requires the least weight of steel in each set of frames. However, the SCWP design is only 1% to 3% less in weight than the SCWB design which is an insignificant difference.

Table 4.1 Design cases included in the study and notation of each designed frame.

| Design basis | Number of storeys | Seismic hazard | Design Philosophy | | |
|---|---|---|---|---|---|
| | | | SCWB | WCSB | SCWP |
| NBCC | six | High (v=0.3 m/s) | H6SCWB | H6WCSB | H6SCWP |
| | | Intermediate (v=0.2 m/s) | I6SCWB | I6WCSB | I6SCWP |
| | | Low (v=0.1 m/s) | L6SCWB | L6WCSB | L6SCWP |
| NBCC* | | Intermediate (v=0.2 m/s) | SP.I6SCWB | SP.I6WCSB | SP.I6SCWP |
| NBCC | ten | Intermediate (v=0.2 m/s) | I10SCWB | I10WCSB | I10SCWP |

NBCC* : The design is based on a maximum storey drift limit of 1% rather than the NBCC limit of 2%, i.e. special drift limit.

Table 4.2 Material properties

| | |
|---|---|
| Yield strength of steel | $F_y = 300$ MPa |
| Modulus of elasticity of steel | E = 200,000 MPa |
| Shear modulus of steel | G = 77,000 MPa |
| Density of steel | $\gamma_{steel} = 78.5$ kN/m$^3$ |
| Density of concrete | $\gamma_{concrete} = 23.5$ kN/m$^3$ |

Table 4.3 The design base shear ($V_{frame}$) for each of the moment resisting frames

| Frame notation | Frame design base shear "$V_{frame}$" kN |
|---|---|
| H6SCWB | 1369 |
| H6WCSB | 1369 |
| H6SCWP | 1369 |
| I6SCWB | 912 |
| I6WCSB | 912 |
| I6SCWP | 912 |
| L6SCWB | 456 |
| L6WCSB | 456 |
| L6SCWP | 456 |
| SP-I6SCWB | 912 |
| SP-I6WCSB | 912 |
| SP-I6SCWP | 912 |
| I10SCWB | 1190 |
| I10WCSB | 1190 |
| I10SCWP | 1190 |

Table 4.4 Member sizes and panel zone designs for the H6 set of frames

H6SCWB Frame — Designed for peak ground velocity = 0.3 m/sec
Design philosophy: Strong column-weak beam

| Storey | Exterior Column | Interior Column | Beam | Doubler plates added to the panel(mm) Exterior Panel - Interior Panel |
|---|---|---|---|---|
| 1 | WWF 400x362 | WWF 450x409 | W 610x140 | 1 PL. @ 8 - 2 PL. @ 16 |
| 2 | WWF 400x362 | WWF 450x409 | W 610x140 | 1 PL. @ 8 - 2 PL. @ 14 |
| 3 | WWF 400x220 | WWF 450x248 | W 610x140 | 2 PL. @ 6 - 2 PL. @ 16 |
| 4 | WWF 400x220 | WWF 450x248 | W 610x125 | 1 PL. @ 8 - 2 PL. @ 12 |
| 5 | WWF 400x178 | WWF 450x228 | W 610x125 | 1 PL. @ 8 - 2 PL. @ 12 |
| 6 | WWF 400x178 | WWF 450x228 | W 530x101 | 1 PL. @ 6 - 2 PL. @ 10 |

H6WCSB Frame — Designed for peak ground velocity = 0.3 m/sec
Design philosophy: Weak column-strong beam

| Storey | Exterior Column | Interior Column | Beam | Doubler plates added to the panel(mm) Exterior Panel - Interior Panel |
|---|---|---|---|---|
| 1 | WWF 350x263 | WWF 400x273 | W 610x241 | 2 PL. @ 16 - 2 PL. @ 30 |
| 2 | WWF 350x263 | WWF 400x273 | W 610x241 | 2 PL. @ 16 - 2 PL. @ 30 |
| 3 | WWF 350x212 | WWF 400x220 | W 610x217 | 2 PL. @ 16 - 2 PL. @ 30 |
| 4 | WWF 350x212 | WWF 400x220 | W610x217 | 2 PL. @ 16 - 2 PL. @ 30 |
| 5 | WWF 350x155 | WWF 400x202 | W610x217 | 2 PL. @ 18 - 2 PL. @ 30 |
| 6 | WWF 350x155 | WWF 400x202 | W610x125 | 2 PL. @ 8 - 2 PL. @ 16 |

H6SCWP Frame — Designed for peak ground velocity = 0.3 m/sec
Design philosophy: Strong column-weak panel

| Storey | Exterior Column | Interior Column | Beam | Doubler plates added to the panel (mm) Exterior Panel - Interior Panel |
|---|---|---|---|---|
| 1 | WWF 400x362 | WWF 450x409 | W 610x140 | No - No |
| 2 | WWF 400x362 | WWF 450x409 | W 610x140 | No - No |
| 3 | WWF 400x220 | WWF 450x248 | W 610x140 | No - 1 PL. @ 6 |
| 4 | WWF 400x220 | WWF 450x248 | W 610x125 | No - No |
| 5 | WWF 400x178 | WWF 450x228 | W 610x125 | No - No |
| 6 | WWF 400x178 | WWF 450x228 | W 530x101 | No - No |

Table 4.5 Member sizes and panel zone designs for the I6 set of frames

I6SCWB Frame Designed for peak ground velocity = 0.2 m/sec
Design philosophy: Strong column-weak beam

| Storey | Exterior Column | Interior Column | Beam | Doubler plates added to the panel(mm) Exterior Panel - Interior Panel |
|---|---|---|---|---|
| 1 | W 310x202 | WWF 400x303 | W 610x125 | 2 PL. @ 6 - 2 PL. @ 16 |
| 2 | W 310x202 | WWF 400x303 | W 610x125 | 2 PL. @ 6 - 2 PL. @ 16 |
| 3 | W 310x143 | WWF 400x220 | W 610x113 | 2 PL. @ 6 - 2 PL. @ 14 |
| 4 | W310x143 | WWF 400x220 | W 610x101 | 2 PL. @ 6 - 2 PL. @ 12 |
| 5 | W 310x107 | WWF 400x178 | W 610x101 | 2 PL. @ 6 - 2 PL. @ 12 |
| 6 | W 310x107 | WWF 400x178 | W 360x64 | 1 PL. @ 8 - 2 PL. @ 8 |

I6WCSB Frame Designed for peak ground velocity = 0.2 m/sec
Design philosophy: Weak column-strong beam

| Storey | Exterior Column | Interior Column | Beam | Doubler plates added to the panel(mm) Exterior Panel - Interior Panel |
|---|---|---|---|---|
| 1 | W 310x202 | W 310x226 | W 610x174 | 2 PL. @ 12 - 2 PL. @ 30 |
| 2 | W 310x202 | W 310x226 | W 610x174 | 2 PL. @ 10 - 2 PL. @ 30 |
| 3 | W 310x129 | W 310x202 | W 610x140 | 2 PL. @ 10 - 2 PL. @ 20 |
| 4 | W310x129 | W 310x202 | W 610x125 | 2 PL. @ 8 - 2 PL. @ 20 |
| 5 | W 310x86 | W 310x118 | W 610x101 | 2 PL. @ 8 - 2 PL. @ 20 |
| 6 | W 310x86 | W 310x118 | W 360x64 | 1 PL. @ 10 - 2 PL. @ 12 |

I6SCWP Frame Designed for peak ground velocity = 0.2 m/sec
Design philosophy: Strong column-weak panel

| Storey | Exterior Column | Interior Column | Beam | Doubler plates added to the panel (mm) Exterior Panel - Interior Panel |
|---|---|---|---|---|
| 1 | W 310x202 | WWF 400x303 | W 610x125 | No - No |
| 2 | W 310x202 | WWF 400x303 | W 610x125 | No - No |
| 3 | W 310x143 | WWF 400x220 | W 610x113 | No - 1 PL. @ 4 |
| 4 | W310x143 | WWF 400x220 | W 610x101 | No - No |
| 5 | W 310x107 | WWF 400x178 | W 610x101 | No - No |
| 6 | W 310x107 | WWF 400x178 | W 360x64 | No - No |

Table 4.6 Member sizes and panel zone designs for the L6 set of frames

L6SCWB Frame — Designed for peak ground velocity = 0.1 m/sec
Design philosophy: Strong column-weak beam

| Storey | Exterior Column | Interior Column | Beam | Doubler plates added to the panel(mm) Exterior Panel - Interior Panel |
|---|---|---|---|---|
| 1 | W 310x202 | W 310x226 | W 460x97 | 1 PL. @ 4 - 2 PL. @ 12 |
| 2 | W 310x202 | W 310x226 | W 460x97 | 1 PL. @ 4 - 2 PL. @ 12 |
| 3 | W 310x129 | W 310x202 | W 460x97 | 2 PL. @ 6 - 2 PL. @ 12 |
| 4 | W 310x129 | W 310x202 | W 410x67 | 1 PL. @ 6 - 2 PL. @ 6 |
| 5 | W 310x74 | W 310x107 | W 410x67 | 2 PL. @ 6 - 2 PL. @ 12 |
| 6 | W 310x74 | W 310x107 | W 250x58 | 2 PL. @ 6 - 2 PL. @ 12 |

L6WCSB Frame — Designed for peak ground velocity = 0.1 m/sec
Design philosophy: Weak column-strong beam

| Storey | Exterior Column | Interior Column | Beam | Doubler plates added to the panel(mm) Exterior Panel - Interior Panel |
|---|---|---|---|---|
| 1 | W 310x158 | W 310x179 | W 530x109 | 2 PL. @ 6 - 2 PL. @ 20 |
| 2 | W 310x158 | W 310x179 | W 530x101 | 1 PL. @ 8 - 2 PL. @ 16 |
| 3 | W 310x118 | W 310x143 | W 530x101 | 2 PL. @ 6 - 2 PL. @ 16 |
| 4 | W 310x118 | W 310x143 | W 460x97 | 2 PL. @ 6 - 2 PL. @ 16 |
| 5 | W 310x74 | W 310x86 | W 460x97 | 2 PL. @ 8 - 2 PL. @ 20 |
| 6 | W 310x74 | W 310x86 | W 360x64 | 2 PL. @ 6 - 2 PL. @ 14 |

L6SCWP Frame — Designed for peak ground velocity = 0.1 m/sec
Design philosophy: Strong column-weak panel

| Storey | Exterior Column | Interior Column | Beam | Doubler plates added to the panel (mm) Exterior Panel - Interior Panel |
|---|---|---|---|---|
| 1 | W 310x202 | W 310x226 | W 460x97 | No - No |
| 2 | W 310x202 | W 310x226 | W 460x97 | No - No |
| 3 | W 310x129 | W 310x202 | W 460x97 | No - No |
| 4 | W 310x129 | W 310x202 | W 410x67 | No - No |
| 5 | W 310x74 | W 310x107 | W 410x67 | 1 PL. @ 6 - 1 PL. @ 2 |
| 6 | W 310x74 | W 310x107 | W 250x58 | 1 PL. @ 6 - No |

Table 4.7 Member sizes and panel zone designs for the SP.I6 set of frames

SP-I6SCWB Frame — Designed for peak ground velocity = 0.2 m/sec
Design philosophy: Strong column-weak beam
Drift limitation: 1% interstorey drift

| Storey | Exterior Column | Interior Column | Beam | Doubler plates added to the panel(mm) Exterior Panel - Interior Panel |
|---|---|---|---|---|
| 1 | WWF 350x315 | WWF 450x409 | W 610x217 | 2 PL. @ 14 - 2 PL. @ 30 |
| 2 | WWF 350x315 | WWF 450x409 | W 610x217 | 2 PL. @ 14 - 2 PL. @ 28 |
| 3 | WWF 350x263 | WWF 450x342 | W 610x195 | 2 PL. @ 12 - 2 PL. @ 22 |
| 4 | WWF 350x263 | WWF 450x342 | W 610x174 | 2 PL. @ 10 - 2 PL. @ 20 |
| 5 | WWF 350x176 | WWF 450x248 | W 610x174 | 2 PL. @ 12 - 2 PL. @ 22 |
| 6 | WWF 350x176 | WWF 450x248 | W 460x74 | 1 PL. @ 4 - 2 PL. @ 6 |

SP-I6WCSB Frame — Designed for peak ground velocity = 0.2 m/sec
Design philosophy: Weak column-strong beam
Drift limitation: 1% interstorey drift

| Storey | Exterior Column | Interior Column | Beam | Doubler plates added to the panel(mm) Exterior Panel - Interior Panel |
|---|---|---|---|---|
| 1 | WWF 350x315 | WWF 400x303 | W 610x341 | 2 PL. @ 18 - 2 PL. @ 38 |
| 2 | WWF 350x315 | WWF 400x303 | W 610x341 | 2 PL. @ 18 - 2 PL. @ 36 |
| 3 | WWF 350x212 | WWF 400x273 | W 610x241 | 2 PL. @ 16 - 2 PL. @ 28 |
| 4 | WWF 350x212 | WWF 400x273 | W 610x217 | 2 PL. @ 16 - 2 PL. @ 28 |
| 5 | WWF 350x155 | WWF 400x202 | W 610x174 | 2 PL. @ 14 - 2 PL. @ 24 |
| 6 | WWF 350x155 | WWF 400x202 | W 530x82 | 1 PL. @ 4 - 2 PL. @ 8 |

SP-I6SCWP Frame — Designed for peak ground velocity = 0.2 m/sec
Design philosophy: Strong column-weak panel
Drift limitation: 1% interstorey drift

| Storey | Exterior Column | Interior Column | Beam | Doubler plates added to the panel (mm) Exterior Panel - Interior Panel |
|---|---|---|---|---|
| 1 | WWF 350x315 | WWF 450x409 | W 610x217 | No - No |
| 2 | WWF 350x315 | WWF 450x409 | W 610x217 | No - No |
| 3 | WWF 350x263 | WWF 450x342 | W 610x195 | No - No |
| 4 | WWF 350x263 | WWF 450x342 | W 610x174 | No - No |
| 5 | WWF 350x176 | WWF 450x248 | W 610x174 | No - No |
| 6 | WWF 350x176 | WWF 450x248 | W 460x74 | No - No |

Table 4.8 Member sizes and panel zone designs for the I10 set of frames

I10SCWB Frame — Designed for peak ground velocity = 0.2 m/sec
Design philosophy: Strong column-weak beam

| Storey | Exterior Column | Interior Column | Beam | Doubler plates added to the panel(mm) Exterior Panel - Interior Panel |
|---|---|---|---|---|
| 1 | WWF 350x315 | WWF 450x409 | W 610x217 | 2 PL. @ 16 - 2PL. @ 30 |
| 2 | WWF 350x315 | WWF 450x409 | W 610x217 | 2 PL. @ 16 - 2 PL. @ 30 |
| 3 | WWF 350x238 | WWF 450x342 | W 610x174 | 2 PL. @ 10 - 2 PL. @ 20 |
| 4 | WWF 350x238 | WWF 450x342 | W 610x174 | 2 PL. @ 10 - 2 PL. @ 20 |
| 5 | WWF 350x176 | WWF 450x248 | W 610x125 | 1 PL. @ 12 - 2 PL. @ 14 |
| 6 | WWF 350x176 | WWF 450x248 | W 610x125 | 1 PL. @ 12 - 2 PL. @ 14 |
| 7 | WWF 350x155 | WWF 400x202 | W 610x113 | 1 PL. @ 12 - 2 PL. @ 14 |
| 8 | WWF 350x155 | WWF 400x202 | W 610x113 | 1 PL. @ 12 - 2 PL. @ 14 |
| 9 | W 310x158 | WWF 350x212 | W 610x113 | 1 PL. @ 10 - 2 PL. @ 16 |
| 10 | W 310x158 | WWF 350x212 | W 310x86 | 1 PL. @ 10 - 2 PL. @ 14 |

I10 WCSB Frame — Designed for peak ground velocity = 0.2 m/sec
Design philosophy: Weak column-strong beam

| Storey | Exterior Column | Interior Column | Beam | Doubler plates added to the panel(mm) Exterior Panel - Interior Panel |
|---|---|---|---|---|
| 1 | W 310x226 | WWF 400x303 | W 610x241 | 2 PL. @ 18 - 2 PL. @ 40 |
| 2 | W 310X226 | WWF 400x303 | W 610x241 | 2 PL. @ 18 - 2 PL. @ 38 |
| 3 | W 310x202 | WWF 400x273 | W 610x241 | 2 PL. @ 18 - 2 PL. @ 38 |
| 4 | W 310x202 | WWF 400x273 | W 610x217 | 2 PL. @ 16 - 2 PL. @ 34 |
| 5 | W 310x179 | WWF 400x243 | W 610x217 | 2 PL. @ 16 - 2 PL. @ 34 |
| 6 | W 310x179 | WWF 400x243 | W 610x217 | 2 PL. @ 16 - 2 PL. @ 34 |
| 7 | W 310x158 | WWF 400x202 | W 610x195 | 2 PL. @ 16 - 2 PL. @ 30 |
| 8 | W 310x158 | WWF 400x202 | W 610x195 | 2 PL. @ 16 - 2 PL. @ 30 |
| 9 | W 310x143 | WWF 350x212 | W 610x174 | 2 PL. @ 14 - 2 PL. @ 30 |
| 10 | W 310x143 | WWF 350x212 | W 610x125 | 2 PL. @ 8 - 2 PL. @ 18 |

I10SCWP Frame — Designed for peak ground velocity = 0.2 m/sec
Design philosophy: Strong column-weak panel

| Storey | Exterior Column | Interior Column | Beam | Doubler plates added to the panel (mm) Exterior Panel - Interior Panel |
|---|---|---|---|---|
| 1 | WWF 350x315 | WWF 450x409 | W 610x217 | No - No |
| 2 | WWF 350x315 | WWF 450x409 | W 610x217 | No - No |
| 3 | WWF 350x238 | WWF 450x342 | W 610x174 | No - No |
| 4 | WWF 350x238 | WWF 450x342 | W 610x174 | No - No |
| 5 | WWF 350x176 | WWF 450x248 | W 610x125 | No - 1 PL. @ 4 |
| 6 | WWF 350x176 | WWF 450x248 | W 610x125 | No - 1 PL. @ 4 |
| 7 | WWF 350x155 | WWF 400x202 | W 610x113 | No - No |
| 8 | WWF 350x155 | WWF 400x202 | W 610x113 | No - No |
| 9 | W 310x158 | WWF 350x212 | W 610x113 | No - No |
| 10 | W 310x158 | WWF 350x212 | W 310x86 | No - No |

Table 4.9 Vibrational periods of the first two modes for each of the moment resisting frames

| Frame notation | First mode period (sec) | Second mode period (sec) |
|---|---|---|
| H6SCWB | 1.92 | 0.64 |
| H6WCSB | 1.84 | 0.62 |
| H6SCWP | 2.00 | 0.66 |
| I6SCWB | 2.24 | 0.78 |
| I6WCSB | 2.17 | 0.78 |
| I6SCWP | 2.34 | 0.81 |
| L6SCWB | 3.00 | 1.15 |
| L6WCSB | 2.92 | 1.05 |
| L6SCWP | 3.10 | 1.18 |
| SP-I6SCWB | 1.82 | 0.64 |
| SP-I6WCSB | 1.75 | 0.63 |
| SP-I6SCWP | 1.95 | 0.68 |
| I10SCWB | 3.06 | 1.07 |
| I10WCSB | 2.91 | 0.98 |
| I10SCWP | 3.10 | 1.09 |

Table 4.10 Deformed mode shapes for the I6 set of frames

| Floor level | Deformed shapes | | | | | |
|---|---|---|---|---|---|---|
| | First mode shape | | | Second mode shape | | |
| | I6SCWB | I6WCSB | I6SCWP | I6SCWB | I6WCSB | I6SCWP |
| 6 | 1.00 | 1.00 | 1.00 | 1.00 | 1.00 | 1.00 |
| 5 | 0.90 | 0.90 | 0.89 | 1.59 | 1.46 | 1.63 |
| 4 | 0.76 | 0.76 | 0.75 | 1.53 | 1.38 | 1.60 |
| 3 | 0.58 | 0.58 | 0.57 | 0.70 | 0.71 | 0.76 |
| 2 | 0.38 | 0.4 | 0.37 | -0.63 | -0.61 | -0.62 |
| 1 | 0.19 | 0.24 | 0.18 | -2.00 | -1.92 | -2.07 |

Table 4.11 Deformed modes shapes for the I10 set of frames

| Floor level | Deformed shapes | | | | | |
|---|---|---|---|---|---|---|
| | First mode shape | | | Second mode shape | | |
| | I10SCWB | I10WCSB | I10SCWP | I10SCWB | I10WCSB | I10SCWP |
| 10 | 1.00 | 1.00 | 1.00 | 1.00 | 1.00 | 1.00 |
| 9 | 0.96 | 0.97 | 0.96 | 0.73 | 0.78 | 0.72 |
| 8 | 0.90 | 0.92 | 0.89 | 0.32 | 0.40 | 0.30 |
| 7 | 0.81 | 0.84 | 0.80 | -0.15 | -0.04 | -0.17 |
| 6 | 0.69 | 0.75 | 0.69 | -0.58 | -0.45 | -0.58 |
| 5 | 0.57 | 0.65 | 0.57 | -0.84 | -0.75 | -0.84 |
| 4 | 0.45 | 0.55 | 0.45 | -0.93 | -0.91 | -0.92 |
| 3 | 0.34 | 0.43 | 0.33 | -0.85 | -0.91 | -0.84 |
| 2 | 0.23 | 0.30 | 0.22 | -0.64 | -0.75 | -0.62 |
| 1 | 0.11 | 0.17 | 0.10 | -0.35 | -0.45 | -0.34 |

Table 4.12 Comparison between the weights of steel (skeleton only) to be used in constructing each of the moment resisting frames

| Frame notation | Weight of steel consumed in constructing the frame (kg) | Percentage of increase or decrease from the standard SCWB design |
|---|---|---|
| H6SCWB | 44520 | 0.0% |
| H6WCSB | 52300 | +17.5% |
| H6SCWP | 43630 | -2.0% |
| I6SCWB | 33490 | 0.0% |
| I6WCSB | 34640 | +3.5% |
| I6SCWP | 32650 | -2.5% |
| L6SCWB | 26400 | 0.0% |
| L6WCSB | 25930 | -1.75% |
| L6SCWP | 25940 | -1.70% |
| SP-I6SCWB | 53520 | 0.0% |
| SP-I6WCSB | 61450 | +15.0% |
| SP-I6SCWP | 51890 | -3.0% |
| I10SCWB | 73440 | 0.0% |
| I10WCSB | 84450 | +15.0% |
| I10SCWP | 71720 | -2.34% |

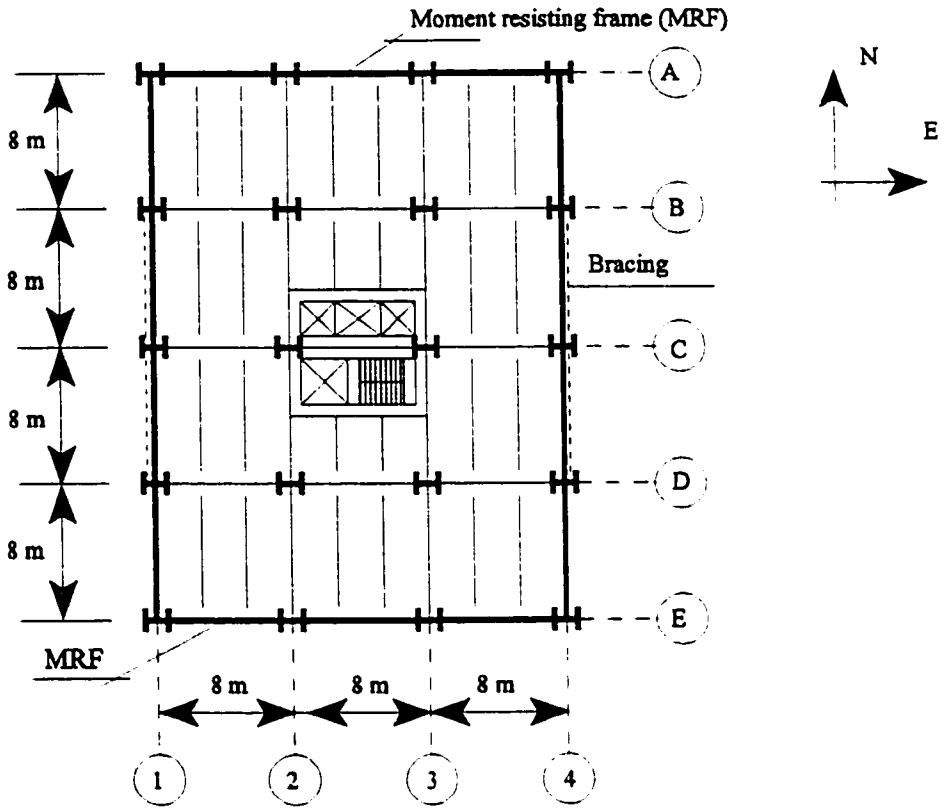


Figure 4.1 Floor plan of the steel office buildings.

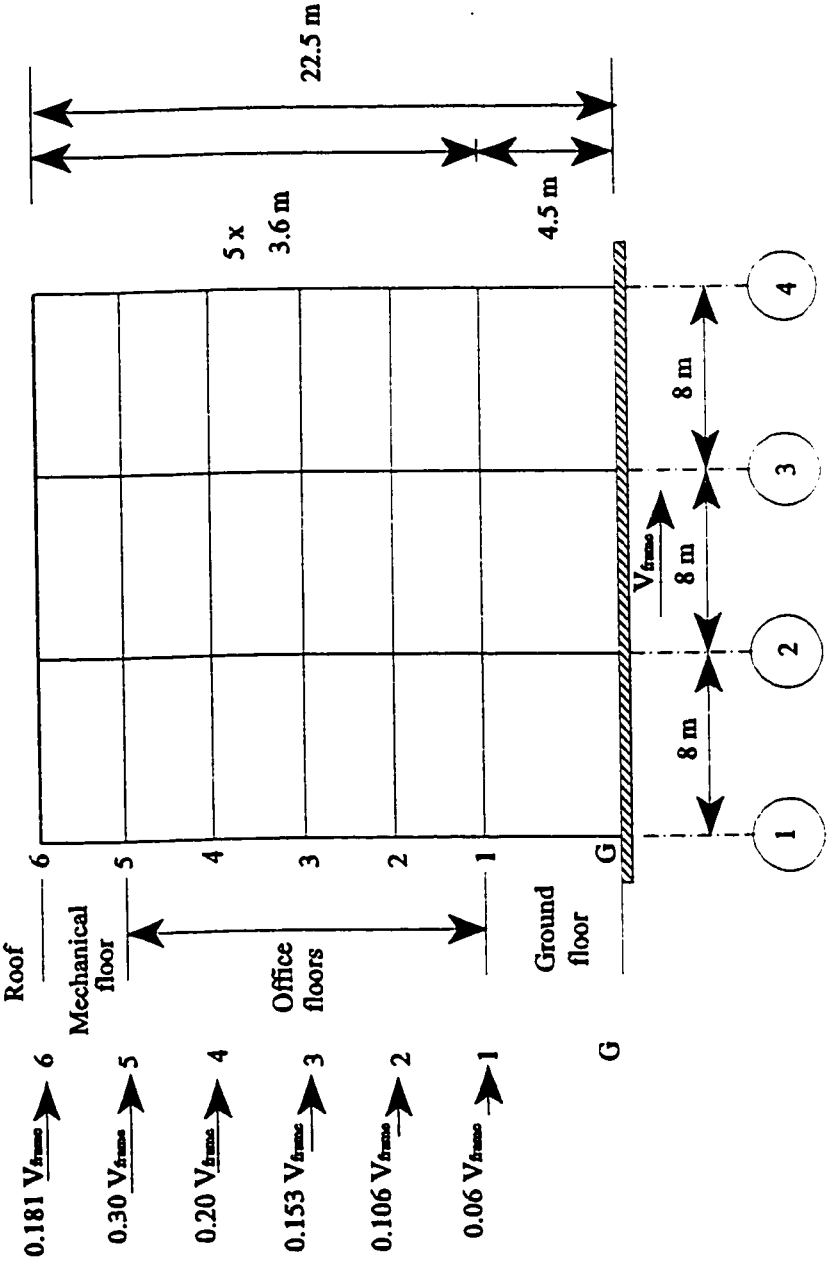


Figure 4.2 Elevation of the six storey moment resisting steel frame (column line A).

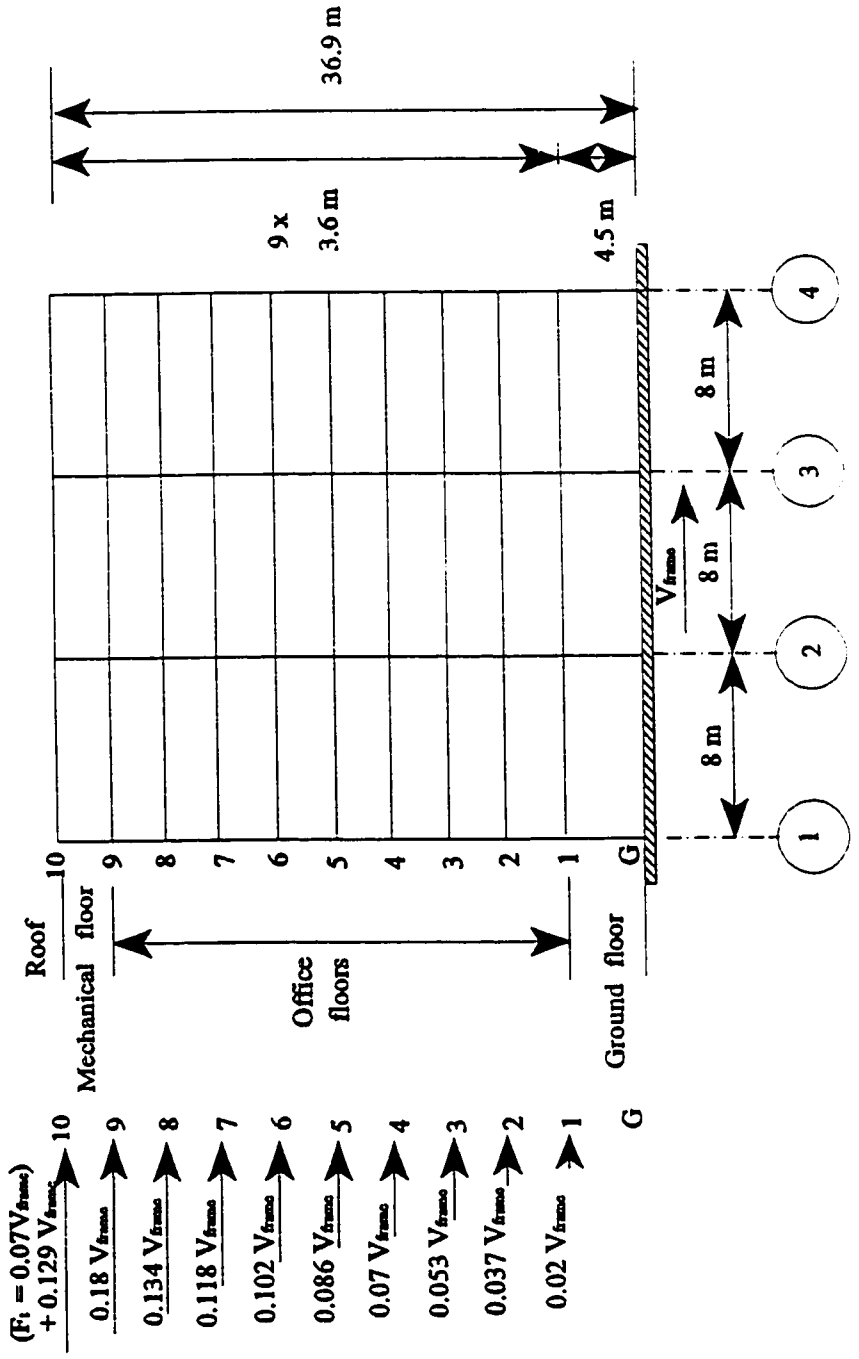


Figure 4.3 Elevation of the ten storey moment resisting steel frame (column line A).

# CHAPTER 5

# INPUT GROUND MOTIONS

## 5.1 GENERAL

This chapter contains a detailed description of the earthquake records selected as input ground motions for this study. Also included in this chapter is an analysis of the selected ground motion data. Different characteristics of the ground motions are presented, including the peak ground acceleration to peak ground velocity (A/V) ratio, and strong-motion duration.

The use of real earthquake records as input for inelastic dynamic analyses provides a realistic simulation of the seismic hazard for determination of structural response. Given the variability of actual ground motion records obtained under very similar conditions, it is important to use a number of different time histories and evaluate their influence on structural response and damage statistically. Visual inspection of different records shows that earthquake ground motions vary greatly from record to record. The intensity, duration of strong shaking and frequency content of any record depend on a number of factors, including the seismo-tectonic environment, the magnitude of the earthquake, the epicentral distance, the local geology and the site soil condition. These differences among records can lead to significant differences in structural responses.

Ground motion characteristics have a significant effect on the seismic response of structures. For ground motion records obtained from the same earthquake event, the peak values, frequency content, and duration of strong shaking may be different due to different distances from the source of energy release and different soil conditions at the recording site. Records from different earthquake events will show considerable variations. For engineering applications, many ground motion characterization parameters were used in the past. These parameters include peak ground motions, response spectra, spectrum intensity, Arias intensity, root mean square (RMS) acceleration or cumulative RMS function, and strong-motion duration. In this study, peak ground acceleration, peak ground velocity, A/V ratio, the spectral values, and strong-motion duration are used for ground motion characterization.

## 5.2 EARTHQUAKE DATA SET

The selection of time-histories to be used in inelastic dynamic analyses is an important task in the evaluation of the level of protection. In this study, while each of the two ensembles of time-histories selected in this study consists of 12 records, a large number of earthquake time-histories were studied in order to choose these 12 records. This number of earthquake records consists of 75 horizontal component of strong motion records from past earthquakes around the world given by Naumoski et al. (1993), in addition to 14 horizontal components from recent earthquake records, such as Landers (1992), Northridge (1994), and Big Bear (1992) earthquakes which were obtained from the strong motion information and data dissemination of California Division of Mines and Geology. All the time-histories are recorded on rock or stiff soil sites.

### 5.2.1 The first ensemble of time-histories (Ensemble "A")

This ensemble consists of twelve ground motion records. The primary criterion for the selection of these records was that the shapes of their response spectra be similar to that of the Newmark-Hall (1982) design spectrum. This was done by matching the mean (M) and mean plus one standard deviation (M+SD) spectral amplification factors with those of the Newmark-Hall spectrum at three periods that cover the range of the fundamental periods of the frames (1.5, 2.2, and 3 sec). Since the intensity of seismic hazard is expressed in terms of peak ground velocity of the record, $v_{max}$, the pertinent amplification factor is $S_a(T)/v_{max}$, in which $S_a(T)$ is the response spectral acceleration ordinate at period T.

Table 5.1 shows the Newmark-Hall spectrum velocity amplification factors for horizontal elastic response (N-H Factor), i.e. $S_v/v_{max}$, in which $S_v$ is the spectral velocity. Using the following relations:

$$S_a(T) = S_v(T).\ \omega = S_v(T) * [2\ \pi\ /\ T] \tag{5.1}$$

$$S_v(T) = v_{max}\ .[\text{N-H Factor}] \tag{5.2}$$

$$S_a(T)/v_{max} = [\text{N-H Factor}]\ .\ [2\ \pi\ /\ T] \tag{5.3}$$

where $\omega$ is the natural frequency under consideration; the target values of $S_a(1.5)/v_{max}$, $S_a(2.2)/v_{max}$ and $S_a(3)/v_{max}$ are presented in Table 5.2. The velocity amplification factors used in the above calculations are those corresponding to 5% damping which is the value assumed by NBCC(1995) for ordinary types of building structures. Tsai and Popov (1988), studied the effects of damping ratios on the response of the SDOF system under various ground acceleration records; they concluded that the response time-histories for 5% damped system are very similar to that of the 3% damped system (which is used for steel structures), and that

the differences are almost negligible.

A second selection criterion was that the records include a wide range of strong-motion durations, since damage will be very much related to the number of cycles of inelastic behaviour. For the purpose of selection of time-histories, the target was that the ensemble should include about 50% of the records with medium duration; 25% with short duration, and 25% with long duration. This distribution enables the variability of duration to be included in the statistical properties of the dynamic response.

Ensemble "A", selected on the basis of the above criteria, consists of twelve time-histories as shown in Table 5.3. The table presents a detailed description of each of the time-histories, including the values of the peak ground acceleration, peak ground velocity and their ratio. The actual statistical values of $S_a(T)/v_{max}$ calculated from the time-histories in ensemble "A" are shown in Table 5.2. The comparison of the actual values to the target values in Table 5.2 shows that the time-histories of ensemble "A" match the required target parameters at all the studied periods.

The strong-motion durations of the earthquake records were determined using Trifunac and Brady (1975) definition (Figure 5.1). Thus, the strong-motion duration is the time interval during which 90% of the integral $\int_o^{t_o} a^2(t)\,dt$ is achieved, where a(t) is the ground acceleration and $t_o$ is the entire duration of the record, with the first and last 5% being deleted.

The strong-motion duration (SMD) of each time-history in ensemble "A" is included in Table 5.3, which shows that the time-histories cover a wide range of strong motion duration that represent the short, medium, and long durations.

The M and M+SD response spectra of the time-histories of ensemble "A" scaled to a peak ground velocity (PGV) of 1 m/sec, using 5% damping, are shown in Figure 5.2. For periods higher than 0.6 sec (i.e. medium and long period range), the M and M+SD response spectra from ensemble "A" match those of Newmark-Hall. As the first and second mode periods for all the frames are higher than 0.6 sec, then the short period range (i.e. less than 0.6 sec), in which the response spectra from ensemble "A" do not match those of Newmark-Hall, has no significant effect on the response of the frames. The twelve response spectra of the time-histories are given in Figure 5.3, which shows the variability which exists between the nature of these time-histories.

Peak ground velocity was used as the scaling parameter for the time-histories in this ensemble. The decision to scale to common peak velocity is first due to the fact that this study deals with long period structures, and the response of medium and long period structures correlates more closely with peak ground velocity or peak ground displacement rather than with peak ground acceleration (Newmark and Hall, 1982). Second, the seismic hazard in NBCC(1995) is expressed explicitly in terms of zonal velocity. Moreover, previous studies by Tso et al.(1992), including spectral analysis of a large number of records having different A/V ratios, showed that there are significant differences in the frequency content for earthquake records having different A/V ratios. If the earthquake ground motions are scaled to a common peak acceleration there would be different energy contents over the moderate and long period ranges for ground motions having different A/V ratios. However, different energy contents would occur only in the short period range for ground motions with different A/V ratios if they are scaled to a common peak velocity.

### 5.2.2 The second ensemble of time-histories (Ensemble B)

The new Canadian seismic hazard results are expressed as uniform hazard spectra (Adams et al., 1996). It should be noted that the uniform hazard spectrum is different than the response spectrum. The response spectrum provide the maximum response of a SDOF system having a range of values of periods and specified damping to a single earthquake ground motion. The uniform hazard spectrum is the envelope of the maximum spectral responses for given damping at different periods; the spectral values at different periods may arise from earthquakes having different distances to source and different magnitude but the same annual probability of exceedance. The new Canadian hazard results incorporate both aleatory (random) and epistemic (model) uncertainties. Thus, the hazard results are presented both in terms of median (50%) and median plus one standard deviation (84%) spectral ordinate levels.

Response and damage analyses to determine performance using the new hazard information can be done by selecting time-histories that have a mean response spectrum which simulate the uniform hazard spectrum for a given location. Realizing that the uniform hazard spectrum involves several earthquake responses, one may approximately simulate it by selecting time-histories that have a mean spectral shape corresponding to that of the site-specific uniform hazard spectrum for that location. The records are then scaled to a specific spectral ordinate from the uniform hazard spectrum, e.g. $S_a(1.0)$.

In this study, the uniform hazard spectrum for Vancouver was used as a basis for selecting an ensemble "B" of time-histories. The time-histories are used as input ground motions for the six storey frames designed for the intermediate level of seismic hazard (zonal

velocity =0.2 m/sec, comparable to Vancouver, B.C.), i.e. I6-frames. The probabilistic seismic hazard estimates for Vancouver, 50%ile and 84%ile, are given in Table 5.4 (Adams et al., 1996). The median (50%ile) uniform hazard spectrum with 5% damping for Vancouver is also shown in Figure 5.4. The selection of time-histories to form ensemble "B" was based on simulating the median (50%ile) uniform hazard spectrum shape at periods of 0.5, 1.0 and 2.0 sec. The mean target spectral ordinate ratios are given in Table 5.5. A large number of trials were performed, after which the final selection was achieved. The achieved mean spectral ordinate ratios from ensemble"B" are also given in Table 5.5. Figure 5.5 shows the mean response spectrum shape of the selected time-histories compared with the median uniform hazard spectrum shape for Vancouver. The figure shows that both curves match very well for periods greater than 0.4 sec, i.e. intermediate and long structural periods.

The time-histories that form the ensemble "B" are given in Table 5.6. The ensemble consists of twelve time-histories. The table presents a detailed description of each of the time-histories, including the values of the peak ground acceleration, peak ground velocity and their ratio. The strong-motion duration (SMD) of each time-history in ensemble "B" is also included in Table 5.6, which indicates that the time-histories cover a wide range of strong-motion duration that represents the short, medium and long durations.

## 5.3 TRUNCATION OF TIME-HISTORIES

For the purpose of reducing computation time, time-histories were truncated. For each time-history, two main factors were considered during the truncation process, the strong-motion duration and the spectral values. The duration of strong shaking is very

important to the response of inelastic systems, this is because the strong-motion duration is closely related to the cumulative fatigue-type damage of structures. Using the strong-motion durations as guide lines during the truncation process and performing several trials, the time-histories were truncated. The truncated records had durations which were close to those calculated using Trifunac and Brady definition. For each time-history, it was confirmed that the response spectrum of the truncated record is approximately the same as the response spectrum resulting when using the entire time-history, i.e. with differences less than 2%.

Table 5.1 Newmark-Hall spectrum velocity amplification factors for horizontal elastic response.

| Damping (%) | One Sigma (84.1 %) $S_v / v_{max}$ | Median (50%) $S_v/v_{max}$ |
|---|---|---|
| 3% | 2.64 | 1.86 |
| 5% | 2.30 | 1.65 |

Table 5.2 Target values of $S_a(T)/v_{max}$ from Newmark-Hall design spectrum against actual values of $S_a(T)/v_{max}$ determined from ensemble "A".

| $S_a(T)/v_{max}$ (g / m/s) | Target values of $S_a(T)/v_{max}$ for selection of the time-histories of ensemble "A" | | | Actual values of $S_a(T)/v_{max}$ determined from the time-histories of ensemble "A" | | |
|---|---|---|---|---|---|---|
| | Period | | | Period | | |
| | 1.5 sec | 2.2 sec | 3.0 sec | 1.5 sec | 2.2 sec | 3.0 sec |
| (M+SD) value | 0.98 | 0.67 | 0.49 | 0.97 | 0.64 | 0.44 |
| (M) value | 0.70 | 0.48 | 0.35 | 0.75 | 0.51 | 0.34 |
| (M-SD) value | 0.42 | 0.28 | 0.21 | 0.53 | 0.38 | 0.24 |

Table 5.3 Description of time-histories included in ensemble "A"

| Record | Earthquake | Date | Magnitude | Station | Component | Maximum Acceleration A(g) | Maximum Velocity V(m/sec) | A/V | SMD* (sec) |
|---|---|---|---|---|---|---|---|---|---|
| NI2 | Kern County California | July 21 1952 | 7.6 | Taft Lincoln School Tunnel | S69E | 0.179 | 0.177 | 1.01 | 29 |
| NI14 | Mexico Earthquake | Sep. 19 1985 | 8.1 | La Union, Guerrero Array | N00E | 0.166 | 0.203 | 0.82 | 24 |
| NI15 | Montenegro Yugoslavia | Apr. 15 1979 | 7.0 | Albatros Hotel, Ulcinj | N00E | 0.171 | 0.194 | 0.88 | 12 |
| NL5 | Mexico Earthquake | Sep. 19 1985 | 8.1 | Zihuatenejo, Guerrero Array | S00E | 0.103 | 0.159 | 0.65 | 19 |
| NVL2 | Long Beach California | Mar. 10 1933 | 6.3 | Subway Terminal, L.A. | N39E | 0.064 | 0.173 | 0.37 | 29 |
| NVL4 | San Fernando California | Feb. 9 1971 | 6.4 | 4680 Wilshire Blvd., L.A. | N75W | 0.084 | 0.209 | 0.4 | 20 |
| NVL8 | Loma Prieta California | Oct. 17 1989 | 7.0 | Pacific Hights, S.F. | N90W | 0.061 | 0.143 | 0.43 | 11 |
| BIG3 | Big Bear Earthquake | June 28, 1992 | 6.6 | San Bernardino-E and Hospitality | N00S | 0.1 | 0.118 | 0.85 | 21 |
| LAN1 | Landers Earthquake | June 28, 1992 | 7.5 | Amboy Station 21081 | E00W | 0.146 | 0.2 | 0.73 | 31 |
| LAN4 | Landers Earthquake | June 28, 1992 | 7.5 | Indio-Coachella canal Station 12026 | E00W | 0.11 | 0.15 | 0.73 | 40 |
| NOR2 | Northridge Earthquake | Jan. 17, 1994 | 6.7 | Arleta-Nordhoff Ave. fire station | E00W | 0.34 | 0.4 | 0.85 | 13 |
| NOR3 | Northridge Earthquake | Jan. 17, 1994 | 6.7 | Los Angeles-Pico and Sentous | E00W | 0.102 | 0.12 | 0.85 | 22 |

NI: Intermediate A/V ratio (0.80 to 1.2)
NL: Low A/V ratio (0.60 to 0.80)
NVL: Very low A/V ratio (0.35 to 0.60)

* SMD = strong-motion duration based on Trifunac and Brady definition

Table 5.4 Probabilistic seismic hazard estimates for Vancouver Uniform Hazard Spectra (Geological Survey of Canada)

| Period (sec) | One Sigma (84%) (g) | Median (50%) (g) |
|---|---|---|
| 0.1 | 0.68 | 0.35 |
| 0.15 | 0.87 | 0.42 |
| 0.2 | 1 | 0.48 |
| 0.3 | 0.76 | 0.38 |
| 0.4 | 0.63 | 0.33 |
| 0.5 | 0.53 | 0.28 |
| 1 | 0.3 | 0.15 |
| 2 | 0.15 | 0.076 |

All values are given for probability of exceedance
10% in 50 years on firm ground
Spectral (5% damped) acceleration values are in (g)

Table 5.5 Target mean spectral shape for selection of time-histories of ensemble "B" against actual mean spectral shape determined from ensemble "B".

| Spectral shape | Target values UHS | Actual values Ensemble "B" |
|---|---|---|
| Sa(0.50)/Sa(2.0) | 3.68 | 3.78 |
| Sa(1.0)/Sa(2.0) | 1.97 | 2.16 |

Table 5.6 Description of time-histories included in ensemble "B"

| Record | Earthquake | Date | Magnitude | Station | Component | Maximum Acceleration A(g) | Maximum Velocity V(m/sec) | A/V | SMD* (sec) |
|---|---|---|---|---|---|---|---|---|---|
| NI2 | Kern County California | July 21 1952 | 7.6 | Taft Lincoln School Tunnel | S69E | 0.179 | 0.177 | 1.01 | 29 |
| NI14 | Mexico Earthquake | Sep. 19 1985 | 8.1 | La Union, Guerrero Array | N00E | 0.166 | 0.203 | 0.82 | 24 |
| NVL2 | Long Beach California | Mar. 10 1933 | 6.3 | Subway Terminal, L.A. | N39E | 0.064 | 0.173 | 0.37 | 29 |
| BIG2 | Big Bear Earthquake | June 28, 1992 | 6.6 | San Bernardino-E and Hospitality | E00W | 0.092 | 0.137 | 0.67 | 21 |
| LAN4 | Landers Earthquake | June 28, 1992 | 7.5 | Indio-Coachella canal Station 12026 | E00W | 0.11 | 0.15 | 0.73 | 40 |
| NOR3 | Northrigde Earthquake | Jan. 17, 1994 | 6.7 | Los Angeles-Pico and Sentous | E00W | 0.102 | 0.12 | 0.85 | 21 |
| NH2 | Parkfield California | June 27, 1966 | 5.6 | Cholame, Shandon No. 5 | N85E | 0.434 | 0.255 | 1.7 | 7 |
| NH8 | San Fernando California | Feb. 9, 1971 | 6.4 | Caltech Seismolog. Lab | S90W | 0.192 | 0.115 | 1.67 | 8 |
| NH14 | Near E. Coast of Honshu, Japan | June 12, 1978 | 7.4 | Ofunato Harbour Works | E41S | 0.226 | 0.141 | 1.6 | 16 |
| NH15 | Friuli Italy | Sep. 15, 1976 | 5.8 | S. Rocco | N00E | 0.119 | 0.061 | 1.95 | 6 |
| NI6 | San Fernando California | Feb. 9, 1971 | 6.4 | 3838 Lankershim Blvd., L.A. | S90W | 0.15 | 0.149 | 1.01 | 12 |
| NI7 | San Fernando California | Feb. 9, 1971 | 6.4 | 3407 6th St., L.A. | S00W | 0.161 | 0.184 | 0.88 | 13 |

NH: High A/V ratio (1.6 to 2.4)
NI: Intermediate A/V ratio (0.80 to 1.2)
NVL: Very low A/V ratio (0.35 to 0.60)

* SMD = strong-motion duration based on Trifunac and Brady definition

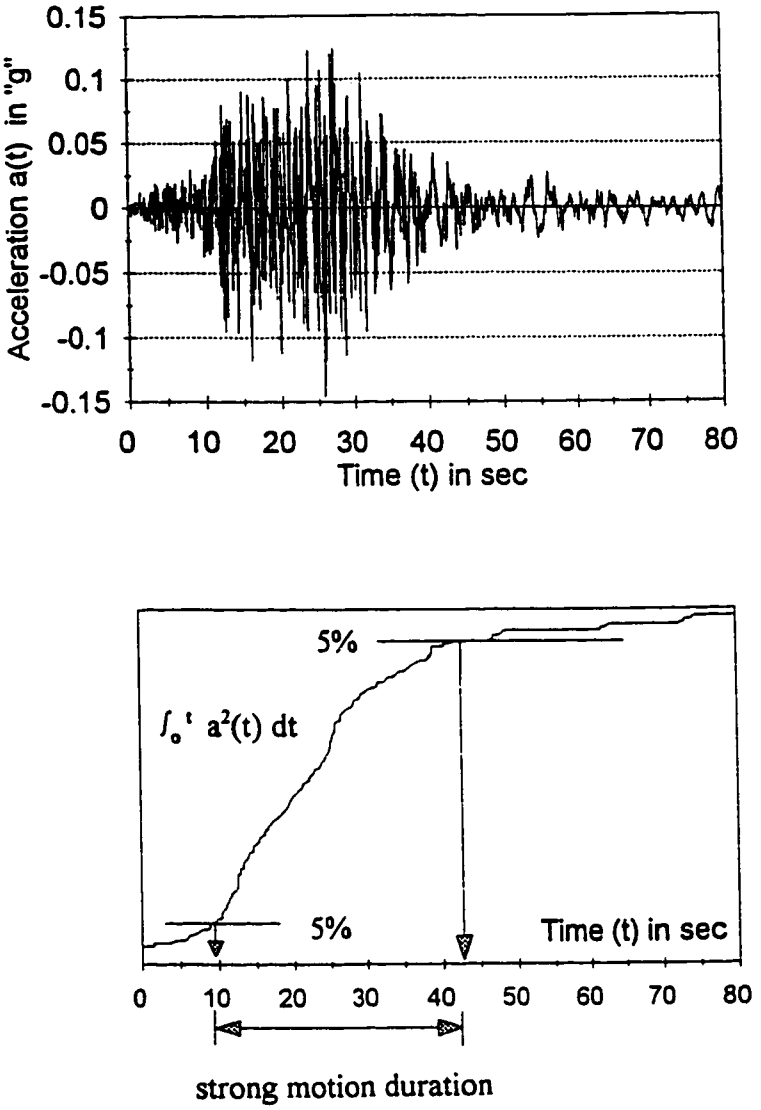


Figure 5.1 Trifunac and Brady definition of strong-motion duration.

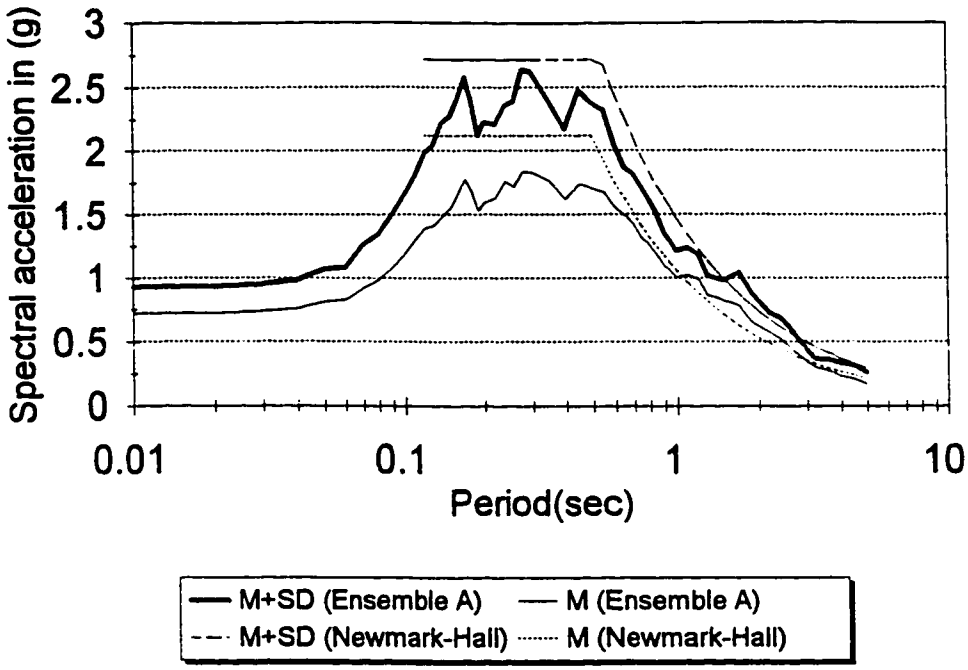


All the records are scaled to a peak ground velocity of 1 m/sec, 5% damping

Figure 5.2 Mean and mean+one standard deviation response spectra for time-histories of ensemble "A".

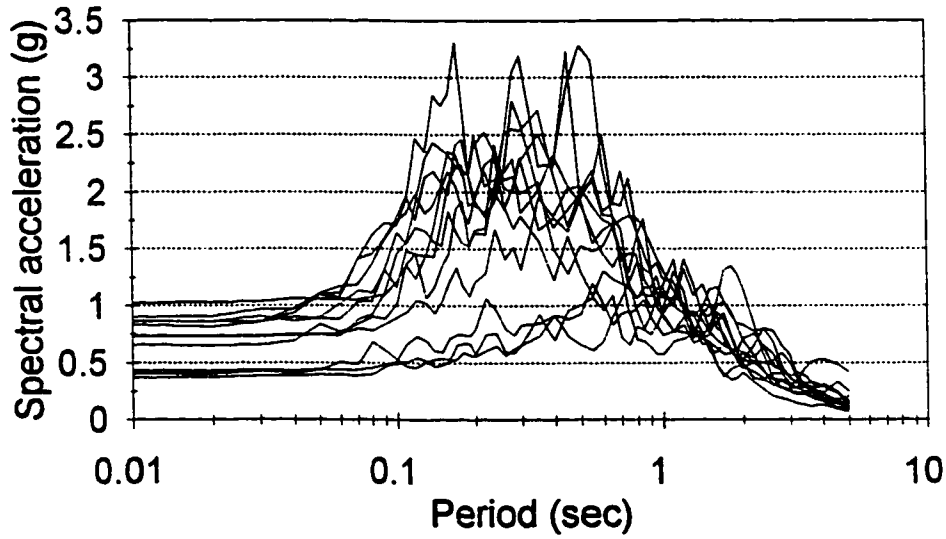


All the records are scaled to a peak ground velocity of 1 m/sec, 5% damping

Figure 5.3 Response spectra for time-histories of ensemble "A".

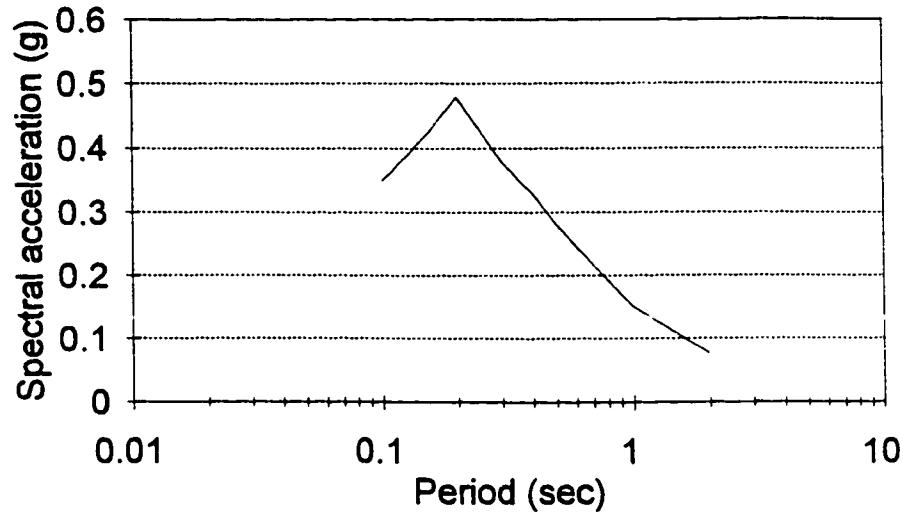


Spectral acceleration are calculated for 5% damping
All values are given for a probability of exceedance 10% in 50 years on firm ground

Figure 5.4 Median uniform hazard spectrum for Vancouver, B.C.

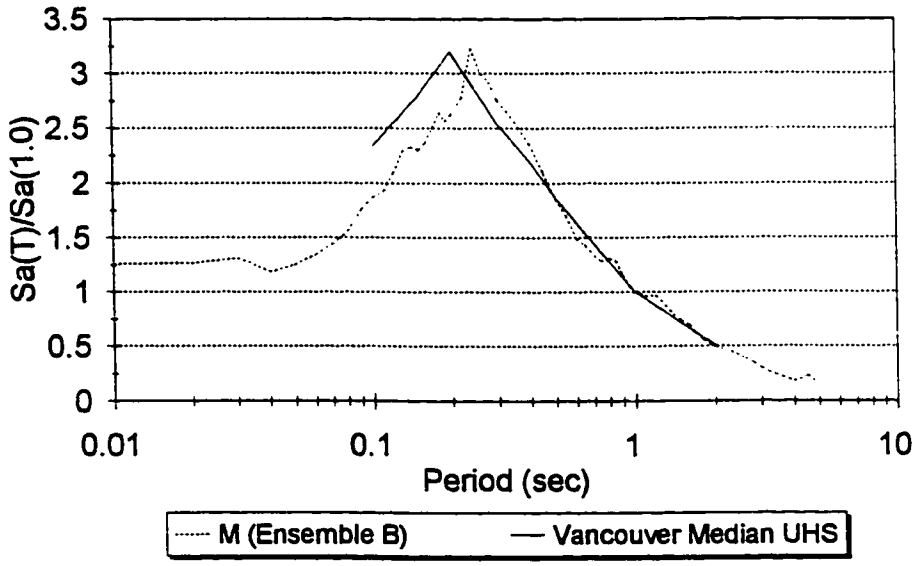


Figure 5.5 Mean spectral shape for time-histories of ensemble "B" compared with Vancouver median uniform hazard spectral shape.

# CHAPTER 6

# NONLINEAR PUSH OVER STATIC ANALYSES

## 6.1 GENERAL

While loading codes specify seismic design forces, the demand imposed by an earthquake on a structure is really a displacement or deformation demand, which is affected by the structure's strength and force-displacement characteristics. The seismic performance is directly related to the deformations of the structural members and the structure as a whole. Thus, the ability of the structure to survive strong seismic ground motions is governed by the deformations which the structure is forced to sustain.

In the current design codes, restrictions are placed on the maximum acceptable values of lateral deflections. Equivalent static load method is used, during which deflections are determined by multiplying the elastic deflections by the applicable structural ductility factor. In general, the actual capability of the structure to sustain those deflections is not evaluated.

In practice, designers use the code specified lateral seismic loads, in combination with factored dead and live loads, to analyze the structure in order to determine the member design forces, which are then used as a basis for selecting the appropriate member shapes and dimensions by ensuring that the strengths of the members exceed the design values. Finally, the deflections calculated from the specified earthquake lateral loads are checked against

specified storey drift and deflection requirements. However, the seismic performance of a structure is directly related to the deformations of the structural members and the structure as a whole, i.e. the capacity of the structure to undergo plastic deformations.

Recent studies on the development of performance based codes for design or rehabilitation of buildings in seismic areas show that a procedure commonly referred to as "push over analysis" is a viable method to evaluate the acceptability of any proposed design, or to assess the damage vulnerability of existing buildings, e.g. ATC 33 (1995) and SEAOC (1995). The objective of the push over analysis is to obtain estimates of the member forces and the global and local deformations a structure is likely to experience in a design earthquake, and to use these estimates to assess the integrity of the structural system.

In brief, a push over analysis is a series of incremental static analyses carried out to examine the deformation and damage pattern of the structure. The push over analysis, which includes lateral sway effects, involves the application of an increasing monotonic static lateral load having the same distribution as the design seismic load (a load pattern that approximately represents the relative inertia forces which are generated at locations of substantial mass); this load is increased until either the structure collapses or until some pre-determined high level of lateral deflection is reached. The code specified load pattern produces the best correlation between static and MDOF dynamic deflection profiles. A carefully performed push over analysis will provide insight into structural aspects that control performance during severe earthquakes.

For structures that vibrate primarily in the fundamental mode, the push over analysis will very likely provide good estimates of global as well as local inelastic deformation

demands. This analysis will also expose design weaknesses that may remain hidden in an elastic analysis. Ductility ratios and plastic hinge rotations can be estimated, as can the global hysteretic energy (area under load-displacement curve) which correlates poorly with the dynamic hysteretic energy dissipation, and is therefore a poor measure of the cumulative damage demand. From the push over analysis, one can also determine the lateral strength of the structure and its load-deflection relationship. The resulting load-deflection relationship, which includes inelastic deformations, represents the capacity of the structure to sustain high levels of lateral deformations. Also, it provides information on the actual strength as well as the amount of lateral deflection which can be sustained. In addition, the performance of each structural element can be monitored and evaluated at various overall displacements or maximum storey drift ratios; this provides useful information on the critical elements in the structure, i.e. those which undergo substantial inelastic deformation.

It is customary to obtain estimates of forces and deformations from the behaviour of the structure at roof (top) displacement predicted during a design earthquake (Lawson et al., 1994). In terms of life-safety protection against strong earthquake ground motions with low annual probabilities of exceedance, the structure has to sustain high levels of roof deflection (e.g. 2% of the building height, Osman et al., 1995, Heidebrecht, 1995) without significant amount of structural damage, i.e. without progressive structural element collapse leading to a collapse mechanism, in order to be deemed satisfactory. Ductile structures designed with a specific energy dissipating mechanism (capacity design) should have little or no difficulty in meeting this requirement.

The push over analysis procedure has been developed by many researchers (e.g. Saiidi and Sozen, 1981; Fajfer and Fishinger, 1988; Qi and Moehle, 1991; Lawson et al., 1994; Fajfar and Gaspersic, 1996) and applied to planar structures. Assuming diaphragm action of the floors, the behaviour of a symmetrical building can be inferred from a push over analysis using two dimensional inelastic analysis programs.

During push over analysis in this study, the gravity loads considered are D+0.5L. The lateral sway effect (P-Δ) is considered as described in Chapter 3. The gravity loads acting on the leaning interior gravity columns are not considered in the (P-Δ) effect.

## 6.2 BASE SHEAR-ROOF DEFLECTION RELATIONSHIPS

The base shear-roof deflection relationship of a frame structure, which includes significant inelastic deformations, gives an indication of the strength of the structure and its capacity to sustain high levels of deformation. In this study, the diagrams presenting the base shear-roof deflection relationships are plotted so that the base shear is normalized to the design base shear of the structure, while the roof deflection is expressed as a percentage of the structure height. Each diagram also includes the points at which specified values of maximum storey drift ratios are reached, including 1.5% and 2.5% drifts, which represent the life-safe and near-collapse drift limits recommended by the SEAOC(1995) Vision 2000 Committee, respectively.

### 6.2.1 Six storey frames

Figure 6.1 shows the base shear-roof deflection relationships for the standard six storey frames. For each set of frames, i.e. H6, I6 or L6 set of frames, all three frames

corresponding to the three design philosophies (SCWB, WCSB and SCWP) have approximately the same initial global stiffness (note that frames in each of the three diagrams have the same design base shear which is used in the normalization process). However, the subsequent inelastic behaviour of each frame is quite different. In general, at any given roof deflection, the SCWP frame in each diagram has the lowest overstrength factor (defined as the base shear divided by the design base shear) because the global strength is controlled by the strengths of the weak joint panel zones. The strengths for both the SCWB and WCSB frames in each diagram are approximately the same at any given roof deflection, even though the members are proportioned by significantly differing design philosophies. Frames designed for different design philosophies also differ in the relationship between maximum storey drift and roof deflection. The largest differences are between the SCWB and WCSB frames; the WCSB frames develop large storey drifts at much smaller roof deflections than for the SCWB frames.

The results of the push over analyses are examined at 1% and 2% roof deflections as well as at 2% and 2.5% maximum storey drifts. The 2% roof deflection is selected to represent a late stage of overall plastic deformation in the roof-deflection relationship of a given frame. Frame structures are likely to exhibit lateral deflections in the neighbourhood of this high value during ground motion excitations that are well above the design level excitation. Thus, this deflection estimate enables the examination of the damage potential at much lower levels of probability of exceedance than that used in design. Whether or not the structure can sustain this deformation without collapse is questionable. The 1% roof deflection is selected to represent an early stage of overall yielding in the roof-deflection

relationship of a given frame, thus, it simulates deflections from low level seismic excitations that are likely to shake the frame structure more frequently. The 2% maximum storey drift represents the limit given by the NBCC (1995) and used during the design of the frames, while the 2.5% maximum storey drift represents the near-collapse limit given by the SEAOC (1995) performance criteria.

The normalized base shear values and maximum storey drift ratios at 1% and 2% roof deflections are summarized in Table 6.1. At 1% roof deflection, the SCWB frames have the smallest maximum drifts followed by the SCWP then the WCSB frames. On the other hand, at 2% roof deflection, the SCWP frames have the smallest maximum drifts followed by the SCWB then the WCSB frames which have very high drifts. The only set of frames for which the maximum drift of the SCWP frame is slightly higher than the SCWB frame is the L6 set of frames (i.e. 2.53% for the L6SCWP frame compared with 2.38% for the L6SCWB frame).

At 2% roof deflection, the maximum drifts occur in the lower portions of the frames in case of SCWB frames (i.e. first or second storey); they occur near the frame-mid height in case of SCWP frames (third storey), while they occur in the first storey in case of WCSB frames. The noticeable very high drifts in case of WCSB frames can be attributed to the fact that the WCSB frames tend to develop maximum drifts in the lowest storey and to do so with little inelastic deformation in the upper part of the building, i.e. very much like a soft storey. By contrast, inelastic deformations are distributed throughout the height in the SCWB frames so that the maximum drifts are not concentrated in the lowest storey. While the base shear-roof deflection relationships for the SCWB and WCSB frames are similar, the SCWB frame is preferable because of these differences.

The normalized base shear values and roof deflections at maximum storey drifts of 2% and 2.5% are given in Table 6.2. From the table, for a given set of six storey frames (i.e. H6, I6 or L6 set of frames), the behaviour of the SCWB and SCWP frames at 2% maximum drift tends to be approximately similar in terms of the roof deflection, while the WCSB frame has a much lower roof deflection, which is basically due to the concentration of drift in the first storey, while the upper storeys have very small storey drifts. On the other hand, the overstrength factors of the SCWB and WCSB frames are similar, while that of the SCWP frame is somewhat smaller.

At 2.5% maximum drift, for each of the six storey set of frames, the SCWP frame tend to have the highest roof deflection followed by the SCWB frame with a slightly lower value of roof deflection, then the WCSB frame which has a much lower value of roof deflection. This clearly indicates that both the SCWB and SCWP frames are well-conditioned structures which have their input energy-dissipation distributed throughout the structure, while the WCSB frame is ill-conditioned which will develop a collapse mechanism with very limited energy-dissipation (i.e. structure with a soft storey, even though its elements may be highly ductile).

In general, the shape of the base shear-roof deflection relationship and the value of the roof deflection at the 2.5% maximum drift level are measures of the extent to which a frame can mobilize ductile inelastic behaviour to help resist large seismic forces. If the roof deflection at the 2.5% drift level is small and relatively near to the apparent "knee" in an approximately bilinear representation of the relationship, then very little ductile behaviour has occurred. All three WCSB frames in Figure 6.1 have that characteristic, which indicates that

these frames, especially in seismically active regions, have relatively limited capacity for ductile behaviour at large deformations. In contrast, the behaviour of the SCWB and SCWP frames illustrated in Figure 6.1 shows quite large deflections which go well beyond the "knee" when the storey drift is 2.5%. This observation indicates that both of these types of frames have considerable capacity for ductile behaviour at large deformations. The foregoing observations indicate that the WCSB frames are not likely to be as satisfactory as those designed using the other two design philosophies. It should be noted here that during push over analyses of the WCSB frames, push over calculations were not carried to deflections large enough for the overall stiffness to become negative.

### 6.2.2 Limited drift designed six storey frames

Figure 6.2 shows the base shear-roof deflection relationships for the limited drift designed six storey frames (i.e. SP.I6SCWB, SP.I6WCSB and SP.I6SCWP). In case of the SCWB and WCSB frames, each frame has a 50% increase in overstrength factors over the corresponding code design frame (i.e. I6SCWB and I6WCSB frames respectively), while there is only 30% increase in the overstrength factor in the SCWP frame. This increase in strength is due to the use of much stronger beam and column sections in order to limit the design storey drift to 1%. At a given roof deflection, the maximum drifts that these special frames experience are very close to those of the corresponding code designed frames. The only advantage of these special frames is that under a given base shear force they will have smaller lateral deflections and drifts as well as less inelastic deformations in the structural members than in the case of the code designed frames.

### 6.2.3 Ten storey frames

Figure 6.3 shows the base shear-roof deflection relationships for the ten storey frames. When these relationships are compared with those of the corresponding six storey frames (I6 set of frames) in Figure 6.1, it may appear that there is not much difference between the two sets of frames. However, by examining the overstrength factors as well as the relationship between roof-deflection and maximum storey drift, which are also given in Tables 6.1 and 6.2, some differences can be detected.

The ten storey frames have similar overstrength factors to the corresponding six storey frames (I6 set of frames). However, at 1% roof deflection, the maximum drift of the I10WCSB frame is 1.97% while that of the I6WCSB frame is 1.5%. This indicates that the ten storey WCSB frame is much more sensitive (ill-conditioned) than the six storey WCSB frame (i.e. I6WCSB) in developing a soft storey behaviour (i.e. a collapse mechanism). For both I10SCWB and I10SCWP frames, the maximum drift occurs just above the frame mid-height level, i.e. in the sixth storey.

For the SCWP frames, the roof deflection of the ten storey frame at 2.5% maximum storey drift is much lower than that of the six storey frame (1.57% compared with 1.97%). This indicates that the I10SCWP frame performs much poorer than its counterpart, the I6SCWP frame. This may be attributed to the difference in heights between the six and ten storey frames (i.e. difference in the deformed shape). A weak panel design of the I10SCWP frame tends to develop high values of storey drifts at the frame's mid-height while the roof deflection is still relatively low. This is also clear from the deformed shape of the I10SCWP frame which is presented in section 6.6.

## 6.3 BASE SHEAR-MAXIMUM STOREY DRIFT RELATIONSHIPS AND LOCATIONS OF PLASTIC DEFORMATIONS

While the base shear-roof deflection relationships in section 6.2 summarize in a global manner the performance during push over analyses, it is of interest to examine the base shear-maximum drift relationships of the frames and the profile of plastic deformation locations at common maximum drift ratios. As the storey drift is an expression of the relative lateral deflections (displacements) between two subsequent floors, it is the main factor that affects the damage of the structural elements in any storey. Figures 6.4 through 6.6 show the base shear-maximum storey drift relationships of the frames. It should be noted that maximum drifts in different frames occur in different storeys. The figures show the drifts at which 1% and 2% roof deflection occur, and the drifts at which a soft first storey mechanism takes place in each of the WCSB frames. When the maximum drift for a given roof deflection is large, the performance is poor. This is because the lateral deformations are concentrated in only one or two storeys rather than throughout the height of the building. For example, the WCSB frames have very high storey drift demands at 2% roof deflection compared with those of the other frames. The L6WCSB frame has better behaviour than that of the other six storey WCSB frames.

Figures 6.4 to 6.6 show the maximum storey drifts at which soft first soft storey mechanism in the WCSB frames occur. It is clear that, with the exception of the L6WCSB frame, a first storey collapse mechanism can occur in WCSB frames at a maximum storey drift in the order of 1.5% rather than the 2.5% stated by SEAOC(1995) performance criteria. In addition, this collapse mechanism in the WCSB frames is expected to correspond to a

maximum roof deflection of 1%.

Figures 6.7 and 6.8 show the locations of plastic deformations in the frames at a maximum drift of 1.5% (life-safe performance limit), while Figures 6.9 and 6.10 show this profile at a maximum drift of 2.5% (near-collapse performance limit). As the storey drifts increase, plastic deformations start to spread throughout the frame. Because of the excellent distribution of plastic deformations in the SCWB frames (i.e. plastic deformations at the base of the first storey columns, in beams at different floor levels and in very few panels) and in the SCWP frames (i.e plastic deformations at the base of the first storey columns and in panels at different floor levels), frames of both design types manage to reach high levels of lateral deflections within acceptable maximum storey drifts. Due to the poor distribution of plastic deformations, the WCSB frames develop a soft first storey mechanism (plastic deformations at the bottom and top ends of the first storey columns), and become more vulnerable to collapse at a maximum drift ratio in the range of 1.4% to 1.6% for the H6WCSB and I6WCSB frames. In the L6WCSB frame, this mechanism is developed at 2% maximum drift.

## 6.4 IMPLICATIONS OF THE DESIGN PHILOSOPHIES

Push over analyses of the frames indicate that the SCWB and WCSB designs produce frames that have approximately similar overstrength factors at the same roof deflection, but with quite different maximum drifts. In general, the SCWP design produces frames that have overstrength factors of about 3/4 that of the frames designed for the other two designs at the same roof deflection.

At 2.5% maximum storey drift, the six storey SCWP frames have the highest roof deflections followed by the SCWB frames with slightly lower roof deflections, while the WCSB frames tend to develop that level of maximum drift at much lower roof deflections. In case of the ten storey frames, the SCWB frame has the highest roof deflection followed by the SCWP frame with slightly lower roof deflection; the WCSB frame behaviour is similar to that of the corresponding six storey frame. Thus, based on the drift performance criteria, the SCWP frames have the best performance in case of the six storey frames, followed by the SCWB frames and then the WCSB frames for which the performance is much poorer. On the other hand, SCWB frame is ranked the best performance in case of the ten storey frames, followed by the SCWP frame and then the WCSB frame which also has much poorer performance.

## 6.5 IMPLICATIONS OF THE SEISMIC HAZARD DESIGN LEVEL

Figure 6.11a shows the seismic hazard level-overstrength factor relationships at 2.5% maximum storey drift for the six storey frames designed using different design philosophies. From the figure, for any design philosophy, the frames in low seismic hazard regions have the highest overstrength factors due to the fact that strength requirements rather than drift limits govern the design of these frames. For each design philosophy, increasing the seismic hazard design level leads to a decrease in the overstrength factor of the frame. For WCSB frames, the decrease in overstrength factor from the L seismic hazard level to the I and H seismic hazard levels is greater than for the other frame types.

While the relative values of overstrength factors for the SCWP frames at different seismic hazard levels are similar to those for the SCWB frames, the actual values are much lower, i.e. ranging from 1.7 to 2.3 compared with a range of 2.25 to 3.1 for the SCWB frames. The overstrength values of the SCWP frames are controlled mainly by the strength of the panels.

Figure 6.11b shows the seismic hazard level-roof deflection relationships at 2.5% maximum storey drift for the six storey frames designed for different design philosophies. From the figure, for a given design philosophy, frames in the H and I seismic hazard regions have comparable roof deflections, while frames in the L region have higher values. In the low seismic hazard region, the code drift requirements do not govern the design; frames are more flexible than the corresponding frames designed for the higher seismic hazard regions. Figure 6.1 does not illustrate the relative stiffnesses of the frames because of using normalized base shear as the dependent variable. However, since seismic design forces in the L, I and H seismic hazard locations are in the proportion 1:2:3, it is clear that the L6 set of frames are significantly more flexible than the H6 and I6 sets of frames.

The roof deflections of the WCSB frames at 2.5% maximum drift are approximately 1.6% in the L seismic hazard region and approximately 1.25% in the other two regions. This indicates that the behaviour of the WCSB frame in regions of low seismic hazard activity is not as poor as in regions of intermediate and high seismic hazard activity. Another observation from Figure 6.11b is that the roof deflections for all three SCWP frames designed for different seismic hazard levels are quite similar, i.e. in the order of 2%. This indicates that the seismic hazard level has very little effect on the behaviour of SCWP frames.

## 6.6 FLOOR DISPLACEMENTS AND STOREY DRIFT RATIOS DISTRIBUTION

Figures 6.12 and 6.13 show the height-wise distribution of floor displacements and storey drifts of the six storey frames when the maximum drift is 2.5%. This maximum drift in the six storey SCWB frames occurs either in the first or the second storey, followed by a gradual decrease of storey drift values in the upper storeys. The six storey WCSB frames have the 2.5% storey drift in the first storey, followed by a sudden decrease to a drift value of about 1.3% in the second through the sixth storey, while the six storey SCWP frames have a more uniform distribution of storey drift along the height with the 2.5% storey drift in the third storey. The height-wise distribution trends for storey drifts of frames designed using the same design philosophy but located in different seismicity regions (different seismic hazard levels) are quite similar. The drift ratio distribution depends mainly on the deflected shape which is affected primarily by the design philosophy and not by the level of seismic hazard. However, in case of the SCWB and WCSB frames in the L6 set of frames, for which the roof deflections are higher than for those in the corresponding H6 and I6 frames, the drift distribution is more uniform along the frame's height.

Figure 6.14 shows the height-wise distribution of floor displacement and storey drifts of the ten storey frames when the maximum drift is 2.5%. The maximum drifts in the SCWB and SCWP frames occur at mid-height. The I10SCWP frame has smaller drifts than those of the I10SCWB frame in the lower storeys. The I10WCSB frame has the 2.5% drift value in the first storey followed by a sudden decrease of drifts in the other storeys, a behaviour which is similar to the corresponding six storey frame (i.e. I6WCSB frame).

At high levels of lateral deflection the differences between the deflected shapes of the frames become much more obvious. The floor displacements at a common roof deflection of 2% are shown in Figure 6.15. The deflected shape of the frame governs the maximum value of storey drift and its location. For instance, this figure shows that the high values of first floor displacements for the WCSB frames are the reasons for high first storey drift values. For the frames designed for WCSB, the soft first storey phenomenon becomes more significant when the level of seismic hazard increases from L to H and also with the increase of the frame's height from six to ten storeys. For all sets of frames, at a common roof deflection of 2%, the SCWP frame has the lowest floor displacements followed by the SCWB frame and then the WCSB frame.

## 6.7 BEAM PERFORMANCE

Since the 2.5% maximum storey drift is considered to be the near-collapse limit by the SEAOC (1995), it is important to consider the performance at the element level when that drift limit is reached. In evaluating this performance during static push over analyses, it should be noted that static analyses do not include the effect of the accumulation of plastic deformation due to cyclic behaviour and the higher mode effects due to the dynamic behaviour of the structural system. Both of these effects, which significantly increase damage, will be discussed in the evaluation of the results of the inelastic dynamic analyses.

Figures 6.16 and 6.17 show the maximum beam rotational ductilities and damage indices for the six storey frames at 2.5% maximum storey drift. The beams in the SCWB frames experience relatively high levels of plastic deformations compared with beams in the

other two frame design types. The beams in the other two frame design types either experience no plastic deformations or negligible values of plastic deformation in very few locations at which yielding has just started. For the six storey SCWB frames, the beam plastic deformations are concentrated at the four bottom floors (see Figure 6.9) with the maximum deformation occurring in the beams of the first floor. For these frames the maximum beam rotational ductility ranges from 4.2 to 5.5, which is within the capacities of compact class 1 sections ($\mu_\theta < 6$), while the maximum beam damage index ranges from 0.5 to 0.7 as the seismic hazard level increases from low to high. Consequently, on the basis of static push over analyses, the beams in the six storey SCWB frames are in moderate to high state of damage (but still below the failure limit) when the maximum drift reaches 2.5%. In the SP.I6SCWB frame, the beam plastic deformations occur only in the first floor with a maximum ductility of 1.8 and damage index of 0.12 (i.e. minor damage). This is due to the stronger beam members (i.e. higher strength and stiffness) in the SP.I6SCWB frame (which is designed for a drift limit of 1%) compared to the beam members in the ordinary I6SCWB frame. Thus, the beam ductilities and damage decrease significantly by designing to a much more restricted drift limit than that specified in the design code, i.e. frame SP.I6SCWB compared with the standard frame I6SCWB.

Figure 6.18 shows the maximum beam rotational ductilities and damage indices for the ten storey frames at 2.5% maximum storey drift. The beams in the I10SCWB frame experience substantial plastic deformation which is distributed throughout the bottom seven storeys (see Figure 6.10), with the maximum beam plastic deformation concentrated in the fifth and sixth floors. The maximum beam rotational ductility is 4.5, which is still within the

capacity of class 1 sections, while the maximum beam damage index is 0.62. Thus, the most damaged beam in the I10SCWB frame can be considered in a moderate to high state of damage at the 2.5% storey drift level. It should be noted that the maximum beam ductility and damage of the I10SCWB frame are comparable to those mentioned above for the I6SCWB frame.

For the I10WCSB frame, the first floor beams experience limited amount of plastic deformations. The interpretation of this observation is that the bottom and top ends of the first storey columns reach high levels of plastic deformations due to the excessive first floor lateral deflection (soft-storey phenomenon), thus, forcing the beam in the first floor to start yielding and experiencing plastic deformations. However, the maximum rotational ductility is 1.25 and the maximum damage index is 0.05, i.e. practically negligible. Consequently, the beams in the I10WCSB frame can be considered to remain elastic until just before the maximum storey drift reaches 2.5%.

The beams in the I10SCWP frame also experience a very limited amount of plastic deformation which occurs only at the third floor beam (see Figure 6.10). For this location, the rotational ductility is 1.5 and damage index is 0.1. This small amount of damage is due to the fact that the 10SCWP frame is basically the same as the I10SCWB frame but without any web panel thickness reinforcement. Thus, some beams can be expected to start experiencing plastic deformation simultaneously with the adjacent panel experiencing plastic shear deformation. Practically, the beams in the I10SCWP frame are also expected to remain elastic until just before the maximum storey drift reaches 2.5%.

## 6.8 COLUMN PERFORMANCE

Figures 6.19 and 6.20 show the performance parameters for the interior columns of the six storey frames; the exterior columns exhibit similar levels and patterns of inelastic behaviour (see appendix II). All the six storey frames (i.e. SCWB, WCSB and SCWP) in all the frame sets (i.e. H6, I6, L6 and SP.I6) experience plastic deformations in first storey columns and no plastic deformations in the columns above that level (see Figure 6.9). While the first storey columns in the WCSB frames are expected to experience extensive plastic deformations at a maximum drift of 2.5%, it can be seen that the maximum deformations and the maximum damage indices for the columns in the SCWB designs are not significantly lower. However, while all the frames experience column plastic deformations at the base, only the WCSB frames experience plastic deformations at both the bottom and top ends of the first storey columns (ductilities in the order of 4 at the top ends of the first storey columns), i.e. potentially achieving a mechanism in the "soft" first storey. Consequently, the WCSB frame design type is highly vulnerable to collapse at the 2.5% drift level even though the maximum damage index ranges from 0.6 to 0.78. These results are consistent with the observations mentioned in section 6.3 regarding the vulnerability of the WCSB frames to exhibit collapse mechanism at lower drifts near 1.5%, especially in seismically active areas. The other two frame design types are not near collapse at this drift level because the column damage is limited to the base (bottom ends of first storey columns) of the structure with maximum damage indices in the range of 0.55 to 0.65.

In all cases, the SCWP frame design type has the lowest column damage when compared to other frame design types; that is because the maximum drifts occur near the

frame mid-height and are mostly resisted by shear deformations in the panels. The sensitivity of the WCSB frame design type to lateral deflections is more obvious in the H6WCSB frame located in regions of high seismicity (i.e. much more vulnerable to collapse at 2.5% drift) than in both the I6WCSB and the L6WCSB frames.

The SP.I6SCWB frame experiences higher values of column damage at the base of the first storey compared with the standard I6SCWB frame. This increase in column damage compensates for the decrease in beam damage which was discussed in section 6.7. Thus, designing a steel MRF for a lower maximum drift leads to a much stiffer frame; this limits the plastic deformations in the beams and upper storey columns, but increases the plastic deformations at the base of the frame. The SP.I6WCSB frame experiences a column damage level that is close to that of the H6WCSB frame rather than the I6WCSB frame, which confirms the conclusion stated above regarding the design for lower drift level.

Figure 6.21 shows the performance parameters for the interior columns of the ten storey frames; the exterior columns exhibit similar levels and patterns of inelastic behaviour (see Appendix II). The performance of the columns in the ten storey frames differ in several respects (see Figure 6.10) from that of the comparable six storey frames (I6 frames). First, there is no inelastic deformation at all in the columns of the I10SCWP frame, as most of the lateral storey deflections of the frame take place in the fourth to the seventh storeys, while relatively small values of lateral deflections occur in the bottom two storeys. Second, inelastic behaviour of the columns in the I10SCWB frame is observed in the fifth and seventh storeys as well as at the base of the first storey; this occurs because the maximum drift in this frame occurs near the mid-height of the structure rather than near the base. This more distributed

plastic deformation also results in a lower damage index in the first storey columns than that of the I6SCWB frame. The pattern and extent of column damage in the I10WCSB frame is similar to that in the I6WCSB frame, i.e. column plastic deformation occurring at both the bottom and top ends of the first storey columns. The maximum column rotational ductilities and damage indices in the I10WCSB frame are higher than in the I6WCSB frame; the ten storey frame is more vulnerable to collapse at the 2.5% drift level.

## 6.9 JOINT PERFORMANCE

When the maximum drift is 2.5%, the joint panel zones are expected to deform in the plastic region, particularly in the case of SCWP design. Figures 6.22 and 6.23 show the performance parameters of the interior joint panel zones for the six storey frames at 2.5% maximum drift. The patterns and extent of damage for the exterior joint panels are similar (see Appendix III).

For the six storey frames, with the exception of the first and/or second floor panels of the SCWB frames, which have just started to yield, only the panels of the SCWP frames experience any plastic deformations (see Figure 6.9). Inelastic deformation occurs in the panels of almost all the floors with maximum values of panel shear ductility and panel damage index occurring in the panels of either the second or the third floor. The maximum panel shear ductility ranges from 10 to 12.5 which is well within the shear deformation capacity of well designed panels ($\mu_\gamma < 20$, Kato et al., 1988). The corresponding maximum panel damage index ranges from 0.55 to 0.68 as one goes from L6SCWP to H6SCWP frame. Although the panels suffer moderate to high levels of damage, the panels of the SCWP frames can be

considered as not being vulnerable to failure at a maximum drift of 2.5%.

The performance parameters of the panels of the SP.I6SCWP frame are slightly higher than those of the corresponding I6SCWP frame; in fact they are in the same order of magnitude as those of the panels of the H6SCWP frame. In case of the SP.I6SCWB frame, although the web panels are reinforced using doubler plates, the exterior first and second floor panels suffer minor damage (damage indices in the range of 0.1 to 0.2), while the interior first and second floor panels have just started to yield.

Figure 6.24 shows the performance of the interior joint panel zones for the ten storey frames at 2.5% drift (see Figure 6.10). The maximum panel shear ductility and damage index in the I10SCWP frame are of the same order of magnitude as those in the I6SCWP frame. However, in this case these maxima occur at the mid-height of the structure (in the fourth to the seventh floors) rather than near the base (the second to the third floors). In both cases, the locations of these maxima correlate well with the locations of the maximum storey drift.

Both the I10SCWB and I10WCSB frames experience a limited amount of panel plastic deformation. For the 10WCSB frame, these maxima occur near the base, with relatively small ductilities ($\mu_\gamma < 3$) and very small damage indices. The panel plastic deformation is more widely distributed throughout the height of the structure in the I10SCWB frame, particularly in the exterior panels (see appendix III), but the maximum ductilities and damage indices are also very low, i.e. $\mu_\gamma < 4$ and DI < 0.18. Consequently, neither the I10SCWB nor the I10WCSB frame are vulnerable to collapse due to failure of the panel zones, because they are either in an elastic or early plastic deformation stage.

The reason that the panels of SCWB and WCSB designs have started to yield or have small values of shear ductilities with minor damage are due to:

1) either the adjacent beams experience high levels of plastic deformations (i.e. suffer extensive damage), thus forcing the panels to start taking their share in the overall frame carrying capacity, or

2) the frame experience very high values of storey drifts, e.g. first storey drift in WCSB frames, as a result, the first storey columns suffer severe damage; the panels are forced to enter into the plastic range due to high levels of shear forces.

## 6.10 MAXIMUM PLASTIC DEFORMATIONS

The maximum value of member plastic deformation is a measure of the amount of damage in a member. While each specific structural element in a typical steel MRF has its own plastic deformation capacity, on average there is a range of plastic rotations in beam-columns or shear strains in joints beyond which any further deformation is considered crucial.

Table 6.3 summarizes the maximum plastic deformations of the structural members at 2.5% maximum drift. For the beams of the SCWB frames, the maximum plastic rotation ranges from 0.020 to 0.026 rad. This range of plastic deformations is consistent with some test results of well designed beams (e.g. Osman, 1991; Tsai and Popov, 1988; Uang and Bondad, 1996) during which the plastic rotational capacity ranges from 0.025 to 0.03 rad. when the drift ratio is in the neighbourhood of 3%. Moreover, the maximum plastic rotations are the basis for calculating the damage indices in case of static analyses. This is clear by relating the maximum beam damage indices (presented in Table 6.4) and the maximum beam

plastic rotations.

For the columns, the plastic deformations for different frames at 2.5% maximum drift are:

1) for the SCWB frames, the maximum column plastic rotation at the base ranges from 0.014 to 0.018 rad.

2) for the WCSB frames, as first storey columns suffer much higher levels of damage; the maximum plastic rotation is in the order of 0.021 rad. Thus, the column plastic rotations of the WCSB designs are on average 30% higher than those of the SCWB designs.

3) for the SCWP frames, the maximum plastic rotation are much lower than those of the SCWB frames, ranging from 0.004 to 0.013 rad.; thus the columns suffer much less damage.

The exact range of column plastic rotational capacity from experimental results depend upon both the value of the axial load and the slenderness of the column section. For this study, where the axial forces are relatively low ($\leq$ 30% of the yielding axial load), some experimental results show that at drifts in the neighbourhood of 3%, the column plastic rotational capacities range from 60% to 70% that of the beams (Lee, 1992), i.e. 0.018 to 0.022 rad.

For the panel zones of the SCWP frames, Table 6.3 also shows that the maximum panel shear strain ranges from 0.021 to 0.027 at 2.5% maximum drift (i.e. panel shear ductility ranging from 10 to 13). These values of shear deformation are below the accepted limits of maximum joint distortions for well designed joints given by Kato et al. (1988), i.e. panel shear ductility < 20. Also, in other experimental studies (Tsai and Popov, 1988; Osman, 1991) panels show stable performance up to plastic shear strains in the order of 0.035.

## 6.11 MAXIMUM STATIC STOREY DRIFT-MAXIMUM ELEMENT PERFORMANCE PARAMETERS RELATIONSHIPS

It is of interest to examine the relationships between maximum critical element performance parameters and maximum storey drift ratios. Figure 6.25 shows diagrams of the maximum element ductilities and damage indices for the critical elements versus the maximum storey drifts from push over analyses. The figure shows that these relationships are very nearly linear. These relationships are useful for estimation of the maximum inelastic deformations and damage of the critical elements for a specific design as a function of the maximum storey drift. Examining these relationships for frames in different seismic hazard areas as well as frames with different heights (six and ten storeys), it can be concluded that the seismic hazard design level and the frame height have slight effect on the relationships, i.e. in each diagram, the slope of the linear relationships are approximately the same but the absolute values of the performance parameters are slightly different. The only relationships that have quite unusual values are those for the beam performance parameters of the SP.I6SCWB frame, for which the parameters are much lower than those of the other SCWB frames. However, this is expected to happen as the drift design limit used for this frame is much lower than that for the other SCWB frames, i.e. 1% compared with 2% drift.

From the diagrams, an approximate estimation of the maximum performance parameters at a specified maximum static storey drift can be determined. For instance, at 2.5% maximum storey drift, the beams in the SCWB frames are expected to exhibit maximum rotational ductility in the order of 4.5 with corresponding damage index in the order of 0.6. The columns in the WCSB frames are expected to experience maximum rotational ductility

in the order of 7 with corresponding damage index in the order of 0.75. The joint panel zones in SCWP frames are expected to exhibit maximum panel shear ductility in the order of 11 with corresponding damage index in the order of 0.6.

## 6.12 SUMMARY OF OVERALL PERFORMANCE

To summarize the overall performance, the maximum performance parameters of the structural elements at 2.5% maximum drift are listed in Table 6.4.

On the basis of element deformation and damage at the 2.5% drift level during push over analyses, the SCWB and SCWP frames for the six and ten storey heights are not near collapse. The maximum beam damage indices range from 0.5 to 0.7 in the SCWB frames, while the maximum panel damage indices range from 0.55 to 0.68 in the SCWP frames. The columns in SCWB and SCWP frames have deformations only at the base with maximum damage indices that ranges from 0.45 to 0.68 in case of the SCWB frames, and from 0.10 to 0.46 in case of the SCWP frames. Consequently, it can be seen that the 2.5% drift limit is slightly conservative for these two design philosophies, in terms of estimating when collapse is imminent.

However, the WCSB frames for the six and ten storey heights are highly vulnerable to collapse at the 2.5% storey drift level. While the maximum column damage indices are only in the range of 0.6 to 0.8, the occurrence of extensive plastic deformation at both the bottom and top ends of the first storey columns provides a strong signal that a plastic collapse mechanism could occur. Also note the maximum column plastic rotations of the WCSB frames listed in Table 6.3. Consequently, the 2.5% drift limit criterion for near collapse is not

conservative for frames designed using the WCSB design philosophy. In fact, results show that the WCSB frames tend to develop a soft first storey collapse mechanism at a maximum drift in the order of 1.5% and maximum roof deflection in the order of 1%; this mechanism will over-ride member deformation capacities as a collapse criterion.

The following conclusions may be drawn from the results of the push over analyses of the frames in this chapter:

The seismic response of steel moment resisting frames depends mainly on the philosophy used in the design, as the inelastic response to seismic forces may be dramatically different when different design philosophies are used.

The push over analysis clearly identify the critical elements in each frame, i.e. those experiencing considerable amount of plastic deformations; therefore the analyses can predict the locations of plastic hinge formation. The push over analysis also expose any frame design weaknesses that may remain hidden in an elastic analysis.

During push over analyses, all the frames possess overstrength factors. The overstrength inherent in a frame structure depends upon the philosophy used in the design. Independent of the seismic hazard level or the frame height, the SCWP frame always has the lowest overstrength, while the strengths of the SCWB and WCSB frames are comparable.

Frames designed for different philosophies have different relationships between the maximum storey drift and roof deflection, the largest differences are between the SCWB frames and WCSB frames; the WCSB frames develop large storey drifts at much smaller roof deflections than for the SCWB and SCWP frames.

The results of the push over analyses show that the SCWB and SCWP frames are

well-conditioned structures with their input energy-dissipation distributed throughout the structure. Thus, they have considerable capacity for ductile behaviour at large deformations; no special preference is given for either of the two frame types. On the other hand, the WCSB frames are ill-conditioned, for which they develop a collapse mechanism (at maximum drift in the order of 1.5%) with very limited energy-dissipation even though their elements may be highly ductile. Therefore, these frames have relatively limited capacity for ductile behaviour at large deformations, especially in seismically active regions. Thus, the performance of WCSB frames are not likely to be as satisfactory as those designed using the other two design philosophies.

At the same level of base shear, the six storey frames designed for 1% drift limit have larger overstrength factors and smaller lateral deflections, drifts, and inelastic deformations compared to those of the six storey frames designed for the code drift limit. At 2.5% maximum drift, the SCWB frame designed for 1% drift limit (i.e. SP.I6SCWB) has much lower beam performance parameters and slightly higher column performance parameters at the base compared with those of the I6SCWB frame, i.e. an increase in the inelastic deformations of the columns at the base compensates for the decrease in beams inelastic deformations.

The behaviour of the ten storey frames is more or less comparable with the behaviour of the corresponding six storey frames. However, the ten storey WCSB frame is more sensitive (more ill-conditioned) than the corresponding six storey frame (I6WCSB) in developing a soft storey behaviour. The ten storey SCWP frame also performs slightly poorer than its six storey counterpart, i.e. the I6SCWP frame.

Based on the maximum storey drift-roof deflection relationship, the six storey SCWP frames are ranked as having the best performance among the six storey frames followed by the SCWB frames then the WCSB frames for which the performance is much poorer. On the other hand, the performance of the ten storey SCWB frame is ranked the best among the ten storey frames, followed by the SCWP then the WCSB frame which also has much poorer performance.

Increasing the seismic hazard design level decreases the overstrength; the decrease is more significant for the WCSB frames. At a given maximum storey drift, frames of the same design type in the H and I seismic hazard regions have comparable roof deflections, however, for the same frame design type in the L seismic hazard region, higher roof deflections are noticeable, i.e. the frames are more flexible.

For the WCSB frames, the soft storey phenomenon becomes more obvious when the level of seismic hazard increases from L to H and also with the increase of the frame's height from six to ten storeys. Also, the behaviour of the WCSB frame in regions of low seismic hazard is not as poor as in the regions of high seismic hazard activity.

There are linearly proportional relationships between maximum critical element performance parameters and maximum storey drifts. These relations are useful for estimation of the maximum inelastic deformations and damage of the critical elements for a specific design as a function of the maximum storey drift.

Table 6.1 Normalized base shears and maximum storey drift ratios at 1% and 2% roof deflections.

| Frame | At 1% Roof Deflection | | | At 2% Roof Deflection | | |
|---|---|---|---|---|---|---|
| | Base Shear* | Max. Drift (%) | Storey | Base Shear* | Max. Drift (%) | Storey |
| H6SCWB | 1.90 | 1.30 | 3rd | 2.32 | 2.87 | 2nd |
| H6WCSB | 1.89 | 1.63 | 1st | 2.47 | 5.47 | 1st |
| H6SCWP | 1.38 | 1.42 | 3rd | 1.75 | 2.70 | 3rd |
| I6SCWB | 2.01 | 1.21 | 3rd | 2.63 | 3.16 | 1st |
| I6WCSB | 2.00 | 1.50 | 1st | 2.56 | 5.00 | 1st |
| I6SCWP | 1.53 | 1.34 | 3rd | 1.86 | 2.54 | 3rd |
| L6SCWB | 2.17 | 1.15 | 5th | 3.09 | 2.38 | 2nd |
| L6WCSB | 2.39 | 1.15 | 3rd | 3.41 | 3.40 | 1st |
| L6SCWP | 1.82 | 1.23 | 3rd | 2.40 | 2.53 | 3rd |
| SP.I6SCWB | 3.06 | 1.19 | 2nd | 4.37 | 3.38 | 1st |
| SP.I6WCSB | 3.12 | 1.46 | 1st | 4.10 | 5.19 | 1st |
| SP.I6SCWP | 1.92 | 1.43 | 3rd | 2.38 | 2.67 | 3rd |
| I10SCWB | 2.10 | 1.21 | 6th | 2.80 | 2.84 | 6th |
| I10WCSB | 2.17 | 1.97 | 1st | 2.86 | 6.80 | 1st |
| I10SCWP | 1.56 | 1.47 | 6th | 2.17 | 3.20 | 6th |

* Base shear is normalized to the design base shear

Table 6.2 Normalized base shears and roof deflections at 2% and 2.5% maximum storey drift ratios.

| Frame | At 2% Maximum Storey Drift | | | At 2.5% Maximum Storey Drift | | |
|---|---|---|---|---|---|---|
| | Base Shear* | Roof Defl.** (%) | Storey of 2% Drift | Base Shear* | Roof Defl.** (%) | Storey of 2.5% Drift |
| H6SCWB | 2.16 | 1.44 | 2nd | 2.25 | 1.76 | 2nd |
| H6WCSB | 2.00 | 1.11 | 1st | 2.06 | 1.24 | 1st |
| H6SCWP | 1.59 | 1.39 | 3rd | 1.71 | 1.82 | 3rd |
| I6SCWB | 2.41 | 1.41 | 1st | 2.51 | 1.66 | 1st |
| I6WCSB | 2.14 | 1.15 | 1st | 2.21 | 1.28 | 1st |
| I6SCWP | 1.73 | 1.52 | 3rd | 1.85 | 1.97 | 3rd |
| L6SCWB | 3.02 | 1.72 | 2nd | 3.12 | 2.08 | 2nd |
| L6WCSB | 3.07 | 1.45 | 1st | 3.23 | 1.63 | 1st |
| L6SCWP | 2.22 | 1.56 | 3rd | 2.33 | 1.98 | 3rd |
| SP.I6SCWB | 3.86 | 1.41 | 1st | 4.10 | 1.62 | 1st |
| SP.I6WCSB | 3.40 | 1.18 | 1st | 3.50 | 1.30 | 1st |
| SP.I6SCWP | 2.18 | 1.41 | 3rd | 2.33 | 1.86 | 3rd |
| I10SCWB | 2.62 | 1.45 | 6th | 2.73 | 1.77 | 6th |
| I10WCSB | 2.18 | 1.01 | 1st | 2.25 | 1.10 | 1st |
| I10SCWP | 1.76 | 1.28 | 6th | 1.95 | 1.57 | 6th |

* Base shear is normalized to the design base shear

** Roof deflections are normalized to the height of the frame structure

Table 6.3 Maximum plastic deformations at 2.5% maximum storey drift

| Frame | Beams plastic rotation rad. | Columns plastic rotation rad. | Panel zones shear strain |
|---|---|---|---|
| H6SCWB | 0.026 | 0.014 | 0.0026 |
| H6WCSB | - | 0.021 | - |
| H6SCWP | - | 0.010 | 0.0270 |
| I6SCWB | 0.020 | 0.018 | - |
| I6WCSB | - | 0.020 | - |
| I6SCWP | - | 0.013 | 0.0248 |
| L6SCWB | 0.024 | 0.014 | - |
| L6WCSB | 0.003 | 0.019 | - |
| L6SCWP | - | 0.004 | 0.0210 |
| SP.I6SCWB | 0.005 | 0.018 | 0.0090 |
| SP.I6WCSB | - | 0.020 | - |
| SP.I6SCWP | - | 0.010 | 0.0257 |
| I10SCWB | 0.020 | 0.012 | 0.0070 |
| I10WCSB | 0.002 | 0.020 | 0.0050 |
| I10SCWP | 0.003 | - | 0.0230 |

Table 6.4 Overall performance at 2.5% maximum storey drift

| Frame | Beams | | Columns | | Panel zones | |
|---|---|---|---|---|---|---|
| | Max. Rot. Duct. | Max. DI | Max. Rot. Duct. | Max. DI | Max. Shear Duct. | Max. DI |
| H6SCWB | 5.6 | 0.69 | 5.6 | 0.56 | 2.2 | 0.10 |
| H6WCSB | - | - | 6.8 | 0.78 | - | - |
| H6SCWP | - | - | 3.6 | 0.31 | 12.5 | 0.68 |
| I6SCWB | 4.2 | 0.60 | 5.9 | 0.60 | - | - |
| I6WCSB | - | - | 6.1 | 0.61 | - | - |
| I6SCWP | - | - | 4.8 | 0.46 | 12.0 | 0.65 |
| L6SCWB | 4.2 | 0.50 | 4.7 | 0.54 | - | - |
| L6WCSB | 1.5 | 0.12 | 5.8 | 0.63 | - | - |
| L6SCWP | - | - | 1.9 | 0.11 | 10.2 | 0.54 |
| SP.I6SCWB | 1.8 | 0.12 | 6.8 | 0.68 | 4.7 | 0.21 |
| SP.I6WCSB | - | - | 7.2 | 0.70 | - | - |
| SP.I6SCWP | - | - | 4.0 | 0.33 | 12.4 | 0.64 |
| I10SCWB | 4.4 | 0.62 | 5.0 | 0.44 | 4.0 | 0.18 |
| I10WCSB | 1.3 | 0.05 | 6.8 | 0.78 | 3.2 | 0.13 |
| I10SCWP | 1.5 | 0.11 | - | - | 11.3 | 0.58 |

Max. Rot. Duct.: Maximum Rotational Ductility
Max. DI: Maximum Damage Index
Max. Shear Duct.: Maximum Shear Ductility

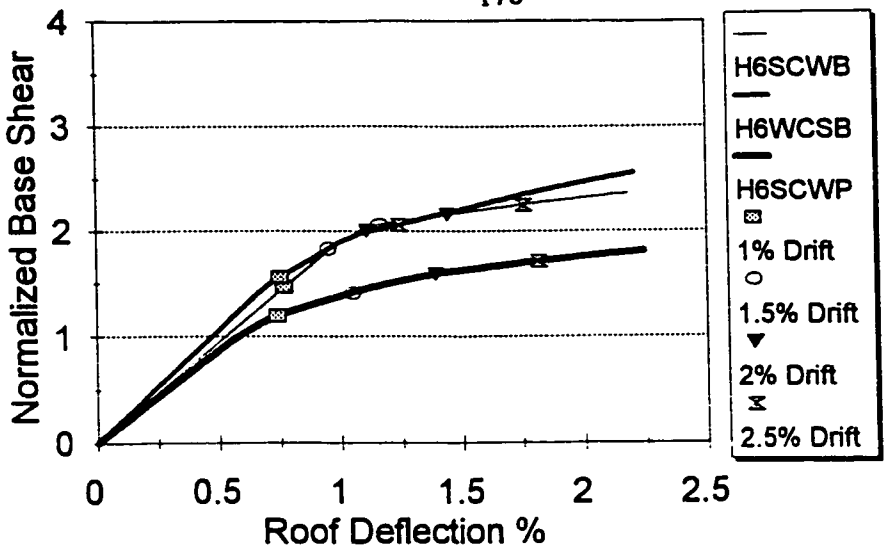


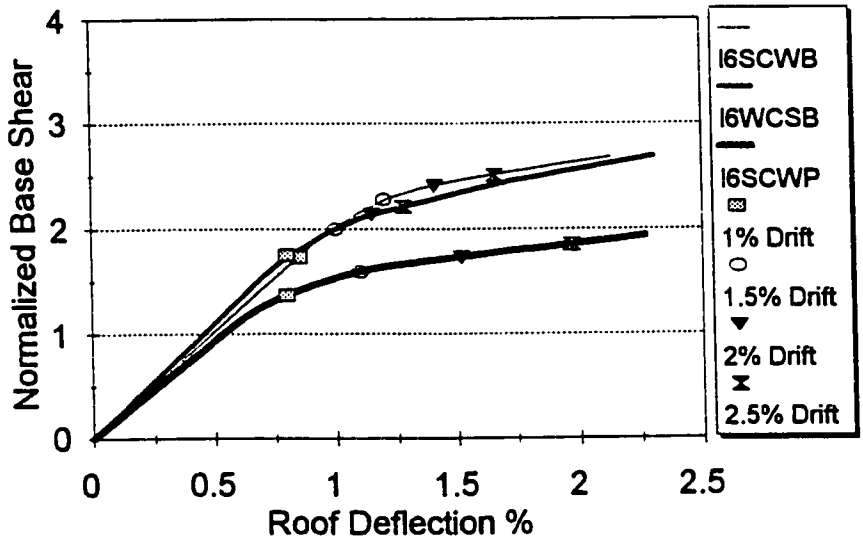


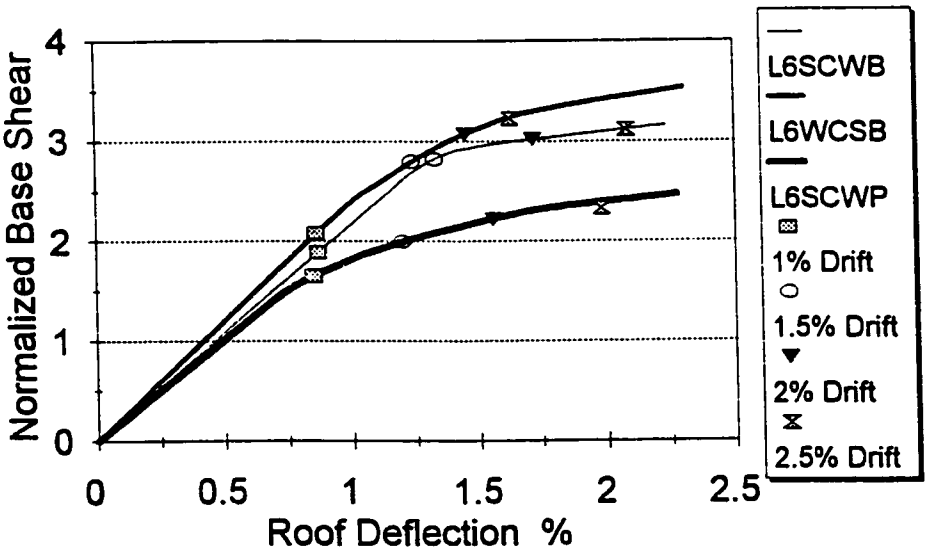


Figure 6.1 Base shear-roof deflection relationships for the six storey frames.

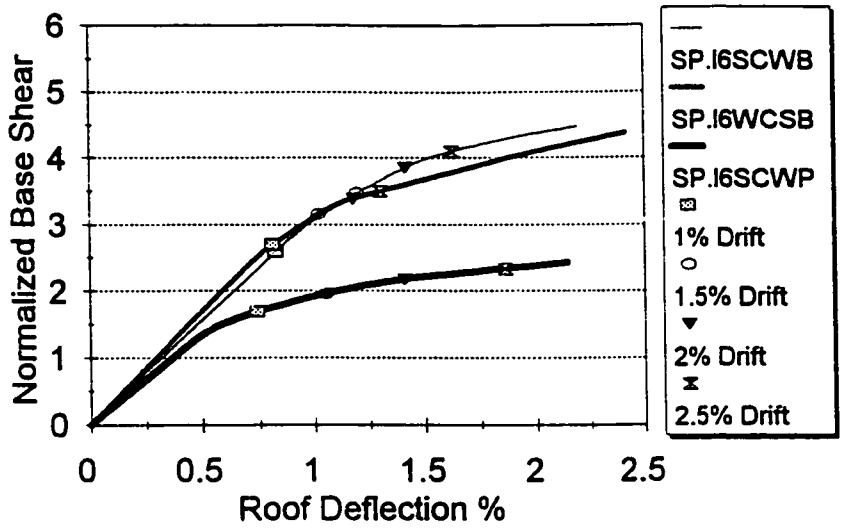


Figure 6.2 Base shear-roof deflection relationships for the six storey frames designed for special storey drift limit of 1%.

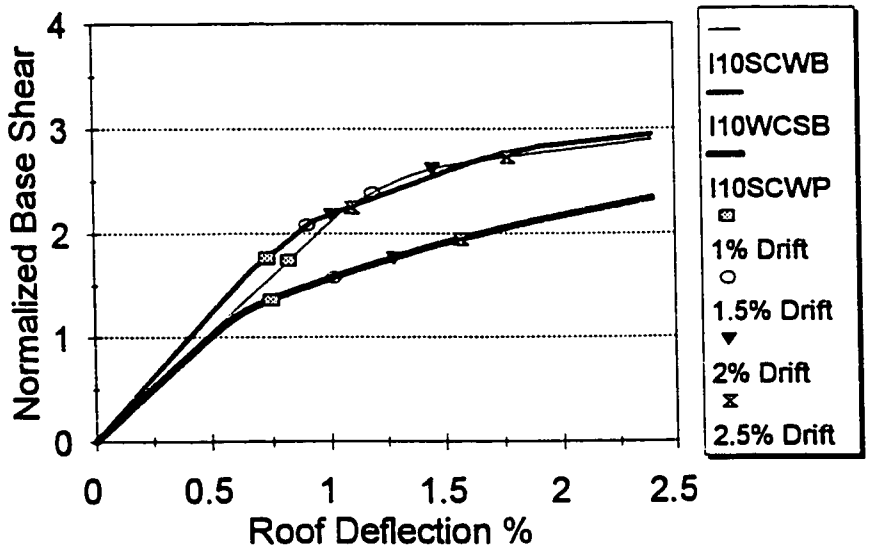


Figure 6.3 Base shear-roof deflection relationships for the ten storey frames.

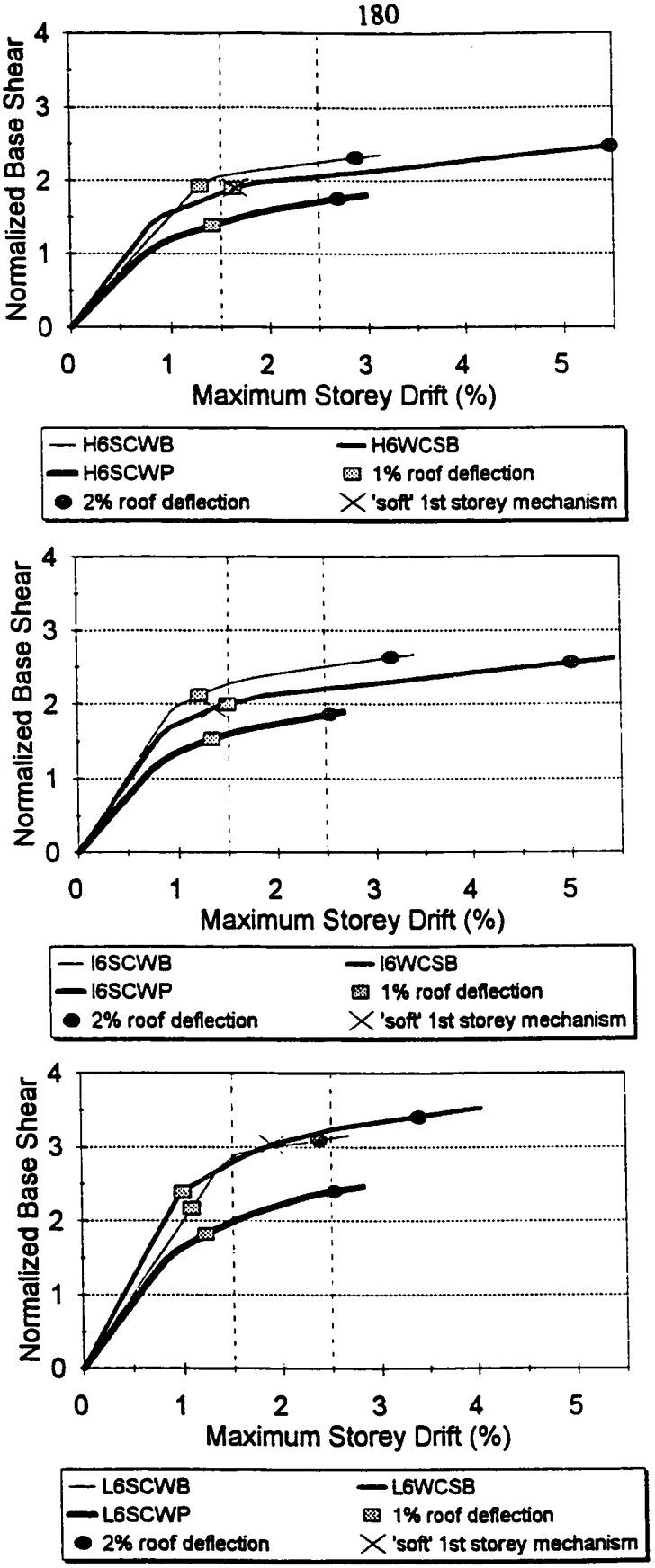


Figure 6.4 Base shear-maximum storey drift relationships for the six storey frames.

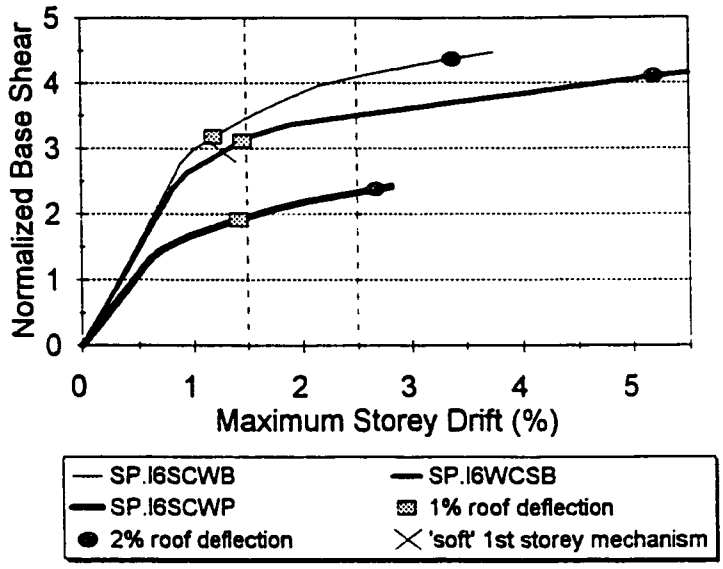


Figure 6.5 Base shear-maximum storey drift relationships for the six storey frames designed for special storey drift limit of 1%.

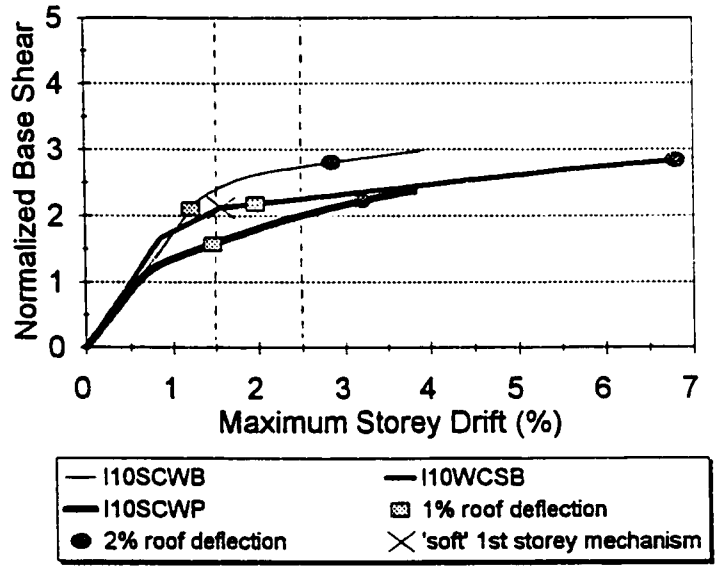


Figure 6.6 Base shear-maximum storey drift relationships for the ten storey frames.

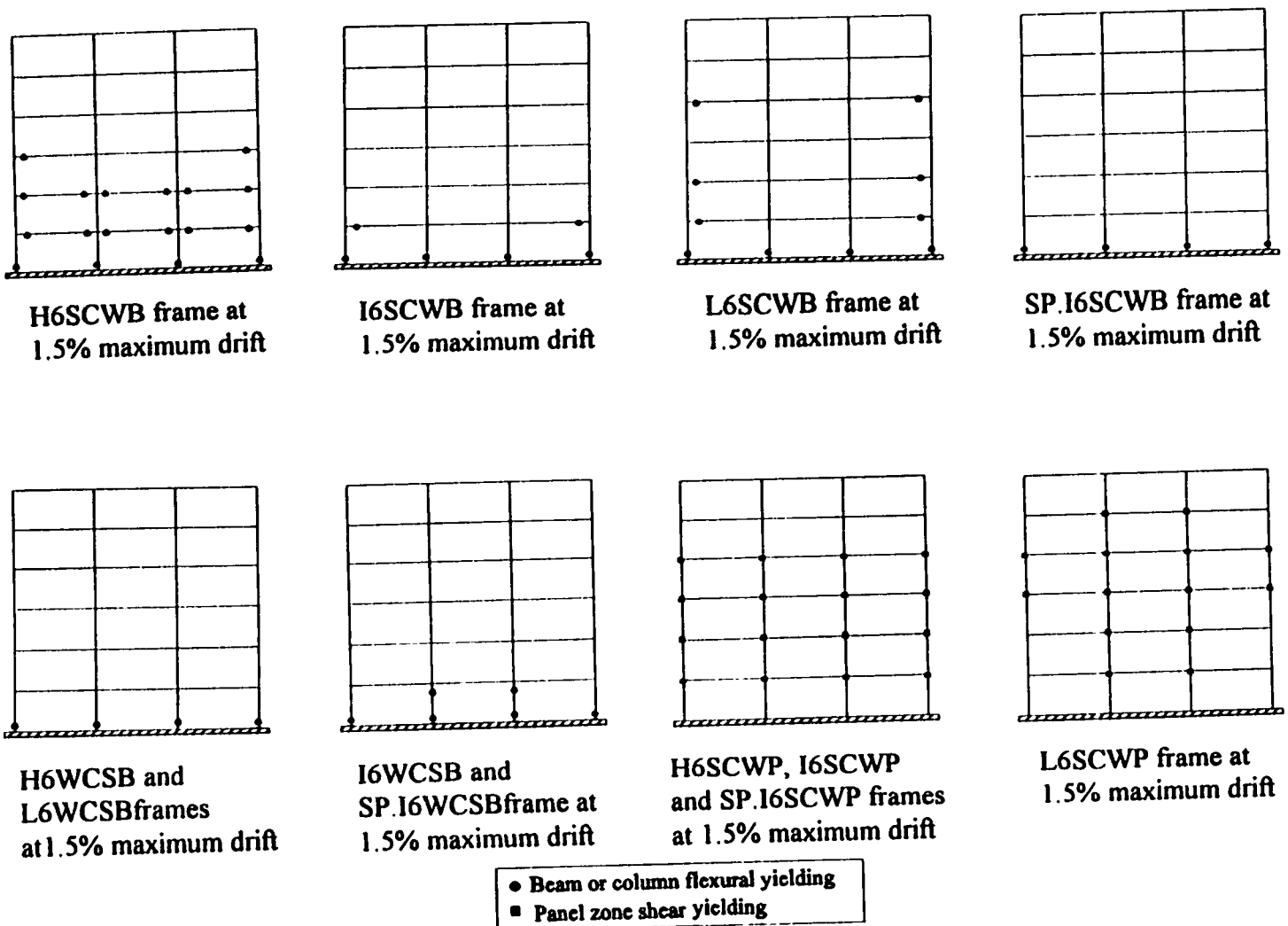


Figure 6.7 Locations of plastic deformations in the six storey frames at 1.5% maximum drift.

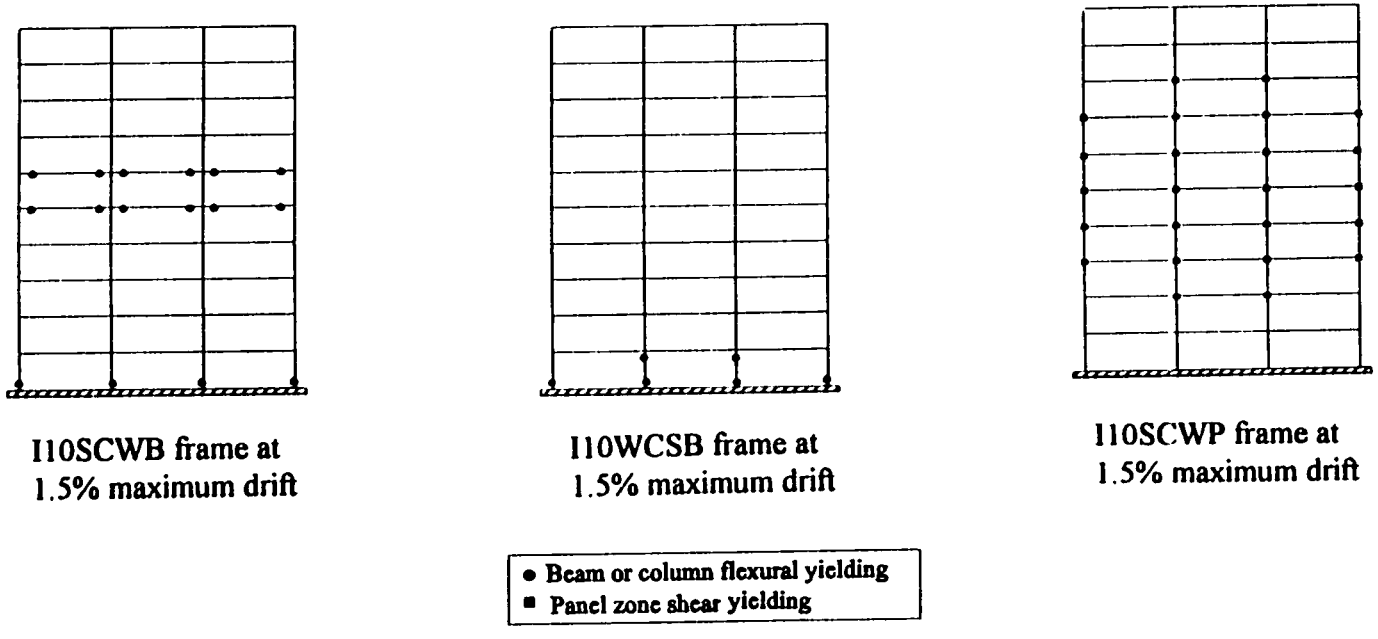


Figure 6.8 Locations of plastic deformations in the ten storey frames at 1.5% maximum drift.

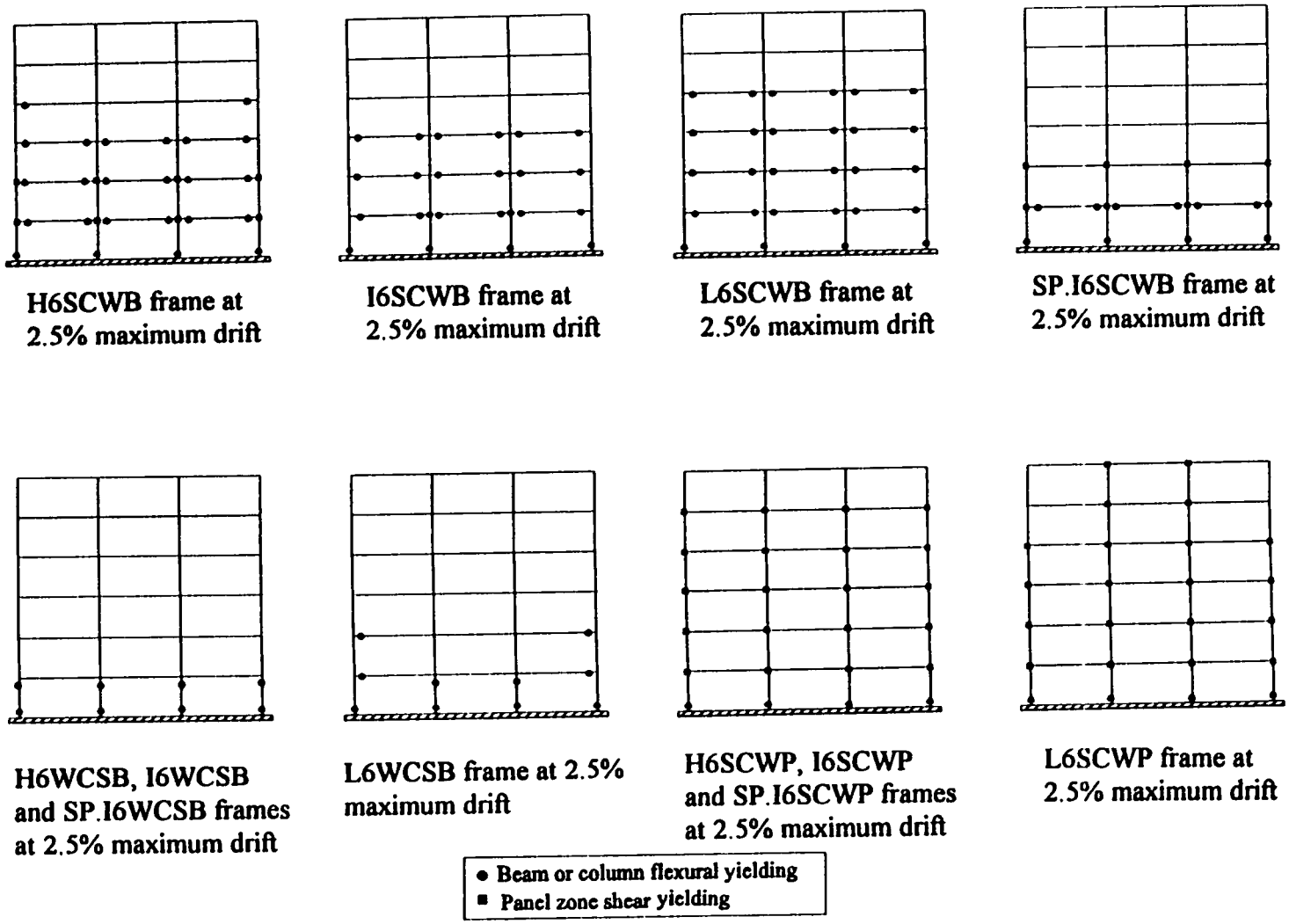


Figure 6.9 Locations of plastic deformations in the six storey frames at 2.5% maximum drift.

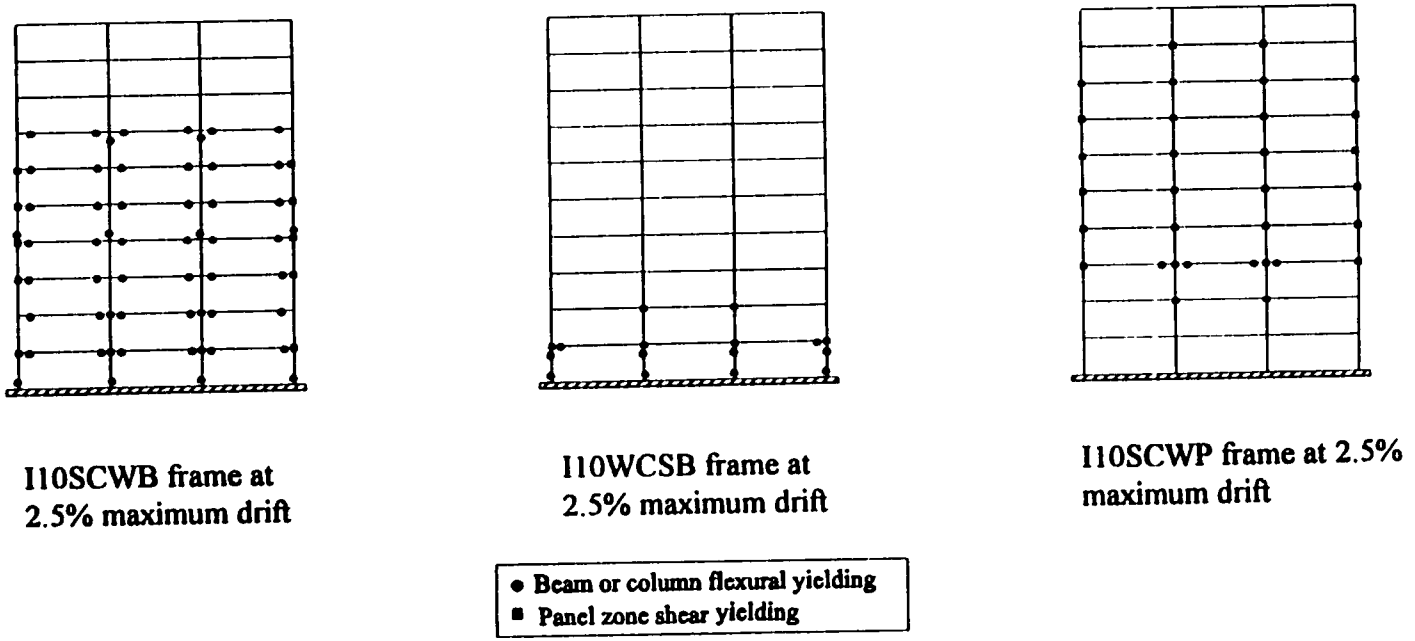


Figure 6.10 Locations of plastic deformations in the ten storey frames at 2.5% maximum drift.

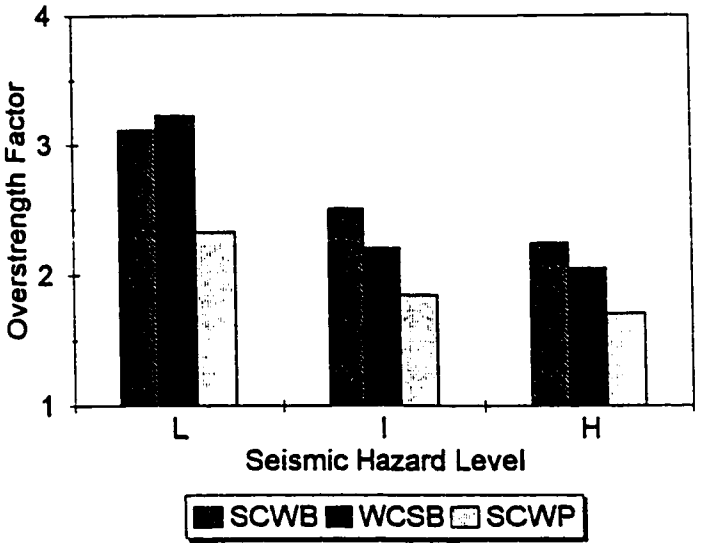


a) Seismic hazard level-overstrength factor relationships at 2.5% maximum drift.

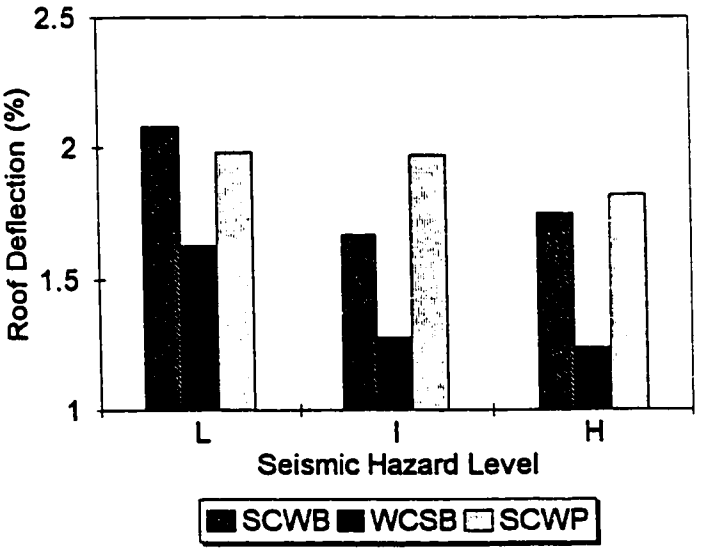


b) Seismic hazard level-roof deflection relationships at 2.5% maximum drift.

Figure 6.11 Effect of the seismic hazard design level on the overstrength factors and roof deflections of the frames.

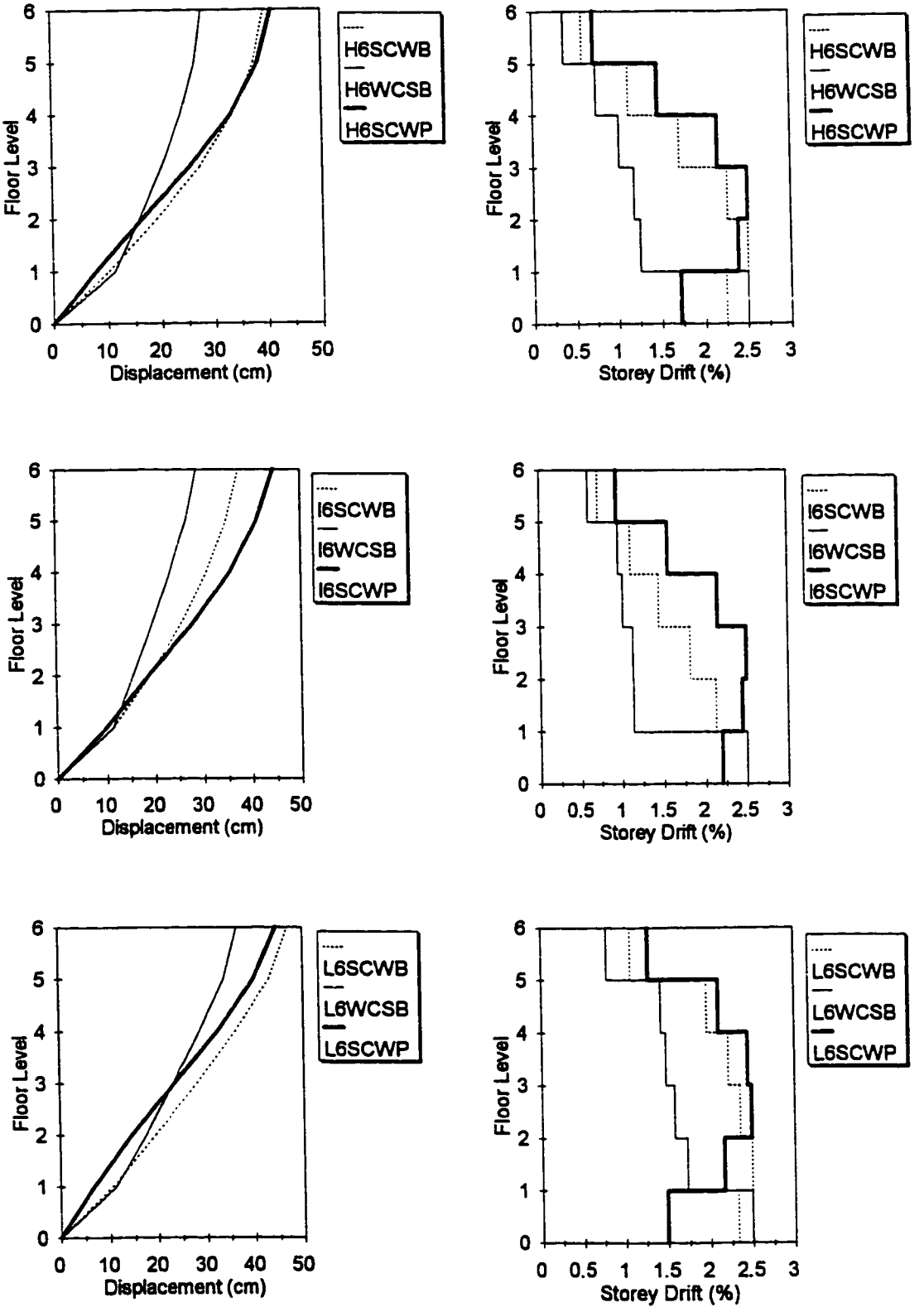


Figure 6.12 Height-wise distribution of floor displacements and storey drifts for the six storey frames at 2.5% maximum storey drift.

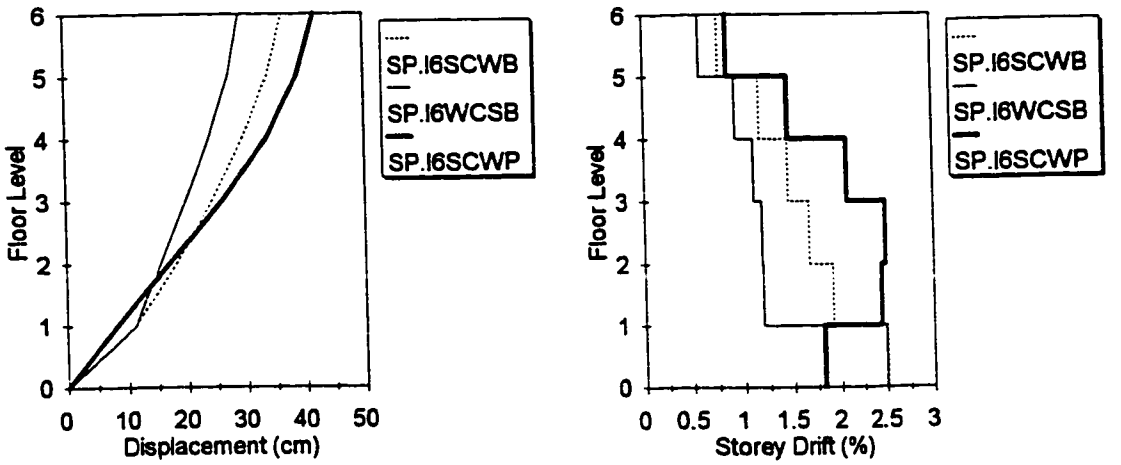


Figure 6.13 Height-wise distribution of floor displacements and storey drifts for the special drift limit designed six storey frames at 2.5% maximum storey drift.

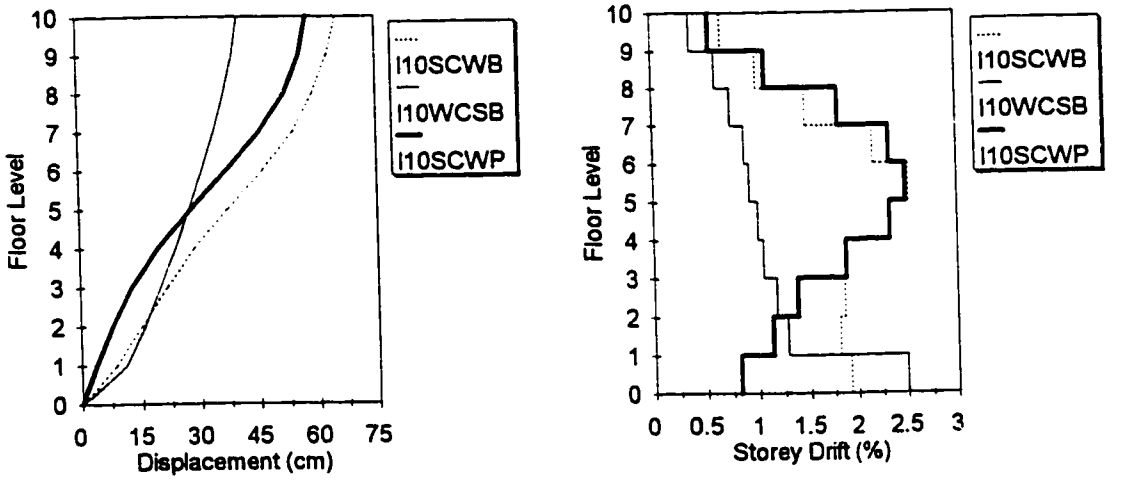


Figure 6.14 Height-wise distribution of floor displacements and storey drifts for the ten storey frames at 2.5% maximum storey drift.

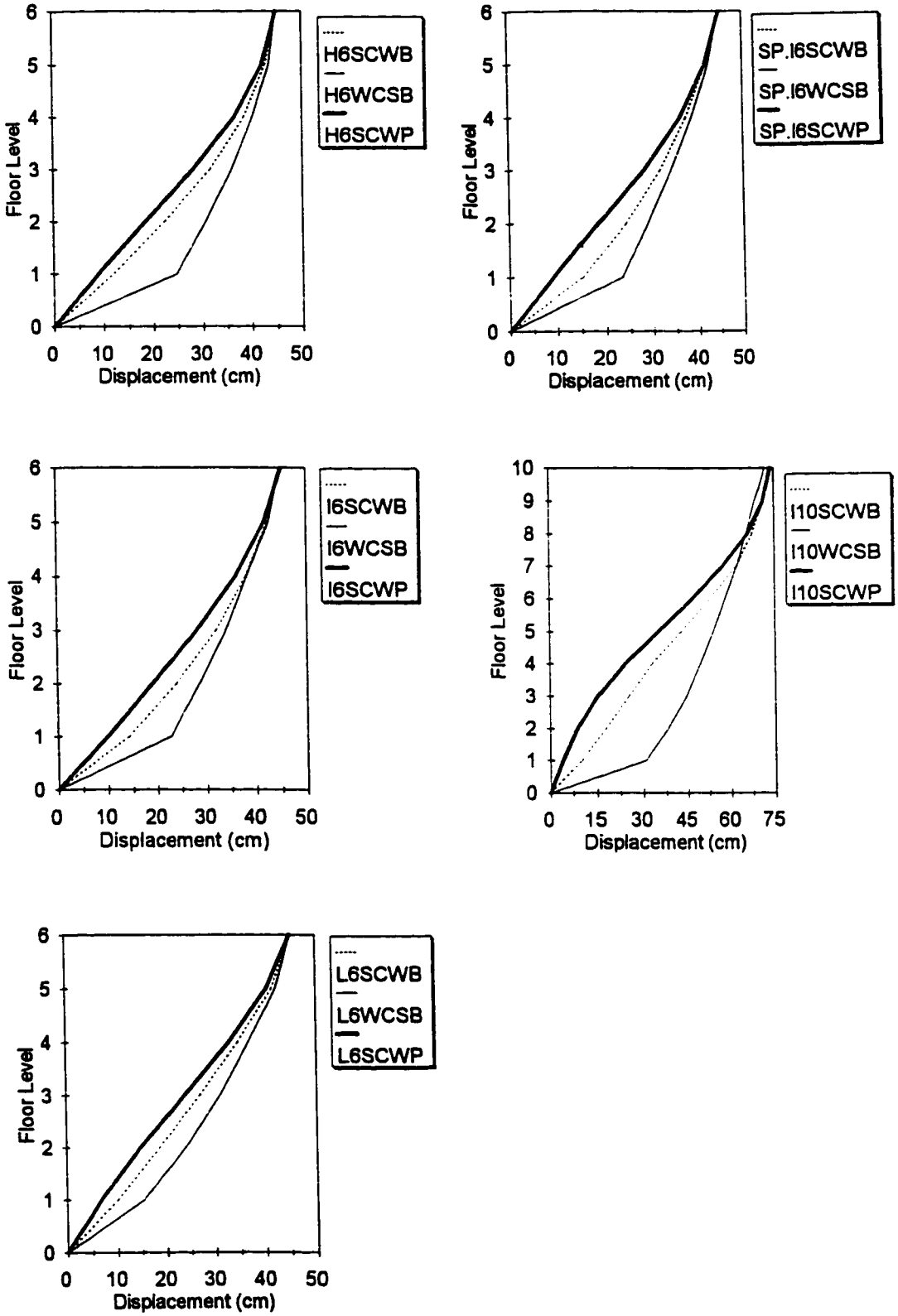


Figure 6.15 Height-wise distribution of floor displacements for all frames at a common roof deflection of 2% of the building height.

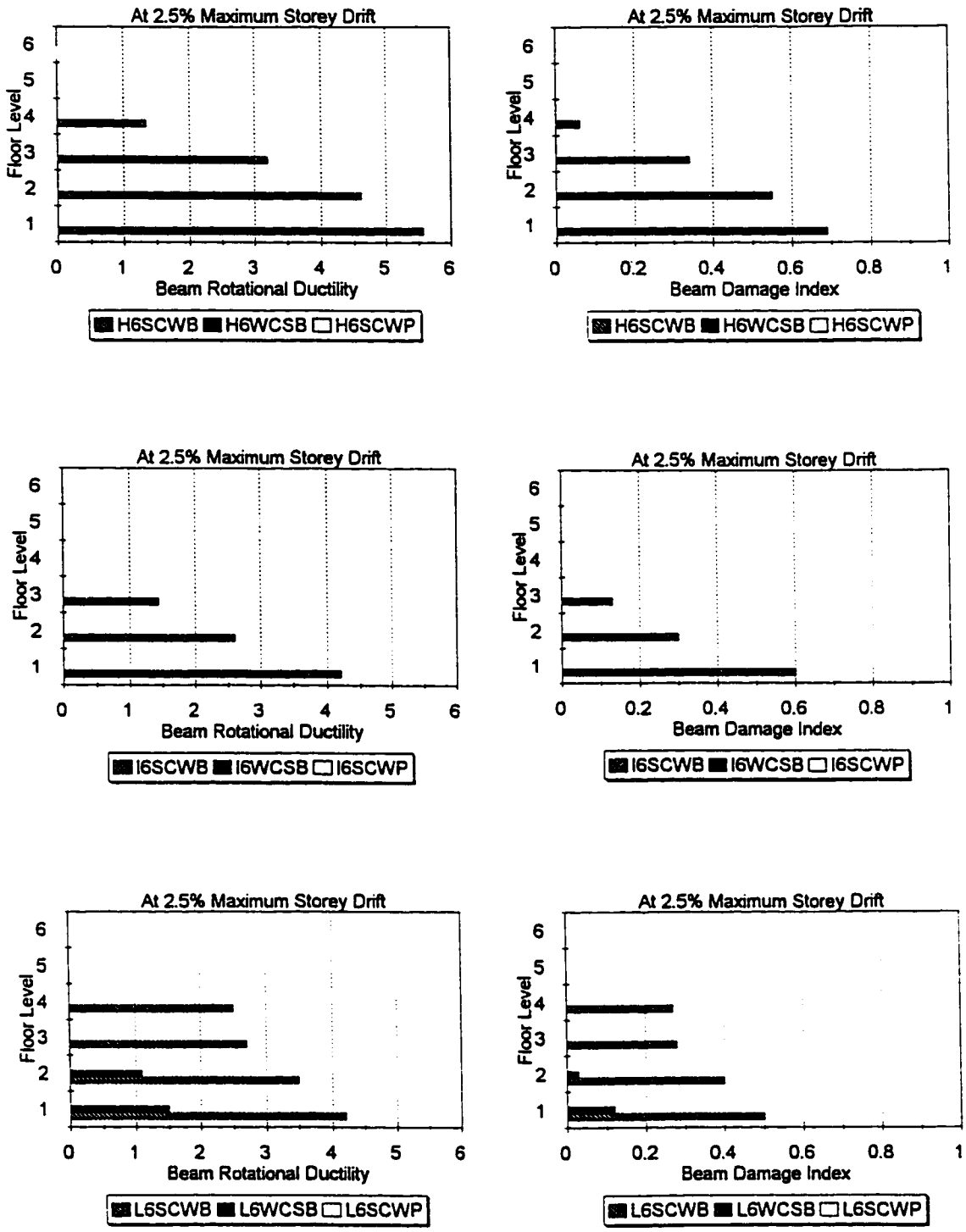


Figure 6.16 Beam performance parameters for the six storey frames at 2.5% maximum storey drift.

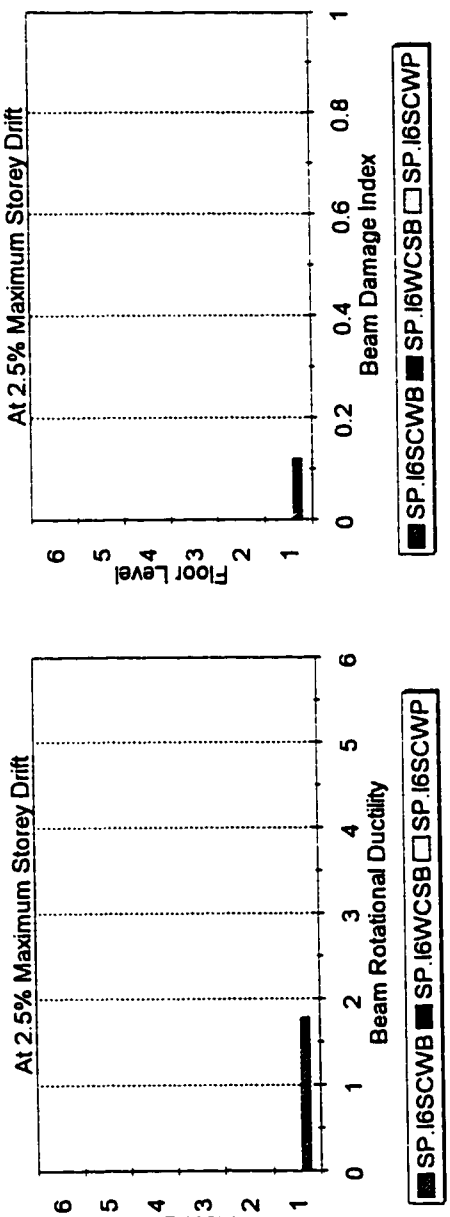


Figure 6.17 Beam performance parameters for the special drift limit designed six storey frames at 2.5% maximum storey drift.

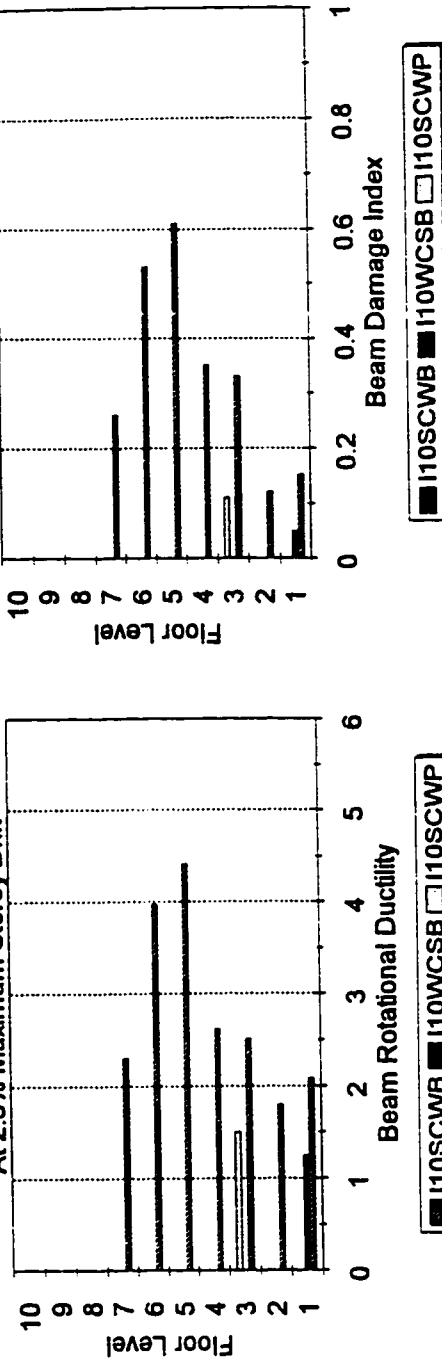


Figure 6.18 Beam performance parameters for the ten storey frames at 2.5% maximum storey drift.

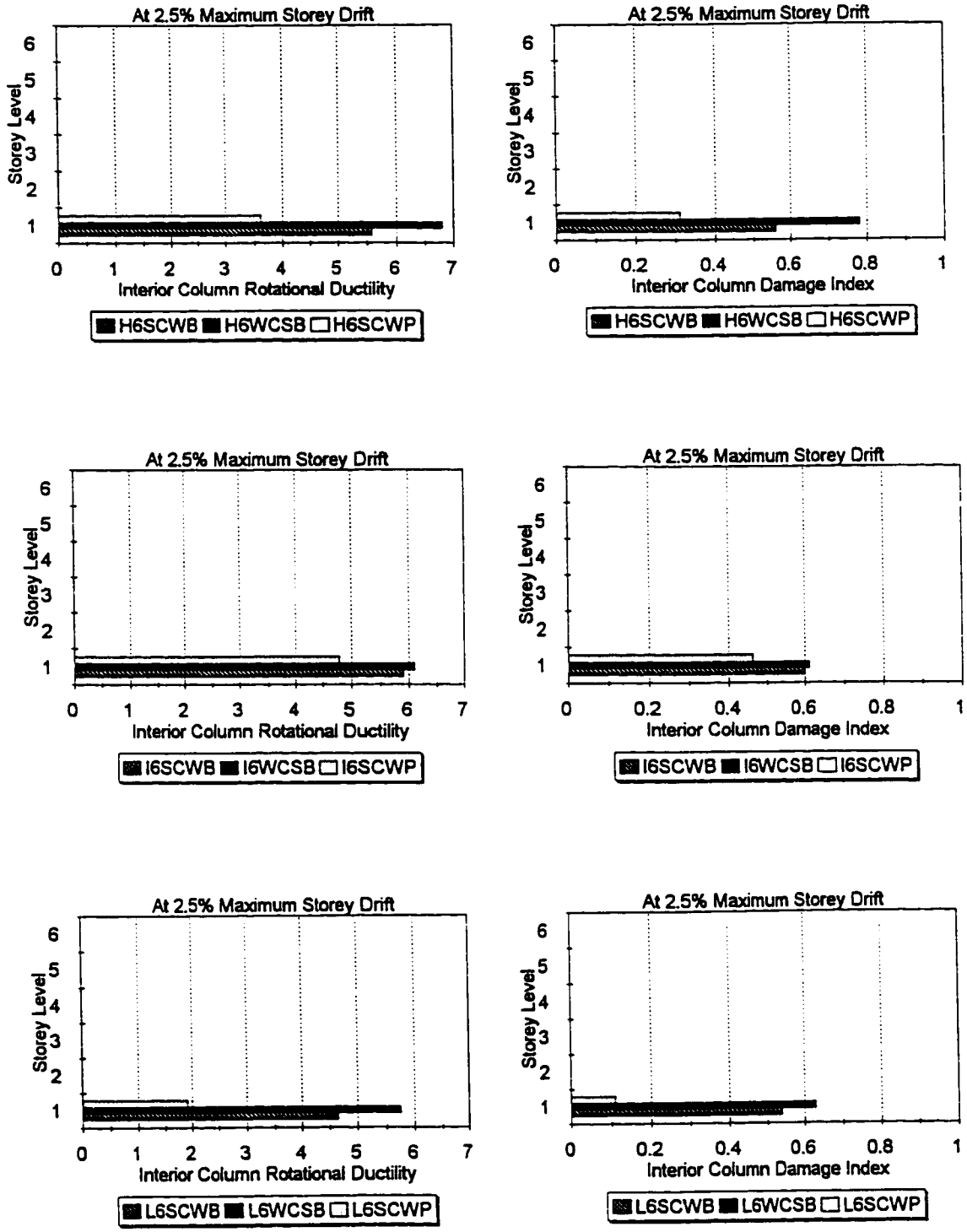


Figure 6.19 Interior column performance parameters for the six storey frames at 2.5% maximum storey drift.

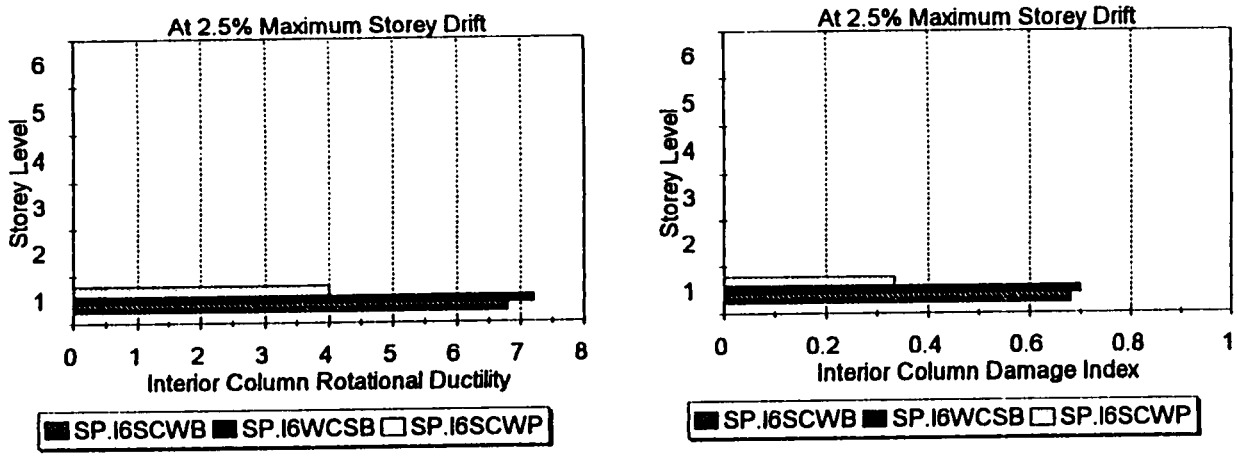


Figure 6.20 Interior column performance parameters for the special drift limit designed six storey frames at 2.5% maximum storey drift.

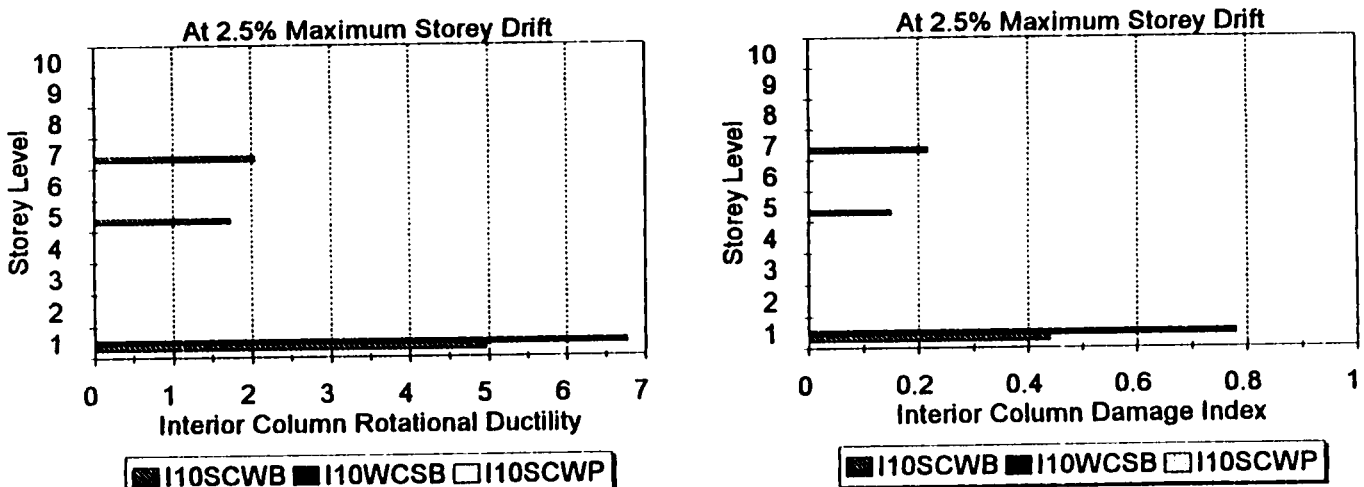


Figure 6.21 Interior column performance parameters for the ten storey frames at 2.5% maximum storey drift.

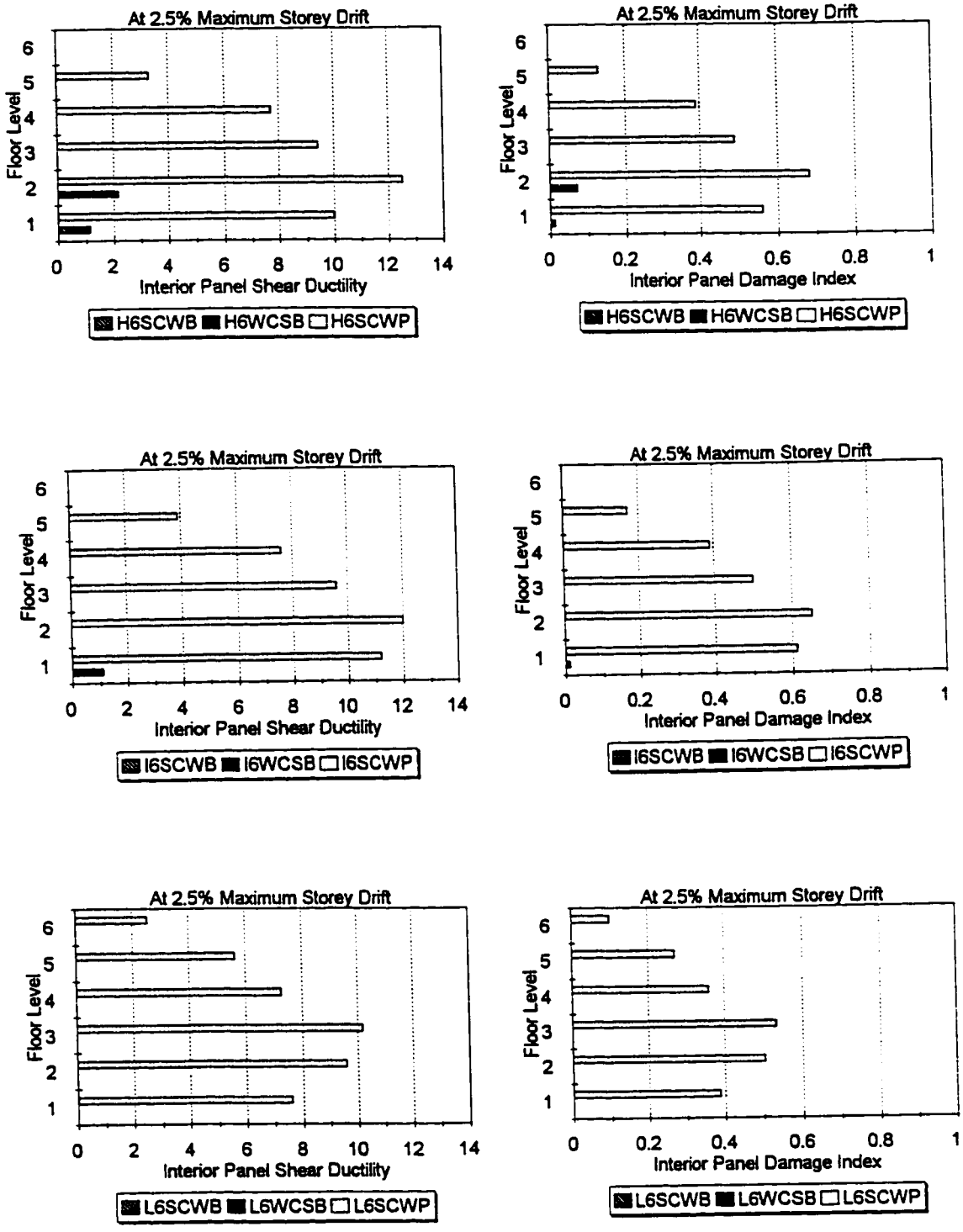


Figure 6.22 Interior panel zone performance parameters for the six storey frames at 2.5% maximum storey drift.

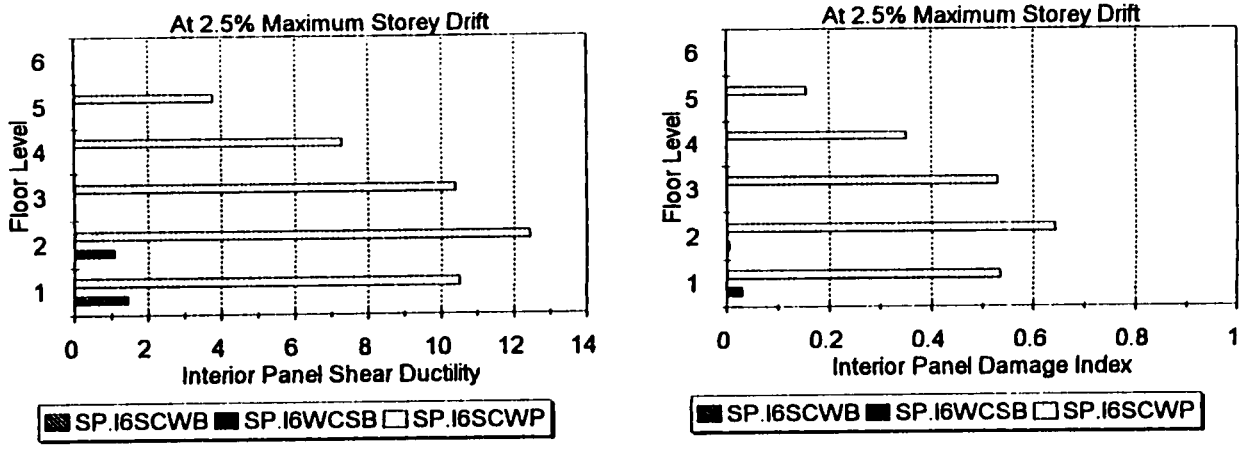


Figure 6.23 Interior panel zone performance parameters for the special drift limit designed six storey frames at 2.5% maximum storey drift.

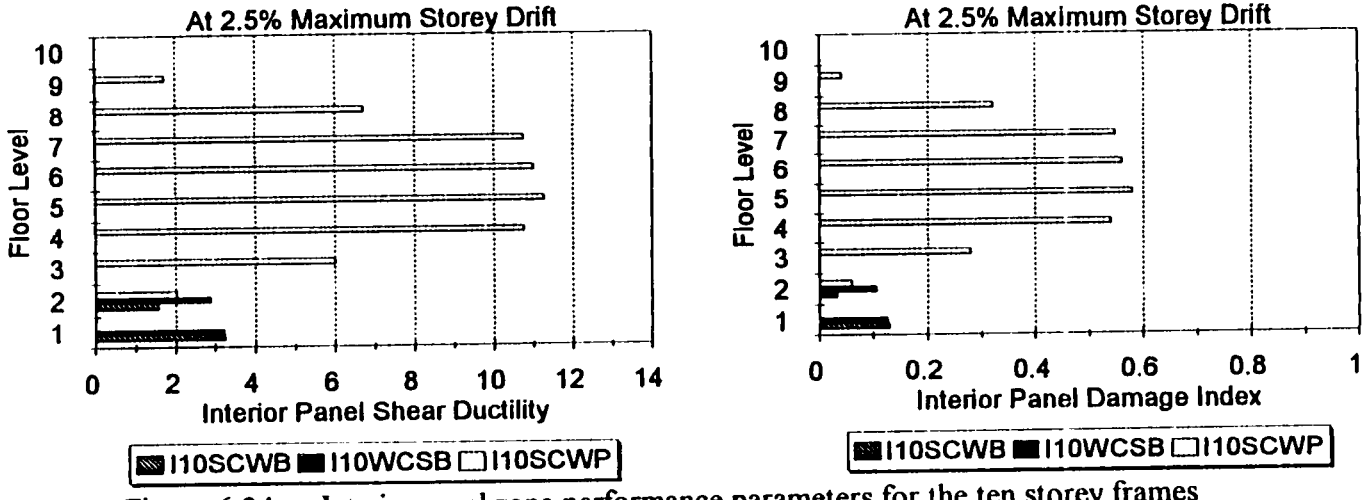


Figure 6.24 Interior panel zone performance parameters for the ten storey frames at 2.5% maximum storey drift.

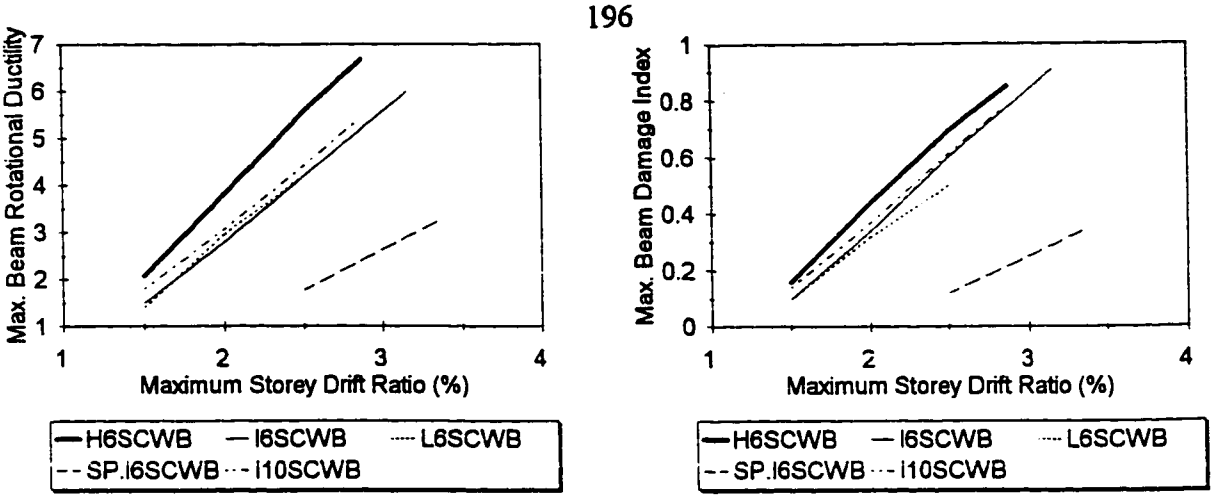


a) Beam Performance Parameters in SCWB frames

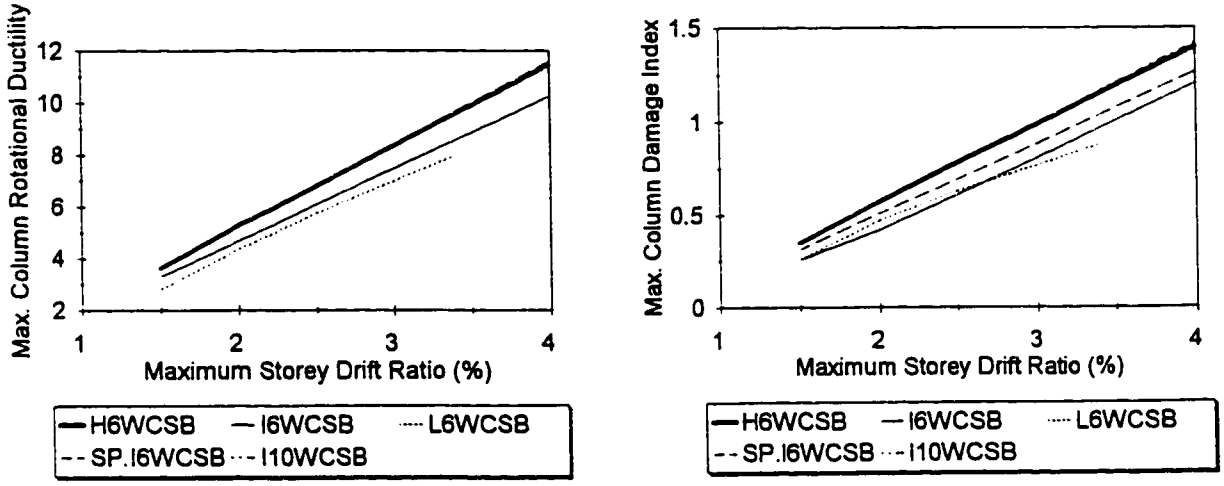


b) Column Performance Parameters in WCSB frames

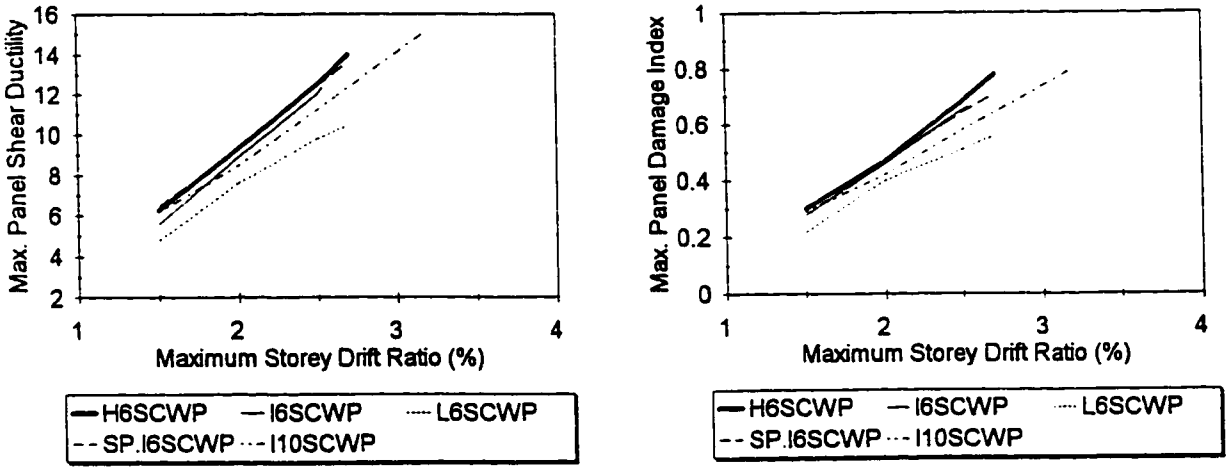


c) Panel Performance Parameters in SCWP frames

Figure 6.25 Maximum critical element performance parameters-maximum storey drift relationships.

# CHAPTER 7

# INELASTIC DYNAMIC ANALYSES

## 7.1 GENERAL

This chapter discusses the dynamic response behaviour of the designed frames subjected to the earthquake records described in Chapter 5. The use of real earthquake records as input for inelastic dynamic analyses provides a realistic simulation of the seismic hazard for determination of structural response. The maximum values of floor displacements, transient storey drifts, element ductilities and damage indices from each time-history excitation were analyzed statistically to determine the mean plus one standard deviation (M+SD) values. The M+SD values are used as the basis for evaluation of performance because of the need for a high level of confidence that damage will be less than some specified value; the M+SD level represents approximately an 84% level of confidence that the damage will be below the calculated value. The mean (M) values of some response parameters are also included in order to provide an indication of the dispersion characteristics within the ensemble of ground motions.

The objective of the inelastic dynamic analyses in this chapter is to investigate the seismic level of protection afforded to steel MRFs from a number of perspectives. This includes an evaluation of the vulnerability of the frames designed for different Canadian locations at ground motion levels that are higher than those used in design. This enables the

examination of the damage potential at lower levels of probability of exceedance than that used in design. The analyses address the question of how vulnerable the designed structures will be if the anticipated earthquake scenario results in much higher ground motions than those for which the structures have been designed (for life-safety objectives). This scenario might occur due to the significant uncertainty associated with determining the seismic hazard at a specific area. In fact, this scenario mentioned above has occurred before in different places all over the world, e.g. in recent earthquakes as 1994 Northridge earthquake and 1995 Hyogo-Ken Nanbu (Kobe) earthquake, for which ground motion levels were well above the design level.

In addition, the damage evaluation includes an assessment of the acceptability of the ranges of predicted (calculated) damage parameters during the time-history analyses. Comparison among the three Canadian locations facilitates the evaluation of the consistency of protection for different levels of seismic hazard. A number of other issues are also addressed in this chapter, e.g. the maximum storey drift-maximum element performance parameters relationships and the effect of peak ground velocity level on the performance (fragility curves). During dynamic analysis in this study, the gravity loads considered are D+0.5L. The lateral sway effect (P-$\Delta$) is considered as described in Chapter 3. The gravity loads acting on the leaning interior gravity columns are not considered in the (P-$\Delta$) effect.

## 7.2 SCALING OF THE TIME-HISTORIES

### 7.2.1 Ensemble "A"

There is a significant degree of uncertainty associated with the determination of

seismic hazard at a specific region. Uncertainties include random uncertainty, i.e. arising from physical variability that is inherent in the unpredictable nature of future earthquake events, and modelling uncertainty, i.e. arising from the expert specification of modelling assumptions. Given this large degree of uncertainty associated with estimates of the design ground motions, even at the same probability of exceedance, the actual ground motions that may excite a building could be higher than the "expected" values used in design, perhaps two or three times the design level (Heidebrecht, 1995). Thus, to evaluate the performance of the frames while taking into account this significant degree of uncertainty about the actual seismic ground motions that might excite the frames, the frames designed for a specified seismic hazard level were subjected to the twelve selected records in ensemble "A" scaled to a peak ground velocity of twice the design zonal velocity, (i.e. scaling to v=0.6 m/s, 0.4 m/s, and 0.2 m/s for H, I, and L seismic hazard zones respectively). In section 7.9, the effect of varying peak ground velocity level on the frame responses is discussed, in which some records were scaled to multiples of the design zonal velocity value (including: 1, 1.5, 2, 2.5, and 3 times the design level).

### 7.2.2 Ensemble "B"

The time-histories in this ensemble were used as input for inelastic dynamic analyses of the I6 set of frames for the purpose of examining the impact of new seismic hazard information. CANCEE (1996) proposed a preliminary formulation for determining the elastic design base shear force "$V_e$" using the uniform hazard spectral ordinates, $S_a^{UHS}(T)$, for possible use in the 2000 edition of the NBCC. For long period structures, for which the periods are larger than 1.0 s, the elastic base shear is based on the spectral ordinate at 1.0 s,

and $T^k$, in which "T" is period of the structure; the exponent "k" differs between eastern and western locations primarily because of the differing frequency content of ground motions in the two regions. The time-histories in ensemble "B" were scaled to the median value of $S_a^{UHS}(1.0)$ for Vancouver (Adams et al., 1996). However the I6 frames were designed based on the current NBCC (1995), for which the factors (v S U) in equations 4.1 and 4.2 in Chapter 4 resembles the factor $S_a^{UHS}(T)$ in determining the elastic base shear.

Therefore, for consistency and in order to compare the responses of the I6 frames when they are subjected to ensemble "B" with those when the frames are subjected to ensemble "A", time-histories in ensemble "B" were scaled to a common spectral acceleration ordinate $S_a(1.0) = 1.33*2* S_a^{UHS}(1.0)$. The factor 2 was used to account for scaling to twice the design level, while the factor 1.33 was used to scale to the same mean spectral acceleration level as that of ensemble "A" at T=1.0 s (Figure 7.1). Consequently, it should be noted that because of scaling factor (1.33), the actual seismic reponse of the I6 frames to the new seismic hazard level may be 30% lower than the results produced in this chapter.

## 7.3 MAXIMUM STOREY DRIFT RATIOS

### 7.3.1 Statistical analyses of the maximum storey drifts

The maximum storey drift is considered by designers as a global performance parameter and damage indicator. In terms of specific values, the SEAOC(1995) Vision 2000 report categorizes maximum storey drift ratios into ranges that correspond to certain levels of damage (see Table 2.1); Sozen (1981) also proposes a similar relationship between a global damage indicator (G.D.I) and the maximum storey drift (see Table 2.2). This drift based

criterion is selected as a basis for the evaluation of performance and overall damage assessment in this study. Table 7.1 presents the statistical parameters of the maximum storey drifts at excitations of twice the design level, as well as the range of the maximum drifts for each frame (i.e. the upper and lower bounds from the time-history analyses). The table also presents the number of time-histories in the ensemble that resulted in maximum drifts in certain ranges, and the storey levels at which maximum drifts occur. It can be seen from the table that the design philosophy as well as the seismic hazard design level have a considerable effect on the maximum storey drifts. The following observations can be drawn from the table:

*(i) SCWB and SCWP frames:* The M+SD drift values indicate that the SCWB and SCWP frames in the H and I seismic hazard zones are capable of sustaining excitations of twice the design level with severe damage but without structural collapse (i.e. M+SD drifts below the collapse drift limit of 2.5%). The M+SD drifts of the six storey SCWB frames and the ten storey SCWP frame slightly exceed the NBCC design drift limit (2%), while those of the six storey SCWP frames and the ten storey SCWB frame are in the neighbourhood of that limit. Both types of frames designed for the L seismic hazard zone suffered only moderate damage (i.e. M+SD drifts that are near the life-safe drift limit of 1.5%).

Based on drift performance criterion, the six storey SCWP frames perform better than the six storey SCWB frames, while the opposite is true for the ten storey frames. The M+SD drifts of the frames designed for the H seismic hazard zone are slightly higher than those for frames designed for the I seismic hazard zone, while drifts of frames in the L seismic hazard zone are significantly lower than those in the H and I seismic hazard zones. The special drift designed frames, i.e. SP.I6 frames, have M+SD drifts similar to those of the standard I6

frames; however, the range of maximum drifts of the SP.I6SCWB frame is much wider than that of the I6SCWB frame. For the I6 frames, the use of ensemble "B" of time-histories results in M+SD drifts comparable to those obtained from the use of ensemble "A", however the ranges of drifts are wider, which may be attributed to the fact that there is more dispersion in spectral values in ensemble "B" than in ensemble "A".

None of the maximum drifts of the six storey SCWP frames is higher than 2.5%, while the same observation is true for the ten storey SCWB frame. For SCWB and SCWP frames in the H and I seismic hazard zones, the majority of maximum drifts are in the range of 1.5% to 2.5%, while most maximum drifts are in the range of 0.5% to 1.5% for frames in the L seismic hazard zone. For SCWB and SCWP frames, the storey of maximum drift may differ from one time-history analysis to another. For the different time-histories included in the ensembles, the location of the maximum storey drift occurs in one of three storey levels. This indicates that the deflected shapes of the SCWB and SCWP frames during a seismic excitation are somewhat dependent on the characteristics of each earthquake time-history.

*(ii) WCSB frames:* The M+SD drifts indicate that the WCSB frames in the H and I seismic hazard zones are very likely to collapse (i.e. M+SD drifts are much larger than the collapse drift limit of 2.5%) when subjected to excitations at twice the design level. For frames H6WCSB and I6WCSB, 50% of the time-history analyses result in maximum drifts larger than 2.5%; the performance is even poorer for the I10WCSB frame in which this percentage is 75%. However, for the L6WCSB frame, the M+SD drift is similar to that of the L6SCWB frame, i.e. it suffers only moderate damage. For all the WCSB frames, the maximum drift always occurs in the first storey (independent of the time-history

characteristics), i.e. always exhibiting soft first storey behaviour, which is similar to what has been observed during the push over analyses. Considering the effect of using ensemble "B" of time-histories on the response of the I6WCSB frame, or the response of the special drift designed frame SP.I6WCSB, similar observations as those mentioned above in case of the SCWB frames are applicable, i.e. M+SD drifts are similar but drift ranges and distribution of drifts are somewhat different when compared with the responses of the I6WCSB frame to the time-histories included in ensemble "A".

### 7.3.2 Base shear-maximum storey drift relationships

The relations between the maximum base shear (normalized to the design value) and the maximum storey drift for all the time-history analyses are presented in Figures 7.2, 7.3, and 7.4 for the SCWB, WCSB, and SCWP frames respectively. As noted in Table 7.1, the maximum storey drifts occur in different storeys of the various frames; for each frame the storey associated with the maximum drift in the majority of the time-history analyses is selected for presentation in these diagrams. Each diagram also shows the same relationship determined from the static push over analysis and highlights the maximum drift associated with the SEAOC Vision 2000 life-safe (1.5%) and collapse (2.5%) performance levels. In addition, the drift at which yielding starts in static push over analysis, i.e. first nonlinear deformation in the base shear-drift curve, is marked on each diagram. For the purpose of discussion, the overall drift ductility factor is defined as the ratio of the maximum drift to that at which the first yielding occurs.

The diagrams show the substantial variability of maximum drift response due to

different excitations (all at twice the design level). The diagrams also show the extent to which the dynamic relationships resemble those obtained during the static push over analyses. In general, the individual dynamic results follow the static relationships quite closely. The largest deviation occur in the SCWP frames, especially in frames L6SCWP and I10SCWP; the static relationship tends to be conservative, i.e. lower base shears than the dynamic values. An examination of the range of individual time-history results gives a clearer picture of the performance of any frame than can be obtained from just knowing the M+SD value of the maximum storey drift. Table 7.2 summarizes the ranges as well as the statistical parameters of the overall drift ductility factor calculated from Figures 7.2 to 7.4. The following are some useful observations from this table and these figures:

*(i) SCWB frames:* (Figure 7.2) Although the absolute values of maximum drifts for the H6SCWB and I6SCWB frames seem to be comparable in both cases and confirm that both frames experience considerable inelastic behaviour, the drift ductility factors (e.g. M+SD drift ductility factor of 1.7 compared with 2.3) indicate that there is more inelastic behaviour in the I6SCWB frame, which may be attributed to the fact that the maximum drift occurs in the first storey rather than in the second storey as for the H6SCWB frame. For the L6SCWB frame, 50% of the maximum drifts from the time-history analyses are in the elastic range and the M+SD drift ductility factor (1.4) is much lower than that of the other SCWB frames, which confirms that this frame can be expected to experience very little inelastic behaviour. The response of the SP.I6SCWB frame is different than that of the standard I6SCWB frame in that the drift values are much more spread along the push over relationship, and the drift ductility factors reaches higher levels. For the effect of using ensemble "B" on

the response of the I6SCWB frame, the drift values and drift ductility factors are generally lower than in the case of using ensemble "A"; only one time-history analysis from ensemble "B" results in a higher drift. The I10SCWB frame experiences less inelastic behaviour than that of the standard I6SCWB frame. Consequently, it can be concluded that frames H6SCWB, I6SCWB, and SP.I6SCWB have little vulnerability of collapsing at an excitation of twice the design level. Frames L6SCWB and I10SCWB are not at all vulnerable to collapse at an excitation of twice the design level.

*(ii) WCSB frames:* (Figure 7.3) In each set of frames, the WCSB frame has the largest drift ductility factors compared to the other frames (i.e. SCWB and SCWP). The diagrams in Figure 7.3 and the maximum drift ductility factors in Table 7.2 (i.e. drift ductility factors of 4 or 5), clearly indicate the poor performance of the WCSB frames in the H and I seismic hazard zones. Frames H6WCSB, I6WCSB and I10WCSB are extremely vulnerable to collapse at an excitation of twice the design level; all time-history excitations result in maximum drifts which exceed that at which a mechanism develops in the static push over analyses. While the SP.I6WCSB frame is also vulnerable to collapse at an excitation of twice the design level, its performance is slightly better than that of the H6WCSB, I6WCSB and I10WCSB frames. Although the maximum drift ductility factors of frame I6WCSB from ensembles "A" and "B" are comparable, ensemble "B" is expected to have smaller damage effect on the frame, i.e. the frame is slightly less vulnerable to collapse. The only WCSB frame that is not vulnerable to collapse at twice the design level is the L6WCSB frame; some of its time-history responses are in the elastic range and all maximum drifts are less than that at which a mechanism develops in the static push over analysis.

*(iii) SCWP frames:* (Figure 7.4) Although the maximum drifts in all SCWP frames do not exceed 2.5%, the drift ductility factors are often higher than those of the comparable SCWB frames. For instance, the drift ductility factor for the H6SCWP frame ranges from 1.8 to 2.8 compared with a range of 1 to 2 for the H6SCWB frame, which indicates that there is more inelastic behaviour in frame H6SCWP than in frame H6SCWB. Consequently, in spite of the lower maximum drifts in frame H6SCWP, it's performance is not as good as that of frame H6SCWB. The same observation can be made when comparing frames I10SCWP and I10SCWB, although this is already clear from the comparison of the M+SD drifts. Similar observations for frames I6SCWP and L6SCWP are also applicable, but in those cases, the drift ductility factors of the SCWP frames are only slightly higher than those of the SCWB frames. The use of ensemble "B" for frame I6SCWP results in a wider range of drift ductility factors than those obtained from the use of ensemble "A"; however, the maximum drift ductility factors are similar. There is no noticeable advantage for frame SP.I6SCWP over frame I6SCWP; the only difference is that the drift ductility factors are more widely distributed in the SP.I6SCWP frame. Based on the drift performance criteria, none of the SCWP frames are likely to be vulnerable to collapse at excitations of twice the design level.

## 7.4 BASE SHEAR-MAXIMUM ROOF DEFLECTION RELATIONSHIPS

The base shear-roof deflection relationship is usually linked to the nonlinear push over static analysis; however, it is of interest to discuss the dynamic relationship and its correlation with the static relationship. The relations between the maximum base shear (normalized to the design value) plotted against the maximum roof deflection (normalized to the building

height) for all the time-history analyses are presented in Figures 7.5, 7.6, and 7.7 for the SCWB, WCSB, and SCWP frames respectively. Each diagram also shows the same relationship determined from the static push over analysis. Because it is not feasible to use the absolute value of the roof deflection as an indicator of the overall ductility demand imposed on a frame, the roof deflection ductility factor is introduced. The roof deflection ductility factor is defined as the ratio of the maximum roof deflection to that at which the first nonlinear deformation (first yielding) occurs in the static base shear-roof deflection relationship. The yielding roof deflection is also marked on each diagram in these figures.

The general conclusions as stated for the base shear-maximum drift relationships are also applicable here, i.e. regarding the variability of the roof deflection response due to different excitations, and that the dynamic relationships follow those determined from the static push over analyses. To assist in the discussion, Table 7.2 includes the overall roof deflection ductility factors determined from Figures 7.5 to 7.7.

The following are some useful observations from that table and these diagrams:

*(i) SCWB frames:* (Figure 7.5) The SCWB frames have the smallest roof deflection ductility demand compared with the other frames (i.e. WCSB and SCWP frames). All the six storey SCWB frames have M+SD roof deflection ductility factors of approximately the same order of magnitude, i.e. 1.5, except for the L6SCWB frame which has an M+SD roof deflection ductility factor of 1.0, i.e. just started to yield. Only the H6SCWB and I6SCWB frames have all their roof deflection ductility factors (from all time-history analyses) above the yielding limit, which indicates higher levels of ductility demands than those for the other six

storey SCWB frames. The I10SCWB frame has a M+SD roof deflection ductility which is slightly above the yielding limit, i.e. the inelastic action is less than that of the standard I6SCWB frame.

*(ii) WCSB frames:* (Figure 7.6) The six storey WCSB frames have roof deflection ductility factors 10% to 20% larger than those of the comparable six storey SCWB frames. Realizing that the lateral deflection in the WCSB frames is concentrated at the first floor level (i.e. inelastic action is concentrated in one storey), those roof deflection ductility factors in the WCSB frames indicate substantial inelastic actions in the critical elements, i.e. in columns.

All the six storey WCSB frames, except frame L6WCSB, have roof deflection ductility factors well above the yielding limit. The L6WCSB frame has 50% of its roof deflection ductility factors below the yielding point, i.e. much less inelastic action than those of other six storey WCSB frames. The I10WCSB frame has a M+SD roof deflection ductility 30% larger than that of the I10SCWB frame, which indicates considerable inelastic deformations in the critical elements (columns).

*(iii) SCWP frames:* (Figure 7.7) The SCWP frames have the largest roof deflection ductility demand compared with the other frames (i.e. SCWB and WCSB frames). For the six storey SCWP frames, increasing the seismic hazard level from L to I to H results in an increase in the M+SD roof deflection ductility factor of 0.5 for each increase in hazard level, which also means an increase in the panel shear ductility demands. The M+SD roof deflection ductility of the I10SCWP frame is comparable with that of the I6SCWP frame, but the range of roof deflection ductilities is much wider.

*(iv) General:* The comparison of roof deflection ductility factors with drift ductility factors indicates that the roof deflection ductility factor alone is incapable of demonstrating the relative performance among different frame design types; the drift ductility factor is a much better parameter for examining such relative performance.

The use of ensemble "B" for all I6 frames results in M+SD roof deflection ductility factors comparable with those resulting from the use of ensemble "A" but with wider ductility range. The SP.I6SCWB and SP.I6WCSB frames have similar M+SD roof deflection ductility factors to those of the standard I6SCWB and I6WCSB frames respectively, but with much wider ductility ranges. The SP.I6SCWP frame shows an increase of 20% in the M+SD roof ductility compared with that of the I6SCWP frame, this of course in addition to having a much wider range of roof deflection ductility.

The force reduction factor "R" specified in NBCC (1995) is directly applied to the elastic design base shear, thus, its value can be explicitly related to the expected overall inelastic behaviour of different structural systems. In general, the overall ductility is associated with the roof deflection ductility factor. One should keep in mind also that the roof deflection ductility factor is always well below the structural element (beam, column, or panel) ductilities. Results show that all roof deflection ductility factors are well below the value of R = 4 specified by NBCC(1995) for steel MRFs. In the extreme case, the roof deflection ductility factor is 2.7 for H6SCWP frame. Consequently, the roof deflection ductility factor is design dependent, and the use of single value to represent all MRFs without recognizing the effects of the design philosophy is inappropriate. This might also show that the use of roof deflection ductility as a measure of the system ductility is not quite consistent.

## 7.5 HEIGHT-WISE DISTRIBUTION OF OVERALL RESPONSE PARAMETERS

### 7.5.1 Floor displacements

Shown in Figure 7.8 are the M+SD values of the maximum floor displacements (envelopes) for all the frames. While the floor displacements cannot strictly be interpreted as displaced shapes (because the maxima at different floor levels may occur at different times), the displacement diagrams provide some indication of the regions of maximum deformations as well as maximum roof displacement. Considering the six storey frames, while the maximum roof deflection increases slightly as the design seismic hazard level goes from L to H, the order of magnitude of the M+SD roof deflection can be considered practically constant (i.e. the average is in the order of 1.4% of the building height, while the range is from 1.3% to 1.5% of the building height). This shows that the increased stiffness of the frames designed at H and I seismic hazard levels compensates for the increased amplitude of ground motions used to excite those frames. The envelope shapes for all the six storey SCWB and SCWP frames are quite smooth. However, the WCSB frames show a marked kink at the first floor level, especially noticeable for frames in the H and I seismic hazard zones. This kink is due to inelastic behaviour at both the bottom and top ends of the first storey columns; the extent of that behaviour increases dramatically as the design seismic hazard level increases.

The envelope shapes show that the maximum deformations occur at the bottom storey for the WCSB frames, at the lower storeys for SCWB frames and at storeys near the mid-height for the SCWP frames. In L seismic hazard zone, frames L6SCWB and L6WCSB have similar envelope shapes. No significant differences are observed between the envelope shapes of the SP.I6 and the I6 frames. The use of ensemble "B" slightly reduces the displacement

envelopes in the upper floors of frame I6SCWB, otherwise, no significant differences are noticed when compared with envelopes resulting from the use of ensemble "A".

For the ten storey frames, the envelope shapes of frames I10SCWB and I10SCWP are quite smooth and similar, while the I10WCSB frame also experiences the first floor kink similar to that of the H6WCSB and I6WCSB frames. The M+SD roof deflections of the ten storey frames are less than those of the six storey frames, i.e. in the range of 1.0% to 1.25% of the building height. The envelope shapes show that the maximum deformations occur at the bottom storey for the I10WCSB frame, while they occur near the mid-height for the I10SCWB and I10SCWP frames.

### 7.5.2 Storey drifts

Shown in Figure 7.9 are the M+SD values of the maximum storey drifts (envelopes) for all the frames. From this figure, the following can be observed:

For the six storey SCWB frames, the height-wise distribution of the drifts is relatively uniform with maxima of about 2.3% (< 2.5%, SEAOC(1995) performance level for collapse) for frames I6SCWB and H6SCWB. The maximum drift occurs in the first storey of the I6SCWB frame and in the second storey of the H6SCWB frame. The maximum for the L6SCWB frame is somewhat smaller, i.e. about 1.6% (≈ at the SEAOC (1995) performance level for life-safety) and occurs in the fifth storey. Given that the design drift limit is 2%, these M+SD drift values and their distribution when the excitation is twice the design value indicate that the lateral deformations of these frames are controlled very well.

For the six storey SCWP frames, the height-wise distribution of the drifts is fairly uniform with maxima slightly lower than those for their SCWB counterparts, i.e. 2.1%, 1.75%

and 1.35% for the H6SCWP, I6SCWP and L6SCWP frames respectively. The maxima occur near the mid-height of the structure, in either the third or the fourth storey. With reference to drift criteria, the performance of each of these frames is slightly better than the corresponding SCWB frame.

For the six storey WCSB frames, excluding the L6WCSB, the height-wise distribution of the drifts starts with a very high M+SD drift in the first storey (i.e. 4% and 3% for frames H6WCSB and I6WCSB respectively); then it decreases to a uniform low value (about 1%) in other storeys. The L6WCSB frame experiences a M+SD first storey drift of 1.6% and values that range from 1% to 1.4% in other storeys. The drift response of the H6WCSB and I6WCSB frames clearly show the soft first storey phenomenon which is consistent with the marked kink in the displacement envelope (Figure 7.8); also their maximum M+SD drifts significantly exceed the SEAOC Vision 2000 limit for expected collapse. The soft first storey feature is not really noticeable in the L6WCSB frame; the M+SD maximum drift, which marginally exceeds the life-safe performance limit, is of the same order of magnitude as that for other L6 frames (i.e. L6SWCB and L6SCWP).

At M+SD level, the drift distribution trends for the I6 frames are also applicable for the SP.I6 frames; the maximum M+SD drifts are comparable for both sets of frames. Practically, the use of ensemble "B" of time-histories for the I6 set of frames results in M+SD drift distribution trends similar to those from the use of ensemble "A".

Based on the above assessment, it can be concluded that the six storey SCWB and SCWP frames perform satisfactorily when designed at all the three seismic hazard levels. The six storey WCSB frames designed at the I and H seismic hazard levels do not perform

satisfactorily. However, the six storey WCSB frame designed at the L seismic hazard level has satisfactorily performance which is practically indistinguishable from that of the six storey SCWB and SCWP frames designed for the L seismic hazard level.

The ten storey SCWB and SCWP frames (i.e. I10SCWB and I10SCWP) have M+SD level drift distributions which are similar to their six storey counterparts (I6SCWB and I6SCWP), except that the maximum drift in the I10SCWB frame occurs at two levels, the first storey and near the mid-height of the building. Both frames have maximum M+SD drifts of about the same order of magnitude ($\approx$ 2%). The drift distribution of the I10WCSB frame is quite similar to that of the I6WCSB frame, except that the maximum drift in the first storey is slightly larger. Consequently, the same conclusions regarding the performance levels can be drawn as for the six storey frames (I6 frames).

By comparing these results with those in chapter 6, it can be concluded that the general distribution trends of the maximum storey drifts during dynamic analyses are similar to those obtained during push over analyses, i.e. the push over analyses can simulate the distribution of the maximum values of the storey drifts obtained from the dynamic analyses.

### 7.5.3 Storey shears

Shown in Figure 7.10 are the M+SD values of the maximum storey shears (envelopes) for all the frames. Each diagram in this figure also shows the design storey shears. The storey shear height-wise distribution trends are similar to those used in the design based on the inertia forces (in which inverted triangular loading was used). The diagrams indicate that in all the six storey sets of frames, the SCWB frames have the largest storey shears and the SCWP frames have the smallest storey shears. For the ten storey frames, the SCWP frame

also has the smallest storey shears, but there is no clear differences between the storey shear distribution of the I10SCWB and I10WCSB frames. At excitation of twice the design level, all the frames exhibit a significant dynamic overstrength (maximum base shear/design base shear). For instance, the M+SD dynamic overstrength for the six storey SCWB and WCSB frames in the H and I seismic hazard zones is in the order of 2.5, while it is in order of 2 for the SCWP frames. Frames designed at the L seismic hazard level have slightly higher values of dynamic overstrength than those mentioned above. The SP.I6SCWB and SP.I6WCSB frames exhibit M+SD dynamic overstrengths of 4 and 3.5 respectively; this is due to their strongest beam and column sections. The ten storey frames exhibit an M+SD dynamic overstrength that ranges from 2.5 to 3.

## 7.6 BEAM PERFORMANCE

### 7.6.1 Performance parameters

Shown in Figure 7.11 are the M+SD beam performance parameters, i.e. beam rotational ductilities and damage indices. It should be mentioned that an M+SD ductility value less than 1.0 (e.g. the third floor beam in frame L6SCWB) does not mean complete elastic behaviour, but means that some time-history analyses resulted in an elastic behaviour (i.e. ductility of zero), while the other time-history analyses resulted in yielding with ductility values which are slightly above 1.0.

*(i) SCWB frames:* It is expected that beams in SCWB frames exhibit considerable inelastic action, as they are the critical elements designed to undergo inelastic deformations. Considering first the six storey frames, at an excitation of twice the design level all three

standard SCWB frames exhibit plastic beam deformations in almost all the floors; the maximum M+SD beam rotational ductility values are 5.5, 4.2, and 2 respectively. As damage is a function of the accumulated plastic deformations, the beam damage indices provide a better indication of the relative damage than the rotational ductilities. The figure shows that for the H6SCWB frame, beams in the first through the third floors can be expected to fail, given that the M+SD beam damage index ranges from 1 to 1.3. For the I6SCWB frame, only the first floor beams suffer a high level of damage (i.e. damage index of 0.85), while the damage is moderate in the beams of the other floors (i.e. damage index of 0.4). Very little damage occurs in the beams of the L6SCWB frame; the maximum M+SD beam damage index is in the order of 0.2. The beams of the SP.I6SCWB frame exhibit limited plastic deformations; the maximum M+SD beam rotational ductility and damage index are 1.7 and 0.15 respectively, which is due to the use of much stronger beam members in order to limit the design drift to 1%. The use of ensemble "B"of time-histories results in M+SD beam rotational ductilities for the I6SCWB frame that are similar to those resulting from the use of ensemble "A", however the M+SD beam damage indices are 25% lower, which means less accumulation of plastic deformations.

Comparison of beam performance parameters in this chapter with those in Chapter 6 indicates that the static push over analyses can estimate maximum beam ductility demand (at a specified drift value) quite well. On the other hand, dynamic analyses result in beam damage indices that can be 60% to 80 % higher than those from static analyses; this difference is due to the accumulation of plastic rotations during reversals which translates directly into more damage.

The most extensive plastic deformations in the beams of the ten storey frames also occur in the SCWB frame, in which the maximum beam deformations are developed near the frame mid-height. Although the height-wise distribution of the beam performance parameters in the I10SCWB and I6SCWB frame is different, the maximum M+SD values are quite similar, i.e. maximum M+SD beam rotational ductility in the order of 4 and damage index in the order of 0.8.

*(ii) WCSB and SCWP frames:* The beams of both the I6WCSB and L6WCSB frames remain elastic at this level of excitation, while the first floor beams of the H6WCSB frame have just started to yield due to the excessive first floor lateral deflection. The beams of both the I6SCWP and L6SCWP frames remain elastic, while the beams of the H6SCWP frame in the first and second floors have limited plastic deformations. This indicates that beams started to share in dissipating the input seismic energy after the panels have suffered extensive plastic shear deformations. The beams in the I10WCSB exhibit no plastic deformation, while the beams in the I10SCWP frame show limited inelastic deformations (the maximum M+SD beam rotational ductility is 2.8 with a corresponding damage index of 0.3).

### 7.6.2 Concluding comments

Based on the above discussion, it can be expected that beams in the H6SCWB frame will fail at an excitation slightly below twice the design level and that beams in the I6SCWB and I10SCWB frames will fail at an excitation slightly above twice the design level. However, at this level of excitation, the beams in the L6SCWB frame can be expected to sustain only moderate damage. In all the WCSB and SCWP frames the beams either remain

elastic or exhibit minor plastic deformations and damage at some very rare locations, i.e. far from being vulnerable to failure.

## 7.7 COLUMN PERFORMANCE

Shown in Figures 7.12 and 7.13 are the M+SD performance parameters of the exterior and interior columns respectively, i.e. column rotational ductilities and damage indices. The figures show that for the WCSB frames, increasing the seismic hazard design level results in a dramatic increase in the plastic deformations of the first storey columns, which occur at both the top and bottom ends, i.e. soft storey behaviour.

### 7.7.1 Exterior column performance parameters

From Figure 7.12, the following can be observed:

*(i) WCSB frames:* at an excitation of twice the design level, the first storey exterior columns of the H6WCSB frame have the poorest performance (the largest ductility (9.5) and damage index >> 1.0) among all exterior columns of the WCSB frames and can be expected to fail at an excitation well below that level. The other WCSB frames, except the L6WCSB frame, also have first storey exterior column damage indices exceeding the failure limit (1.0) with a corresponding ductility of 7 and can be expected to fail at this level of excitation. In addition, column plastic deformations start to develop at upper storeys, which are more obvious in case of the I6WCSB frame. This might be attributed to two factors, first is the contribution of the higher modes of vibration to the frame dynamic response, and second is the relative lateral strengths of the upper storeys with respect to the lower storeys, including the relative strengths of the columns, which is function of the final selection of the member

sections during the design process. For the L6WCSB frame, the first storey exterior columns suffer only minor damage (damage index of 0.4).

*(ii) SCWB and SCWP frames:* the columns of the six storey SCWB frames undergo plastic deformations only at the bottom of the first storey, i.e. at the base, with moderate levels of ductility and damage for the H6SCWB, I6SCWB and SP.I6SCWB frames, while these levels are minor for the L6SCWB frame. Based on the deterministic capacity design approach given by Paulay and Priestley (1992), in which a kinematically admissible plastic mechanism is chosen, plastic hinge formation is expected at ground floor of the first storey or at foundation level, where full base fixity of a column is normally assumed. In addition, at the ground level, the moment demand does not depend on the strength of the adjacent members, such as components of the foundation system. The first storey columns of the I10SCWB frame also undergo plastic deformations at the base with moderate damage. Moreover, limited plastic deformations occur in the columns located at storey levels near the mid-height of the ten storey frame. This is due to extensive plastic deformations in beams located at the adjacent floor levels. The columns of all the SCWP frames have minor plastic deformations only at the bottom of the first storey (at the base), except for the L6SCWP frame in which they remain elastic.

### 7.7.2 Interior column performance parameters

In general, the observations mentioned above for the exterior columns are also applicable for the interior columns, but with higher levels of plastic deformations and damage. From Figure 7.13, the following can be observed:

*(i) WCSB frames:* more significant damage occurs in the upper storey interior columns compared with that in the exterior columns. Given the values of damage indices in the first storey interior columns (>> 1.0), it can be expected that in all the WCSB frames, except frame L6WCSB, these columns will fail at excitations well below twice the design level, especially the columns of the H6WCSB and I10WCSB frames. The L6WCSB frame suffers only moderate damage in its first storey interior columns and only minor damage in the columns at upper storey levels. It should be noted that the results of static analyses in Chapter 6 did not predict such high maximum column rotational ductility demands nor the pattern of inelastic deformations throughout the height of the buildings. In general, the dynamic analyses result in more column deformations and damage than are predicted by the static analyses; sometimes column damage indices from dynamic analyses are two to three times those from static analyses.

*(ii) SCWB and SCWP frames:* the first storey interior columns of the six storey SCWB frames exhibit plastic deformations at the base of the frames, but with higher damage indices than in the exterior columns, particularly for frames in the H and I seismic hazard zones. For instance, the M+SD interior column damage indices at the base are 0.9 and 1.0 for the H6SCWB and I6SCWB frames respectively; both have M+SD column ductilities in the order of 6. For the stiffer frame SP.I6SCWB, the situation is slightly worse, as the column damage index at the base is slightly larger than 1.0, this compensates for the minor level of beam damage that this frame suffers. The interior columns of the I10SCWB frame exhibit similar behaviour to its external columns, but with slightly larger values of the performance parameters; the M+SD column damage index at the base is 0.65, i.e. the columns

of this frame are not yet near failure. For SCWB frames, the column rotational ductilities are similar to those obtained form the push over static analyses in Chapter 6, however, the column damage indices are 50% higher than those obtained from the push over analyses.

For the SCWP frames, the interior columns experience minor to moderate levels of damage, which occur mainly at the bottom of the first storey (i.e. at the base). The interior columns of the L6SCWP frame do not experience any plastic deformations. The column performance parameters are lower than those determined during static push over analyses.

### 7.7.3 Concluding comments

Based on the performance of columns, it can be concluded that both the H6WCSB and I10WCSB frames can be expected to fail at an excitation level well below twice the design level. The I6WCSB and SP.I6WCSB frames can be expected to fail at an excitation level which is slightly below twice the design level, while the L6WCSB frame sustains only moderate damage at this excitation level. At an excitation of twice the design level, the columns of the SCWB frames are in a moderate to high state of damage at the base, but are not expected to cause structural collapse of the frames. The columns of the SCWP frames suffer only minor or moderate damage at the base.

## 7.8 JOINT PANEL PERFORMANCE

Shown in Figures 7.14 and 7.15 are the M+SD performance parameters of the exterior and interior panels respectively, i.e. panel shear ductilities and damage indices. Most of the joint panels in the SCWB and WCSB frames remain elastic, while the joint panels in the

SCWP frames exhibit significant plastic shear deformations as they are the elements responsible for seismic energy dissipation. In all the SCWP frames, inelastic panel zone shear deformations occur throughout the height of the structure; maximum values typically occur in the second and the third floor panels for the six storey SCWP frames, while they occur in the fourth and fifth floor panels for the ten storey SCWP frame. Inelastic deformations and damage are always more extensive in the interior panels.

### 7.8.1 Exterior panel performance parameters

From Figure 7.14, the following can be observed:

*(i) SCWP frames:* in all the SCWP frames, the maximum M+SD panel shear ductility is in the range of 8 to 9, except for frame L6SCWP in which it is only 4. Severe panel damage (i.e. maximum M+SD damage index in the order of 0.9) occurs in frames H6SCWP and I6SCWP, while the panels in frame L6SCWP are only lightly damaged. The larger panel web thicknesses in frame SP.I6SCWP slightly reduce the panel damage compared with that in frame I6SCWP. The use of ensemble "B" of time-histories results in less damage in the panels of the I6SCWP frame compared with that resulting from the use of ensemble "A". Although the panels of the I10SCWP frame have M+SD shear ductilities similar to those of the I6SCWP frame, they suffer less damage (maximum M+SD panel damage index of 0.65 compared with 0.9), i.e. lower cumulative hysteretic damage effects, probably because the longer period of this frame results in fewer cycles of large amplitude response.

*(ii) SCWB and WCSB frames:* the panels of the SCWB and WCSB frames have either no or very limited plastic shear deformations. In the rare cases in which the panels of

these frames start to experience plastic deformations, the maximum M+SD panel shear ductility are in the neighbourhood of 3 with corresponding damage indices of 0.2 or less, i.e. practically negligible.

### 7.8.2 Interior panel performance parameters

From Figure 7.15, the following can be observed:

*(i) SCWP frames:* at an excitation of twice the design level, the interior panels in floors from the first through the fourth in both the H6SCWP and I6SCWP frames are expected to fail (i.e. M+SD panel damage index $\geq$ 1.0), while the interior panels of the L6SCWP frame exhibit only moderate damage. For frames H6SCWP, I6SCWP and L6SCWP, the maximum M+SD panel shear ductilities are 12, 9 and 5; the corresponding damage indices are 1.6, 1.2 and 0.4 respectively.

Although the panel shear ductilities in frame SP.I6SCWP are similar to those in frame I6SCWP, the larger panel web thicknesses reduces the panel damage compared with that in frame I6SCWP, i.e. maximum M+SD panel damage index of 0.75 compared with 1.2. The use of ensemble "B" of time-histories results in shear ductilities in the panels of the I6SCWP frame which are similar to those resulting from the use of ensemble "A", however, the panel damage indices are less, e.g. the maximum M+SD panel damage index of 0.8 compared with 1.2.

The performances of the interior and exterior panels of the I10SCWP frame are approximately comparable, i.e. they have shear ductilities similar to those of the I6SCWP frame but they only suffer moderate damage.

For the SCWP frames, the distribution of panel zone deformations along the building height during dynamic analyses is comparable with that obtained during push over static analyses in Chapter 6. However, comparison of the results indicate that during the static analyses, the panels tend to exhibit lower damage indices with much higher shear ductilities than those obtained during dynamic analyses, i.e. the accumulation of hysteretic damage during dynamic response increases the damage indices significantly.

While the ductility demands imposed on the critical elements in SCWP frames (i.e. panel zone elements) are relatively higher than those of beams and columns in SCWB and WCSB frames respectively, this does not automatically mean poor behaviour when compared with other frames, because inelastic behaviour in panel elements is completely different from that in beam-column elements, as panel behaviour is dominated by shear deformation, while beam-column behaviour is dominated by flexural deformation. In addition, the ductility capacity for a panel element (shear ductility capacity) is different from that of a beam-column element (rotational ductility capacity).

*(ii) SCWB and WCSB frames:* similar observations as those mentioned above for the exterior panels of SCWB and WCSB frames are also applicable for the interior panels, i.e. either no damage or the damage is practically negligible.

### 7.8.3 Concluding comments

Based on the performance of joint panels, it can be concluded that panels of the H6SCWP can be expected to fail at an excitation which is below twice the design level, while the panels of the I6SCWP can be expected to fail at an excitation only slightly below twice

the design level. The panels of the L6SCWP frame suffer only moderate damage at an excitation of twice the design level. The panels of the SP.I6SCWP and I10SCWP frames can sustain excitations above twice the design level prior to reaching failure. The panels of the SCWB and WCSB frames deform either elastically or with minor levels of plastic deformations in only very few locations, i.e. they are not at all vulnerable to failure at an excitation of twice the design level.

## 7.9 EFFECT OF PEAK GROUND VELOCITY LEVEL

Since frames H6WCSB and I10WCSB are expected to fail at an excitation level well below twice the design level, time-history analyses for both frames were also performed at the design level excitation using the records in ensemble "A". Figure 7.16 shows the M+SD maximum storey drift height-wise distribution for both frames at the design level and twice the design level excitations. While at the design level excitation the first soft storey drift is significantly less than that at twice the design level excitation, the H6WCSB frame still has a poor performance with a maximum first storey drift that is only slightly below the collapse drift limit. The I10WCSB frame has somewhat lower storey drift at the design excitation, i.e. a maximum first storey drift that is approximately at the life-safe drift limit.

Using the same format, Figure 7.17 shows the M+SD interior column performance parameters for both frames at the design level and twice the design level excitations. From the figure, it can be seen that at the design level excitation, frame H6WCSB has a high M+SD rotational ductility at the first soft storey with a corresponding damage index that slightly exceeds 1.0. This indicates that for this frame, failure could well occur at the design level

excitation. At the design level excitation, the performance of the I10WCSB frame is somewhat better than that of the H6WCSB frame; the M+SD column rotational ductility and damage index at the soft first storey show that the I10WCSB frame can be expected to sustain an extensive state of damage concentrated at its first storey, i.e. very near to the collapse state.

To further investigate the effect of peak ground velocity level on the response of the various frame design types, the I6 set of frames (i.e. I6SCWB, I6WCSB and I6SCWP) were subjected to three time-histories scaled to several multiples of the design peak ground velocity level. The three time-histories were selected as the most damaging records in ensemble "A", NI14, BIG3 and LAN1 ground motions. Consequently, for each frame, the average response to those three excitations represents approximately the M+SD response to the earthquakes in ensemble "A". The earthquake records were then scaled to 1, 1.5, 2, 2.5 and 3 times the design peak ground velocity level, i.e. 0.2, 0.3, 0.4, 0.5 and 0.6 m/sec.

Shown in Figure 7.18 are the effect of peak ground velocity level on the maximum storey drifts and the maximum roof deflections of the I6 set of frames. It is clear that the maximum storey drift of the I6WCSB frame is the most sensitive parameter to the level of peak ground velocity. On average, it is expected that the I6WCSB frame will exhibit a maximum drift of 1.5% (life-safe drift limit) at the design level excitation, a maximum drift of 2.5% (collapse drift limit) at an excitation of 1.5 times the design level, and a much larger drift of 4% or 5% at an excitation of three times the design level.

The maximum drift of the I6SCWB frame also increases with velocity level, however the rate of increase is less than that for the I6WCSB frame. It is expected that the I6SCWB

frame will exhibit a maximum drift of 2.5% at an excitation of twice the design level, and a maximum drift of 3% at an excitation of three times the design level.

The behaviour of the I6SCWP frame is quite different from the other two frames in which the maximum storey drift is almost insensitive to the velocity level and only increases by a very small rate at the higher velocities. The I6SCWP frame is expected to exhibit a maximum drift of 2.5% at an excitation of three times the design level, while it only exhibits a maximum drift of 1% at the design level excitation.

Considering the maximum roof deflection, there are no significant differences among the frames. In general, there is a linear relationship between the maximum roof deflection and the velocity level, in which roof deflections are in the order of 1% at the design level excitation, and increase to 1.5% and 2% at excitations of two and three times the design level respectively.

Shown in Figure 7.19 are the effect of the peak ground velocity level on the performance parameters of the critical elements in the frames. For the I6SCWB frame, in which beams are the critical elements, Figure 7.19a shows that beam failure can be expected at excitation levels higher than twice the design level, but very minor beam damage can be expected at the design level excitation. It can also be seen that beam rotational ductilities of approximately 5 or larger are associated with beam damage indices larger than 1.0 (i.e. beam failure).

For the I6WCSB frame, in which columns are the critical elements, Figure 7.19b shows that column failure can be expected at excitations that range from the design level to 1.5 times the design level. In addition, column rotational ductilities of approximately 6 or

larger are likely to be associated with column failure.

For the I6SCWP frame, in which panels are the critical elements, Figure 7.19c shows that panel failure can be expected at excitation levels of twice the design level and higher. However, at the design level excitation, only moderate panel damage occurs (i.e. ductility in the order of 4). Panel shear ductilities of approximately 10 or larger are likely to be associated with panel damage indices larger than 1.0 (i.e. panel failure).

## 7.10 MAXIMUM STOREY DRIFT-MAXIMUM ELEMENT PERFORMANCE PARAMETERS RELATIONSHIPS

Figure 7.20 shows diagrams of the maximum element ductilities and damage indices for the critical elements versus maximum storey drifts for all the time-history responses. Maximum ductilities have an approximate linear relationship with maximum drifts for every frame. This linear relationship is similar to what was observed during push over analyses (Figure 6.25). This proportionality indicates that there is a consistent pattern of deformation associated with each frame design philosophy (i.e. SCWB, WCSB or SCWP) which produces a proportionate increase in the critical element ductility demand as the overall lateral deformation increases. The beam ductility demands in the SP.I6SCWB frame are much smaller than those for the I6SCWB frame because of the much stronger members used to limit the drift. The proportionality mentioned above facilitates linking the maximum element ductility capacities with the maximum drift limits associated with specific performance levels. For example, in SCWB and WCSB frames (Figure 7.20 a and b), beam and column rotational ductilities in the range of 2 to 3 are associated with a life-safe drift limit of 1.5%, while

rotational ductilities in the range of 5 to 6 are associated with a collapse drift limit of 2.5%. In section 7.9, for the I6 frames, beam and column ductilities in the range of 5 to 6 were identified as approximate values that correlate with critical element failure, i.e. damage index of 1.0. This indicates first that the 2.5% maximum drift proposed by SEAOC(1995) as a collapse limit is applicable to both the SCWB and WCSB frame design types, and second that these approximate ductility values are somewhat independent of the hazard level and are likely to be associated with critical element failure. For the WCSB frames, while the above statements might be theoretically true, however practically, those frames tend to develop a soft first storey sway mechanism at a maximum drift of 1.5% as indicated before during push over analyses, especially in seismically active regions. Therefore, this mechanism is most likely to govern the collapse of those frames rather than member deformation capacities as a collapse criterion.

In SCWP frames (Figure 7.20c), panel zone shear ductilities in the range of 6 to 8 are associated with a drift limit of 1.5%, while panel shear ductility in the order of 14 is associated with a drift limit of 2.5% (using an extrapolation of the relationship). In section 7.9, panel shear ductility of 10 was identified as an approximate value that correlates with panel failure, i.e. damage index of 1.0. Thus, a maximum drift value of approximately 2% is probably more appropriate as a collapse drift limit for the SCWP frames rather than the 2.5% collapse drift limit proposed by the SEAOC (1995).

In contrast, the relationships between maximum damage indices and maximum drifts are not proportional, especially at the larger values of maximum drifts. The reason for this non-proportionality is the variability of the cumulative plastic deformation associated with the

varying durations of the time-histories used to excite the frames. The variability of the damage indices at any particular maximum drift level shows clearly the importance of time-history strong-motion duration. For instance, consider the response of the frames designed for the H seismic hazard level. For frame H6SCWB, about one-half of the time-history analyses resulted in beam damage indices of 1.0 or higher, though these values are associated with maximum drifts ranging from about 1.5% to 2.5%; there is one case of maximum drift of 2.5% resulting in a beam damage index of only 0.4. Results show that for that frame, given two excitations that result in approximately the same maximum drift (1.8%), the one that has a strong-motion duration of 24sec produces a maximum beam damage index of 0.55, while the other that has a strong-motion duration of 40sec produces a maximum beam damage index of 0.90.

For frame H6WCSB, although there is no proportionality between maximum column damage index and maximum drift, it can be seen that all of the nine cases with maximum drifts of 2.5% or higher have damage indices of 1.0 or higher. Thus, even short duration excitations producing large drifts are expected to cause column failure in this frame.

For frame H6SCWP, while the maximum drift is slightly above 2%, panel damage indices at that drift level range from 0.5 to 2. One-half of the total responses result in panel damage indices above 1.0. These results indicate that, while there is good control of maximum drift in the SCWP frames, these frames are particularly vulnerable to damage due to cumulative plastic deformation in the panel zones. Comparing the ranges and distribution of damage indices confirms that the SCWP frames have somewhat poorer performance than the corresponding SCWB frames.

As the columns of the SCWB and SCWP frames also exhibit plastic deformations, particularly at the base (bottom ends of first storey columns), Figure 7.21 shows diagrams of maximum column ductilities and damage indices versus maximum storey drifts for all the time-history responses. Similar to the WCSB frames, there is proportionality between the maximum column ductilities and maximum storey drifts in the SCWB frames, while no proportionality can be seen in the SCWP frames, which is most probably due to the difference in deformation types at the plastic hinge locations, i.e. flexural yielding in the columns at the base and shear yielding in the joint panels. The maximum column ductilities in the SCWB frames are smaller than those in the WCSB frames, and much smaller yet in the SCWP frames. There are only very few cases in which the column damage indices for the SCWB frames are slightly above 1.0, while in most of the cases they are below 1.0, i.e. the column damage is very likely to be controlled. For the SCWP frames, the columns damage indices range from 0 (elastic) to a maximum of 0.5, i.e. in the extreme case the columns suffer only moderate damage.

## 7.11 SUMMARY OF OVERALL PERFORMANCE

### 7.11.1 Summary of maximum plastic deformations

Presented in Table 7.3 are the maximum plastic deformations of the critical elements. By examining the values included in that table, the following can be observed:

At an excitation of twice the design level, the maximum beam plastic rotations in the SCWB frames range from 0.01 to 0.025 rad. as the seismic hazard increases from L to H. Thus, the maximum value of this range is consistent with the beam plastic rotation capacities

obtained during some experimental results in the literature (at maximum storey drifts in the neighbourhood of 3%) as mentiond in Chapter 6, section 6.10. The table shows that a beam ductility of approximately 5 is likely to be associated with beam plastic deformation capacity. On the contrary, most of the maximum column plastic rotations for the WCSB frames are well above the acceptable capacities, i.e. much larger than the acceptable range of plastic rotation capacity (0.018 to 0.022 rad.) discussed in Chapter 6, except for the L6WCSB frame in which the maximum column plastic rotation is well below that range. The table shows that a column ductility of approximately 6 is likely to be associated with column plastic rotation capacity. In all the SCWP frames, the maximum panel plastic shear strains range from 0.01 to 0.024 as the seismic hazard increases form L to H. While the maximum value in this range (0.024) is below the acceptable plastic shear strain capacities from experimental results (0.03 to 0.035), results show that this level of plastic shear strain is likely to be associated with panel failure due to accumulated plastic strains during time-history responses.

### 7.11.2 Overall performance in relation to potential collapse

For the purpose of describing overall performance in relation to potential collapse, the collapse prevention ratio (CPR) is defined as the ratio of the excitation velocity level at which structural collapse can be expected (at the M+SD level of response) to the design velocity level. A summary of the overall performance and approximate CPR values for all the frames is given in Table 7.4. Based on this table as well as the foregoing discussions of M+SD level storey drifts and element damage parameters in this chapter, the following conclusions can then be drawn:

The drift ductility factor correlates with the relative performance of frames designed for different design philosophies much better than the roof deflection ductility factor (Table 7.2), i.e. the actual maximum storey drift value and the drift ductility factor are capable of distinguishing which frames have the best performance and which have the poor performance.

For the SCWB frames, the 2.5% maximum storey drift proposed by the SEAOC (1995) as a collapse limit correlates well with the results obtained from the dynamic analyses, including damage indices. However, maximum drifts of lower values are more appropriate as collapse limits for the other frame types, i.e. 1.5% for the WCSB frames and 2% for the SCWP frames.

The level of seismic hazard in a specific region has a substantial effect on determining the acceptability of the performance for each specific frame design philosophy. In regions of high seismic hazard, the performance of both the H6SCWB and H6SCWP frames is more or less comparable; the CPR for both frames is slightly less than 2. However, reference to the overall drift ductility (Table 7.2) as well as the values of the damage indices and their distribution indicates that the performance of the H6SCWB frame is slightly better than that of the H6SCWP frame. On the other hand, the performance of the H6WCSB frame is very much poorer as it can be expected to collapse at excitations well below twice the design level (i.e. CPR $<<$ 2); some collapses can even be expected at the design level excitations (see section 7.9).

In regions of intermediate seismic hazard, the performance of both the I6SCWB and I6SCWP frames are also comparable with CPR values in the neighbourhood of 2. While the CPR for the I6WCSB frame is slightly below 2, its performance is inferior to other cases for

which CPR is slightly below 2 (i.e. H6SCWB and H6SCWP) based on the range of overall drift ductilities (Table 7.2) and the distribution of column damage indices. For the I10 set of frames, the performance of both the I10SCWB and I10SCWP frames are also comparable with CPR values greater than 2. However, based on M+SD drift values as well as the overall drift ductility (Table 7.2), the performance of the I10SCWB frame is expected to be slightly better than that of the I10SCWP frame. In contrast with the performance of the I10SCWB and I10SCWP frames, the performance of the I10WCSB frame is significantly poorer with CPR well below 2, i.e. it is even poorer than the performance of its six storey counterpart, the I6WCSB frame.

The SP.I6 frames exhibit M+SD drift levels that are similar to those of their counterpart, i.e. the I6 frames. The reduction in beam damage in the SP.I6SCWB frame is compensated for by an increase in the column damage at the base, thus keeping the CPR value in neighbourhood of 2. As the SP.I6WCSB frame is much more stiffer than the I6WCSB frame, its performance is poorer with a CPR well below 2. The only advantage is for the SP.I6SCWP frame, in which the panel damage is reduced due to the larger web panel thicknesses resulting from the use of stronger column members, with a CPR > 2.

The use of ensemble "B" of time-histories, which represents the new hazard information, as an input for the I6 frames results in storey drifts and ductility factors comparable to those resulting from the use of ensemble "A", however, the damage indices are on average 20% less, i.e. ensemble "B" produces less accumulation of plastic deformations. Realizing that the time-histories in ensemble "B" were scaled to have the same mean spectrum as that of ensemble "A" at the periods of interest, the results indicate that the new hazard

information for Vancouver is likely to result in a seismic hazard activity level which is approximately 25% less than that specified by the current NBCC(1995). This can be attributed to both the slightly lower ground motion intensity level described in the new hazard information and the characteristics of the earthquake time-histories that are used to match the mean uniform hazard spectrum for Vancouver, i.e. some of the records used are high frequency content records.

In regions of low seismic hazard, the performance of all three types of frames (i.e. L6SCWB, L6WCSB and L6SCWP frames) is comparable with M+SD drifts in the neighbourhood of the life-safe limit (1.5%) and CPR values greater than 2.

In general, a static push over analysis to an approximate collapse-level maximum storey drift can satisfactorily simulate the primary features of the frame performance during dynamic analysis. Push over analysis is capable of predicting the storey levels which will experience the maximum drifts during dynamic analysis. In addition, the static push over analysis is capable of distinguishing the critical differences among the behaviour of frames designed using different philosophies. However, the drawback of using push over analysis is that it cannot include the effects of higher mode contribution in the lateral deformation of the frame, neither can it account for the effect of accumulation of plastic deformations of the critical elements during the cyclic response of the frame when subjected to dynamic loading. Consequently, the damage indices for the critical elements during dynamic analysis are much larger than those predicted from a static push over analysis, i.e. damage indices from dynamic analyses can sometimes be 50% to 100% larger than those obtained from static analyses.

There is no absolute way of judging whether or not a CPR of 2 is acceptable. However, the recent version of the Canadian seismic hazard (Adams et al., 1996) indicates that the standard deviation of seismic hazard estimates due to uncertainty in the modelling of seismicity parameters results in a ratio of M+SD to mean hazard of approximately 2. This result suggests that structures which are designed and constructed on the basis of life safety criteria should, with a high level of confidence, be able to sustain twice the design ground motions without collapse, i.e. have a CPR of 2 or more. On the basis of this simplified criteria, the WCSB frames are clearly not acceptable for the intermediate and high seismic hazard regions. While the CPR is slightly below 2 for the H6SCWB and H6SCWP frames, the overall performance of these frames is such that both the SCWB and SCWP frames can be considered acceptable for both the intermediate and high seismic hazard regions. There is a slight preference for the SCWB frames based on the range of drift ductilities and the distribution of damage indices. At the low seismic hazard level, all three frames (SCWB, WCSB or SCWP) have CPR which exceed this simplified criterion, i.e. CPR > 2, which means satisfactorily performance.

In general, there is a linearly proportional relationship between maximum critical element ductilities and maximum storey drift ratios, which is more or less independent of the hazard level for each design philosophy; this proportionality enables the determination of the element ductility capacities which are required in order to prevent collapse due to excessive storey drifts, e.g. as those given in sections 7.9 and 7.10. The relation between maximum element damage indices and maximum storey drift ratios is non-proportional, because damage depends mainly on the accumulation of plastic deformations which is affected significantly by the duration of the strong ground motion.

Table 7.1 Maximum storey drift ratios for excitation at twice the design level.

| Frame | Ensemble of time-histories | (M)* Drift (%) | (M+SD)** Drift (%) | Range of drift (%) | Number of time-history responses | | | Storey of maximum drift |
|---|---|---|---|---|---|---|---|---|
| | | | | | Range I | Range II | Range III | |
| H6SCWB | A | 1.95 | 2.35 | 1.50 - 2.75 | 1 | 9 | 2 | 1st or 2nd |
| H6WCSB | A | 3.00 | **4.10** | 1.70 - 4.90 | 0 | 5 | 7 | 1st |
| H6SCWP | A | 1.85 | 2.15 | 1.25 - 2.25 | 2 | 10 | 0 | 2nd, 3rd or 4th |
| I6SCWB | A | 1.90 | 2.30 | 1.40 - 2.60 | 3 | 8 | 1 | 1st or 2nd |
| I6WCSB | A | 2.50 | **3.00** | 1.80 - 3.30 | 0 | 6 | 6 | 1st |
| I6SCWP | A | 1.60 | 1.80 | 1.10 - 2.00 | 4 | 8 | 0 | 2nd, 3rd or 4th |
| L6SCWB | A | 1.25 | 1.60 | 0.60 - 1.80 | 8 | 4 | 0 | 1st, 4th or 5th |
| L6WCSB | A | 1.25 | 1.60 | 0.60 - 1.90 | 9 | 3 | 0 | 1st |
| L6SCWP | A | 1.15 | 1.40 | 0.60 - 1.80 | 11 | 1 | 0 | 3rd, 4th or 5th |
| SP.I6SCWB | A | 1.80 | 2.45 | 1.00 - 3.25 | 4 | 6 | 2 | 1st or 2nd |
| SP.I6WCSB | A | 2.15 | **2.90** | 1.10 - 4.00 | 2 | 6 | 4 | 1st |
| SP.I6SCWP | A | 1.50 | 1.80 | 1.05 - 1.90 | 6 | 6 | 0 | 2nd, 3rd or 4th |
| I6SCWB | B | 1.70 | 2.20 | 1.20 - 2.90 | 4 | 7 | 1 | 1st or 2nd |
| I6WCSB | B | 2.15 | **2.85** | 1.35 - 3.60 | 3 | 7 | 2 | 1st |
| I6SCWP | B | 1.60 | 2.05 | 0.70 - 2.10 | 4 | 8 | 0 | 2nd, 3rd or 4th |
| I10SCWB | A | 1.60 | 1.90 | 0.80 - 2.10 | 5 | 7 | 0 | 1st or 6th |
| I10WCSB | A | 2.60 | **3.35** | 1.00 - 3.55 | 1 | 2 | 9 | 1st |
| I10SCWP | A | 1.70 | 2.20 | 0.85 - 2.70 | 6 | 4 | 2 | 4th, 5th or 6th |

* (M) = Mean value.
** (M+SD) = Mean plus one standard deviation value.
Drifts are given to the nearest 0.05% .

Range I: 0.5% < maximum drift < 1.5% (G.D.I. = 0.0 to 0.5)
Range II: 1.5% ≤ maximum drift < 2.5% (G.D.I. = 0.5 to 1.0)
Range III: 2.5% ≤ maximum drift (G.D.I > 1.0)
G.D.I = Global Damage Indicator.

Table 7.2 Drift and roof deflection ductility factors.

| Frame | Ensemble of time-histories | Drift ductility factors | | | | Roof deflection ductility factors | | | |
|---|---|---|---|---|---|---|---|---|---|
| | | Lower bound | Upper bound | (M)* | (M+SD)** | Lower bound | Upper bound | (M)* | (M+SD)** |
| H6SCWB | A | 1.1 | 2.0 | 1.4 | 1.7 | 1.1 | 1.8 | 1.4 | 1.6 |
| H6WCSB | A | 1.8 | 5.2 | 3.2 | 4.3 | 1.3 | 2.3 | 1.7 | 2.0 |
| H6SCWP | A | 1.8 | 2.8 | 2.3 | 2.6 | 1.8 | 2.7 | 2.3 | 2.6 |
| I6SCWB | A | 1.1 | 2.6 | 1.9 | 2.3 | 1.2 | 1.7 | 1.4 | 1.6 |
| I6WCSB | A | 1.6 | 3.7 | 2.8 | 3.4 | 1.3 | 1.8 | 1.6 | 1.7 |
| I6SCWP | A | 1.5 | 2.6 | 2.1 | 2.5 | 1.5 | 2.1 | 1.8 | 2.0 |
| L6SCWB | A | 0.6 | 1.6 | 1.0 | 1.4 | 0.3 | 1.2 | 0.8 | 1.0 |
| L6WCSB | A | 0.6 | 1.9 | 1.2 | 1.6 | 0.4 | 1.4 | 1.0 | 1.2 |
| L6SCWP | A | 0.6 | 1.8 | 1.1 | 1.4 | 0.6 | 1.8 | 1.2 | 1.5 |
| SP.I6SCWB | A | 1.0 | 3.5 | 1.9 | 2.7 | 0.8 | 1.8 | 1.3 | 1.5 |
| SP.I6WCSB | A | 1.1 | 4.6 | 2.4 | 3.4 | 1.0 | 2.0 | 1.5 | 1.8 |
| SP.I6SCWP | A | 1.3 | 3.0 | 2.2 | 2.7 | 1.3 | 2.5 | 2.0 | 2.4 |
| I6SCWB | B | 1.0 | 3.1 | 1.8 | 2.3 | 0.8 | 1.7 | 1.3 | 1.5 |
| I6WCSB | B | 1.2 | 4.0 | 2.3 | 3.1 | 1.0 | 2.0 | 1.5 | 1.7 |
| I6SCWP | B | 0.9 | 2.6 | 1.9 | 2.4 | 0.9 | 2.5 | 1.7 | 2.2 |
| I10SCWB | A | 0.8 | 2.2 | 1.5 | 1.9 | 0.5 | 1.2 | 1.0 | 1.2 |
| I10WCSB | A | 1.1 | 4.0 | 2.9 | 3.8 | 0.7 | 1.7 | 1.3 | 1.5 |
| I10SCWP | A | 1.0 | 3.4 | 2.5 | 3.1 | 0.8 | 2.5 | 1.7 | 2.1 |

* (M) = Mean value.

** (M+SD) = Mean plus one standard deviation value.

Table 7.3 Summary of maximum plastic deformations (Excitation at twice the design level).

| Frame | (M+SD) Maximum plastic deformations | | | | | |
|---|---|---|---|---|---|---|
| | Beams | | Columns | | Panel zones | |
| | Plastic rotation (rad.) | Associated rotational ductility | Plastic rotation (rad.) | Associated rotational ductility | Plastic shear strain | Associated shear ductility |
| H6SCWB | **0.025** | 5.5 | 0.015 | 5.9 | 0.005 | 3 |
| H6WCSB | 0.004 | 1.5 | **0.036** | 11.5 | 0.002 | 1.7 |
| H6SCWP | 0.005 | 2 | 0.007 | 3.5 | 0.024 | 12 |
| I6SCWB | 0.019 | 4.2 | 0.016 | 5.7 | 0.001 | 1.2 |
| I6WCSB | - | elastic | **0.024** | 7.5 | - | elastic |
| I6SCWP | - | elastic | 0.006 | 2.7 | 0.019 | 9.7 |
| L6SCWB | 0.01 | 2.2 | 0.005 | 2.2 | - | elastic |
| L6WCSB | - | elastic | 0.009 | 3.2 | - | elastic |
| L6SCWP | - | elastic | - | elastic | 0.01 | 5.3 |
| SP.I6SCWB | 0.006 | 1.7 | **0.019** | 7.2 | 0.004 | 2.8 |
| SP.I6WCSB | - | elastic | **0.025** | 8.3 | 0.002 | 2 |
| SP.I6SCWP | - | elastic | 0.002 | 1.25 | 0.017 | 8.5 |
| I10SCWB | 0.015 | 3.7 | 0.01 | 4.5 | 0.005 | 3.1 |
| I10WCSB | - | elastic | **0.03** | 9.5 | 0.003 | 2.4 |
| I10SCWP | 0.01 | 2.8 | 0.005 | 2.8 | 0.019 | 10 |

Typical estimates for element plastic deformation capacity :

Beam plastic rotation: 0.025 to 0.03 rad.

Column plastic rotation: 0.018 to 0.022 rad.

Panel zone shear strain: 0.03 to 0.035.

Table 7.4 Summary of overall performance (Excitation at twice the design level).

| Frame | (M+SD) Maximum performance parameters | | | | | | | CPR* |
|---|---|---|---|---|---|---|---|---|
| | Drift (%) | Beams | | Columns | | Panel zones | | |
| | | Duct. | D.I. | Duct. | D.I. | Duct. | D.I. | |
| H6SCWB | 2.35 | 5.5 | **1.3** | 5.9 | 0.9 | 3 | 0.15 | < 2 |
| H6WCSB | 4.1 | 1.5 | 0.1 | 11.5 | **3.6** | 1.7 | 0.1 | << 2 |
| H6SCWP | 2.15 | 2 | 0.2 | 3.5 | 0.4 | 12 | **1.6** | < 2 |
| I6SCWB | 2.3 | 4.2 | 0.85 | 5.7 | 1 | 1.1 | 0.05 | ≈ 2 |
| I6WCSB | 3 | elastic | 0 | 7.5 | **1.5** | elastic | 0 | < 2 |
| I6SCWP | 1.8 | elastic | 0 | 2.7 | 0.2 | 9.7 | **1.2** | ≈ 2 |
| L6SCWB | 1.6 | 2.2 | 0.25 | 2.2 | 0.2 | elastic | 0 | > 2 |
| L6WCSB | 1.6 | elastic | 0 | 3.2 | 0.5 | elastic | 0 | > 2 |
| L6SCWP | 1.4 | elastic | 0 | elastic | 0 | 5.3 | 0.4 | > 2 |
| SP.I6SCWB | 2.45 | 1.7 | 0.15 | 7.2 | **1.3** | 2.8 | 0.2 | ≈ 2 |
| SP.I6WCSB | 2.9 | elastic | 0 | 8.3 | **1.8** | 2 | 0.1 | << 2 |
| SP.I6SCWP | 1.8 | elastic | 0 | 1.25 | 0.05 | 8.5 | 0.75 | > 2 |
| I10SCWB | 1.9 | 3.7 | 0.8 | 4.5 | 0.65 | 3.1 | 0.25 | > 2 |
| I10WCSB | 3.35 | elastic | 0 | 9.5 | **2.3** | 2.4 | 0.2 | << 2 |
| I10SCWP | 2.2 | 2.8 | 0.3 | 2.8 | 0.2 | 10 | 0.7 | > 2 |

Duct.: Beam rotational ductility
Column rotational ductility
Panel zone shear ductility

D.I.: Damage Index

* CPR = Collapse Prevention Ratio, i.e. ratio of excitation velocity expected to cause structural collapse (at M+SD response level) to the design velocity.

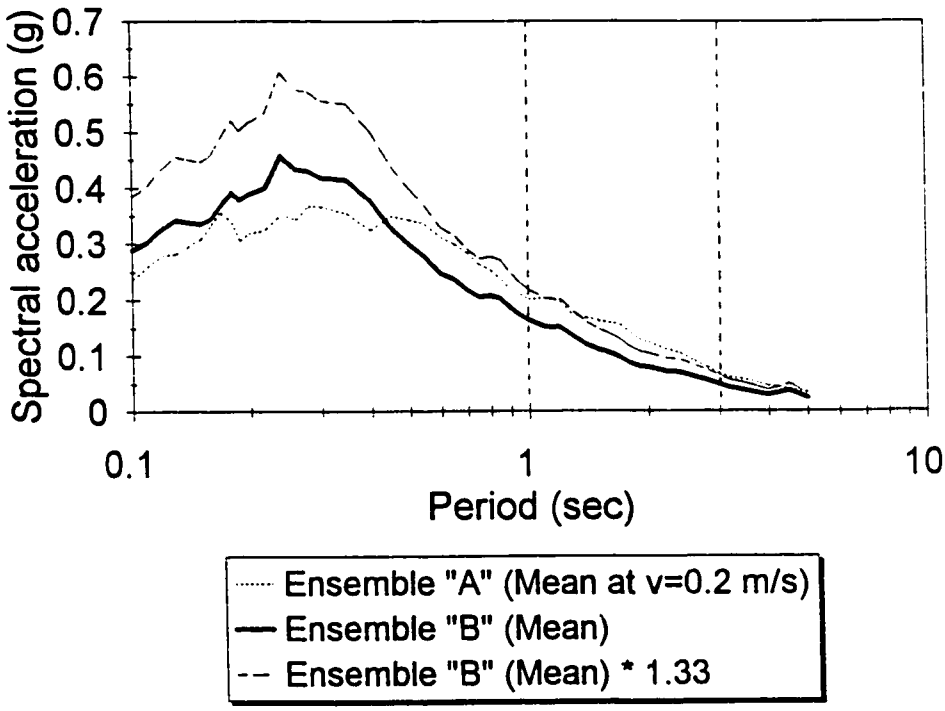


Figure 7.1 Scaling level for the time-histories in ensemble "B".

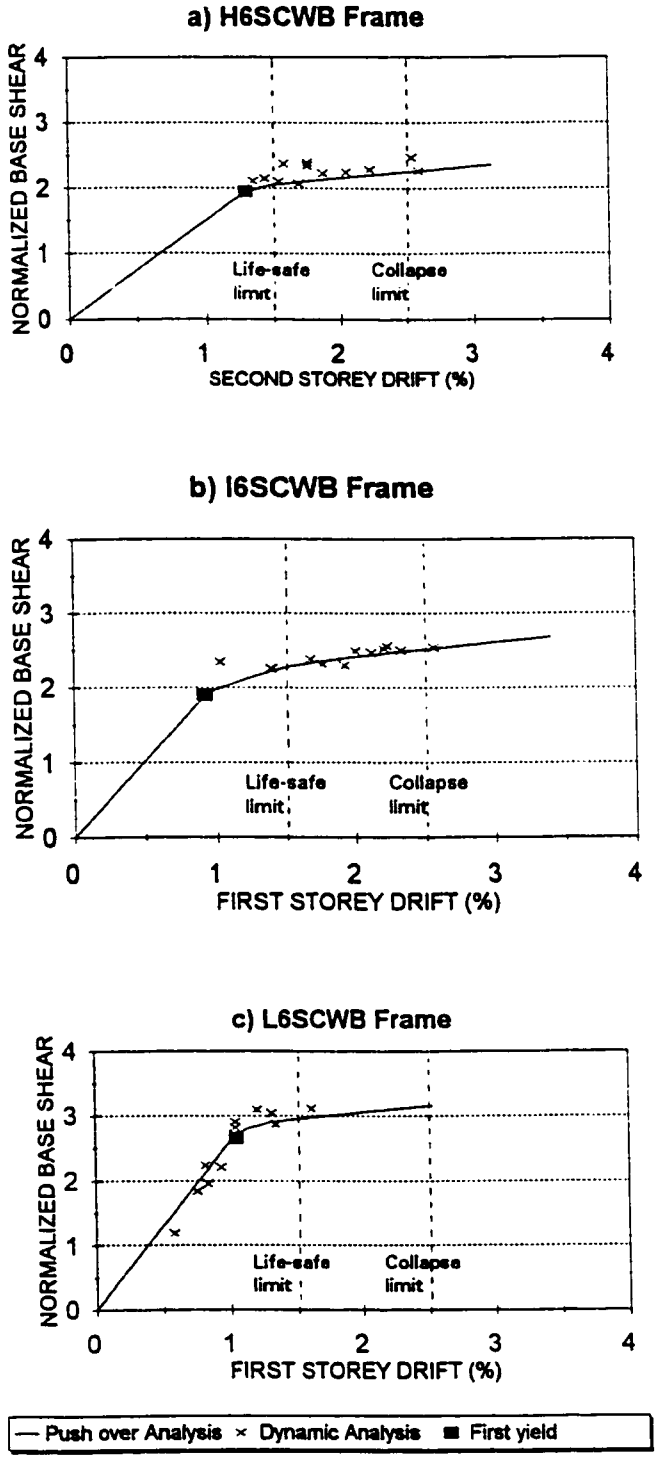


Figure 7.2 Base shear-maximum storey drift relationships for the SCWB frames, evaluation of the different time-history responses.

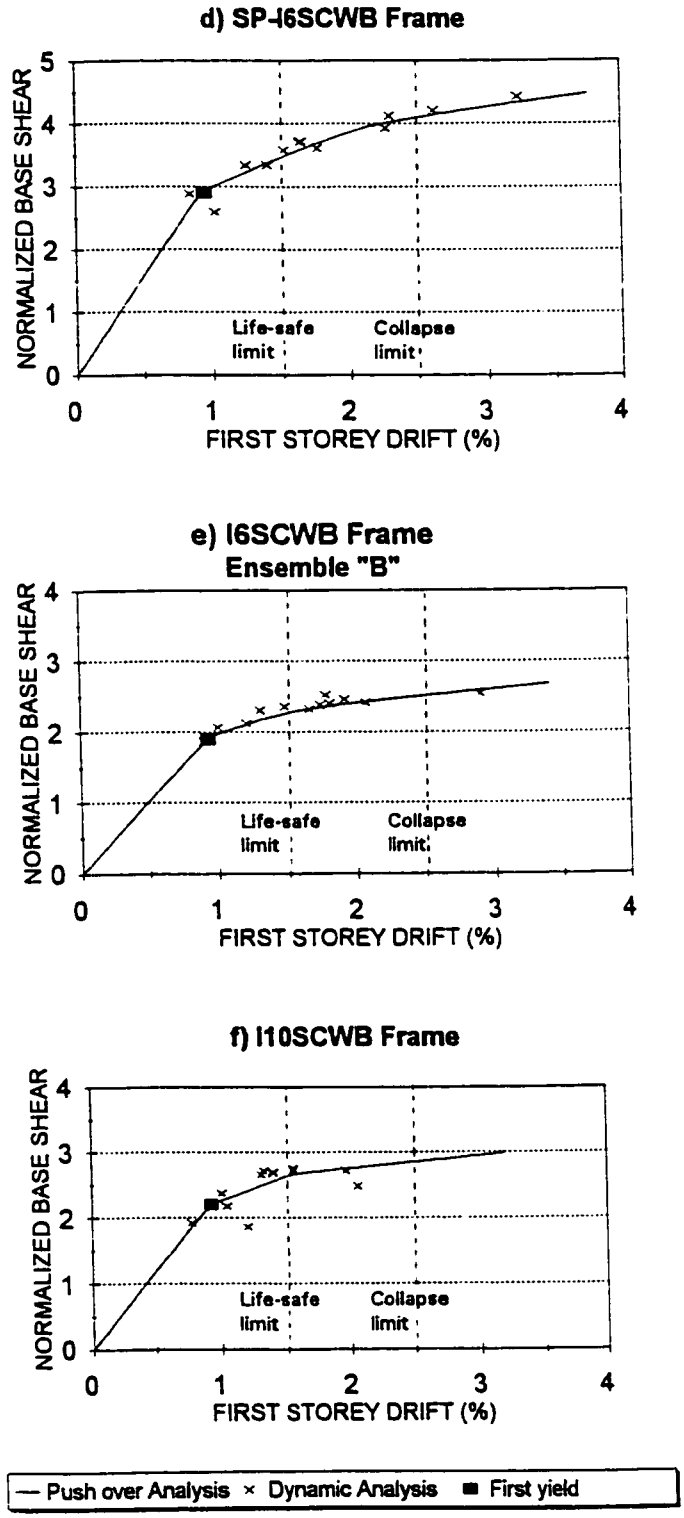


Figure 7.2 Continued

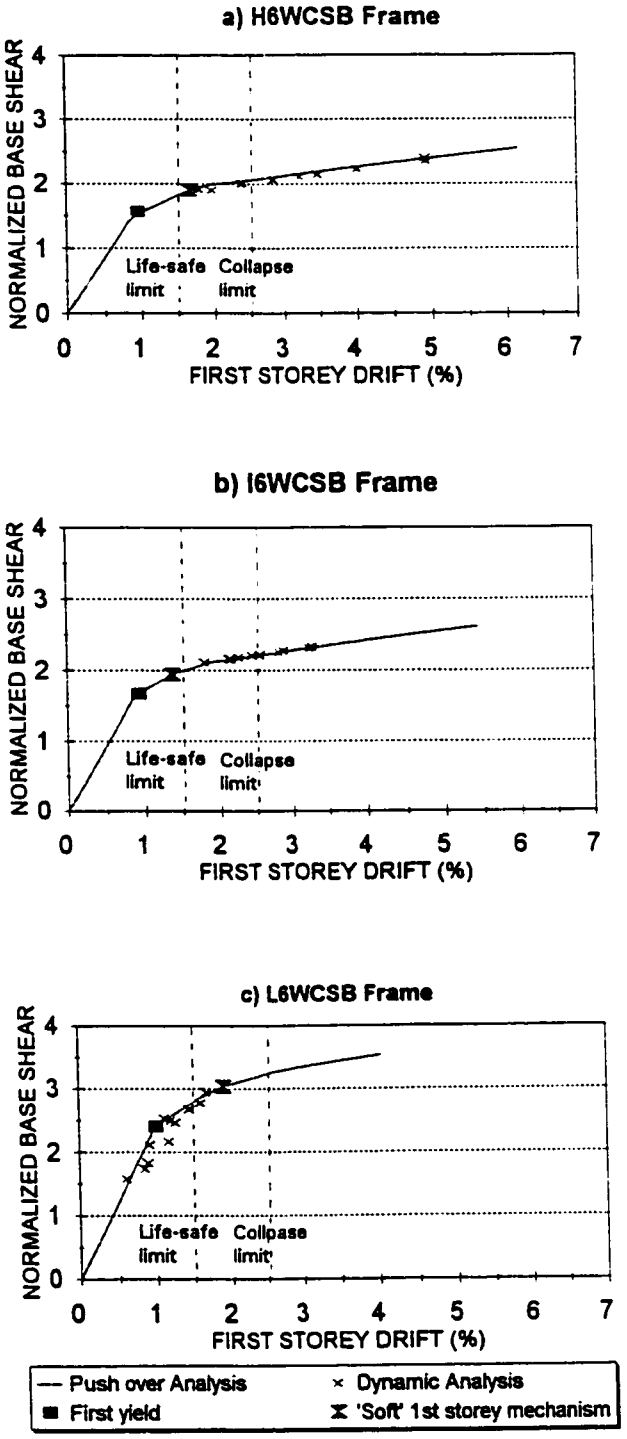


Figure 7.3 Base shear-maximum storey drift relationships for the WCSB frames, evaluation of the different time-history responses.

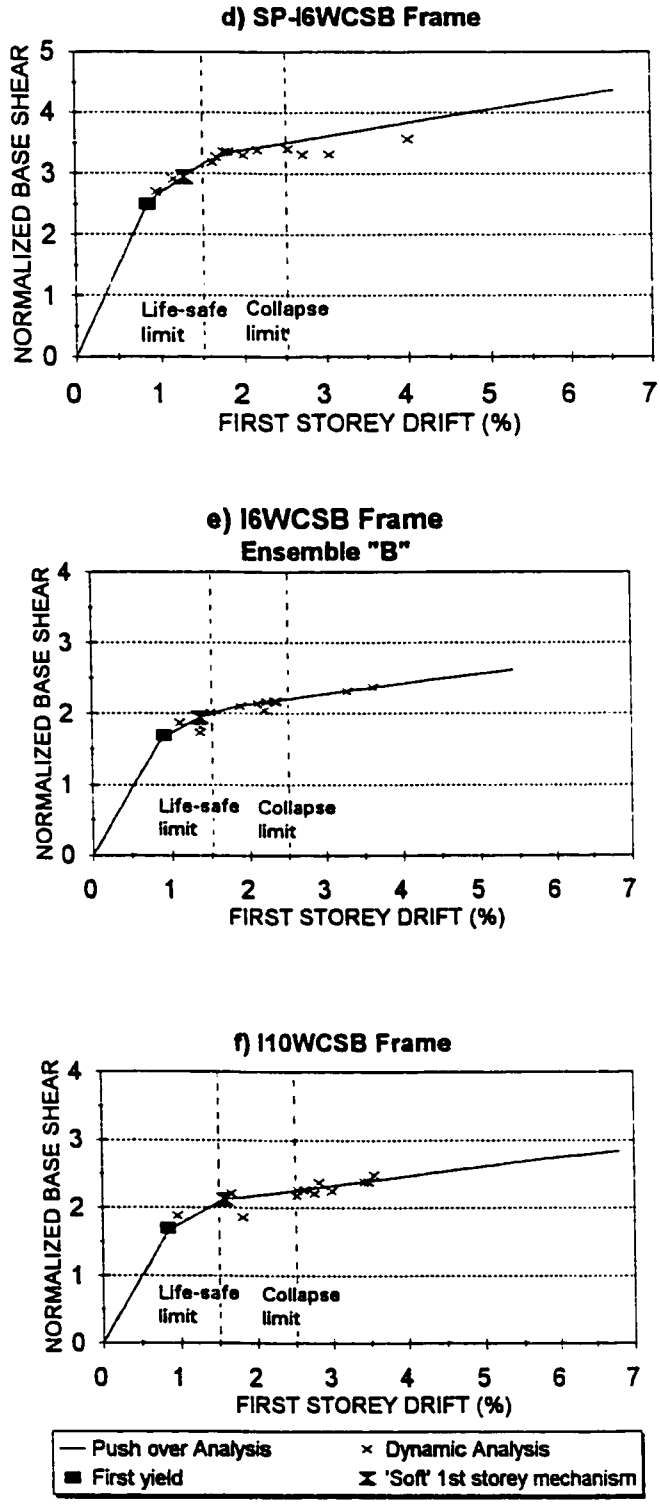


Figure 7.3 Continued

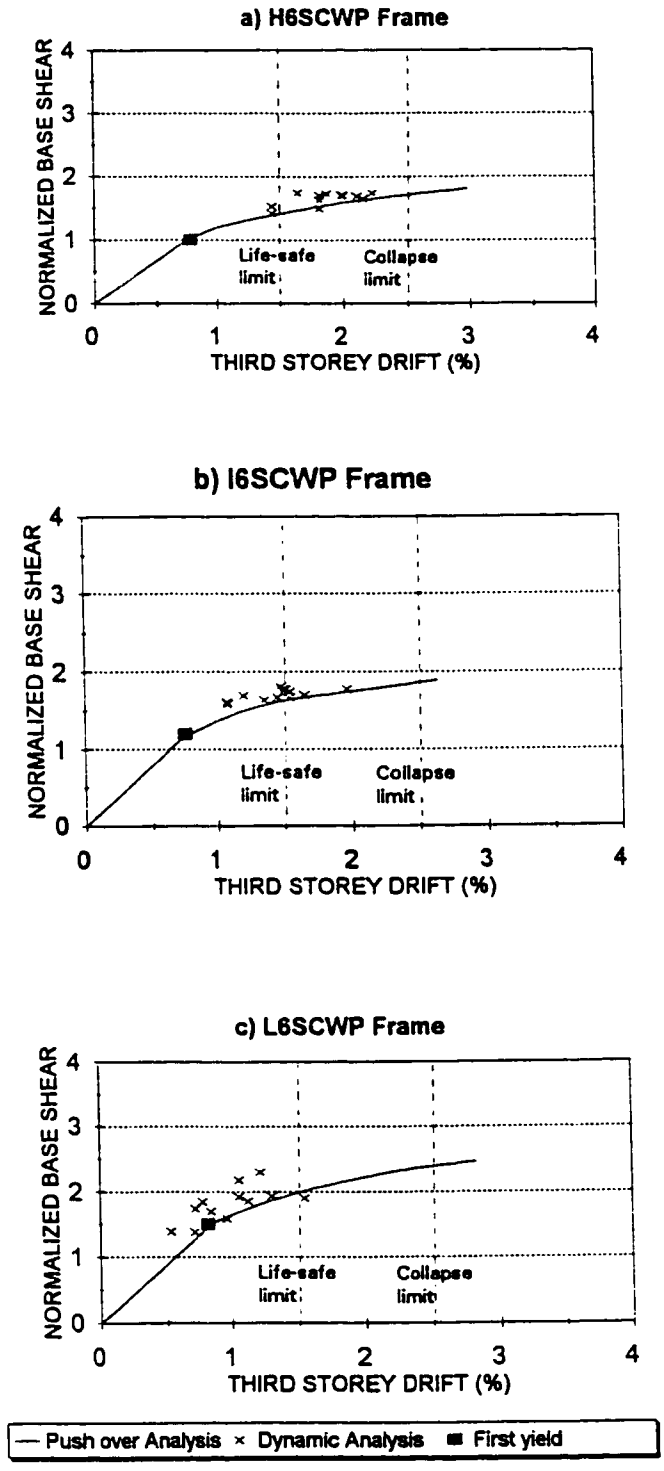


Figure 7.4 Base shear-maximum storey drift relationships for the SCWP frames, evaluation of the different time-history responses.

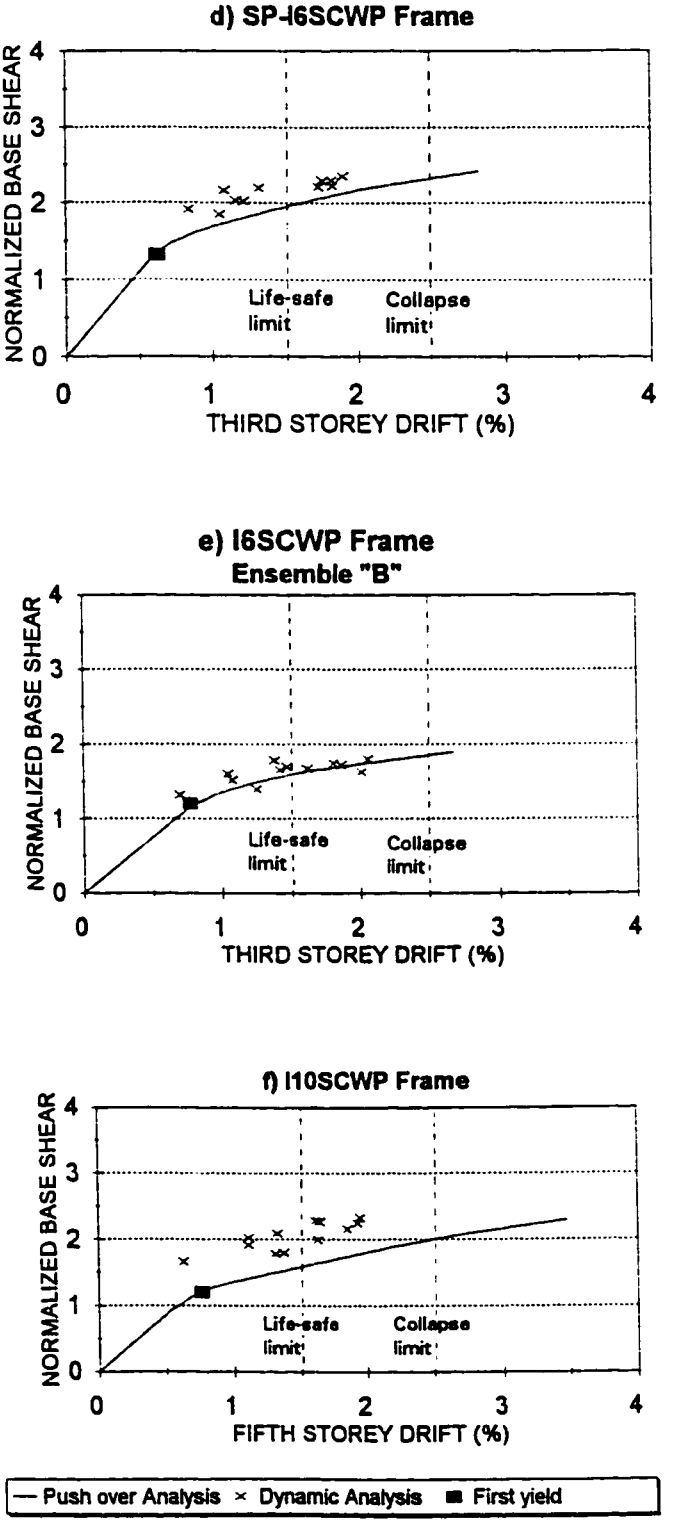


Figure 7.4 Continued

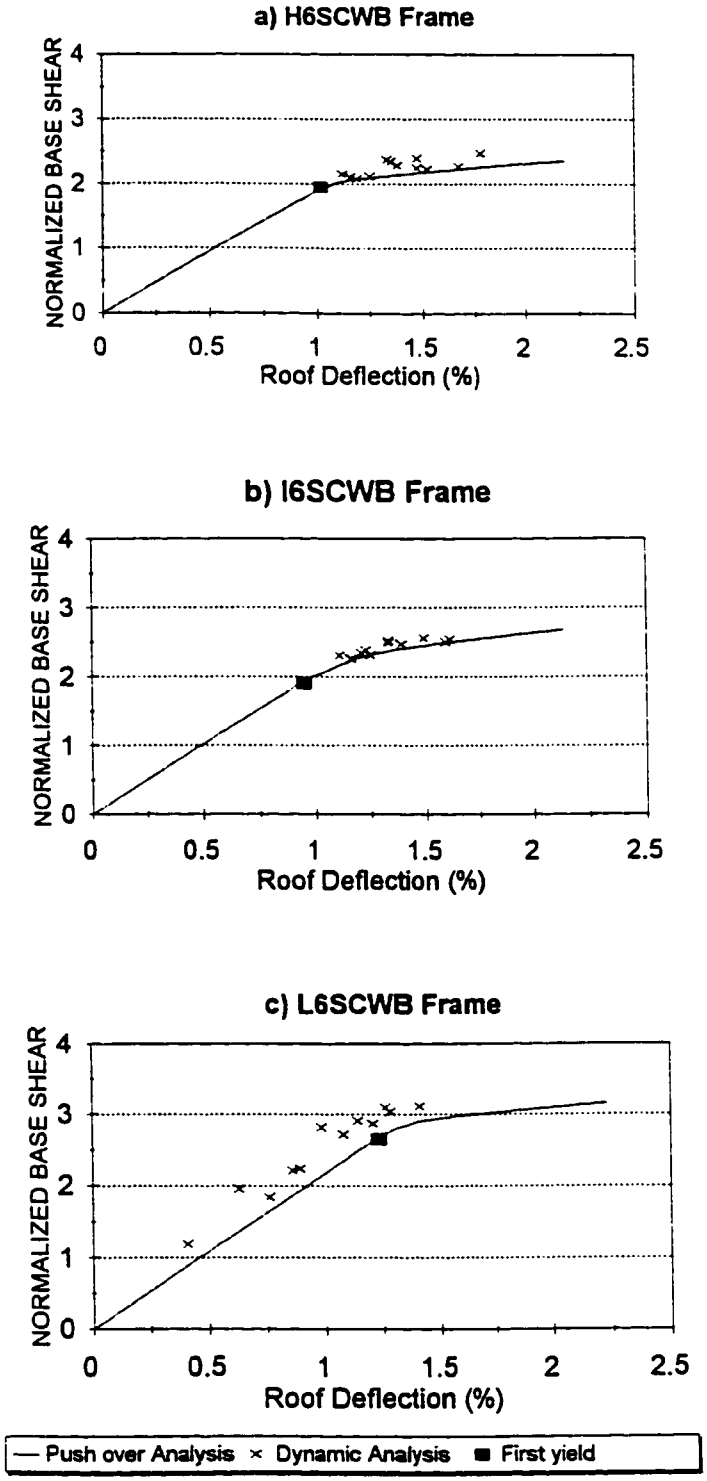


Figure 7.5 Base shear-maximum roof deflection relationships for the SCWB frames, evaluation of the different time-history responses.

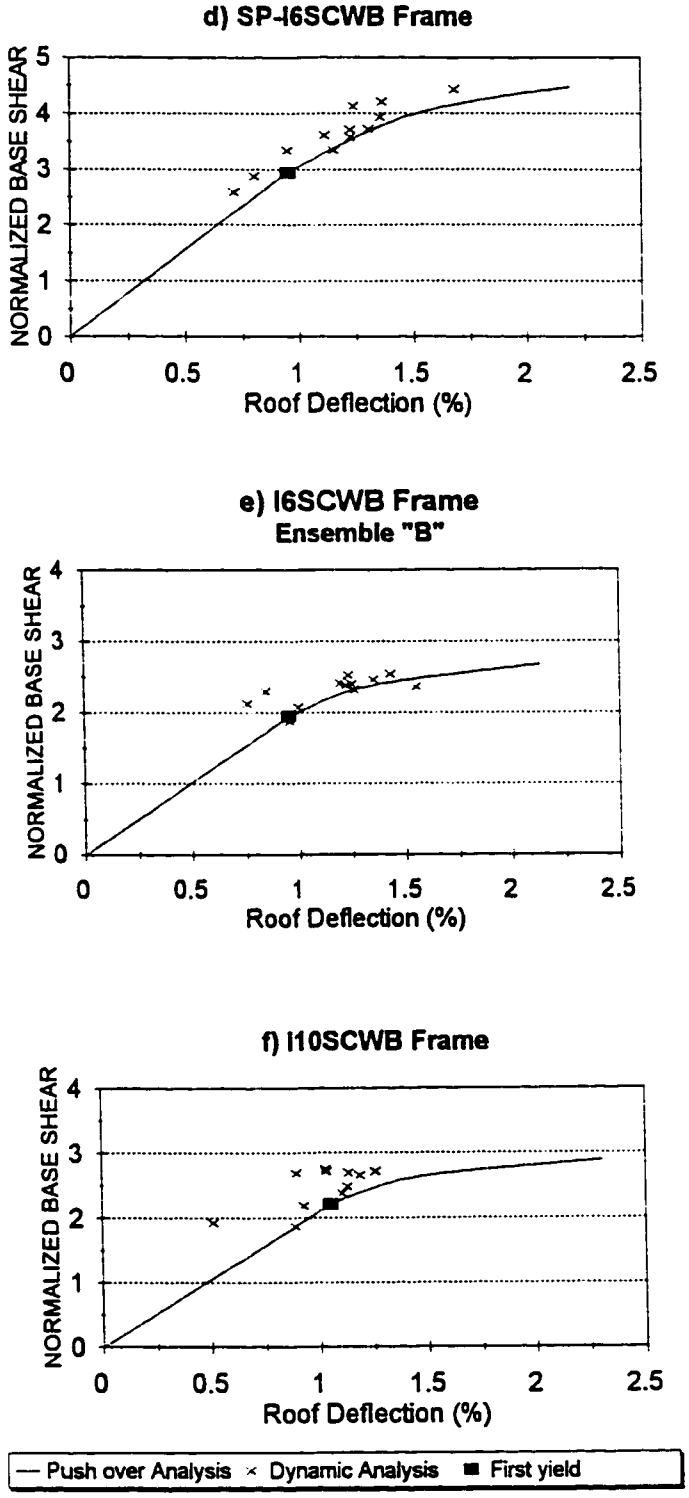


Figure 7.5 Continued

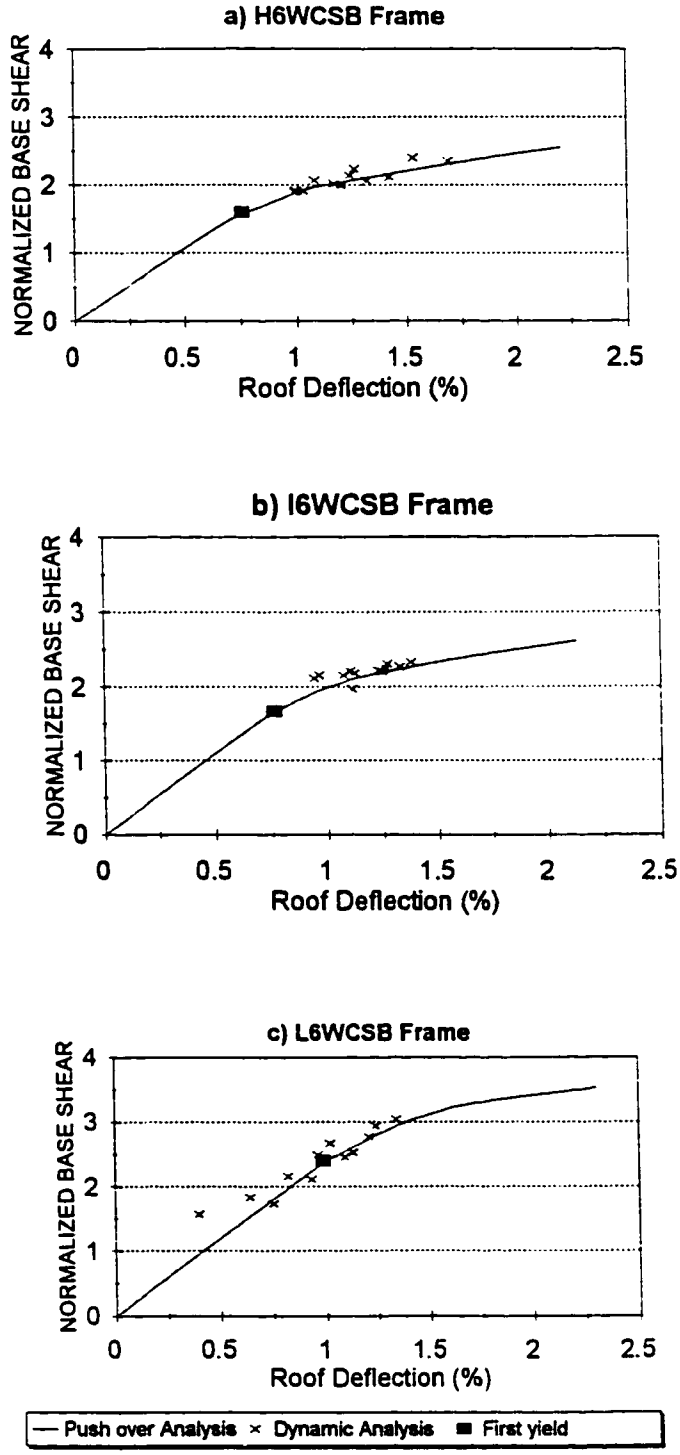


Figure 7.6 Base shear-maximum roof deflection relationships for the WCSB frames, evaluation of the different time-history responses.

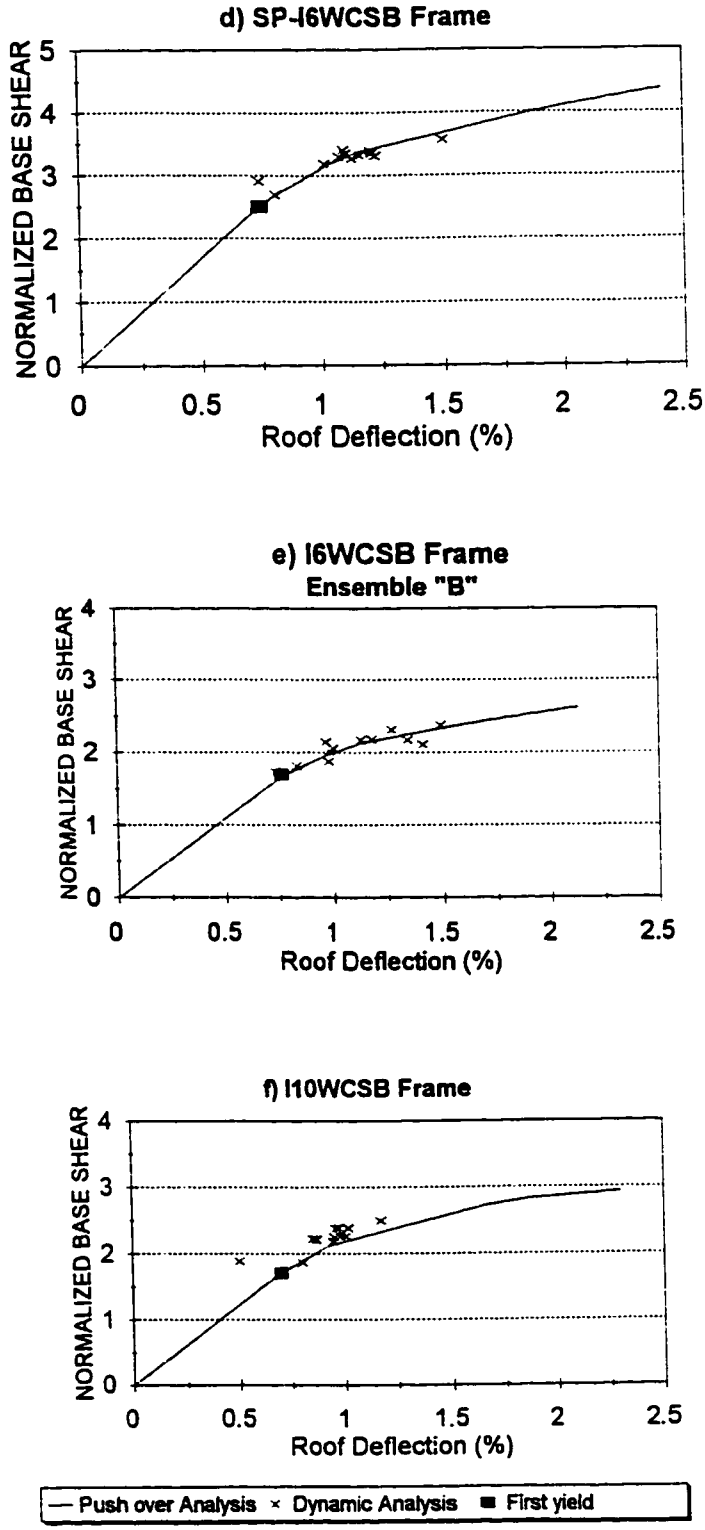


Figure 7.6 Continued

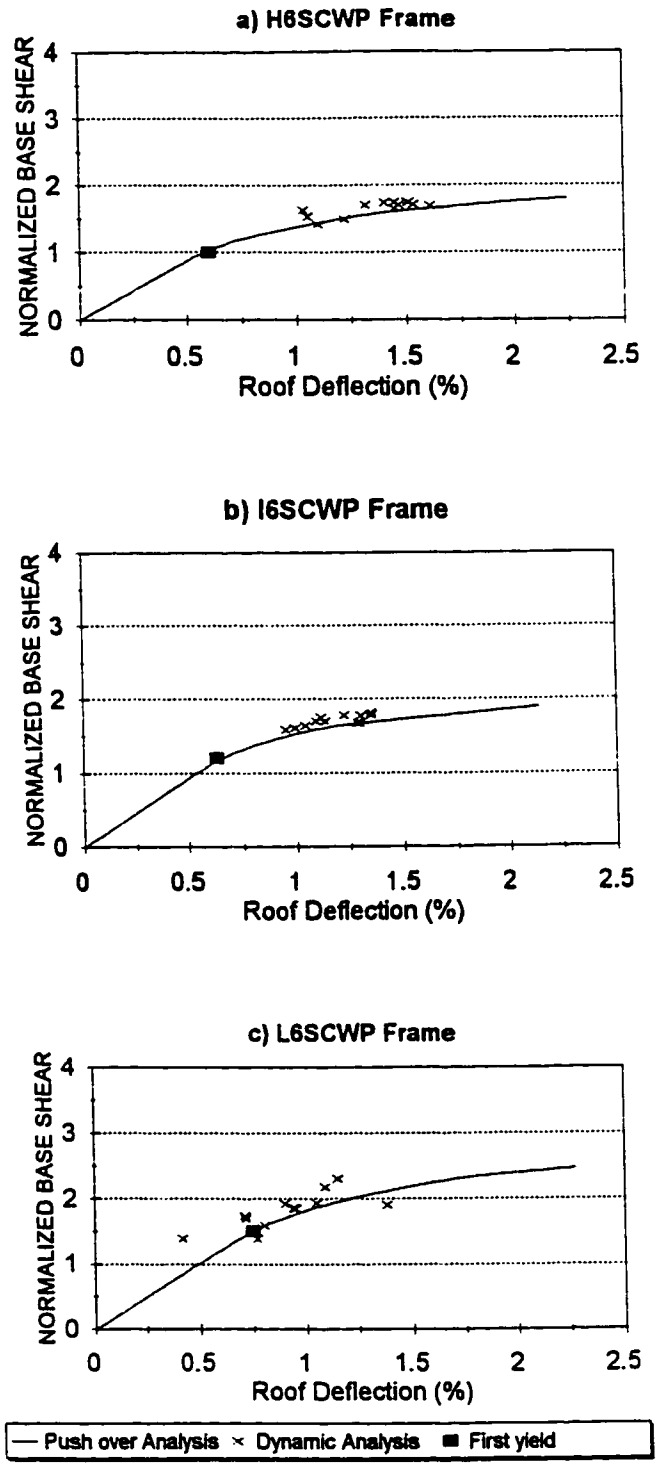


Figure 7.7 Base shear-maximum roof deflection relationships for the SCWP frames, evaluation of the different time-history responses.

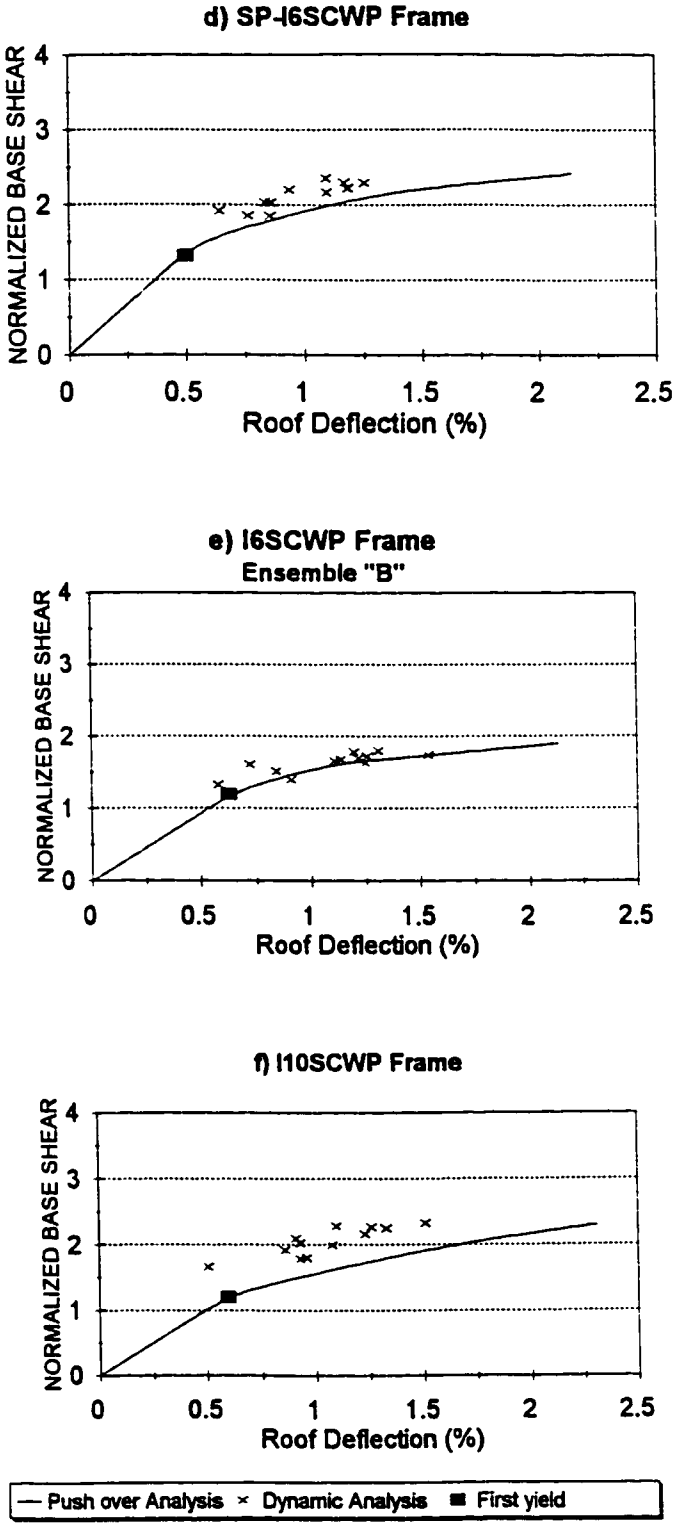


Figure 7.7 Continued

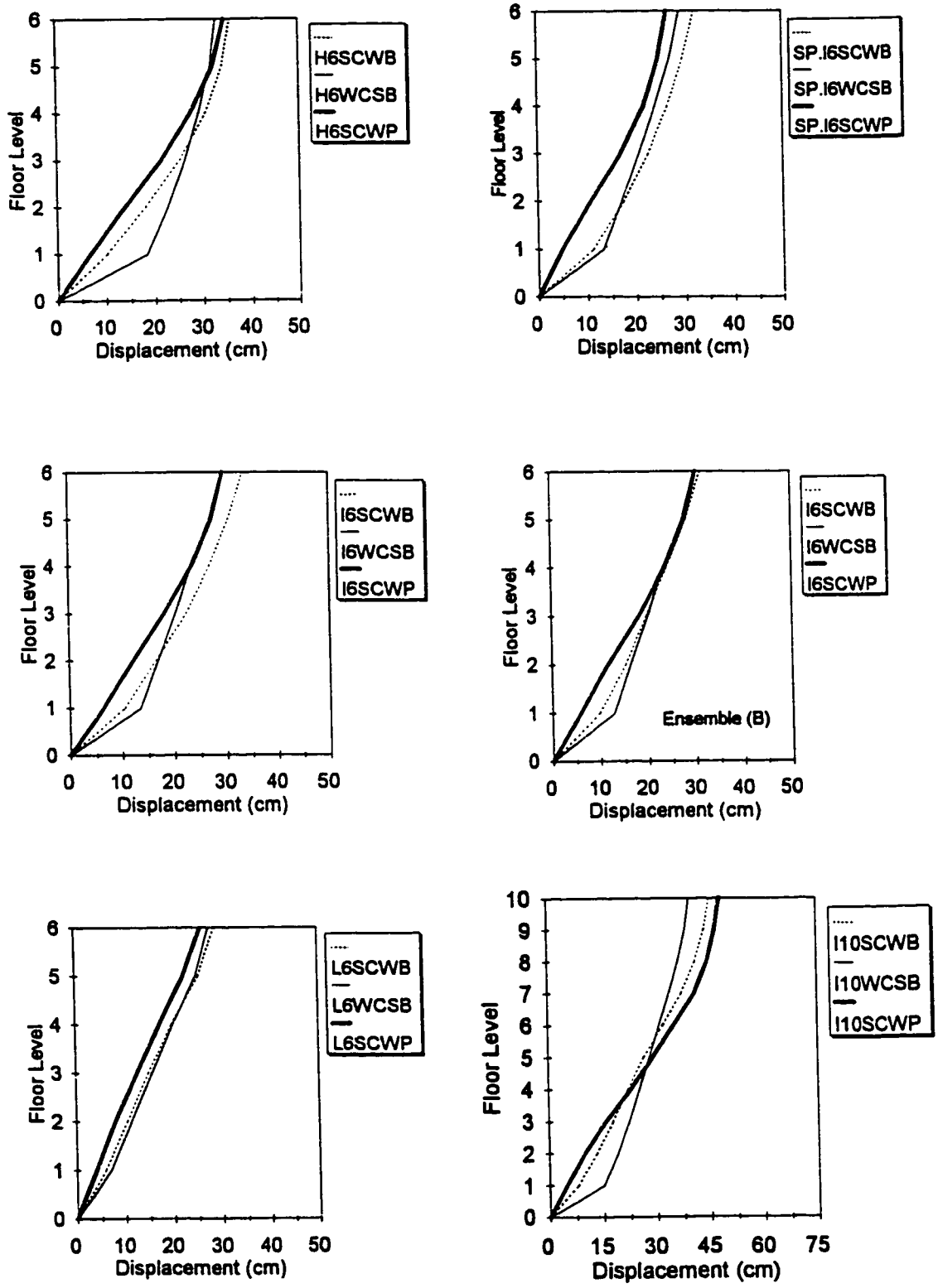


Figure 7.8 Height-wise distribution of maximum floor displacements, M+SD values.

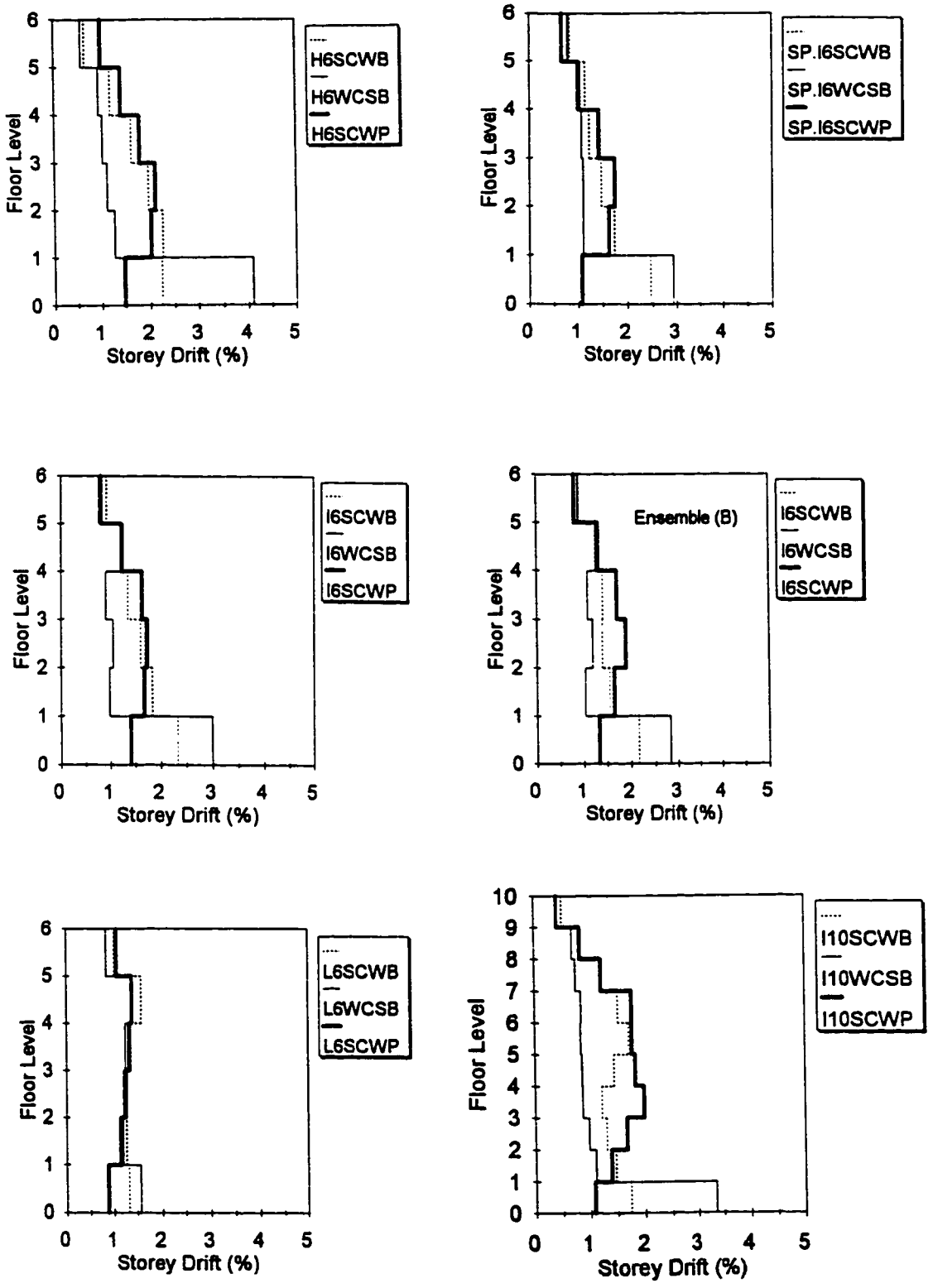


Figure 7.9 Height-wise distribution of maximum storey drifts, M+SD values.

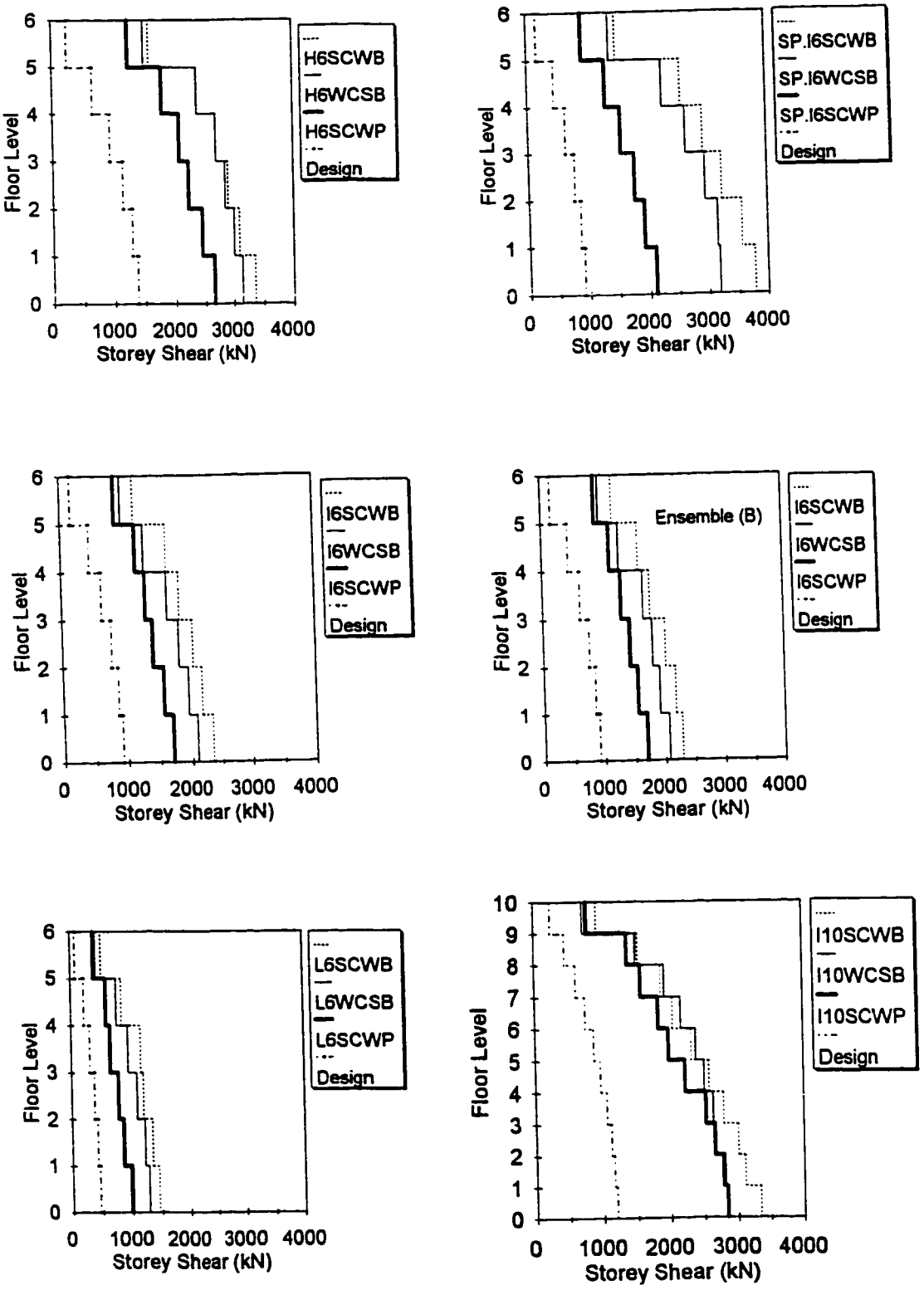


Figure 7.10 Height-wise distribution of maximum storey shears, M+SD values.

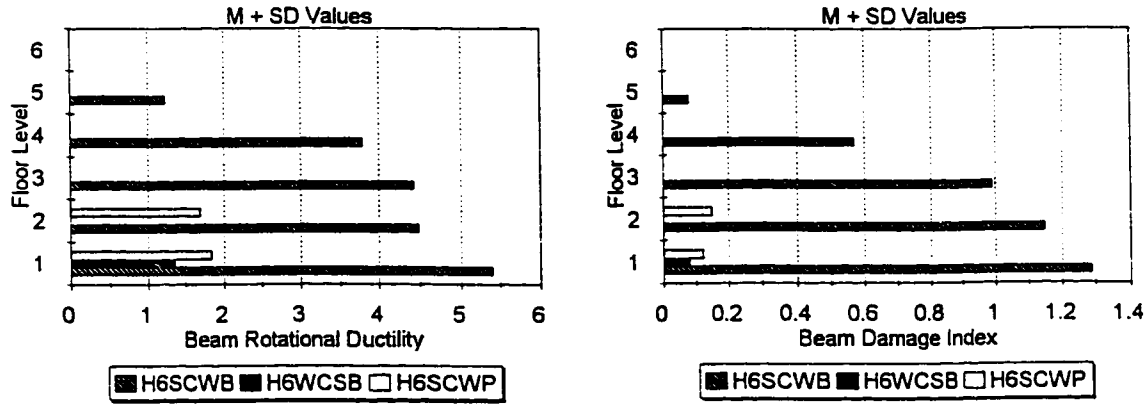


a) H6 frames

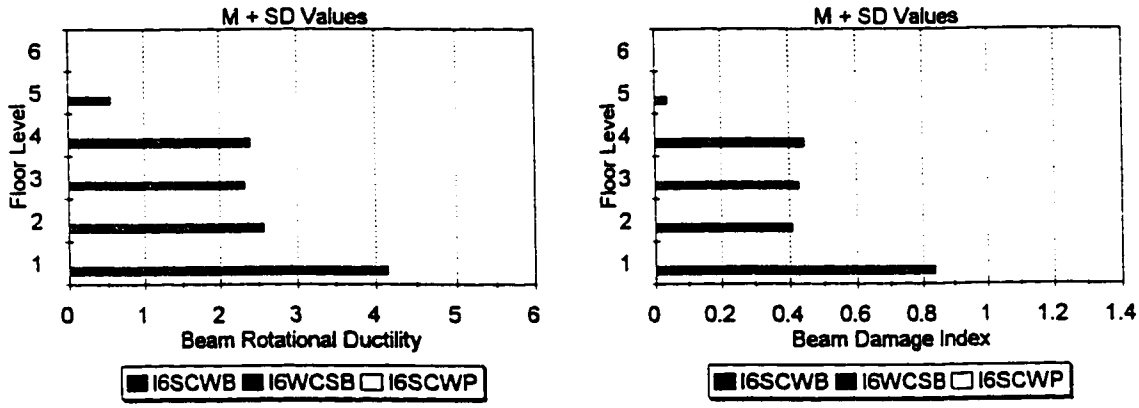


b) I6 frames

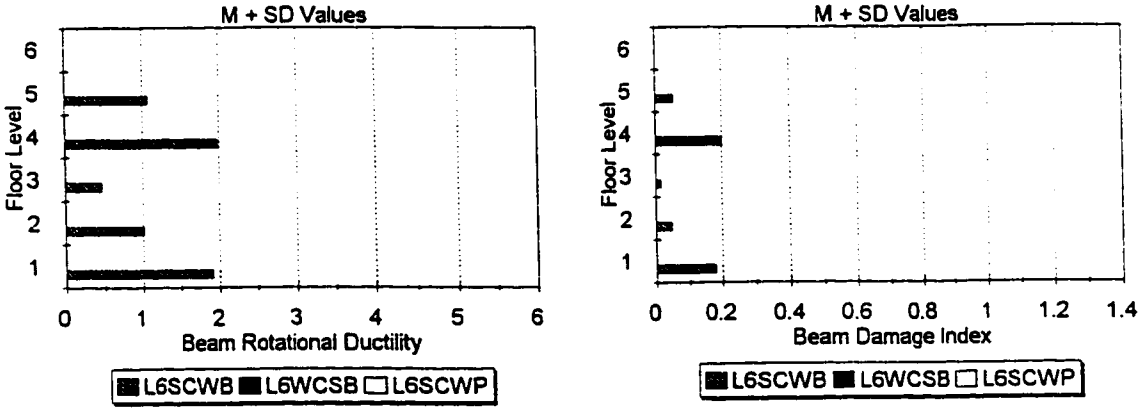


c) L6 frames

Figure 7.11 Beam performance parameters, M+SD values.

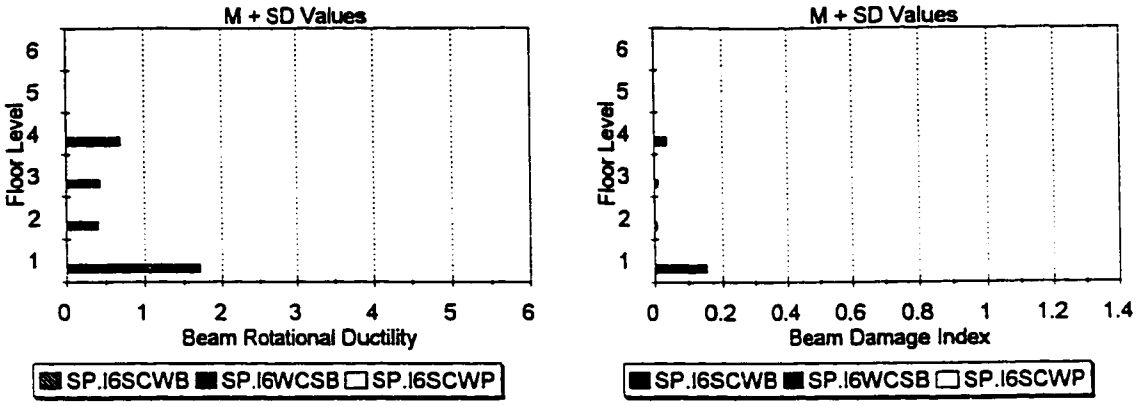


d)SP-I6 frames

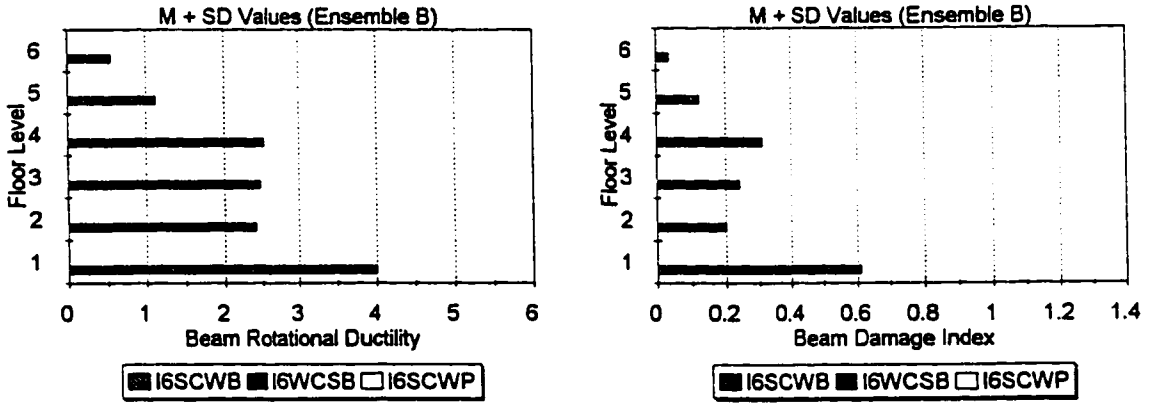


e) I6 frames (ensemble "B")

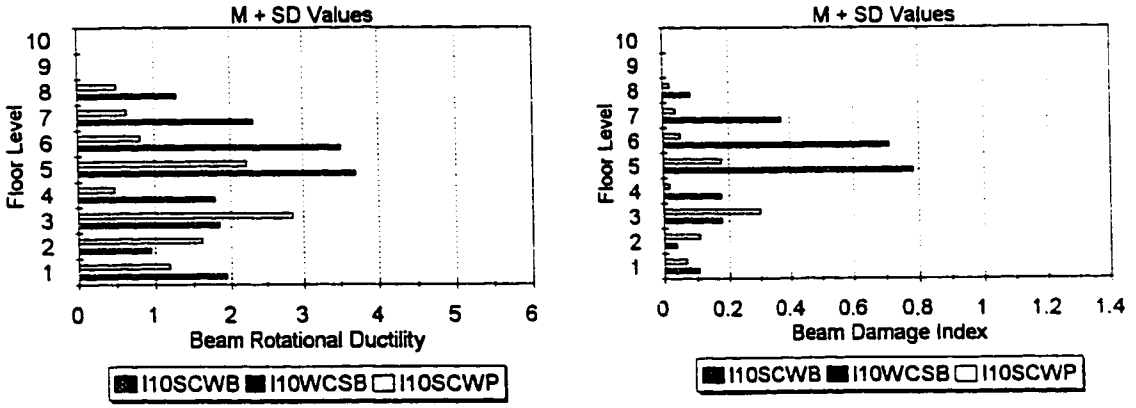


f) I10 frames

Figure 7.11 Continued

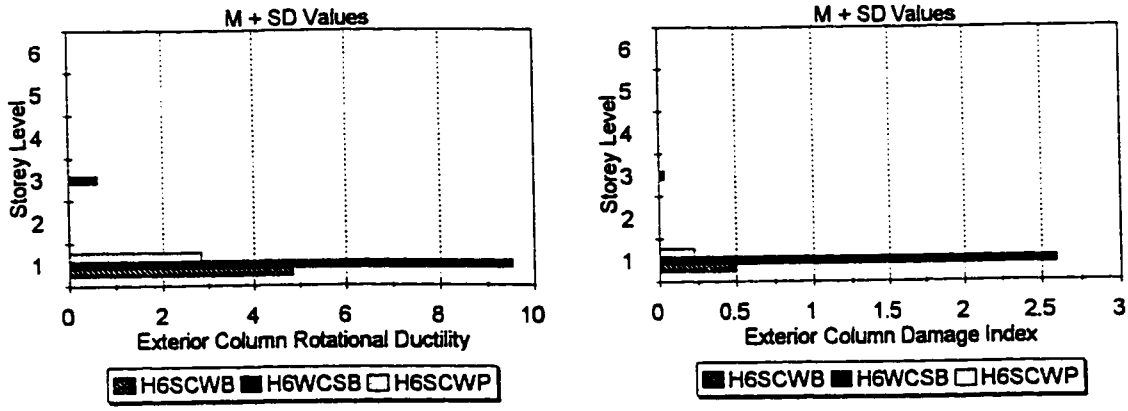


a) H6 frames

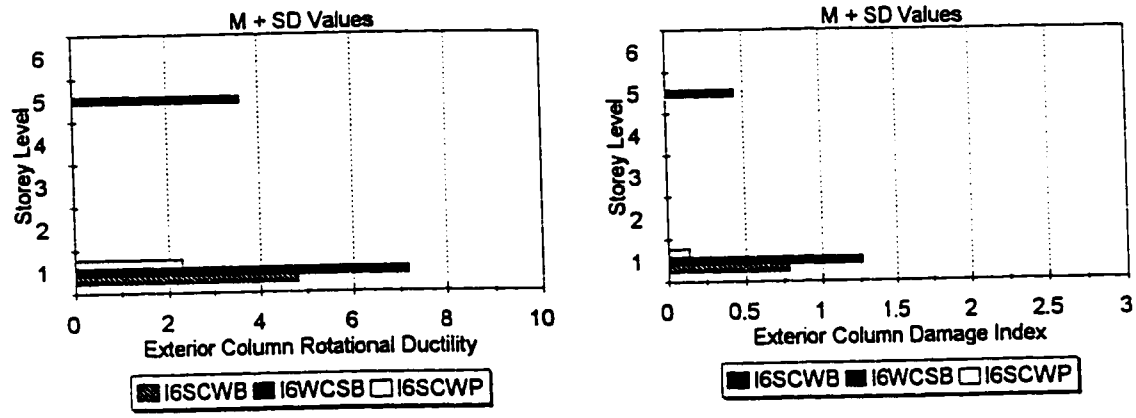


b) I6 frames

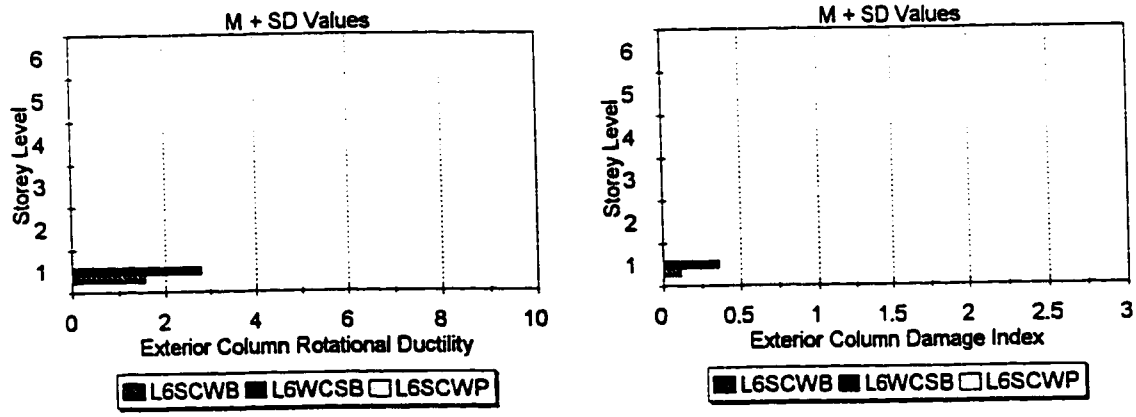


c) L6 frames

Figure 7.12 Exterior column performance parameters, M+SD values.

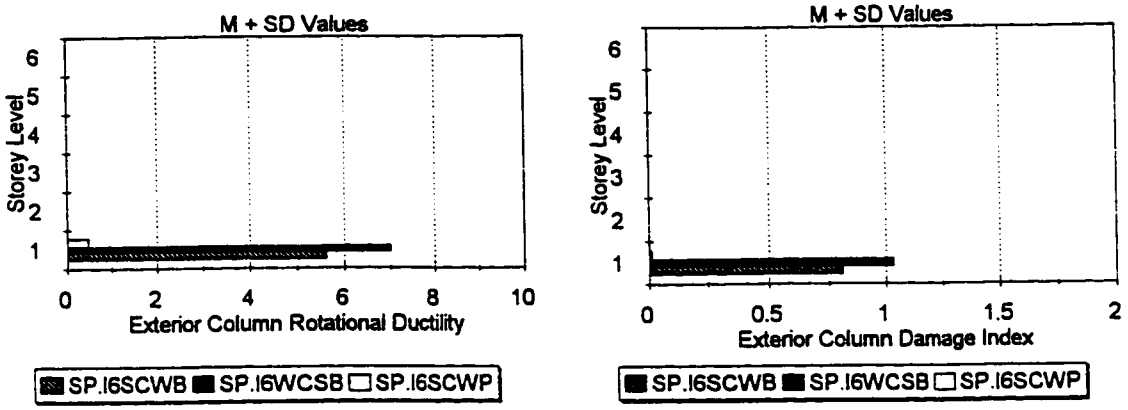


d)SP-I6 frames

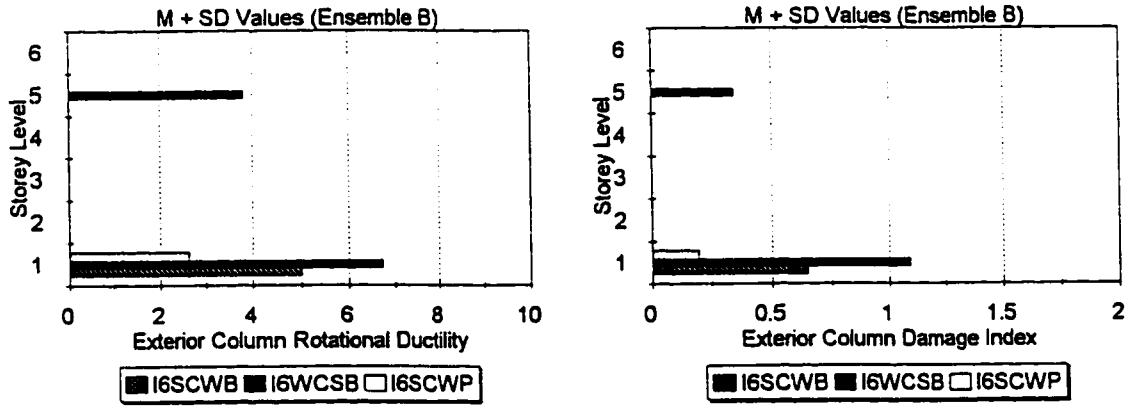


e) I6 frames (ensemble "B")

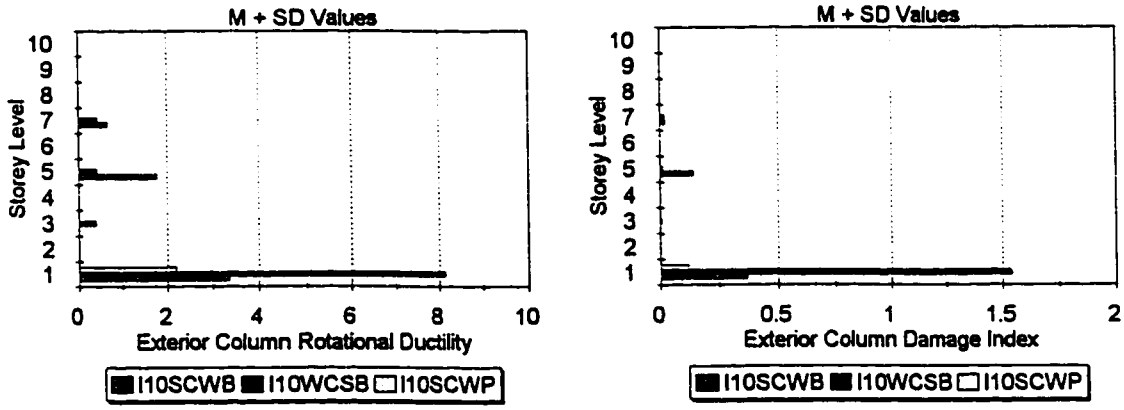


f) I10 frames

Figure 7.12 Continued

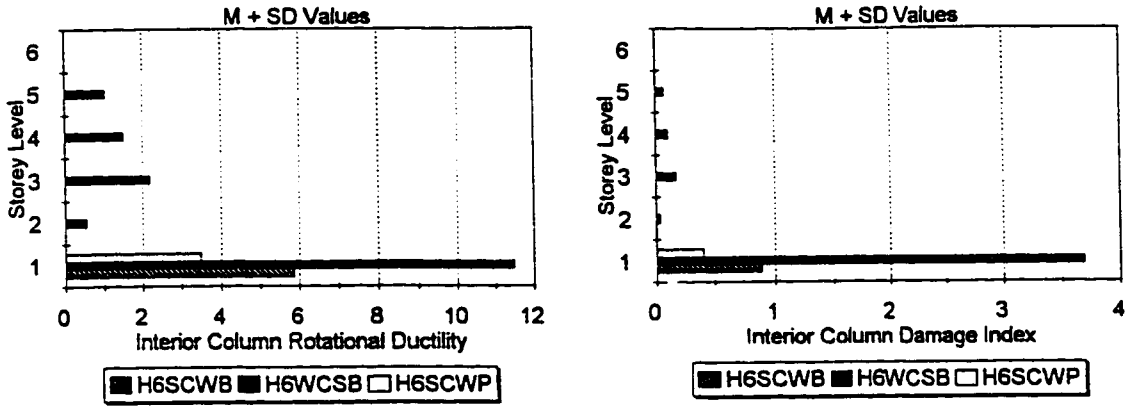


a) H6 frames

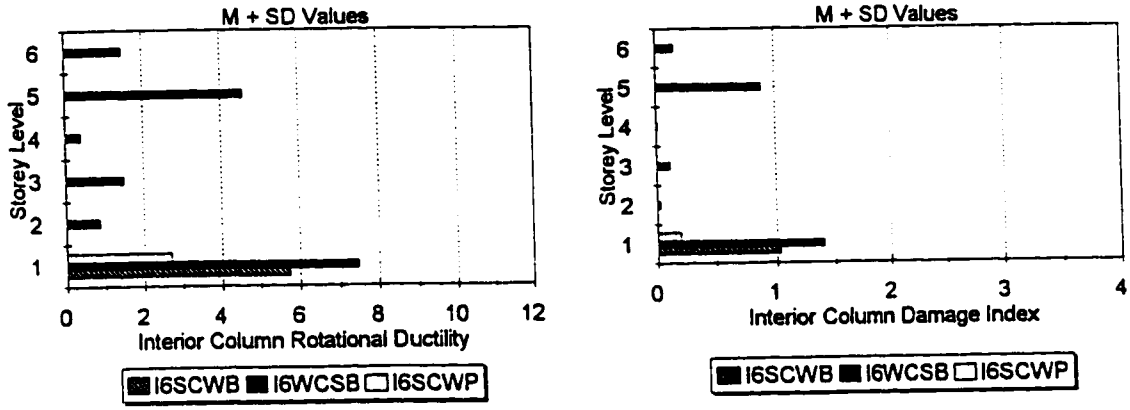


b) I6 frames

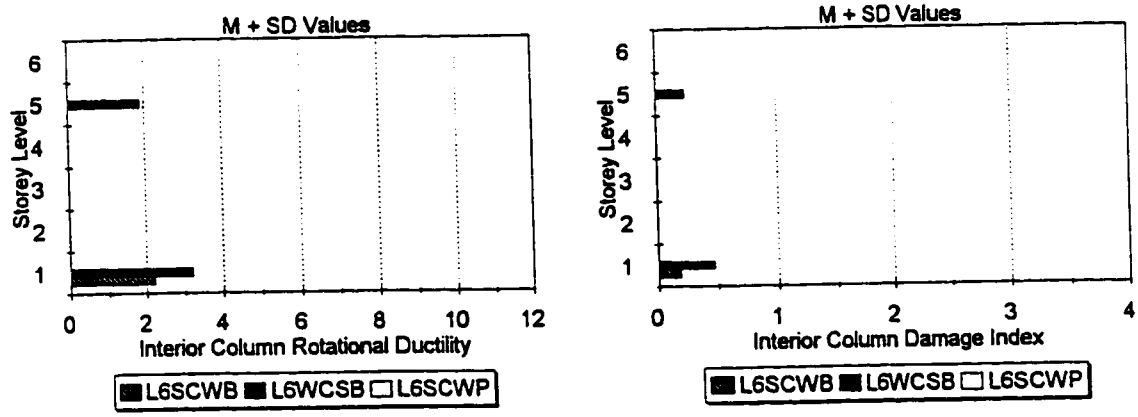


c) L6 frames

Figure 7.13 Interior column performance parameters, M+SD values.

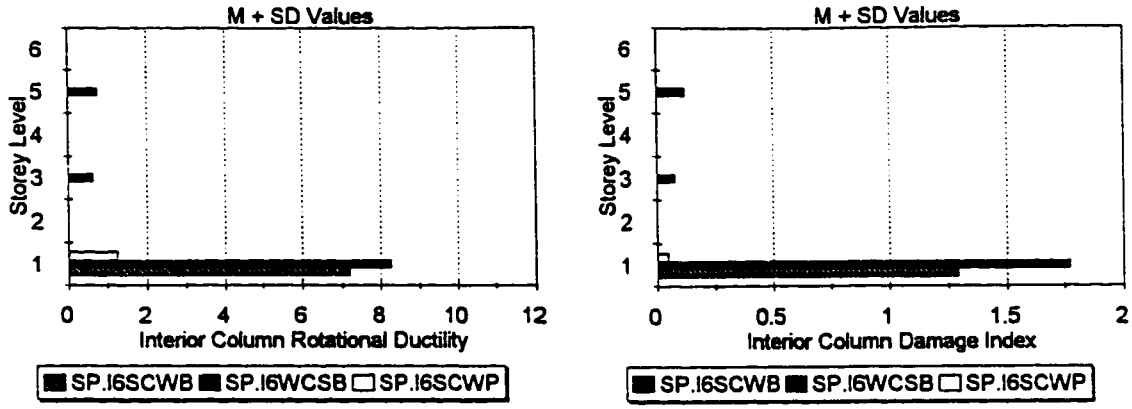


d)SP-I6 frames

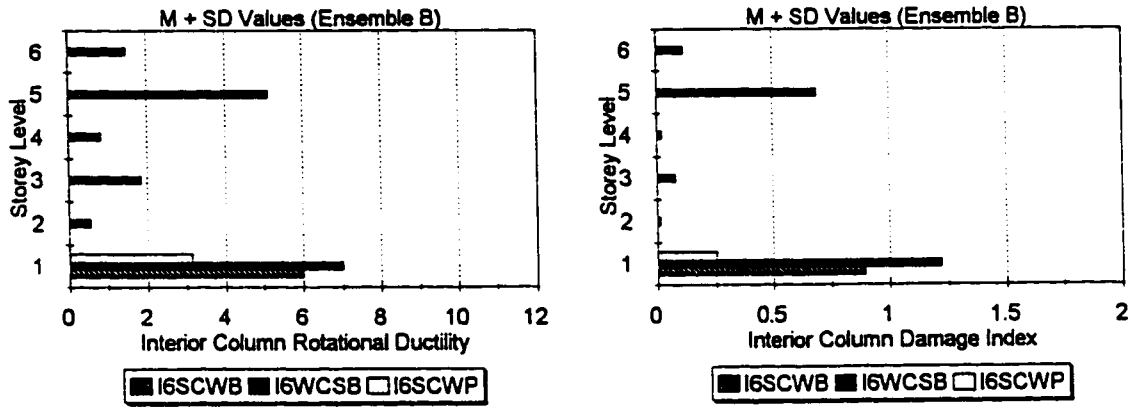


e) I6 frames (ensemble "B")

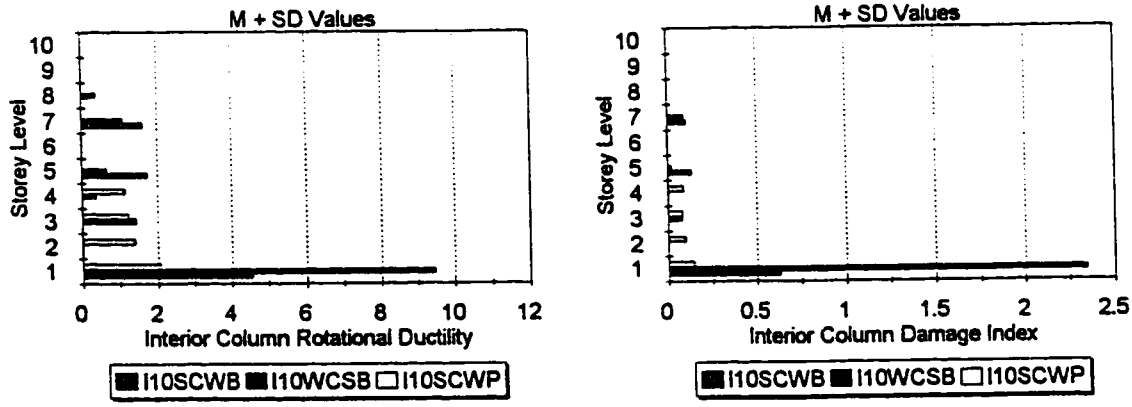


f) I10 frames

Figure 7.13 Continued

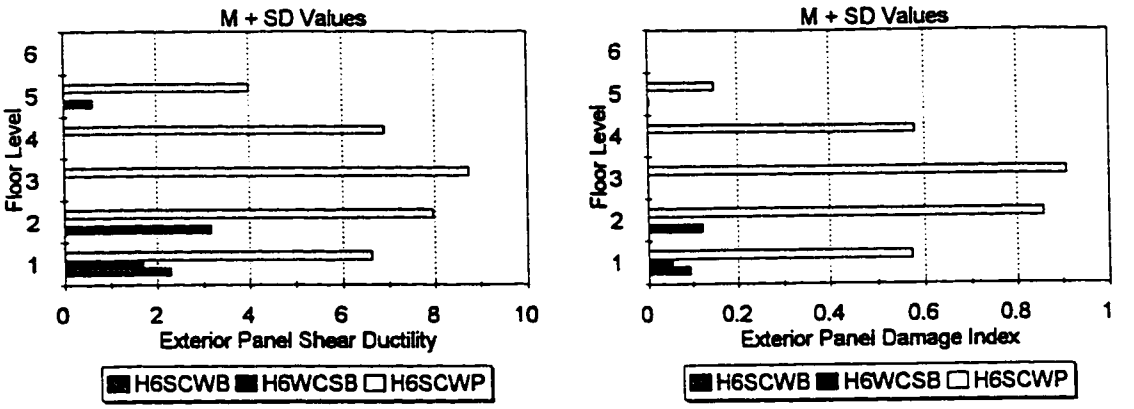


a) H6 frames

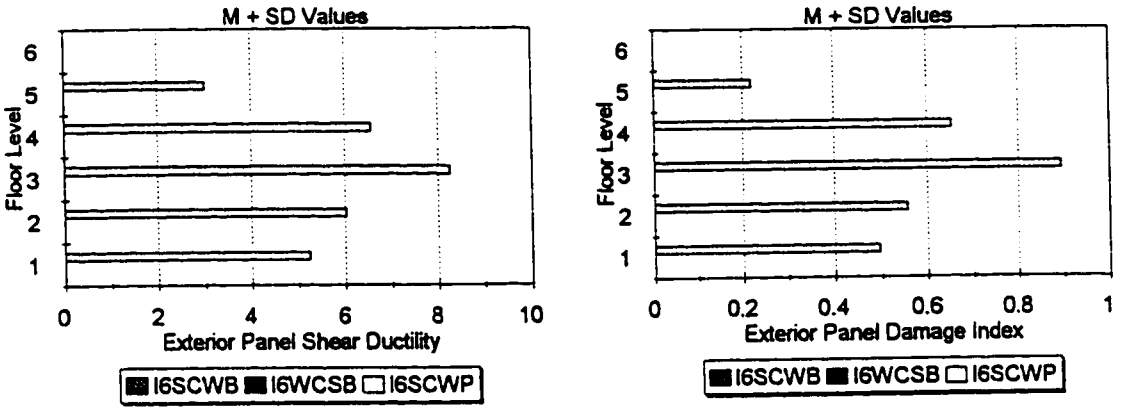


b) I6 frames

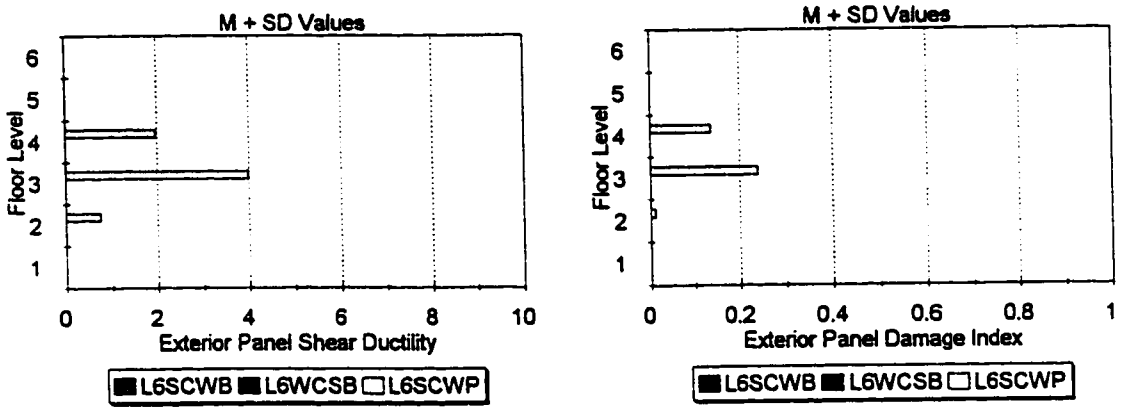


c) L6 frames

Figure 7.14 Exterior panel zone performance parameters, M+SD values.

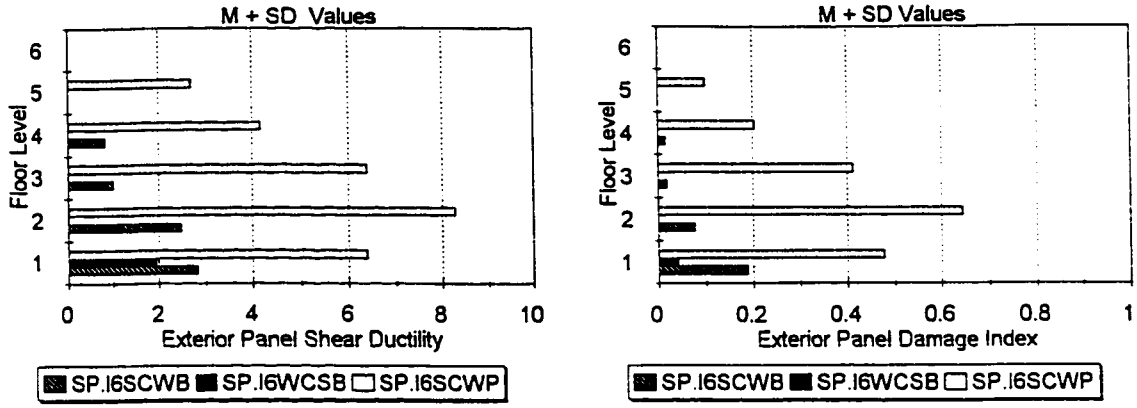


d)SP-I6 frames

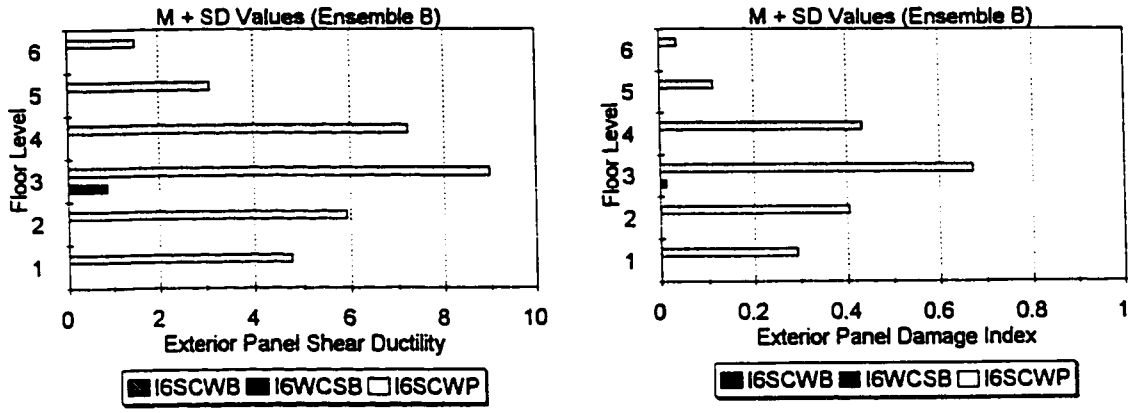


e) I6 frames (ensemble "B")

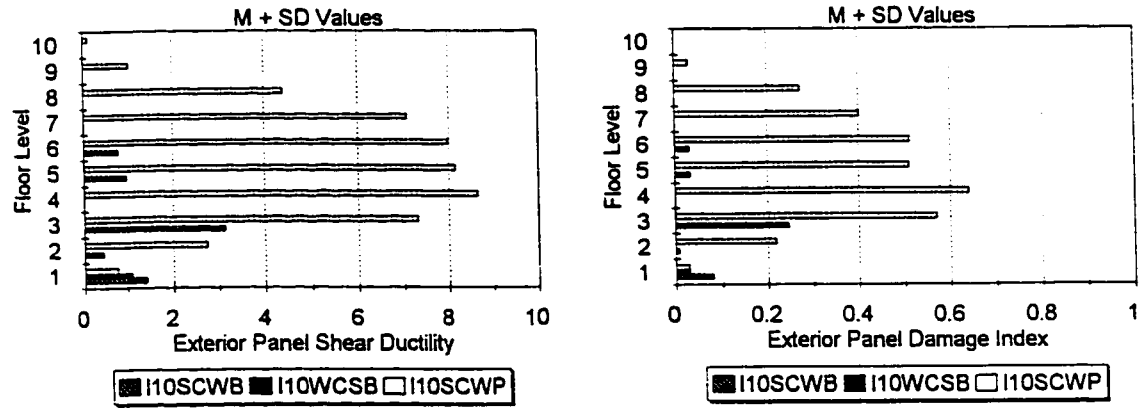


f) I10 frames

Figure 7.14 Continued

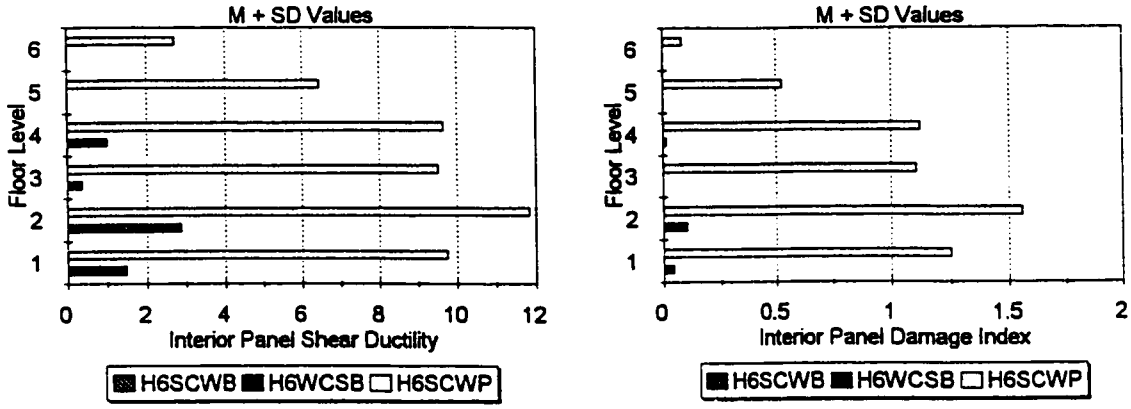


a) H6 frames

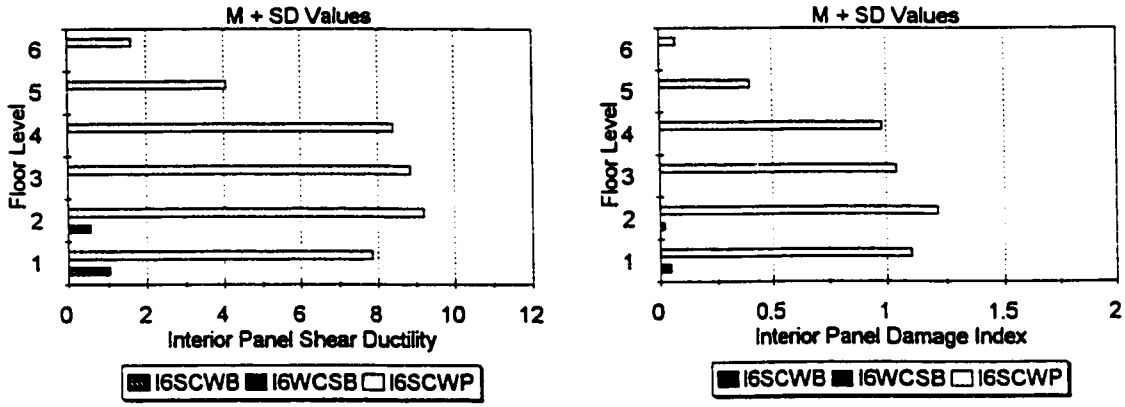


b) I6 frames

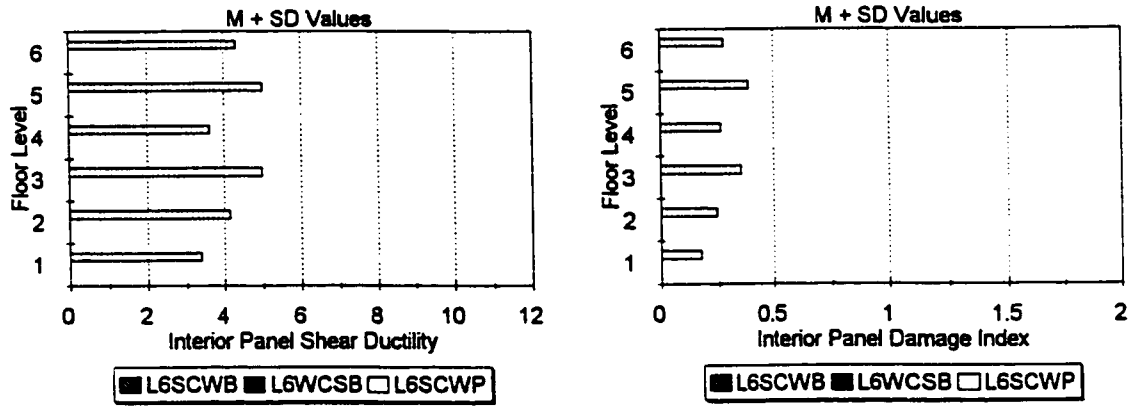


c) L6 frames

Figure 7.15 Interior panel zone performance parameters, M+SD values.

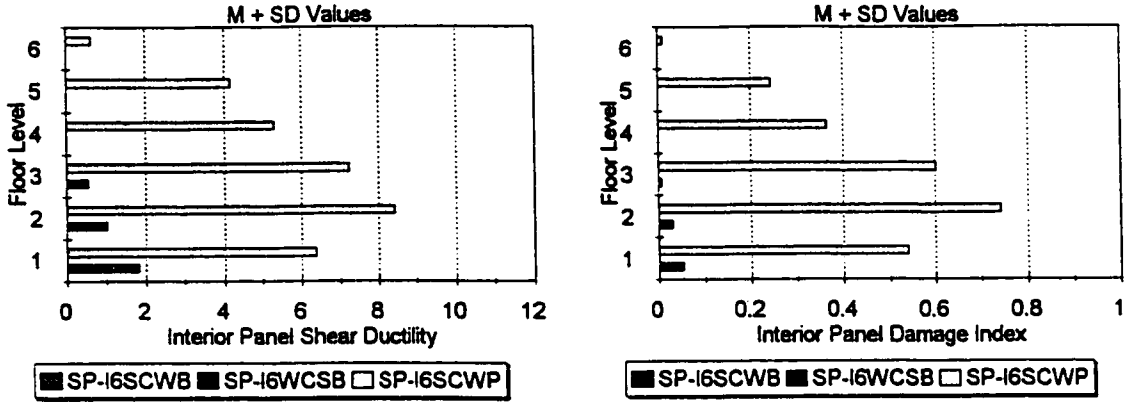


d)SP-I6 frames

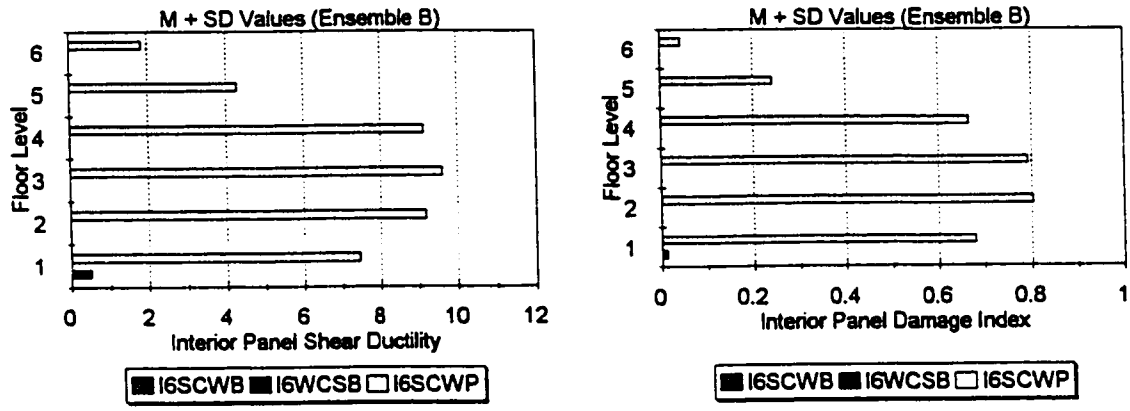


e) I6 frames (ensemble "B")

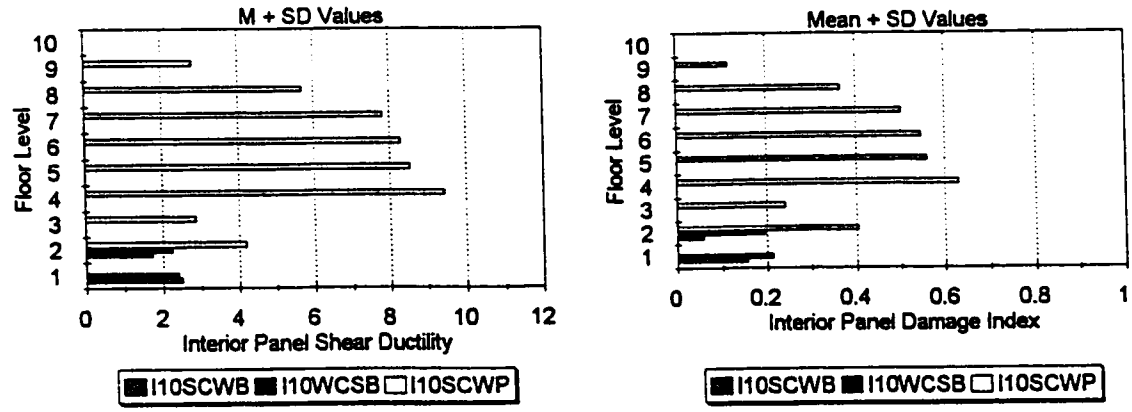


f) I10 frames

Figure 7.15 Continued

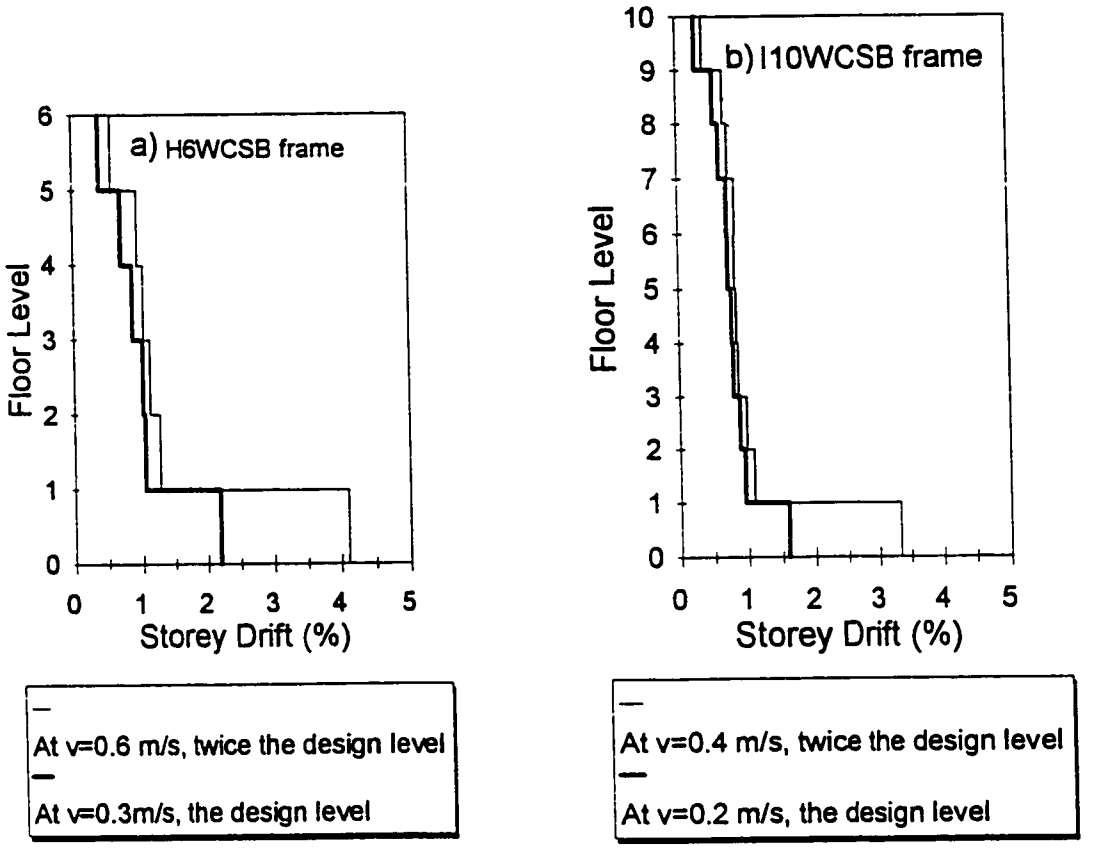


Figure 7.16 Comparison between M+SD maximum storey drifts at the design level and twice the design level excitations, a) for H6WCSB frame, b) for I10WCSB frame.

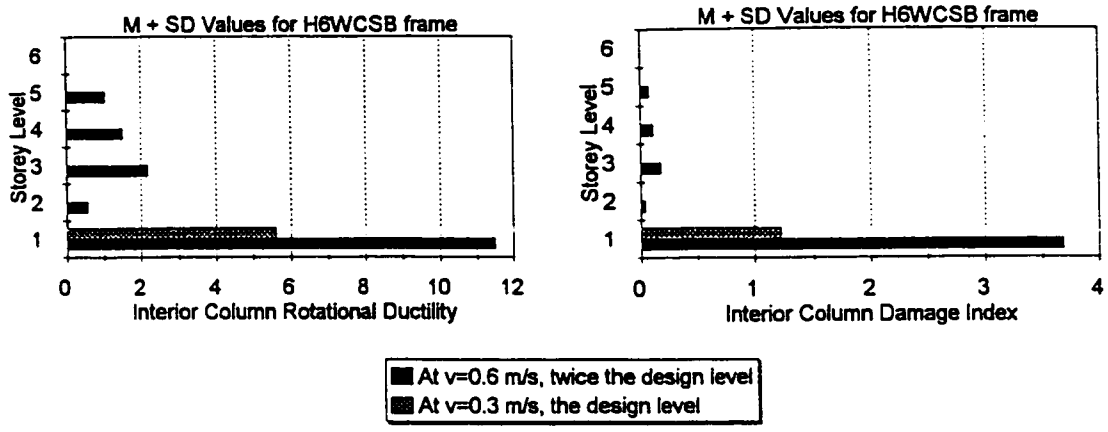


a) H6WCSB frame

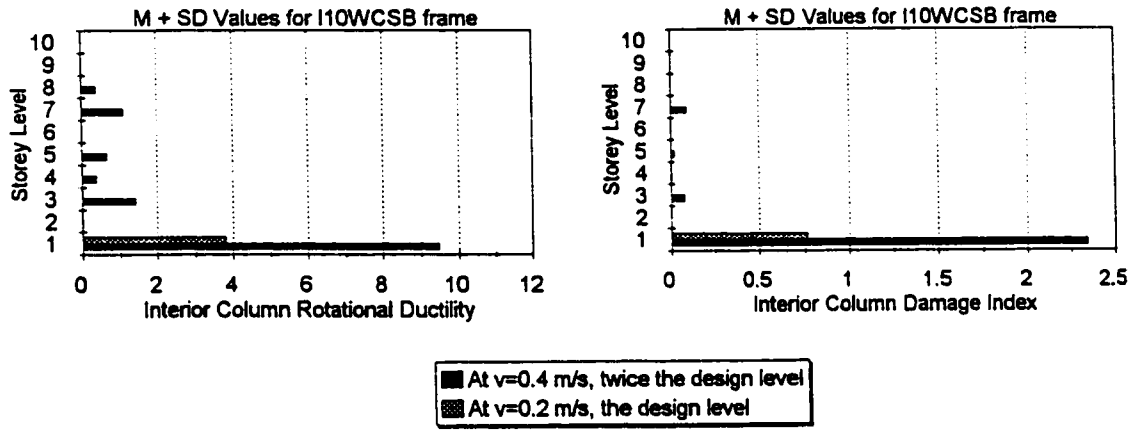


b) I10WCSB frame

Figure 7.17 Comparison between M+SD interior column performance parameters at the design level and twice the design level excitations, a) for H6WCSB frame, b) for I10WCSB frame.

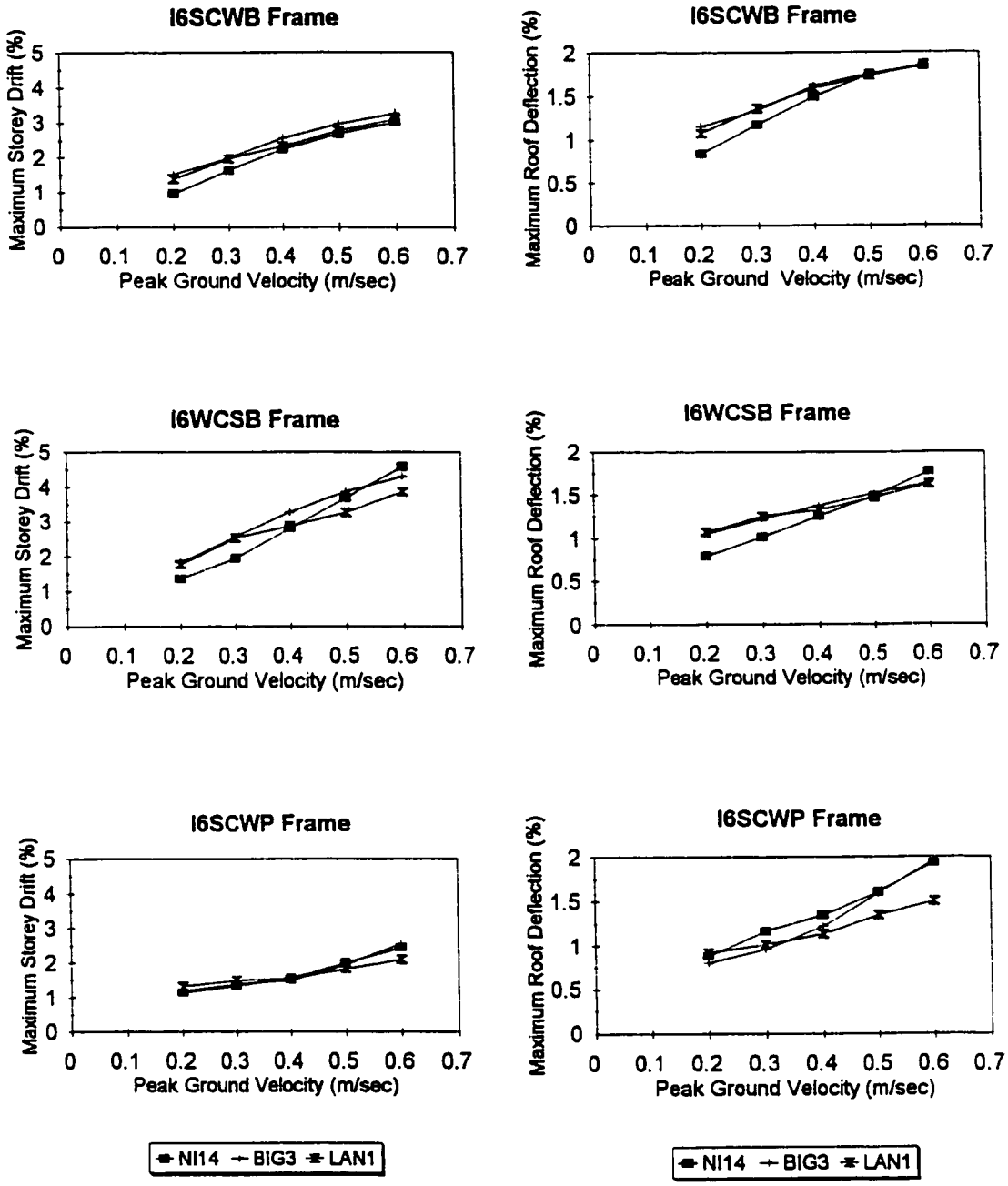


Figure 7.18 Effect of the peak ground velocity level on the maximum storey drifts and maximum roof deflections of the I6 frames.

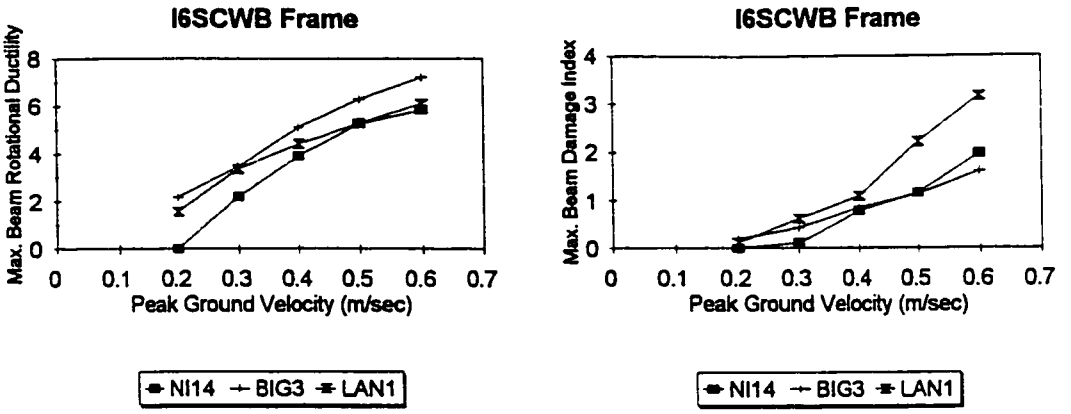


a) Maximum beam performance parameters in I6SCWB frame

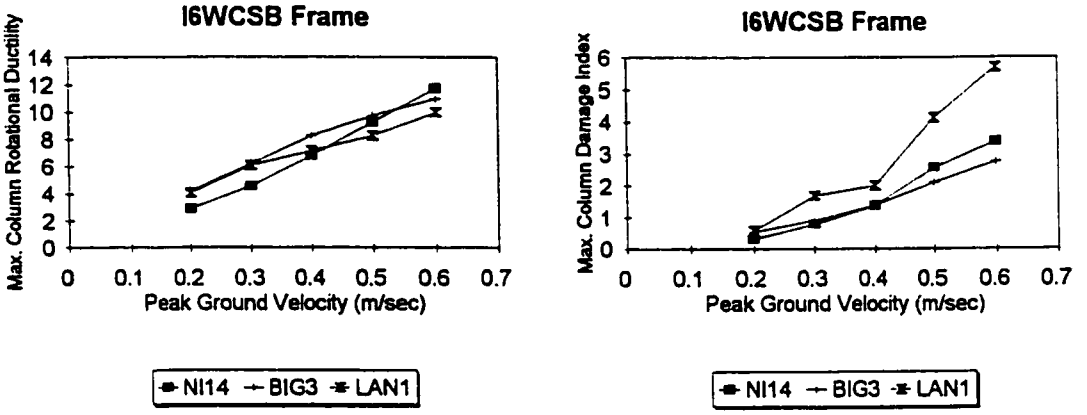


b) Maximum column performance parameters in I6WCSB frame

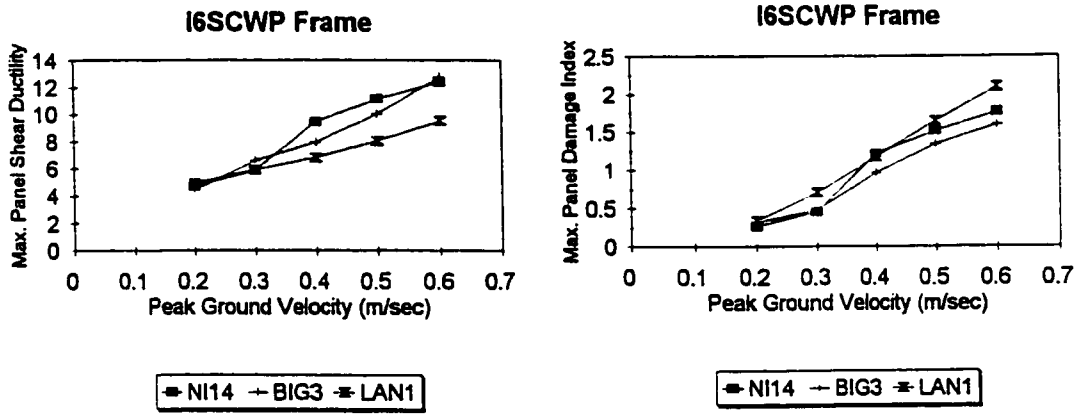


c) Maximum panel performance parameters in I6SCWP frame

Figure 7.19 Effect of the peak ground velocity level on the critical element maximum performance parameters in the I6 frames.

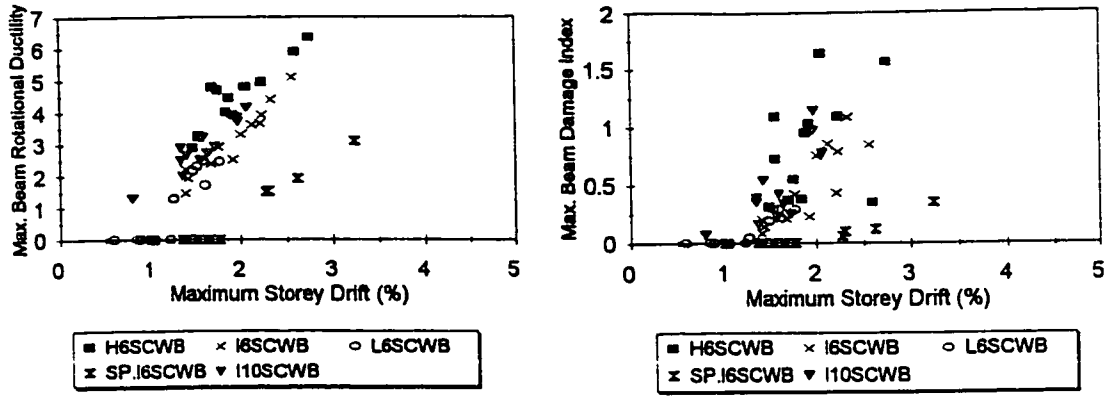


a) Beam performance parameters in SCWB frames

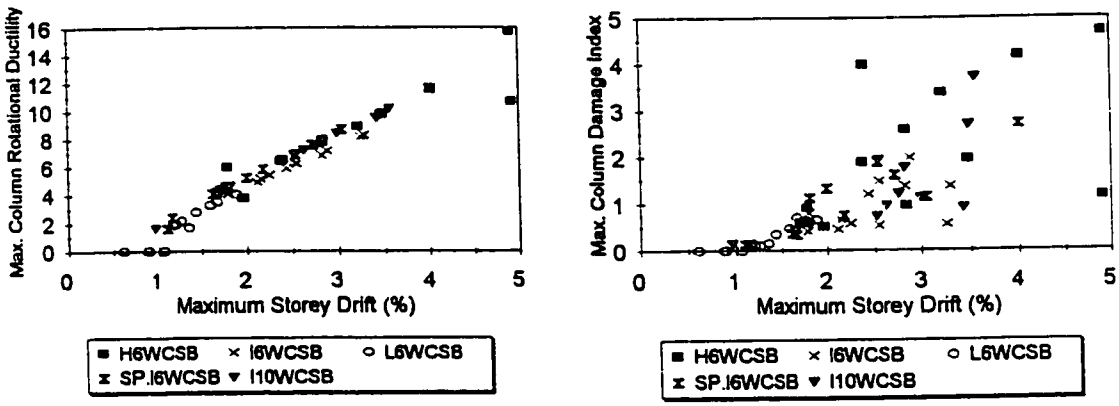


b) Column performance parameters in WCSB frames

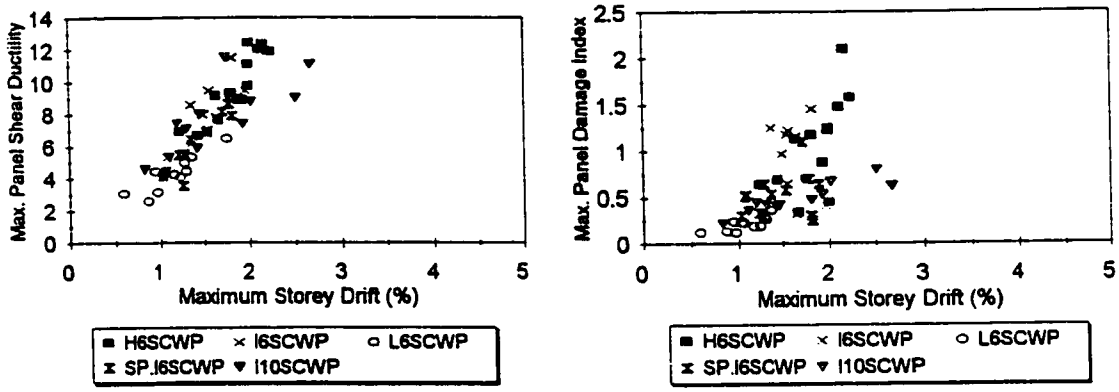


c) Panel performance parameters in SCWP frames

Figure 7.20 Maximum critical element performance parameters-maximum storey drift relationships.

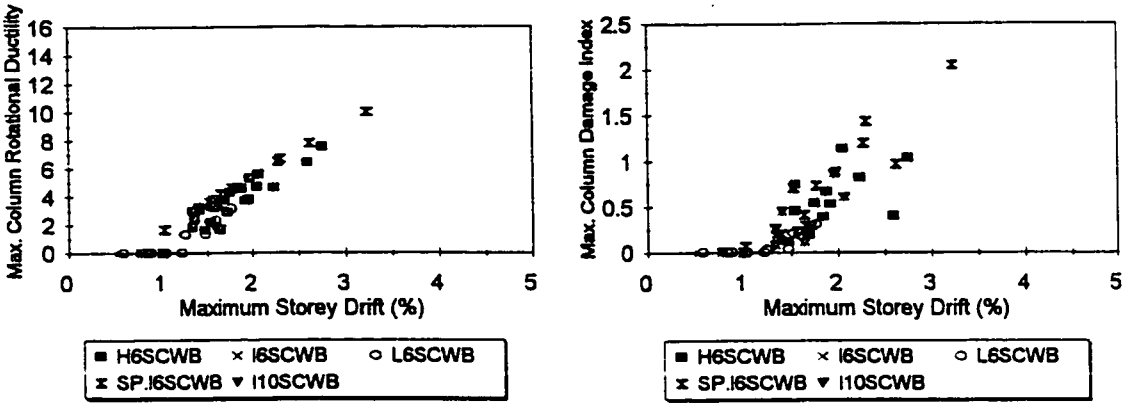


a) Column performance parameters in SCWB frames

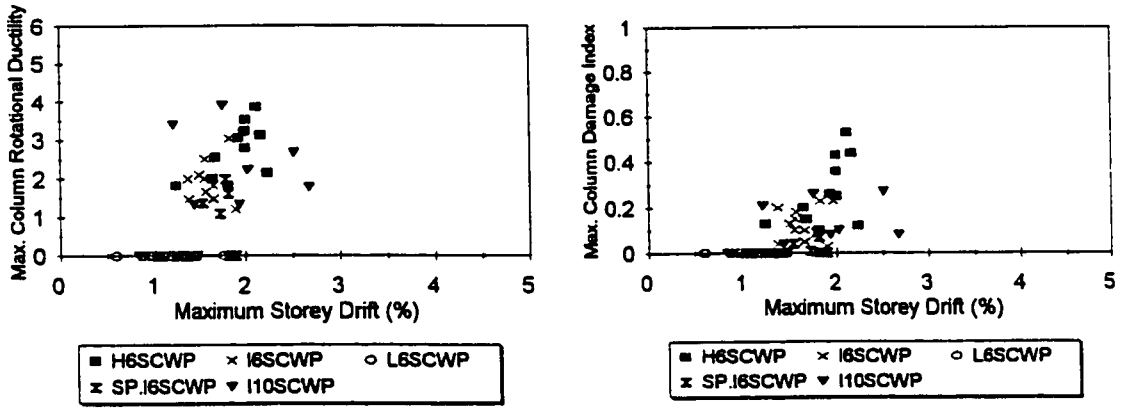


b) Column performance parameters in SCWP frames

Figure 7.21 Maximum column performance parameters-maximum storey drift relationships for the SCWB and SCWP frames.

# CHAPTER 8

# CONCLUSIONS

## 8.1 SUMMARY

This research study was concerned primarily with the evaluation of the seismic level of protection provided by the current Canadian code provisions to medium-rise moment resisting steel frame buildings, i.e. six and ten storey heights. In particular, most of the emphasis has been devoted to the assessment of the performance of the perimeter moment resisting frames (MRFs) in those buildings when subjected to actual strong earthquake ground motion records. The study involved several design philosophies and seismic hazard activity levels. The evaluation of the seismic level of protection was based on investigating the damage potential associated with each design case.

To achieve this principal objective, a comprehensive analytical study was undertaken involving several phases; they are briefly summarized as follows:

1) A definition was given for each design philosophy (i.e. SCWB, WCSB or SCWP) used in the research study. Following this, a total of three analytical computer element models, namely a beam-column element that accounts for gradual spreading of inelastic deformations, a spring connection element that accounts for its flexibility, and a panel zone finite element that accounts for the different joint panel deformations, were modified and incorporated into the PC-ANSR computer program. The analytical model predictions were

compared with some experimental results for validation purposes. Results showed that the model is capable of predicting the overall performance of steel MRFs. Response parameters were then defined, including the overall response parameters and the local member response parameters (element ductilities and damage indices).

2) The layouts of a six and ten storey steel office buildings were given. The buildings were used for the evaluation of seismic performance process. The study was concerned with the perimeter MRFs that are responsible for resisting seismic lateral loading. Six storey MRFs were designed in accordance with the Canadian code provisions for the different combinations of three design philosophies, namely SCWB, WCSB and SCWP, with three levels of seismic hazard activity levels, namely, high, intermediate and low. Also, six storey MRFs were designed for the three design philosophies at the intermediate seismic hazard level but using a special storey drift limit of 1% rather than the 2% code drift limit. In addition, ten storey MRFs were designed in accordance with the Canadian code provisions for the three design philosophies at the intermediate seismic hazard level.

3) Two ensembles of actual earthquake time-histories, each consisting of twelve records, were selected for use as inputs during the dynamic analyses. The records of the first ensemble were selected based on the criterion that the shapes of their mean (M) and mean plus one standard deviation (M+SD) response spectra match those from the Newmark-Hall design spectra for the periods range of interest. The records of the second ensemble were selected based on the criterion that the shape of their (M) response spectrum match that of the median uniform hazard spectrum for Vancouver, i.e. representing the new seismic hazard information. For both ensembles, the records represented a wide range of strong-motion

durations.

4) Nonlinear push over static analyses were performed for all the frames. The base shear-roof deflection relationship for each frame was studied, from which both the actual frame strength and capacity to sustain high levels of lateral deflections were examined. The base shear-maximum storey drift relationships for the frames were also discussed. The critical elements in each frame were identified, i.e. those which undergo substantial inelastic deformations. Implications of both the design philosophies and the seismic hazard design level were investigated. The height-wise distributions of the floor displacements and storey drifts were presented. Special consideration was given to the performance of the structural elements at a maximum storey drift of 2.5% which is the drift collapse limit defined by the SEAOC(1995). Beam, column, and panel zone performance parameters were evaluated in order to predict the damage potential associated with each design. For each frame, the relationship between the maximum storey drifts and maximum critical element performance parameters was also investigated.

5) Inelastic dynamic analyses (time-history analyses) were performed for all the frames. The dynamic responses of the frames were analyzed statistically. Maximum values of floor displacements, storey drifts, element ductilities and damage indices were analyzed to determine the M+SD values, which were later used in the evaluation process. The analyses included an evaluation of the vulnerability and damage potential of the frames at seismic ground motion levels that are higher than those used in the design. Based on the drift performance criteria and the values of the beam, column, and panel zone performance parameters, an assessment of the seismic performance of each frame was done, which

included the determination of the acceptability of the ranges of predicted damage. A number of other aspects were also addressed, including the maximum storey drift-maximum element performance parameters relationships and the effect of the peak ground velocity level on the performance. Finally, the performance expectations of the various frames were evaluated and compared, leading to conclusions regarding the overall level of protection provided by the current Canadian code provisions, and the status of each frame design type performance in a specific seismic hazard activity zone, i.e. best, acceptable, or unacceptable performance.

## 8.2 CONCLUSIONS

On the basis of the current research study on the evaluation of seismic performance and level of protection afforded to steel MRFs, the following conclusions are drawn:

### 8.2.1 Push over static analyses

1) In general, a static push over analysis to an approximate collapse-level maximum storey drift can satisfactorily simulate the primary features of the frame performance, i.e. order of magnitude and the distribution of element damage. Push over static analysis is capable of distinguishing the main differences among the behaviour of frames designed using different philosophies. The analysis clearly identifies the critical elements in each frame, i.e. those experiencing considerable amount of plastic deformations; also it can expose any frame design weaknesses that may remain hidden in an elastic analysis.

2) The push over static analyses show that the overstrength inherent in a specific frame depends upon the philosophy used in the design. Independent of the seismic hazard level, the SCWP frame always has the lowest overstrength compared to the other frame

design types, i.e. the SCWB and WCSB frames which have comparable overstrengths. For the same frame design type, increasing the seismic hazard level decreases the overstrength; the decrease is more significant for the WCSB frame design type.

3) The results of the push over analyses show that the SCWB and SCWP frames have considerable capacity for ductile behaviour at large deformations; no special preference is given for any of the two frame types.

4) The WCSB frames are vulnerable to collapse at large deformations; this vulnerability can be seen in the relatively small displacements at which large storey drifts are developed; these large drifts are associated with the early development of plastic hinges at both the bottom and top ends of the first storey columns which is the primary reason that the performance of these frames is less than satisfactory, especially in seismically active regions. Results show that in the high and intermediate seismic hazard regions, the WCSB tend to develop a soft storey collapse mechanism at approximately 1.5% maximum storey drift and 1% roof deflection. This mechanism will over-ride member deformation capacities as a collapse criterion.

5) Push over analyses show that the six storey frames designed for 1% drift limit have larger overstrengths and smaller lateral deflections and drifts compared to those of the corresponding frames designed for the code drift limit. Compared with the I6SCWB frame, the SP.I6SCWB frame has much lower beam plastic deformations and damage which are compensated for by slightly higher column plastic deformations at the base.

6) Push over analyses show that the behaviour of the ten storey frames is more or less comparable with the behaviour of the corresponding six storey frames. However, the ten

storey WCSB frame is more sensitive than the corresponding six storey frame in developing a soft storey behaviour. The ten storey SCWP frame also performs slightly poorer than its six storey counterpart, i.e. the I6SCWP frame.

7) A simple push over analysis cannot include the effects of higher mode contributions in the lateral deformation of the frame; therefore only maximum values of deformation parameters (and their locations) rather than detailed distributions can be used to evaluate structural performance.

8) Push over analysis cannot account for the effect of accumulation of plastic deformations of the critical elements during the cyclic response of the structure during dynamic loading. The results of the dynamic analyses show that the damage indices for the critical elements are usually much larger (e.g. 50% to 100% larger) than those predicted from a static push over analysis.

9) In general, there is a linearly proportional relationship between the maximum storey drift ratios and both the maximum critical element ductilities and damage indices, which is more or less independent of hazard level for each design philosophy.

### 8.2.2 Inelastic dynamic analyses

An evaluation of the performance of the frames to seismic excitations at twice the design level using a simplified definition of expected collapse performance shows the following:

1) The performance of the special drift designed six storey frames shows that there is no specific advantage for designing steel frames for a more restricted drift limit than that

given by the NBCC.

2) The new seismic hazard information (UHS) given by the Geological Survey of Canada for Vancouver (B.C.) is likely to result in a seismic hazard intensity level which is slightly less than that given by the current NBCC(1995), i.e. less seismic damage to structures.

3) In regions of high seismic hazard activity, the six storey SCWB and SCWP frames perform satisfactorily with comparable CPR (Collapse Prevention Ratio) values that are slightly less than 2. However, based on the drift ductility factors and the values of the damage indices, the performance of the SCWB frame is slightly better than that of the SCWP frame. On the other hand, the six storey WCSB frame does not perform satisfactorily and it has a CPR value << 2 (i.e. can be expected to collapse at excitations well below twice the design level); some collapses can even be expected at the design level excitation.

4) In regions of intermediate seismic hazard activity, the six storey SCWB and SCWP frames also perform satisfactorily with comparable CPR values that are in the neighbourhood of 2. While the CPR for the six storey WCSB frame is slightly below 2, its performance is inferior to other cases for which CPR is slightly below 2 (e.g. the SCWB and SCWP frames in the H seismic hazard zone); based on the range of the overall drift ductilities and the distribution of column damage indices, this frame does not perform satisfactorily.

The ten storey SCWB and SCWP frames perform somewhat better than the corresponding six storey frames; they both have CPR values greater than 2. This better performance is attributed to the fact that the ten storey frames have longer periods and are therefore not subject to the same level of input seismic energy as the six storey frames. The

performance of the ten storey SCWB is expected to be slightly better than that of the ten storey SCWP frame. In contrast with the performance of the ten storey SCWB and SCWP frames, the performance of the ten storey WCSB frame is significantly poorer and not satisfactory. This frame has a CPR well below 2, i.e. it's performance is even poorer than that of the corresponding six storey WCSB frame.

5) In regions of low seismic hazard activity, the performance of all three types of frames (i.e. SCWB, WCSB and SCWP) is comparable and very well satisfactory. The CPR values for all frames are larger than 2.

6) In general, there is a linearly proportional relationship between maximum critical element ductilities and maximum storey drift ratios, which is more or less independent of hazard level for each design philosophy; this proportionality enables the determination of the element ductility capacities which are required in order to prevent collapse due to excessive storey drifts.

7) The relation between maximum element damage indices and maximum storey drift ratios is non-proportional. This is because damage during dynamic analyses depends mainly on the accumulation of plastic deformations which is affected significantly by the duration of the strong ground motion excitation. Thus, it is expected that both the intensity and the strong-motion duration of an earthquake play important roles in determining the seismic structural damage.

### 8.2.3 Overall performance

Based on the recent version of the Canadian seismic hazard informations, in which results suggest that structures designed for life safety criteria should, with a high level of

confidence, sustain twice the design ground motion without collapse, it can be concluded that in both the high and intermediate seismic hazard regions, the performance of the SCWB and SCWP frames can be considered acceptable with a slight preference for the SCWB frames, while the performance of the WCSB frames is totally unacceptable. In low seismic hazard regions, all three frame design types have comparable and acceptable performance.

The conclusions mentioned in this chapter for the overall seismic performance of six and ten storey moment resisting steel frames can be applicable to frames that range from several storeys to approximately fifteen storeys, i.e. low to medium-rise moment resisting steel frames.

It should be noted that the overall seismic performance of SCWP frames may be altered if totally welded beam-to-column connections are used (i.e. if the connection type is different than those assumed in Chapter 2 of this study). This is because the yielding of the panel zones may be detrimental for the connections.

## 8.3 RECOMMENDATIONS FOR FUTURE RESEARCH

The following general ideas are put forward as a suggestion for future research:

1) The level of protection framework need to be applied using more sophisticated models in order to take into account the following aspects:

a) the actual geometry of a specific connection type during the dynamic analyses.

b) the influence of local buckling (i.e. local instability in the plastic range) of the component plates of a cross-section on the stiffness and load carrying capacity of the member.

2) The level of protection framework needs to be applied to frames that have some flaws or imperfections in the design, e.g. in the connections or joint panels.

3) In seismically active regions, buildings built to prior codes or older buildings which were designed and built without specific seismic consideration may be vulnerable. Thus, the performance of those buildings has to be examined and rehabilitation strategies should be developed to upgrade such buildings and improve their performance and hence the level of protection afforded to them.

4) The effect of the rigidity of the floor slabs and the stiffnesses of the non-structural members including walls on the performance of the frames need to be studied.

## REFERENCES


Adams, J., Weichert, D.H., Halchuk, S., and Basham P.W. 1995. "Towards fourth generation seismic hazard maps of Canada", Proceeding of the 7th Canadian Conference on Earthquake Engineering, Montreal.

Adams, J., Weichert, D.H., Halchuk, S., and Basham, P.W. 1996. "Trial seismic hazard maps for Canada-1995: final values for selected Canadian cities", Geological Survey of Canada, Ottawa, Ontario, Open File Report 3283.

Anagnostopoulous, S.A., 1981. "Inelastic beams for seismic analysis of structures", Journal of Structural Division, ASCE, Vol.107, pp. 1297-1312.

Ang, K.M., and Morris, G.A., 1984. "Analysis of three dimensional frames with flexible beam-column connections", Canadian Journal of Civil Engineering, Vol. 11, pp. 245-254.

Associate Committee on the National Building Code. 1995. National Building Code of Canada (NBCC), National Research Council of Canada, Ottawa, Ontario, Canada.

ATC, 1995. Guidelines for the seismic rehabilitation of buildings. ATC 33.03: Applied Technology Council, Redwood City, California.

Banon, H., Biggs, J., and Irvine, H., 1981. "Seismic damage in reinforced concrete frames", Journal of Structural Division, ASCE, Vol 107, No. ST9, pp. 1713-1729.

Banon and Veneziano, 1982. "Seismic safety of RC members and structures ", Earthquake Eng.and Structural dynamics, Vol 10, pp.179-193.

Basham, P.W., Weichert, D.H., Anglin, F.M., and Berry, M.J., 1985. "New probabilistic strong motion maps of Canada", Bulletin of the Seismological Society of America, Vol. 75, pp. 563-595.

Becker, R., 1975. "Panel zone effect on the strength and stiffness of steel rigid frames", Eng. Journal, AISC 12, pp. 19-29.

Bertero, V.V., Popov, E.P., and Krawinkler, H., 1972. "Beam-column subassemblages under repeated loading", Journal of Structural division, ASCE, Vol. 98, pp. 1137-1159

Bertero, V.V., Anderson, J.C., and Krawinkler, H. 1994. "Performance of steel buildings during the Northridge earthquake", Report UCB/EERC-94/09, Earthquake Engineering Research Center, University of California, Berkeley, California

Biddah, A., and Heidebrecht, A.C., 1998. "Seismic performance of ductile six storey steel frame structures", Six U.S. National Conference on Earthquake Engineering, Seismic Design and Mitigation for the Third Millennium, Seattle, Washington, USA, May.

Biddah, A., and Heidebrecht, A.C., 1998. "Evaluation of the seismic level of protection afforded to steel moment resisting frame structures designed for different design philosophies", Accepted for publication in the Canadian Journal of Civil Engineering.

Biddah, A., and Heidebrecht, A.C., 1998. "Seismic performance of moment resisting steel frame structures designed for different levels of seismic hazard", Submitted for publication in the Earthquake Spectra.

Canadian National Committee on Earthquake Engineering (CANCEE),1996. "Preliminary formulation of elastic seismic forces using spectral ordinates".

Canadian Standards Association (CSA). 1992. Structural Quality Steels, CAN/CSA-G40.21-92, Rexdale, Ontario, Canada.

Canadian Standards Association (CSA). 1994. Limit States Design of Steel Structures, CAN/CSA-S16.1-94, Rexdale, Ontario, Canada.

Chen, S., 1994. "Seismic behaviour of unbraced steel building frames", M.Eng. Thesis, Department of Civil Engineering, McMaster University, Hamilton, Canada, 209 pages.

Chen, W.F. and Atsuta, T., 1976. "Theory of beam-columns", Vol.1, Published by McGraw-Hill.

Chen, W.F., and Patel, K.V., 1981. "Static behaviour of beam-to-column moment connections", Journal of the Structural Division, ASCE, ST9.

Chen, W.F., and Lui, E.M., 1991. "Stability design of steel frames", CRC Press, Boca Raton, Fla.

Cheng, F.Y., Oster, K.B., and Kitipitayangkul, P., 1979. "Establishment of ductility factors based on energy absorption and evaluation of present methods", Proc. of 3 CCEE, Vol 1, pp. 719-744

Chi, H-M., and Powell, G.H., 1973. "Computational procedure for inelastic finite element analysis", Report No UC SESM 73/02, University of California, Berkeley, California.

Clough, R. and Penzien, J., 1993. Dynamics of Structures. McGraw-Hill, second edition.

Cosenza, E., Manfredi, G., and Ramasco, R., 1993. "The use of damage functionals in earthquake engineering: a comparison between different methods", Earthquake Eng. and Struc. Dynamics, Vol. 22, pp. 855-868.

Daali, M. L., and Korol, R. M., 1994. "Damage assessment in locally stiffened beams under seismic type of loading", Eng. Mech. Symposium of CSCE, Winnipeg

Daali, M.L., and Korol, R.M., 1995. "Prediction of local buckling and rotation capacity at maximum moment", Journal of constructional Steel Research, Vol. 32, pp. 1-13.

Daali, M.L., and Korol, R.M., 1996. "Adequate ductility in steel beams under earthquake-type loading", Engineering Structures, Vol. 18, pp. 179-189.

Engelhardt, M., Kim, K., Uzarski J., Husain, A., Sabol, T., Ho, L., and Kim, H.-I. 1995. "Parametric studies on inelastic modelling of steel moment frames", Technical Report SAC 95-05: Parametric Analytical Investigation of Ground Motions and Structural Response, Earthquake of January 17, 1994, SAC Joint Venture, Sacramento, California.

Fajfar, P., and Fischinger, M., 1988. "N2- A method for nonlinear seismic analysis of regular buildings", Proc. 9th World Conference on Earthquake Engineering, Tokyo, Japan, Vol. 5, pp. 111-116.

Fajfar, P., and Gaspersic, P., 1996. "The N2 method for the seismic damage analysis of RC buildings", Journal of Eathquake Eng. and Structural Dynamics, Vol. 25, pp. 31-46.

Frye M.J., and Moris, G.A., 1975. "Analysis of flexibly connected steel frames", Canadian Journal of Civil Engineering, Vol 2, pp 280-291.

Geberson, M.F., 1969. "Two nonlinear beams with definitions of ductility", Journal of the Structural Division, ASCE, Vol. 95, No. ST2, pp. 137-157.

Ghobarah A., Osman A., and Korol R.M., 1990. "Behaviour of extended end-plate connections under cyclic loading", Engineering Structures, Vol. 12, January.

Ghobarah, A., Korol, R.M., and Osman, A. 1992. "Cyclic behaviour of extended end plate-joints", Journal of Structural Engineering, ASCE, Vol. 118, pp. 1333-1353.

Goel, R.K., and Chopra, A.K., 1996. "Evaluation of code formulas for fundamental period of buildings", Eleventh World Conference on Earthquake Engineering, Acupolco, Mexico, paper No. 1127.

Harper, Jr. W.L., Bradburn, J.H., Dickerson, J.R., and Radziminski, J.B., 1990. "Static and cyclic behaviour of semi-rigid bolted and welded beam-column connections", A report from the Department of Civil Engineering, University of South Carolina, Columbia.

Harriot, J.D., and Astaneh, A., 1990. "Cyclic behaviour of steel top-and-bottom plate moment connections", Report UCB/EERC-90/19, Earthquake Enginnering Research Center, University of California, Berkeley, California.

Heidebrecht, A.C. 1995. "Insights and challenges associated with determining seismic design forces in a loading code", Bulletin of the New Zealand National Society for Earthquake Engineering, Vol. 28, pp. 224-246.

Heidebrecht, A.C. 1997. "Seismic level of protection for building structures", Canadian Journal of Civil Engineering, Vol. 24, pp. 20-33.

Heidebrecht, A.C., Basham, P.W., and Finn, W.D.L. 1995. "Overview of major issues involved in preparing new seismic loading provisions for the 2000 edition of the National Building Code of Canada", Proceedings of the 7th Canadian Conference on Earthquake Engineering, Montreal, Que., pp. 993-1000.

Housner, G.W., and Brady, A.G., 1963. "Natual periods of vibration of buildings", ASCE, Journal of Engineering Mechanics Division, Vol. 89, No. EM4, pp. 31-65.

International Conference of Building Officials. 1994. Uniform Building Code (UBC), 1994 edition, Whittier, California.

Kato, B., 1982. "Beam-to-column connection research in Japan", J. Struct Div., Proc. ASCE 108, pp. 343-360

Kato, B., Chen, W.F., and Nakao, M. 1988. "Effect of joint-panel shear deformations on frames", Journal of Constructional Steel Research, Vol. 10, pp. 269-320.

Korol, R.M., Ghobarah, A., and Osman, A. 1990. "Extended end-plate connections under cyclic loading: Behaviour and design", Journal of Constructional Steel Research, Vol. 16, pp. 253-280.

Krawinkler, H., Bertero, V.V., and Popov, E.P., 1971. "Inelastic behaviour of steel beam-to-column subassemblages", Report EERC 71/07, Earthquake Enginnering Research Center, University of California, Berkeley, California.

Krawinkler, H., Bertero, V.V., and Popov, E.P., 1975. "Shear behaviour of steel frame joints", Journal of Structural Division, ASCE, Vol. 101, No. ST11.

Krawinkler H., 1978. "Shear in beam-column joints in seismic design of steel frame", Engineering Journal, AISC, Vol.15(3), PP82-91

Krawinkler, H., and Popov, E.P., 1982. "Seismic behaviour of moment connections and joints", Journal of Structural Division, ASCE, Vol. 108, ST2, pp. 372-391.

Krawinkler, H., and Zohrei, M., 1983. "Cumulative damage in steel structures subjected to earthquake ground motions", Computers and Structures, Vol 16, pp.1-4

Krawinkler, H., and Mohasseb, S. 1987. "Effects of panel zone deformations on seismic response", Journal of Constructional Steel Research, Vol. 8, pp. 233-250.

Lawson, R.S., Vance, V., and Krawinkler, H., 1994. "Nonlinear static pushover analysis-Why, When and How?", 5th U.S. National Conference on Earthquake Engineering, Chicago, Illinois, Vol. 1, pp. 283-292.

Lee, E-T., 1992. "Inelastic cyclic behaviour of loaclly buckled plastic hinges of steel members", Ph.D. Thesis , State University of NewYork at Buffalo.

Liew, J.Y.R., and Chen, W.F., 1995. "Analysis and design of steel frames considering panel joint deformations", Journal of Structural Engineering, ASCE, Vol. 121, No. 10, pp. 1531-1540.

Lui, E.M., and Chen, W.F. 1986. "Frame analysis with panel zone deformation", International Journalof Solids and Structures, Vol. 22, pp. 1599-1627.

Maison, B.F., 1992. PC-ANSR: A computer program for nonlinear structural analysis, 1992 Version. University of California, Berkeley, California.

Meyer, C., Roufaiel, M.S., and Arzoumanidis, S.G., 1983. "Analysis of damaged concrete frames for cyclic loads", Earthquake Engineering and Structural Dynamics, Vol.11, pp. 207-228.

Miner, M. A., 1945. "Cumulative damage in fatigue", Journal of the Mechanical Division, ASME, pp. 159-164.

Mondkar, D.P. and Powell, G.H., 1974. "ANSR-1, General purpose program for analysis of nonlinear structural response", Report No. EERC 75/37, Earthquake Enginnering Research Center, University of California, Berkeley, California.

Mondkar, D.P. and Powell, G.H., 1975. "ANSR-1 static and dynamic analysis of nonlinear structures", Report No. EERC 75/10, Earthquake Enginnering Research Center, University of California, Berkeley, California.

Mzzalani, F.M., 1987. "Mathematical model for semi-rigid joints under cyclic loads", Proceeding of State-of-the-art workshop on connections and behaviour, strength and design of steel structures, Laboratorie de Mecanique et Technologie, Cachan, France.

Nader, M.N., and Astaneh, A. 1989. "Experimental studies of single story steel structure with fixed, semi-rigid and flexible connections", Report UCB/EERC-89/15, Earthquake Enginnering Research Center, University of California, Berkeley, California.

Nader, M.N, and Astaneh, A., 1992. "Seismic behaviour and design of semi-rigid steel frames", Report UCB/EERC-92/06, Earthquake Engineering research center, University of California, Berkeley, California.

Nakao, M., 1975. "Research on the Behaviour of Steel Beam-to-Column Rigid Connections", Ph.D. Thesis, University of Tokyo, Tokyo, Japan.

Naumoski, N., Heidebrecht, A.C. and Rutenberg, A.V., 1993. "Representative ensembles of strong motion earthquake records", Earthquake Engineering Research Group, McMaster University, Hamilton, Ontario, Canada, EERG Report 93-01.

Newmark, N.M., 1959. "A method of computing for structural dynamics", Journal of Engineering Mechanic Division, ASCE, Vol. 85.

Newmark, N.M., 1962. "A method of computation for structural dynamics", Transactions, ASCE, Vol. 127, pp. 1406-1435.

Newmark, N.M., and Hall, W.J. 1982. Earthquake spectra and design. Monographs Series, EERI, Department of Civil Eng., University of Illinois at Urbana-Champaign, Illinois.

Oliveira, C.S., 1975. "Seismic risk analysis for site and metropolitan area", Report No. EERC-75-3, University of California, Berkeley, California.

Osman, A., Ghobarah, A., and Korol, R.M., 1990. "Moment-rotation relationship for extented end-plate connections", Proc. fourth CSCE Conf., Hamilton, Ontario, Canada, pp. 517-536.

Osman, A., 1991. "Extended end-plate beam-column joints in seismic moment resisting frames", Ph.D. Thesis, Department of Civil Engineering, McMaster University, Hamilton, Canada, 316 pages.

Osman, A., Ghobarah A., and Korol R.M. 1993. "Seismic performance of moment resisting frames with flexible joints", Engineering structures, Vol. 15, pp. 117-134.

Osman, A., Ghobarah A., and Korol R.M. 1995. "Implications of design philosophies for seismic response of steel moment resisting frames", Earthquake Engineering and Structural Dynamics, Vol. 24, pp. 127-143.

Otani, S., and Sozen, M.A., 1972. "Behaviour of multistory reinforced concrete frames during earthquakes", Structural research series No. 392, Civil Engineering studies, University of Illinois, Urbana Ill.

Otani, S., 1974. "Inelastic analysis of R/C frame structures", Journal of Structural Division, ASCE, Vol. 100, pp. 1433-1449.

Packer, J.A., and Morris, L.J., 1977. "Alimit state design method for the tension region of bolted beam-column connections", Journal of the Institution of Structural Engineers, Vol. 55, No.10.

Park and Ang, 1985. "A mechanistic seismic damage model for reinforced concrete", Journal of Structural Eng., Vol 111, No. 4

Paulay, T., and Priestly, M., 1992. "Seismic design of reinforced concrete and masonry buildings", Published by John Wiley and Sons Inc.

Pinkney, R.B., and Popov, E.P., 1967. "Behaviour of steel building connections subjected to repeated inelastic strain reversal-experimental data", Report No. UCB/SEMM 67-31, University of California, Berkeley, California.

Popov, E.P., 1968. "Introduction to mechanics of solids", Prentice-Hall, Englewood Cliffs, N.J.

Popov, E.P., and Bertero, V.V., 1973. "Cyclic loadings of steel beams and connections", Journal of Structural Division, ASCE, Vol. 99, No. ST6.

Popov, E.P., Bertero, V.V., and Chandramouli, S., 1975. "Hysteretic behaviour of steel columns", Proc. U.S. National Conf. Earthquake Eng., Ann Arbor, Michigan, pp. 245-254

Popov, E. P., 1983. "Seismic moment connections for moment-resisting steel frames", Report UCB/EERC-83/02, Earthquake Engineering Research Center, University of California, Berkeley, California.

Popov, E. P., Amin, N. H., and Louie, J.C., 1985. "Cyclic behaviour of large beam-column assemnlies", Earthquake Spectra, pp. 201-237.

Popov, E.P., 1987. "Panel zone flexibility in seismic moment joints", Journal of Construc. Steel Research. Vol. 8, pp. 91-118.

Popov, E. P., and Tsai, K.C., 1989. "Performance of large seismic steel moment connections under cyclic loads", Engineering Journal, AISC, 2nd Quarter, pp. 51-60.

Popov, E.P., Tsai, K. and Engelhardt, M.D. 1989. "On seismic steel joints and connections", Engineering Structures, Vol. 11, pp. 148-162.

Powell, G. and Allahabadi, R., 1988. "Seismic Damage prediction by deterministic methods: Concepts and procedures", Earthquake Eng. and Structural Dynamics, Vol 16, pp. 719-734

Qi, X., and Moehle, J.P., 1991. "Displacement design approach for reinforced concrete structures subjected to earthquakes", Report UCB/EERC-91/02, Earthquake Engineering Research Centre, University of California, Berkeley, California.

Redwood, R., Lefki, L., and Amar, G., 1990. "Earthquake resistant design of steel moment resisting frames", Canadian Journal of Civil Engineering, Vol. 17, pp. 659-667.

Roeder, C.W., Schneider, S.P., and Carpenter, J.E. 1993. "Seismic behaviour of moment resisting steel frames: I - Analytical Study", Journal of Structural Engineering, ASCE, Vol. 199, pp. 1866-1885.

Saidii, M., and Sozen, M., 1981. "Simple nonlinear seismic analysis of R/C structures", Journal of Structural Division, ASCE, Vol. 107, pp. 937-952.

Schneider, S.P., and Amidi, A. 1998. "Seismic behaviour of steel frames with deformable panel zones", Journal of Structural Engineering, ASCE, Vol. 124, pp. 35-42.

Sivakumaran, K.S. 1988. "Seismic response of multi-storey steel buildings with flexible connections", Engineering Structures, Vol. 10, pp. 239-248.

Soleimani, D., Popov, E.P., and Bertero, V.V., 1979. "Nonlinear beam model for RC frame analysis", Proc. 7th ASCE conf. on Electronic computation, St. Louis, MO, USA.

Sozen, M.A., 1981. "Review of earthquake response of reinforced concrete buildings with a view to drift control", State of the art in earthquake engineering, Turkish National Committee on Earthquake Engineering, Istanbul, Turkey, pp. 383-418.

Tahara, T., and Kamei, T.T., 1988. "Comparative design of 10-storey steel building using ATC 3-06, L.A. city code and current Japanese code", 9th WCEE Vol.5, Tokyo, pp. 1113-1118

Tremblay, R., Timler, P., Bruneau, M., and Filiatrault, A., 1995. "Performance of steel structures during the 1994 Northridge earthquake", Canadian Journal of Civil Engineering, Vol. 22, pp. 338-360.

Tremblay, R., Bruneau, M., Nakashima, M., Prion, H., Filiatrault, A., and DeVall, R., 1996. "Seismic design of steel buildings: lessons from the 1995 Hyogo-ken Nanbu earthquake", Canadian Journal of Civil Engineering, Vol. 23, pp. 727-756.

Trifunac, M.D., and Brady, A.G., 1975. "A study on the duration of strong earthquake ground motion", Bulletin of the Seismological Society of America, Vol. 65, No.3, pp. 581-626.

Tsai, K.C., and Popov, E. P. 1988. "Steel beam-column joints in seismic moment resisting frames", Report UCB/EERC-88/19, Earthquake Engineering Research Center, University of California, Berkeley, California.

Tsai, K.C., and Popov, E.P., 1989. "End-plate moment connections for cyclic loads", ASCE Structures Congress, May.

Tsai, K.C. , and Popov, E.P., 1990. "Cyclic behaviour of end-plate moment connections", Journal of Structural Engineering, ASCE, Vol. 116, No.11, pp. 2917-2930.

Tso, W.K., Zhu, T.J. and Heidebrecht, A.C., 1992. "Engineering implication of ground motion A/V ratio", Soil Dynamics and Earthquake Engineering, Vol. 11, pp. 133-144.

Uang, C-M. and Bondad, D., 1996. "Improving the seismic performance of pre-Northridge steel moment frame connections with haunches", National Steel Construction Conference, Phoenix, Arizona.

Vision 2000 Committee. 1995. Performance based seismic engineering of buildings. Structural Engineers Association of California (SEAOC), San Francisco, California.

Waterloo Engineering Software, 1996. "Structural Optimization Design and Analysis: Version 3.3.1, User Manual".

Wilson, E.L. and Habibullah, A., 1987. "Static and dynamic analysis of multi-storey buildings including P-Delta effects", Earthquake Spectra, Vol.3, No.2, pp. 289-298.

# APPENDIX (I)

## STRAIN-DISPLACEMENT MATRIX OF THE WEB PANEL FINITE ELEMENT MODEL

$$
\mathbf{B}_w = \begin{bmatrix}
\frac{-1}{4w}(2-3\eta+\eta^3) & 0 & \frac{h}{8w}(1-\eta-\eta^2+\eta^3) \\
0 & \frac{-1}{2h}(1-\xi) & 0 \\
\frac{1}{4h}(1-\xi)(-3+3\eta^2) & \frac{-1}{2w}(1-\eta) & \frac{1}{8}(1-\xi)(-1-2\eta+3\eta^2)
\end{bmatrix}
$$

$$
\begin{bmatrix}
\frac{-1}{4w}(2+3\eta-\eta^3) & 0 & \frac{h}{8w}(-1-\eta+\eta^2+\eta^3) \\
0 & \frac{1}{2h}(1-\xi) & 0 \\
\frac{1}{4h}(1-\xi)(3-3\eta^2) & \frac{-1}{2w}(1+\eta) & \frac{-1}{8}(1-\xi)(-1+2\eta+3\eta^2)
\end{bmatrix}
$$

$$
\begin{bmatrix}
\frac{1}{4w}(2+3\eta-\eta^3) & 0 & \frac{-h}{8w}(-1-\eta+\eta^2+\eta^3) \\
0 & \frac{1}{2h}(1+\xi) & 0 \\
\frac{1}{4h}(1+\xi)(3-3\eta^2) & \frac{1}{2w}(1+\eta) & \frac{-1}{8}(1+\xi)(-1+2\eta+3\eta^2)
\end{bmatrix}
$$

$$
\begin{bmatrix}
\frac{1}{4w}(2-3\eta+\eta^3) & 0 & \frac{-h}{8w}(1-\eta-\eta^2+\eta^3) \\
0 & \frac{-1}{2h}(1+\xi) & 0 \\
\frac{1}{4h}(1+\xi)(-3+3\eta^2) & \frac{1}{2w}(1-\eta) & \frac{-1}{8}(1+\xi)(-1-2\eta+3\eta^2)
\end{bmatrix}
$$

in which

$h$ = height of the panel zone
$w$ = width of the panel web.

# APPENDIX (II)

## PERFORMANCE OF EXTERIOR COLUMNS DURING PUSH OVER ANALYSES

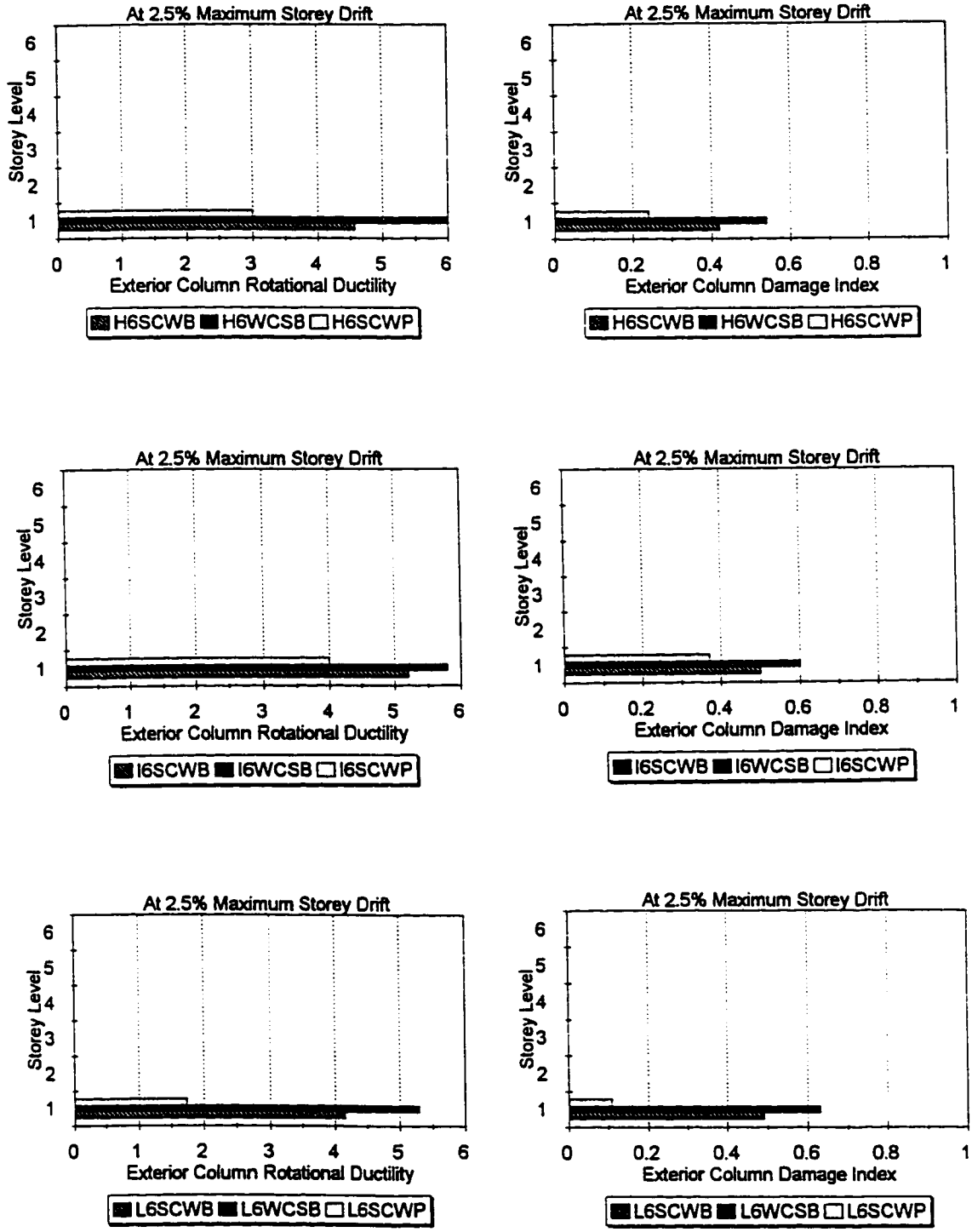


Figure II. 1 Exterior column performance parameters for the six storey frames at 2.5% maximum storey drift.

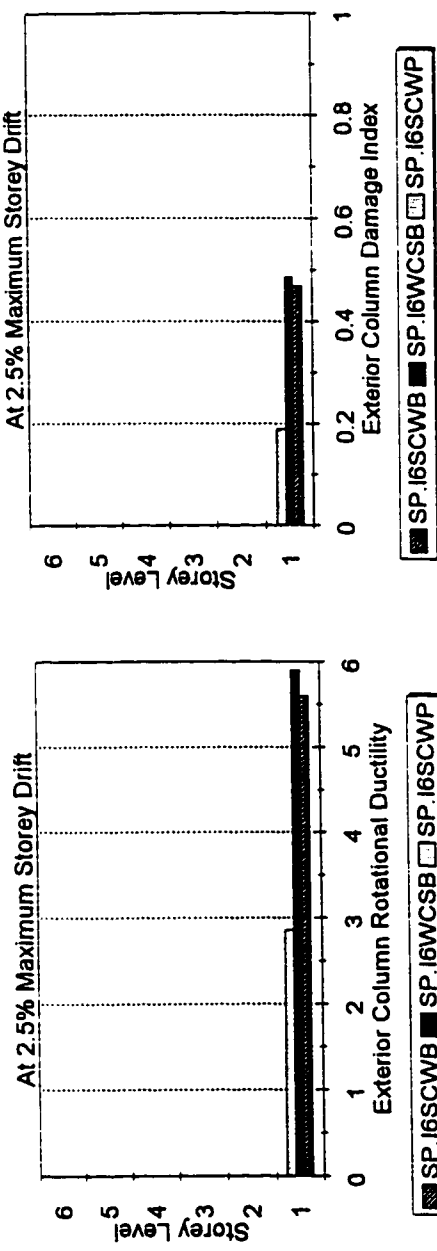


Figure II.2 Exterior column performance parameters for the special drift limit designed six storey frames at 2.5% maximum storey drift.

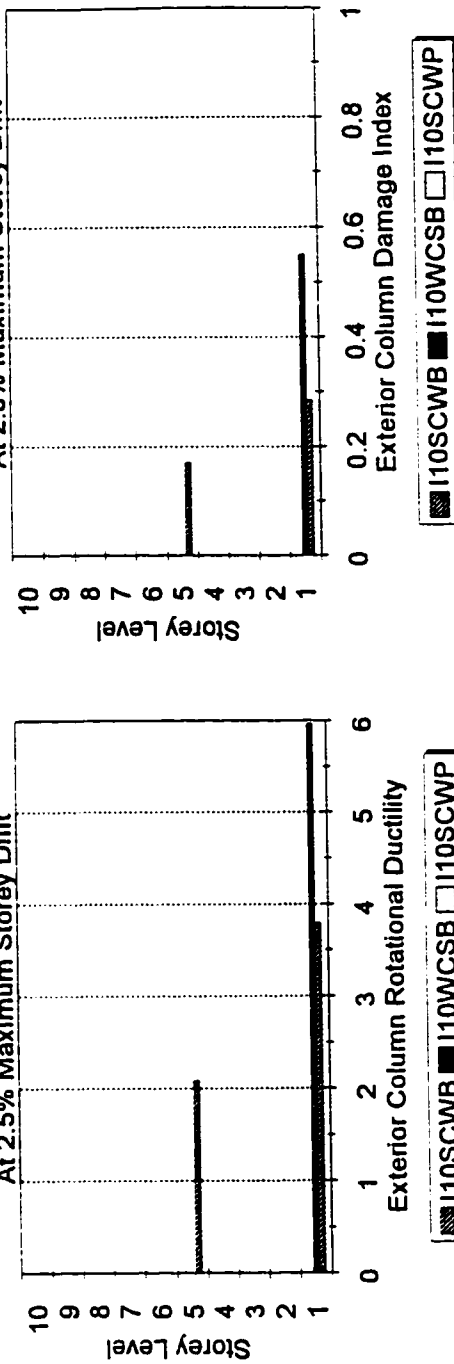


Figure II.3 Exterior column performance parameters for the ten storey frames at 2.5% maximum storey drift.

# APPENDIX (III)

## PERFORMANCE OF EXTERIOR PANEL ZONES DURING PUSH OVER ANALYSES

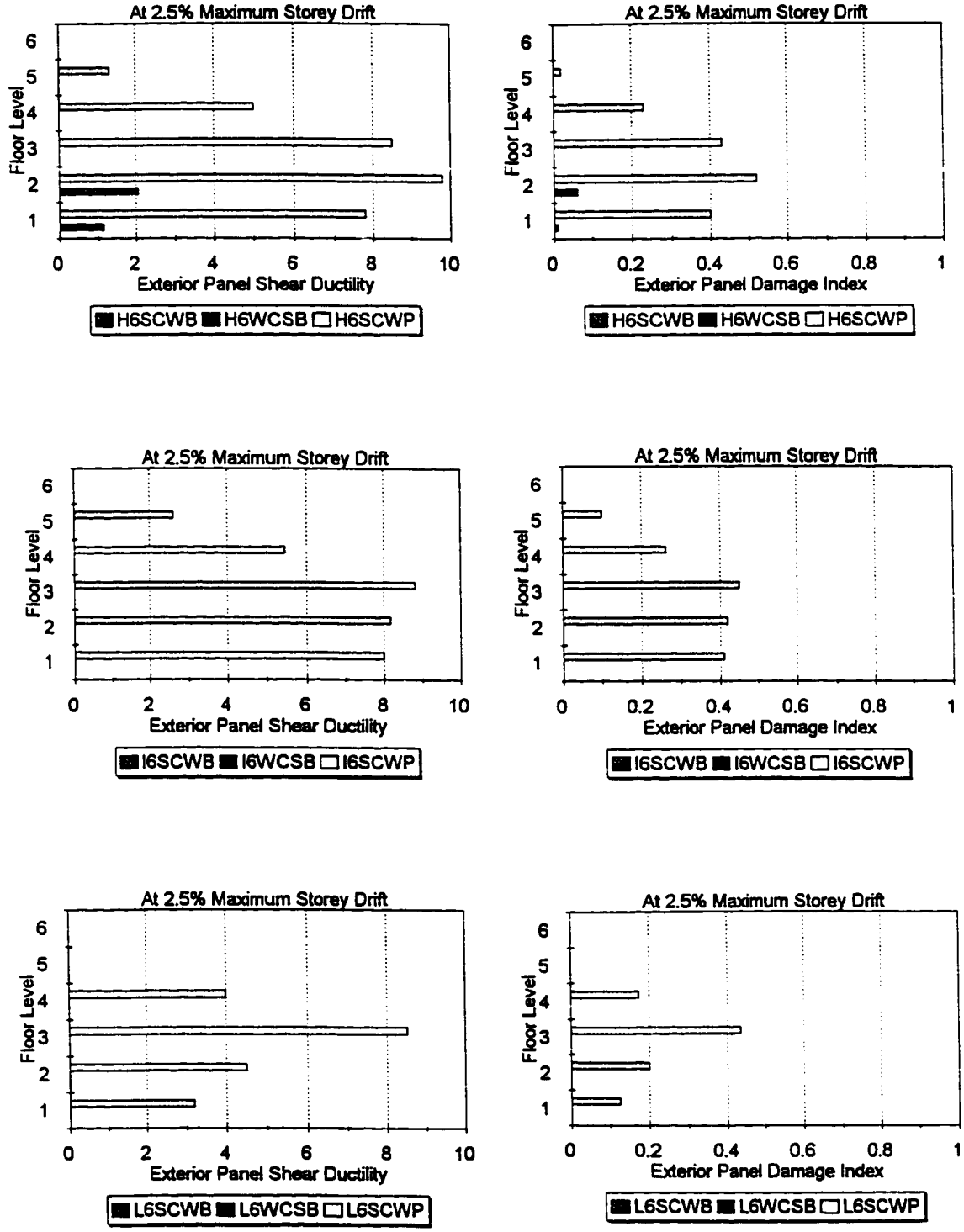


Figure III.1 Exterior panel zone performance parameters for the six storey frames at 2.5% maximum storey drift.

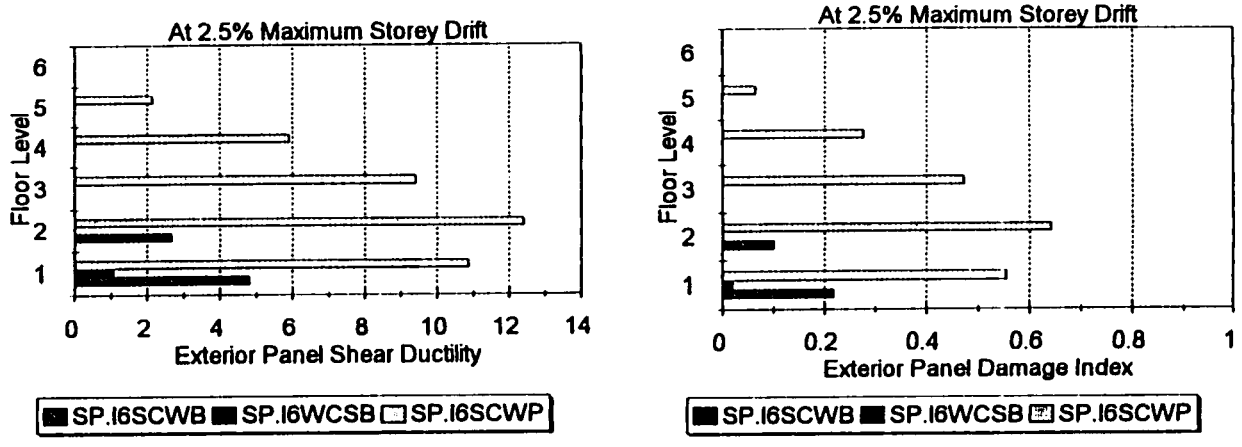


Figure III.2 Exterior panel zone performance parameters for the special drift limit designed six storey frames at 2.5% maximum storey drift.



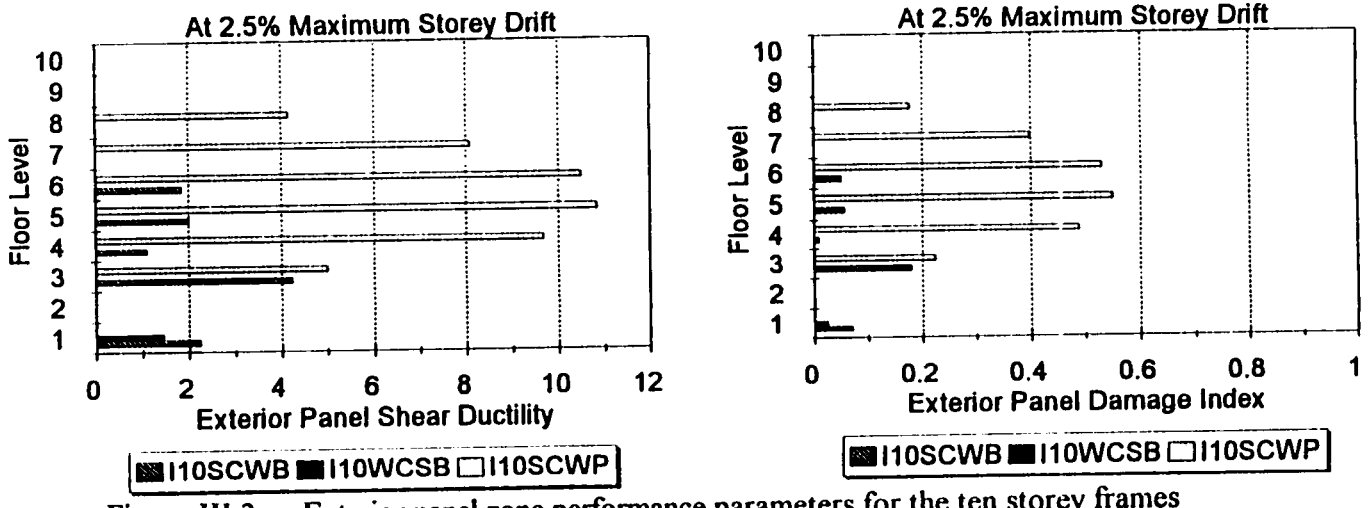


Figure III.3 Exterior panel zone performance parameters for the ten storey frames at 2.5% maximum storey drift.